THE INFLUENCE OF VEGETATION INDUCED MOISTURE TRANSFER ON UNSATURATED SOILS

BY

NAZRI ALI

Submitted for the degree of Doctor of Philosophy University of Cardiff

The School of Engineering
University of Cardiff

NOVEMBER 2007

ProQuest LLC
789 East Eisenhower Parkway
P.O. Box 1346
Ann Arbor, MI 48106-1346

ABSTRACT

This study explores issues related to the numerical simulation of moisture migration patterns in the unsaturated zone and in the vicinity of established vegetation. A one-dimensional water-uptake model was first developed to simulate moisture migration beneath uniform vegetation (crop) cover. The main thrust of the research was then to develop a practicable water-uptake model that can be used to simulate moisture migration patterns beneath mature trees.

The moisture flow model used is based on Richard's Equation extended to incorporate a sink term and integrated with appropriate water-uptake models (i.e. 1D, 2D, and 2D axi-symmetric form). A numerical solution was achieved via the finite element method for spatial discretisation along with a finite difference time-marching scheme. A series of numerical simulations have been presented that demonstrate the newly introduced sink term functioned correctly and that the model is capable of representing typical water extraction processes from a variety of crop types. A new two-dimensional axi-symmetric model was then developed and applied to simulate moisture migration near established trees. In particular, the approach adopted utilizes radial symmetry and assumes a linear distribution of water extraction rate with both depth and radius. The new model has been validated by direct comparison to field measurements recorded (by others) for mature trees located on a clay sub-soil. The model has been shown to be capable of representing water-uptake over a full-annual cycle. Time dependent boundary conditions, based on rainfall data, and hysteresis effects have also been explored. Overall, a good correlation between field data and simulated results has been achieved. Hysteresis effects, when the soil has already experienced repeated wetting and drying cycles, were not found to be of great significance for the class of problem considered.

The research also provides a preliminary assessment of the significance of tree induced water content (and therefore suction) changes on the stability of unsaturated soil slopes. The 'typical' example considered, indicated that relatively small suction changes (in the order of 10 kPa) can influence the factor of safety against slope failure by approximately 7%. These findings should be considered in addition to the variety of other vegetation related strength effects.

In conclusion, a relatively straight forward approach to modelling water-uptake by vegetation has been developed. The resulting model is thought to be valuable for a range of geoengineering problems.

DECLARATION

The work submitted in this thesis is the result of investigations carried out by the author. Acknowledgement is given directly in the text or by means of references where the work of others is discussed.

The material in this thesis has not already been accepted for any degree and is not concurrently submitted in candidature for any degree.

Signed

CANDIDATE

Signed

DIRECTOR OF STUDIES

ACKNOWLEDGEMENTS

This study was undertaken while I was a PhD student at the School of Engineering, University of Cardiff. I would like to express my sincere thanks to Dr. Stephen William Rees for his close supervision, guidance and encouragement at all stages of works.

This research has been sponsored by the University Technology of Malaysia and Higher Education of Malaysia. Their financial support is appreciated.

The completion of this thesis has been greatly helped by the support and understanding shown by my wife, Shalhaa Ismail, my kids, Nasha and Naiman and friends. I am very grateful and fortunate.

CONTENTS

LIST OF FIGURES

LIST OF TABLES

LIST OF SYMBOLS

$C(\psi)$	Specific moisture capacity (cm^{-1})
c'	Effective Cohesion (kPa)
G_j , g_j	Prescribe known functions or operators
i	Hydraulic gradient
K_s	Saturated hydraulic conductivity (cm/s)
$K(\phi), K(\psi)$	Unsaturated hydraulic conductivity (cm/s)
N	Total normal force on the base of the slice (kN)
N_i, N_r, N_s	Shape Function
O	The centre of slip surface rotation
R, R_Ω	The residual or error introduced by the approximation
r_{rj}, r_r	Maximum rooting radial (cm)
S	Matric Suction (kPa)
S_m	Shear force mobilized on the base of each slice (kN)

$S_{max}, S(\psi), S(\psi, z), S(\psi, z, r)$	Sink term ($cm^3/cm^3/s$)
T, T_j	Potential Transpiration rate (cm/s)
t	Time (s)
u	Functions in Ω
u_a	The pore-air pressure (kPa)
u_w	The pore-water pressures (kPa)
$\hat{u}$	The approximation to the function u
V, V_w	Volume of water (cm^3)
v_x, v_y, v_z	Velocity of water flow (cm/s)
W	Total weight of a slice (kN)
W_l	The weighting functions
x, r, z	Cartesian co-ordinates (cm)
z_{rj}, z_r	Maximum rooting depth (cm)
$\alpha(\psi)$	Pressure head dependent reduction factor
α, l, m, n	Soil specific parameter
β	Angle between the tangent to the centre of the base of each slice and the horizontal (degree)

γ	Density (kN/m^3)
θ	Volumetric moisture content (%)
$\theta 1, \theta 2$	Contact angle of an interface
θ_r	Residual water content (%)
θ_s	Saturated water content (%)
σ_n	Normat stress (kPa)
ψ	Capillary potential (cm)
$\hat{\psi}$	The approximation to the ψ (cm)
ϕ	Total potential for moisture flow
ϕ'	Angle of friction (degrees)
ϕ^b	Angle indicating the rate of increase in shear strength relative to matric suction (degrees)
$\hat{\phi}$	The approximation to the ϕ
Ω	Domain
Γ	Boundary
λ	Water flux at the boundary (cm/s)

CHAPTER ONE

INTRODUCTION

1.1 RESEARCH BACKGROUND

It is now well established that soil suction is a limiting parameter for water-uptake, and hence nutrient intake, for many types of vegetation. Therefore, in agricultural science, the optimisation of crop yield depends on a sound knowledge of the interplay between the plant-root system and the soil water. However, it is becoming increasingly recognised that the variation in soil suction that occurs in the presence of vegetation, and indeed those that can occur on removal of vegetation, have an important role to play in the analysis of a number of geotechnical and geoenvironmental problems.

This study explores the development of a numerical model capable of representing the extraction of water from the soil by the roots of various types of vegetation – the so called water-uptake process. The work initially focuses on

relatively simple forms of water-uptake models capable of representing the behaviour beneath uniform crop/grass cover. The main thrust of the research is then aimed at the consideration of water-uptake in the vicinity of established trees. The research can be extended and applied to a range of geoengineering problems as indicated below.

The stability of soil slopes, naturally occurring or man-made, gives rise to significant problems in many countries. Safe design and an ability to predict behaviour under a variety of field conditions is becoming increasingly important. This is a problem that is exacerbated by climate change and increasingly intense rainfall events (Dehn et al, 2000; Turner, 2001). In many circumstances soil slopes will be populated by some form of vegetation ranging from grass cover to more established shrubs and trees. Repair maintenance and operation of railway and road embankments is a particular area where these factors are important (Ridley et al. 2004). Recent research indicates that progress is now being made to incorporate the influence of vegetation within the framework of slope stability analysis (Greenwood et al. 2004). Whereas, good progress is being made with regard to the contribution of roots to the overall shear strength, the direct influence of suction variations still appears to need further consideration.

In the UK the shrinkage and swelling of clay soils, particularly when influenced by trees, is the single most common cause of foundation movements which may damage domestic buildings. The value of insurance claims for subsidence and heave damage to domestic properties has been estimated to be in the region of £300 - £400 million per annum (BRE, 1999; BRE, 2004). Furthermore, the prediction of heave/shrinkage is fundamentally dependent on changes in soil moisture content.

Within this context, a predictive capability that will enable the extent to which trees cause moisture content (and hence deformation) changes is clearly of importance.

More widely, the hydro-dynamic influence of trees on surface water flows is receiving increasing attention within the context of effective floodplain utilization. This aspect of the problem is beyond the scope of the current programme of work; however, an improved understanding of groundwater variation near trees will contribute to the assessment of overall water balance (run-off, infiltration etc).

At the start of this research programme an existing finite element solution of the Richard's equation for unsaturated soil was available (Rees and Thomas, 1990). The code was written in Fortran and was set-up for two-dimensional, Cartesian flow problems. The current research required significant development and extension of this code as indicated in some of the objectives listed below.

1.2 OBJECTIVES

The overall objective of this research is to develop a new two-dimensional axi-symmetric model capable of simulating moisture migration near established trees. The new model will be capable of including time varying boundary conditions and soil hysteresis that occur over a full-annual cycle. Detailed objectives of this investigation are to:

i. Introduce a volumetric sink term into the governing equation for unsaturated moisture flow and pre-existing finite element code (Rees and Thomas, 1990).

ii. Identify a theoretical model for one-dimensional water-uptake by vegetation.

iii. Implement the selected 1D water-uptake model within the finite element framework.

iv. Verify and validate the new 1D model.

v. Develop a theoretical model for two-dimensional axi-symmetric water uptake processes associated with an established tree.

vi. Implement the 2D axi-symmetric model within the finite element formulation.

vii. Incorporate the root zone geometry and control routines related to the water uptake models within the finite element code.

viii. Validate the 2D axi-symmetric model by comparison with experimental data.

ix. Investigate water-uptake from an established tree over a seasonal time frame.

x. Investigate the influence of hysteresis in the water retention characteristics on seasonal wetting/drying trends.

xi. Provide a preliminary assessment of the role of vegetation in slope stability analysis.

1.3 SCOPE AND LIMITATIONS

The current work is aimed at providing a framework for the simulation of moisture migration due to vegetation that will be of potential value for a range of

geoengineering applications (as mentioned previously). Therefore, an underlying principle of maintaining the simplest acceptable approach has been adopted. As a consequence of this, the resulting models will inevitably exclude or simplify some aspects of the problem.

One-dimensional water-uptake was considered briefly in the first instance. This work was primarily undertaken to ensure that the volumetric sink terms and overall water-extraction process could be implemented correctly within the finite element formulation. Therefore the water-uptake model was kept as simple as possible by utilizing a linear distribution of water extraction with depth.

Root growth can be accommodated in the new model, however since the current work is primarily aimed at developing an approach for the simulation of established trees, this aspect of behaviour is only considered briefly within the context of the 1D modelling approach and is excluded entirely from the work on simulation of moisture migration near trees.

When the behaviour associated to single, isolated, trees is under consideration, radial symmetry is assumed to exist. Therefore, a two-dimensional axi-symmetric formulation is assumed adequate for this class of problem. Clearly, more complex behaviour will occur when adjacent trees interact – this aspect of the problem is not considered here.

Most roots must have oxygen for growth; therefore, the necessary rates of diffusion of oxygen can only be achieved in a non-saturated soil. Many of the practical problems of interest are also dominated by near surface behaviour. Therefore, this research focuses only on moisture flow occuring in unsaturated soils.

Unsaturated flow is described by a partial differential equation and solved by approximate numerical methods. In particular, the finite element method is used to

achieve spatial discretisation and the finite difference method is used to achieve time discretisation. There are unavoidable approximations implicit in this approach. However, every effort has been made to ensure that discretisation errors are kept to a minimum.

It is recognized that flow parameters may also be temperature dependent; however, this effect is considered second order and is not included here. Isothermal conditions are therefore assumed to exist. Non-linearity of moisture transfer parameters and hysteresis effects are included in this work.

Some soils will exhibit volume change in relation to variations in soil moisture content. Analysis of this problem requires coupled flow and deformation to be considered. However, this is beyond the scope of the current work and constant volume models are developed here.

Tree roots are often found mostly below 0.3 m depth from the ground surface. This is often attributed to competition between different root species, for example, roots of trees frequently extend beyond the rooting depth of grasses and crops (Buresh and Tian, 1998, Dawson et al, 2001, Moreno et al, 2005). Although, in reality the uppermost layer of soil will often contain a higher organic content and may have significantly different hydraulic properties from soil at depth. In the current work, a homogenous soil profile is assumed throughout. The generic model developed, is however, capable of including layered soils although this is not explicitly demonstrated in the current developmental work.

Normally grass roots are shallow in depth ranging from 0.15 m to 0.35 m depth and widespread near the ground surface (Karen and Phillip, 1999, Tufekcioglu et al, 1999, Polley et al, 2002). Since trees also use significantly more water than most other types of vegetation (Nisbet, 2005) the influence that surrounding grass

may have on the overall moisture migration patterns has not been given any separate attention here.

A preliminary assessment of the influence of trees on soil slope stability is also attempted. However, this aspect of the work is limited to the influence of suction changes on shear strength only. This is achieved by utilising an extended form of the Mohr-Coulomb equation (Fredlund et al, 1978). There are implicit limitations with this approach that are beyond the scope of this investigation. Furthermore, no consideration is given to the mechanical effects associated to the strength of roots.

1.4 THESIS LAYOUT

An overview of related research work to the analysis of root water uptake in unsaturated soil is presented in Chapter 2. The review provides a commentary on the general significance of the water-uptake process. It then provides a summary of the key mechanisms involved and aims to provide some background information that can be utilised in subsequent simulation work. The review also summarises developments in modelling the root-water-uptake process.

The theoretical basis for describing moisture flow in an unsaturated soil is presented in Chapter 3. Some of the fundamental concepts used to describe moisture flow due to water uptake plant by roots are also introduced. This chapter is divided into two main parts. The first part describes the derivation of the moisture flow equation and the second part describes the derivation of the water uptake model.

Chapter 4 presents an approximate numerical solution of the theoretical model framework presented in Chapter 3. The problem addressed is one in which both spatial and time variations of the unknown variable, capillary potential in this case,

are required. A numerical solution is then described to achieve discretisation of a two-dimensional axi-symmetric space domain and the time domain.

Chapter 5 presents some preliminary applications of the new numerical model. In the first instance, attention is given to a basic assessment of the robustness of the new code. This chapter considers one-dimensional water uptake only and aims to provide confidence in the implementation of the new sink term and the basic form of the water uptake model. The performance of the model is checked against independent results for a range of test problems.

Chapter 6 then moves on to explore the numerical simulation of moisture migration patterns in the vicinity of mature trees. In particular the axi-symmetric form of the model presented in Chapter 3 and 4 is explored here. The model is applied to simulate field measurements recorded (by others) for a mature lime tree located on a Boulder Clay sub-soil. Non-linear hydraulic properties are obtained from independent published data. This first application of the full model aims to simulate only a spring/summer drying period and does not include a full seasonal wetting/drying cycle.

Chapter 7 develops the work presented in Chapter 6 with the aim of exploring a full seasonal time frame. In particular, a simulation is presented that covers a full annual cycle starting from field capacity in winter, extending through a full spring/summer drying period and including the subsequent autumn recharge. The simulation attempts to include time dependent variations in boundary conditions based on daily rainfall patterns. In addition hysteresis in the soil water retention curve is also explored.

Chapter 8 considers how the new model may be employed to provide an assessment of the significance of water content (and therefore suction) changes on the stability of unsaturated soil slopes. Typical slope geometry and a range of initial conditions and tree locations are considered. The corresponding variation of the Factor of Safety against failure is examined.

Overall conclusions are presented in Chapter 9. Suggested further research is also discussed at this stage.

1.5 REFERENCES

Biddle, P. G., "Tree Root Damage to Buildings." Willowmead Publishing Ltd, Wantage, 1998.

BRE. "Low-rise building foundations: the influence of trees in clay soils." A Building Research Establishment Publication, 1999.

BRE. "Controlling Water Use of Trees to Alleviate Subsidence Risk." Horticulture LINK project 212, University of Cambridge, 2004.

Buresh, R. J. & Tian, G. "Soil improvement by trees in sub-Saharan Africa. " Agroforestry Systems, 38: 51–76, 1998.

Dawson, L.A., Duff, E.I., Campbell, C.D. & Hirst, D.J. "Depth distribution of cherry (Prunus avium L.) tree roots as influenced by grass root competition." Plant and Soil, 231: 11–19, 2001.

Dehn, M., Burger, G., Buma, J. and Gasparetto, P., "Impact of Climate Change on Slope Stability using expanded downscaling." Eng. Geology 55, p193-204, 2000.

Fredlund, D.G., Morgenstern, N. R. and Widger, R. A., "The shear strength of unsaturated soils." Canadian Geotechnical Journal, 15, 313 – 321, 1978.

Greenwood, J. R., Norris, J. E., and Wint, J., "Assessing the contribution of vegetation to slope stability." Geotechnical Engineering, 157(GE4), 199 - 207, 2004.

Karen, J. E. & Philip, W. R. " Comparative patterns of phenology and growth form diversity in two winter rainfall deserts: the Succulent Karoo and Mojave Desert ecosystems." Plant Ecology, 142: 97–104, 1999.

Moreno, G., Obrador, J.J., Cubera, E. & Dupraz, C. "Fine root distribution in Dehesas of Central-Western Spain." Plant and Soil, 277:153–162, 2005

Nisbet, T. R. "Water Use by Trees." Forestry Commission, Edinburgh, 1 – 8, 2005.

Polley, H.W., Hyrum B. J. and Charles R. T. " Woody invasion of grasslands: evidence that CO2 enrichment indirectly promotes establishment of Prosopis glandulosa." Plant Ecology, 164: 85–94, 2002.

Rees, S. W., "Seasonal Ground Movement Effects on Buried Services," PhD, University of Wales, Cardiff, 1990.

Rees, S. W., and Thomas, H. R., "Modelling Field Infiltration into Unsaturated Clay." Journal of Geotechnical Engineering, 116(10), 1483 – 1501, 1990.

Ridley, A., McGinnity, B., and Vaughan, P., "Role of pore water pressure in embankment stability". Geotechnical Engineering, 157, Issue GE4, p193-198, Paper 13714, 2004.

Tufekcioglu, A., Raich, J. W., Isenhart, T. M. and Schultz, R. C. " Fine root dynamics, coarse root biomass, root distribution,and soil respiration in a multispecies riparian buffer in Central Iowa, USA." Agroforestry Systems, 44: 163–174, 1999.

Turner, S., "Climate change blamed as landslip incidents treble." New Civil Engineer, 8, 2001.

CHAPTER TWO

LITERATURE REVIEW – UPTAKE OF WATER BY VEGETATION

2.1 INTRODUCTION

An understanding of the movement and distribution of soil water in the presence of vegetation is important in the analysis of a number of geotechnical and geoenvironmental problems (see Chapter 1). This chapter provides the reader with a broader indication of the significance of these processes and an outline of the key behavioural mechanisms involved. A summary of the historic development of theoretical/numerical models related to specific vegetation types and field conditions is also presented.

The primary objective of the current work relates to consideration of water-uptake near trees. However, it is also necessary to consider, in brief, some of the previous research undertaken in relation to the analysis of water-uptake by crops.

These primarily one-dimensional models have largely formed the basis for axi-symmetric (and/or 3D) models that may be applied to simulate the behaviour of water-uptake near trees.

2.2 ROOT-WATER UPTAKE

2.2.1 Context and Significance

The amount of water used by trees has been the subject of international research for over one hundred years (Bosch and Hewlett, 1982; McCulloch and Robinson, 1993; Nisbet 2005). This aspect of behaviour is of interest to many different fields of study such as; agricultural, geoenvironmental engineering, ecology, building management, hydraulic/hydro-environmental engineering and geotechnical Engineering.

Jackson et al (2000) states one of the most significant facts that provides scale to the problem. In their work on root-water uptake and transport in global predictions, they state that, globally, plants recycle more than half of the 110,000 km^3/yr (approx.) of precipitation that falls on land each year. It would appear, therefore, that the role that vegetation has on the global hydrological cycle is difficult to over-estimate.

More locally, BRE (2004) stated that the Highways Agency (HA) in United Kingdom has an extensive roadside estate that extends to 30,000 hectares, which supports more than 25 million trees. In addition, there are even more trees on non-highway land, including those on private and public property. Many trees are located close to structures/buildings, roads, and pavements and an ability to predict the influence of related soil drying is a potentially important management tool in these

situations. A similar picture exists for the rail industry where track maintenance and repair are recognised as a key aspect of asset management. Vegetation on embankments and cuttings requires careful consideration (Network Rail, 2006).

Trees can extract water from below the foundations causing some particular clay sub-soils to shrink, ultimately leading to failure of the foundations and cracks to appear. As mentioned in Chapter 1, the cost of repairing such subsidence damage of domestic house foundations is of the order of £300-£400 million annually (BRE, 1999; BRE, 2004). Although not all of this damage can be attributed to the presence of tree roots, some 73 % of cases are claimed to have been caused, at least to some extent, by tree roots (Loss Prevention Council, 1995).

Quantifying soil moisture content redistribution within an unsaturated soil in the presence of a rooting system is also a practical problem in surface hydrology and climate research (Protopapas and Bras, 1992; Kleidon et al, 1998; Zeng et al, 1998; Lai and Katul, 2000). For example, Nisbet (2005) states that in order to achieve a good surface-water and groundwater status by 2015, the European Water Framework Directive requires a deeper understanding of the role that trees play in the hydrological process. This requires recognition of how forests affect water supply, downstream flooding and erosion control. This is set against the background that water companies have to deal with the dual threat of rising water demand and the possibility of reduced supplies due to climate change.

Feddes et al (2001) suggests that the research of the Anglo-Brazilian Amazonian Climate Observation Study (Gash and Nobre, 1997) and the inter-comparison of different land surface parameterization schemes given by Pitman et al. (1999) provide clear evidence that root-zone structure and water-uptake may have a direct effect on form of the land surface. In addition, evaluation of water uptake by

roots is also necessary to estimate correctly the antecedent soil-water condition in many rainfall-runoff models (Stephenson and Freeze, 1974; Grayson et al, 1995; Kim et al, 2005).

Water-uptake by roots can also contribute to an improved understanding of chemical fluxes in the unsaturated zone in both ecological and hydrological studies (Somma et al, 1998; Vrugt et al, 2001a). The process can control the timing and the amount of chemical pollutant loading to the groundwater through elimination of preferential flow paths of both water and chemicals, or by regulation of absorption of nutrients, thus reducing their concentration levels in the deep unsaturated zone or groundwater (Clothier and Green, 1994). Furthermore, the rhizosphere area (i.e. the zone that surrounds the roots of plants) might be responsible for accelerated breakdown of organic chemicals by biodegradation (Walton and Anderson, 1990).

Remediation of contaminated unsaturated zone has been an issue of increasing interest (Chang and Corapcioglu, 1997; Alexander, 1999; Wise and Trantolo, 1994; Sung et al, 2002). Vegetation can reduce water entry into the soil by blocking soil pores and by extracting water from the soil via transpiration (see below for further discussion). The presence of roots may change the soil composition and distribution of micro-organisms in the soil. Soil temperature and moisture content influence microbial activity, root-growth and chemical reactions in the soil. Since temperature can vary with depth, biological and chemical reactions can respond to this temperature profile (Schelde et al, 1998). Water uptake by roots may therefore play a role in the prediction of contaminant fate and transport in remediation systems. Deliberate utilization of vegetation to assist with the clean-up process is known as phytoremediation (Salt et al., 1995).

Water uptake by plant roots is fundamental to many applications in agriculture (WUCOLS, 2000; Zhuang et al, 2001) and water management practice (Rasiah and Kohl, 1989; Gong et al, 2006). The interaction between soil water and plant roots is key to successful growth (Ojha and Rai, 1996; Wu et al, 1999; Dardanelli et al, 2004; Braud et al, 2005). Shortage of water in the root zone results in reduced plant growth and affects the crop yield, as well as the quality and quantity of infiltration recharge to groundwater systems (Wallach, 1990; Schmidhalter et al, 1994). During this period, the capability of crop roots to extract soil water is primarily dependent on the distribution and depth of its root system. Therefore, predicting water uptake becomes crucial for modelling plant growth under those conditions.

2.2.2 The Root-Water Uptake Process

The process of water uptake by roots within unsaturated soil layers is quite complex and depends on many interrelated factors. The overall result is controlled by meteorological, soil physical and plant factors (Homaee et al, 2002; Green et al, 2003; Nisbet, 2005). Figure 2.1 shows a simplified illustration of the main factors involved.

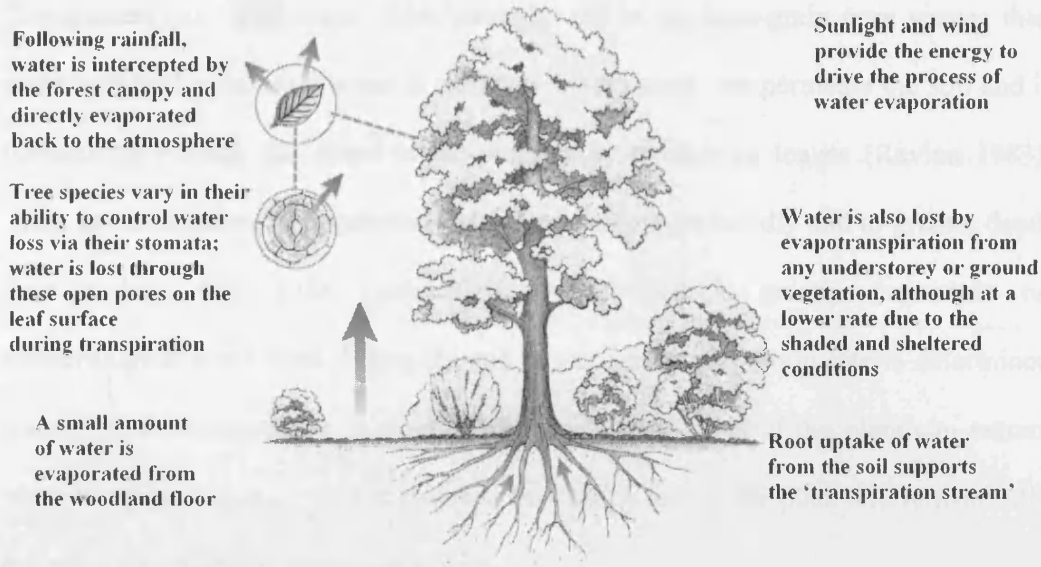

Figure 2.1 Water use by Trees, modified after Nisbet (2005)

Nisbet (2005) provides a summary of the way that trees use, or lose, water in terms of two separate processes. The first process is where water is taken up by tree roots from the soil, transported from the roots to the leaves through the plant tissue (called the xylem) and then evaporated through the leaves to the atmosphere. This is termed 'transpiration' and is a physiological process, which responds to soil and atmospheric factors. The second process is the interception of water by the surfaces of leaves, branches and trunk(s) during rainfall and its subsequent evaporation. Interception losses are enhanced by the high atmospheric turbulence created by forest canopies due to their height and rough aerodynamic profile. Taken together, these two processes are referred to as 'evapotranspiration'. Both are strongly affected by the amount of sunlight, the air temperature, the air humidity and the wind speed. In the current work, the focus of attention is on prediction of water uptake by roots from the soil and therefore transpiration is the key process of interest here.

Soil type also influences the amount of evapotranspiration that takes place; fine-grained soils hold water more strongly within the inter-grain pore spaces than coarse-grained soils. Soil water is extracted by the roots that permeate the soil and is transmitted through the stems to the continually transpiring leaves (Ravina 1983). Thus, in the presence of vegetation the soil may dry more rapidly and to greater depth than a bare soil. Like evaporation, transpiration is greatly dependent on meteorological conditions. When the soil is wet, the transpiration rate is determined mainly by the evaporative demand. Provided that the roots of the plant can extract water from the soil at a rate that matches the canopy losses, the plant will remain fully hydrated and maintain its normal activity.

However, when the rate of water uptake by the roots falls below the rate of transpiration, the plant will begin to lose water and if this situation persists, it will cause the plant to wilt. As soil moisture is diminished and soil suction increases, the hydraulic conductivity may become too low to transmit soil water to the roots at the desired rate. In addition, the soil suction may exceed that of the root system and the soil will reach the wilting point moisture content. The water retention characteristic of the soil enables a definition of the approximate wilting point as the moisture content at a capillary potential of -15000 cm (suction of 1500 kPa) (Feddes et al, 1978).

Different species of tree vary in terms of moisture demand and in terms of their rooting configuration. Cutler and Richardson (1989) provided a guide to the maximum height and the horizontal root spread that can be expected for commonly planted trees in Britain. This information is repeated here in Table 2.1. It appears that the average horizontal root spread is about 5.75 m for a tree of an average height

of 17.8 m. Thus, root spread would appear to be roughly one-third of the height of the tree, although some variation to this clearly occurs.

Table 2.1 Horizontal root spread of commonly planted trees in Britain, modified after Cutler and Richardson (1989)

No	Trees	Max height (m)	Horizontal root spread (m)
1	Apple	10	4
2	Pear	12	4
3	Ash	14	6
4	Beech	20	6
5	Birch	14	4
6	Cherries	12	3
7	Plums	8	3
8	Damsons	8	3
9	Elm	25	8
10	False Acacia	20	7
11	Hawthorn	10	5
12	Horse Chestnut	25	7.5
13	Lime	24	6
14	Maples	24	6
15	Oak	23	9.5
16	Plane	30	5.5
17	Poplar	28	11
18	Rowan	12	5
19	Service Tree	12	5
20	Sycamore	24	6
21	White Beam	12	5
22	Willow	25	7

Cutler and Richardson identified this data as part of an investigation of the distance between trees and buildings in cases where building damage may have occurred due to the presence of a tree. It is therefore, not based on a direct measurement of root length in-situ.

Trees produce roots to provide support, water, nutrients and act as a food storage organ. Genetic influences on rooting habits do exist, but the dominant effect on rooting structure is environmentally based (Crow, 2004). Opportunities to examine the entire root systems of mature trees are rare; however, storms in October, 1987 produced many wind-thrown trees that allowed root plate dimensions to be surveyed by the Royal Botanical Gardens at Kew as shown in Figure 2.2.

Figure 2.2 Storm blown tree showing root plate typical of that found during the Kew survey, after Crow (2004)

Of the 4511 wind thrown trees surveyed by Cutler et al (1990) after the storm, only 2.4 % were found to have deep roots or taproots. Typically, trees have relatively shallow but wide-spread root systems (Dobson and Moffat, 1993; Dobson, 1995). It is unusual for roots to penetrate to a depth greater than 2 m.

Dobson and Moffat (1993) made some generalisations about the rooting characteristics of major woodland species as shown in Table 2.2. Characteristics were studied for different species of natural regeneration, grown on well aerated sandy soils and grouped into three different types:

a. Taproot - where a strong main root descends vertically from the underside of the trunk.
b. Surface roots - where large horizontal lateral roots extend below the surface, from which smaller roots descend vertically.
c. Heart root - where large and small roots descend from the trunk diagonally into the soil

This type of information, although limited, provides useful guidance for the modelling work presented in Chapter 6 of the thesis.

Table 2.2 Rooting information and relative water demands for some common tree species, modified after Crow (2004)

Species	Typical root architecture	Typical root depth (metre)	Water requirements 1 = lowest, 6 = highest
Ash	Surface	1.1	2 – 4
Aspen	Surface	1.3	4 – 6
Birch	Heart	1.8	1 – 2
Beech	Heart	1.3	2 – 3
Common alder	Heart/Surface	2.0	2
Corsican pine	Tap	-	1
Douglas fir	Heart	2.0	1 – 2
English oak	Tap	1.5	3 – 6
Eucalyptus	-	-	5 – 6
European larch	Heart	2.0	1
Hornbeam	Heart	1.6	2
Japanese larch	Heart	-	1
Lime	Heart	1.3	3 – 4
Norway maple	Heart	1.0	2 – 3
Norway spruce	Surface	2.0	1
Poplar	-	-	4 – 6
Red oak	Heart	1.6	3 – 6
Scots pine	Tap	2.1	1
Sessile oak	Tap	1.5	3 – 6
Silver fir	Tap	2.0	1
Sycamore	Heart	1.3	2 – 3
White pine	Surface	1.7	1

2.2.3 Transpiration Rate

Transpiration rate is one of the important values employed in modelling the water-uptake process. As indicated above, transpiration rate is influenced by many factors including; tree species, condition, canopy volume, temperature, xylem volume, wind speed, soil type, soil moisture, root volume, length of daylight and strength of daylight (Kramer 1969, Roberts, 1983; Nisbet, 2005; Indraratna, 2006). Some typical transpiration rates based on independent published data and are shown in Table 2.3.

Table 2.3 Transpiration rate for trees

Authors	Type of Tree	Rate (mm/d)
Nisbet (2006)	Broadleaves	2
Indraratna et al (2006)	Lime	3
Takagi et al (2006)	Lotus	7
Dunin et al (1985)	Gum	9
Vrught et al (2006)	Almond	4
USGS (2005)	Oak	5
Biddle (1998)	Common	5

There are wide differences among plants of different species with respect to the depth, spread and amount of branching of the root. The larger the volume of soil occupied by root system, the larger the volume of water is transpiration. Smith (1917) claims that Sorghum fine roots have nearly twice as many when compared to Corn.

Changes in light intensity and temperature cause variation in leaf resistance through stomatal (leaf cells through which most of the water escapes) aperture and vapour pressure. Stomatal control of water losses through transpiration has been identified as an early event in plant response to water deficit (Chaves, 1991; Cornic and Massacci, 1996; Bacelar et al, 2007). An increase in temperature increases transpiration because it increases the steepness of the vapour pressure gradient from leaf to air (Meyer and Anderson, 1952).

Wind acts directly to increase transpiration by sweeping away the boundary layer of moist air surrounding leaves (Kramer, 1969). This factor is directly influenced by the leaf area, arrangement and structure. The leaf arrangement also affects the exposure of leaves to sun and has some effect on the amount of energy received.

The xylem is mainly responsible for the transportation of water and mineral nutrients throughout the plant. The total potential of the root cells is often greater than that in the soil - usually due to the concentrations of solute in the root cell. Therefore, water can move by osmosis into the root (Tyree and Zimmermann, 2002). As a result, increasing the volume of xylem in the roots will increase water transported into the tree.

2.3 WATER-UPTAKE MODELS

2.3.1 One-Dimensional Water Uptake

For the reasons already stated, the development of methods of analysis of vegetation induced moisture migration is of considerable practical interest. In describing water uptake by plant roots, there are two main approaches (Feddes et al, 1976; Mathur and Rao, 1999). The first strategy typically considers radial soil water flow to a single root and is therefore known as the 'microscopic' approach. In contrast, the second approach is based on a 'macroscopic' view of the problem and considers the root system treated as a single unit.

A considerable amount of research has been published using microscopic approach starting with early contributions from Philip (1957). This work assumed flow towards individual roots to be radial. The root system was considered to represented by a network of cylindrical roots embedded into cylindrical soil volumes. The hydraulic conductivity was assumed to be independent of water content, and the evaporative demand was also assumed constant with time.

Further developments appeared in the literature shortly afterwards by many researchers (Gardner 1960; Cowen 1965; Passioura and Cowen, 1968; Molz and Remson, 1970; Hillel et al, 1975; Molz and Hornberber, 1973; Pages et al, 1989; Nobel and Alm, 1993; Steudle, 1994; Personne et al, 2003) which followed the microscopic approach and modified the steady-state model of Philip (1957). However, the microscopic approach is generally limited by the difficulty in measuring

the time-dependent geometry of the root system. This approach also cannot be experimentally tested, and boundary conditions cannot be easily defined (Simunek et al, 1992; Vogel et al, 1992; Wu et al, 1999; Vrugt et al, 2001b, Li et al, 2006).

Gardner (1964) was the first researcher to propose a macroscopic mathematical model to describe the water uptake by a non-uniform root system. The study aimed to determine the rooting distribution associated with various depth increments. The model results were compared to experimental data for a sorghum plant. Good agreement was achieved between the experimental and theoretical water-uptake. Further developments appeared in the literature shortly afterwards also using the macroscopic approach (see for example Whisler et al, 1968; Molz and Remson, 1970; Nimah and Hanks, 1973; Raats, 1974; Feddes et al, 1976, 1978; Afshar and Marino, 1978; Hoogland et al, 1981; Landsberg and Fowkes, 1978; Rowse et al, 1978; Molz, 1981; Belmans et al, 1983; Prasad, 1988).

In the macroscopic approach, the root system is treated as a single unit and the approach does not take into account the effect of the individual roots, thus eliminating the difficulty in measuring the time-dependent geometry of the root system. The entire root zone is assumed to extract moisture from small differential volumes of the root zone at some rate, and the water uptake by roots is usually represented by a volumetric sink term in the unsaturated flow equation. The boundary conditions are specified at the soil surface of the composite soil plant system and at the water table. These macroscopic models also allow natural interaction with the transpiration process.

The inclusion of a volumetric sink term in Richard's equation to accommodate water-uptake is an approach that has been used quite widely; Whisler et al, 1968; Feddes et al, 1978; Molz, 1981; Clausnitzer and Hopmans, 1994. Usually, the sink

term is expressed as the volume of water per unit volume of soil per unit time (cm^3 water. cm^{-3} soil. sec^{-1}). A macroscopic water uptake model is then required to effectively distribute the volume of water extracted from the root zone in a pattern that mimics that observed in the field.

For the practical reasons stated above, this study also employs a macroscopic approach. The precise approach developed here is described in detail in Chapters 3 and 4.

Returning to the general overview, a number of different approaches to modelling the macroscopic water uptake process have been considered in past. For example, Feddes et al (1978) proposed a scheme in which potential transpiration was first distributed over the rooted zone and then reduced to actual root-water-uptake by the use of a soil water stress reduction function. Based on this conceptualization, numerous root-water-uptake models have since been developed (Li et al 2006).

Gardner (1991) proposed a sink term based on the root depth parameter and an extractable water parameter and distributed sink moving downward through the soil profile. However, the moving sink does not explicitly explain the observed uptake patterns completely.

Prasad (1988) use linear root distribution functions based on Feddes et al (1978) and Hoogland et al (1981) to represent water uptake. Prasad suggested a linear root water extraction term that varies with time and assumes a zero root water extraction rate at the bottom of the root zone. Validation of the model was attempted using the experimental results of Erie et al (1965) - the results were found to agree well. This approach provided an important development in water-uptake modelling. Prasad's model was conceptually simple and shown to be capable of representing real behaviour.

Mathur and Rao (1999) presented a numerical model that incorporated a sinusoidal root growth function that takes into account the root growth with time. However, the time dependent nature of root behaviour was not fully demonstrated due to fact that the simulation was run for a relatively short time period.

Raats (1974) was among the first researchers to provide a nonlinear root distribution function. However, the Raats' model ignored the effect of soil water content on the distribution of root water uptake, which is in stark contrast to the work of Feddes et al (1978). Further developments of the non-linear model can also be found in the literature (Jarvis, 1989; Tiktak and Bouten, 1992; Li et al, 2001; Vrugt et al, 2001a, 2001b).

Vrugt et al (2001a) presented six different possible configurations of normalized water uptake distribution (see Figure 2.3). The first four water uptake models (A, B, C and D) have maximum root water uptake at the soil surface whereas the other two (E and F) have maximum uptake at depths of 0.2 m and 0.5 m, respectively. It was suggested that these two (latter) distributions may arise in relation to subsurface drip irrigation. The figure indicates that the most common distribution form adopted assumes maximum root water uptake to occur at the soil surface.

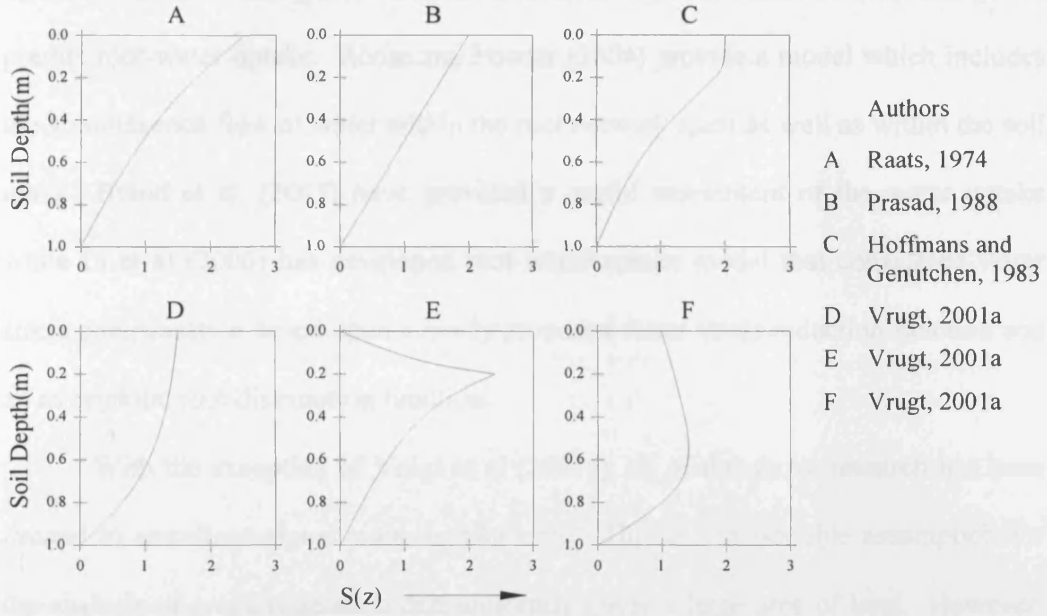

Figure 2.3 Some possible water uptake patterns, modified after Vrugt (2001a)

Li et al (2001) examined the difference between linear and non-linear root distribution functions. In particular, Prasad's linear model and an exponential model developed by Li et al (1999) were compared. After the first 30 days of simulation, the cumulative water uptake from both models was found to be the same. After 60 days, at the end of simulation, the cumulative water uptake for the linear and exponential model differed by only 5 %. This comparison suggested that for some practical problems the cumulative water uptake predicted by a simple linear model may be adequate. In circumstance where the exact geometry of the resulting moisture migration pattern is of more importance, non-linear models may offer advantage.

Further contributions have been published more recently. For example, Lai and Katul (2000) considered the role of root-water-uptake on the relationship between actual and potential transpiration. Homaee et al. (2002) used an extraction term in the simulation of salinity stress. Dardanelli et al. (2004) developed a simplified water-

uptake model that uses generalizations from measured soil water content changes to predict root-water-uptake. Roose and Fowler (2004) provide a model which includes the simultaneous flow of water within the root network itself as well as within the soil mass. Braud et al. (2005) have provided a useful assessment of the water uptake while Li et al (2006) has developed root water uptake model that considered water stress compensation based upon a newly proposed water stress reduction function and an asymptotic root distribution function.

With the exception of Vrugt et al (2001a), all of the above research has been limited to one-dimensional water-uptake only. This is a reasonable assumption for the analysis of crops/vegetation that uniformly cover a large area of land. However, for other types of vegetation, notably trees, this simplification would not appear appropriate.

2.3.2 Multi – Dimensional Water Uptake

Neuman et al. (1975) was among the first researchers to consider multi-dimensional water-uptake by roots. In this work, a numerical simulation was used to solve two-dimensional non-steady flow in porous media. Their methods made a great contribution to the understanding of the movement of the soil moisture. However, their method are not appropriate for irrigation in actual field service because of the restrictions on the performance of computers, limitations of mathematical knowledge and problems in the stability of calculation.

Warrick et al (1980) presented a mathematical model to simulate plant water uptake assuming steady state conditions and an unsaturated hydraulic conductivity as

an exponential function of pressure head. The geometries considered possess radial symmetry (points, discs and cylinders shape) and are appropriate in situations such as trickle irrigation. However, as mentioned by Warrick et al, this model is limited only to uniform soil, negligible surface loss and no time dependent.

Based on experimental data, Coelho and Or (1996) proposed parametric models for two-dimensional water-uptake intensity patterns under drip irrigation. These models offer parameters that may be useful for modelling and comparisons between crops, locations, and management scenarios. Different water uptake patterns associated with four basic plant dripper configurations, (surface, subsurface, within and between crop rows) were identified and measured in field and greenhouse experiments. However, the proposed models were limited based on the experimental work without any numerical simulations and more focus on water-uptake by crops, which are more relevant to agricultural field.

Somma et al (1998) expand work by Clausnitzer and Hopmans (1994) to present a finite elements model to allow the simultaneous, dynamic simulation of root growth and water and solute transport and uptake in three dimensions. The model provided a tool for studying the interactive relationships between changing soil-water and nutrient status and root activity. Solute transport modelling includes passive and active nutrient uptakes by roots are the main concern in their study. However, the model only validated for short periods of time (25 days) and there are the limitations of the model, including the lack of root formulation. Somma et al also suggest that much experimental work is needed to provide the model with the correct parameter values and functional relationships.

Vrugt et al (2001a) and Vrugt et al (2001b) presented two-dimensional and three-dimensional root water uptake models to be integrated in a flow code provided by Simunek et al (1992). They employed the model developed by Raats (1974) and extended it to include a radial component for two-dimensional problems and a thickness term for three-dimensional cases. To validate the model, Vrugt et al (2001a) measured water content around a sprinkler-irrigated almond tree for a 16-day period. Their model is flexible and allows spatial variations of water uptake as influenced by non-uniform and uniform water application patterns. However, this model is limited to deal with types of root distribution and parameters of the model were difficult to determine. The model has also been validating for the short period only.

Recently, Gong et al (2006) provided two-dimensional model of root water uptake for single apple tree and validate the model with soil water content measurements in an orchard. The model includes root density distribution function, potential transpiration and soil water stress-modified factor. However, this model is validated against the measurement data for a seven year old apple tree for an eight week period. Root growth was the main concern and this model was not applied to consider seasonal variations.

Indraratna et al (2006) have developed a two-dimensional water uptake model employing to the commercially available software, ABAQUS. Their simulation was compare with experimental data provided by Jaksa et al (2002) for a Gum Tree and data provided by Biddle (1998) for a Lime Tree. However, as state by Indraratna, direct comparison of suction values is not possible, due to the fact that the proposed numerical model could predict only the matric suction changes, whereas the measurements obtained by Jaksa et al were in total suction. A number of

uncertainties and assumptions in relation to the specification of some soil parameters when using ABAQUS (i.e. variety of empirical and experimental root coefficients, densities and compression index). There also no seasonal variations effects (e.g. rainfall and hysteresis) were included in this work.

To date, water uptake models appear to have been validated only for relatively short periods of time (as relevant to the particular problems considered) and more focus on agricultural field. However, within the context of some of the geoengineering problems (i.e. slope stability) mentioned earlier, the seasonal and long term influence of vegetation becomes more important (Blight, 2003). Therefore, this research aims to explore the simulation of water uptake from an established tree over a typical full annual cycle. Time dependent boundary conditions due to rainfall and hysteresis effects are also explored in the current work.

2.4 CONCLUSIONS

A general overview of the literature related to root water uptake in unsaturated soils has been presented. The state of art of modelling root water uptake has been presented from one-dimensional to multi-dimensional models. Literature has been cited that addresses specific aspects of the particular problem in hand. The specific useful findings from this chapter are state below.

The review indicated that trees have relatively shallow but wide-spread root systems and most distribution from various researchers shows that the maximum root water uptake is at the soil surface. Transpiration rate for a single tree based on independent data published in the literature are range from 2mm/day to 9mm/day.

This comparison of transpiration rate would appear to suggest that the assumed rate in this study within the range of previously published data.

In this study, the macroscopic approach for the water uptake model is employed due to this approach does not take into account the effect of individual roots because of the difficulty in measuring the time-dependent geometry of the root system. The entire root zone is assumed to extract moisture from each differential volume of the root zone at some rate and the water uptake by roots is represented by a volumetric sink term or sink term.

Most root-water uptake models from review are based on one-dimensional behaviour and for two-dimensional models are applied relatively for short time periods. There also no seasonal effect involved in the water uptake models. One-dimensional model is a reasonable assumption for the analysis of crops/vegetation that uniformly covers a large area of land. However, for other types of vegetation, notably trees, this simplification would not appear appropriate. Due to the sink term employed to represent water-uptake near an established tree, a two-dimensional axi-symmetric formulation looks more appropriate to apply rather than one-dimensional and standard two-dimensional unsaturated model. Therefore, further work two-dimensional axi-symmetric on seasonal water uptake for trees is necessary.

The review also indicates that the cumulative water uptake for the linear and exponential model is 5 % different. This comparison indicates that small percentage of different in the cumulative water uptake between the linear and exponential water uptake. Therefore, in this study a linear root water extraction term that varies with time is used. This relatively straight forward and simplicity approach is thought to be suitable for development for axi-symmetry two-dimensional water uptake models which can be used and more related to geoengineering problems like slope stability

and shrinkage. Prasad's approach was found to be conceptually simple and shown to be capable of representing real behaviour. For this reason, Prasad's work has been chosen as the basis for the root-water model developed in this study (see Chapters 3 and 4).

2.5 REFERENCES

Afshar, A., and Marino, M. A. "Model for simulating soil water content considering evaporation." Hydro, 37, 309-322, 1978.

Alexander, M. "Biodegradation and Bioremediation." San Diego, CA, 1, 453, 1999.

Bacelar E. A., Pereira,J. M., Goncalves, B. C., Ferreira, H. F. and. Correia, C. M. "Changes in growth, gas exchange, xylem hydraulic properties and water use efficiency of three olive cultivars under contrasting water availability regimes. " Environmental and Experimental Botany, 60, 183–192, 2007.

Belmans, C., Wesseling, J. G., and Feddes, R. A. "Simulation model of the water balance for the cropped soil: SWATRE. " J. Hydro., 63, 271–275, 1983.

Biddle, P. G., "Tree Root Damage to Buildings." Willowmead Publishing Ltd, Wantage, 1998.

Blight, G. E., "The vadose zone soil-water balance and transpiration rates of vegetation." Geotechnique, 53(1), 55 64, 2003.

Bosch, J. M. and Hewlett, J. D. "A review of catchment experiments to determine the effects of vegetation changes on water yield and evapotranspiration. " Journal of Hydrology, 55, 1982.

Braud, I., Varado, N., and Olioso, A., "Comparison of root water uptake modules using either the surface energy balance or potential transpiration." Journal of Hydrology, 301, 267 – 286, 2005.

BRE. "Low-rise building foundations: the influence of trees in clay soils." A Building Research Establishment Publication, 1999.

BRE. "Controlling Water Use of Trees to Alleviate Subsidence Risk." Horticulture LINK project 212, University of Cambridge, 2004.

Chang, Y. Y. and Corapcioglu, M. Y. "Effect of Roots on Water Flow in Unsaturated Soils. " Journal of Irrigation and Drainage Engineering, 202 – 209, 1997.

Chaves, M. M. "Effects of water deficits on carbon assimilation. " J. Exp. Bot. 42, 1–16, 1991

Clausnitzer, V. and Hopmans, J. W. "Simultaneous modeling of transient three-dimensional root growth and soil water flow. " Plant and Soil, 164, 299–314, 1994.

Clothier, B. E. and Green, S. R. "Rootzone processes and the efficient use of irrigation water." Agric. Water Manage., 25, 1–12, 1994.

Coelho, F. E., and Or, D., "A parametric model for two-dimensional water uptake intensity by corn roots under drip irrigation." Soil Sci. Am. J., 60, 1039-1049, 1996.

Cornic, G. and Massacci, A. "Leaf photosynthesis under drought stress." Photosynthesis and the Environment, Netherlands, 347–366, 1996.

Cowen, I. R. "Transport of water in the soil-plant-atmosphere system." J. Appl. Ecology, 2, 221–239, 1965.

Crow, P. "Trees and Forestry on Archaeological sites in the UK: A review document." Forest Research, 2004.

Cutler, D. F., and Richardson, I. B. K., "Tree roots and buildings.", Longman Scientific and Technical, Singapore, 1989.

Cutler, D.F., Gasson, P.E and Farmer, M.C. "The wind blown tree survey: Analysis of results. " Arboricultural Journal, 14, 265-286, 1990.

Dardanelli, J. L., Ritchie, J. T., Calmon, M., Andriani, J. M., and Collino, D. J., "An empirical model for root water uptake." Field Crops Research, 87, 59 – 71, 2004.

Dobson, M.C. "Tree root systems. " Arboriculture Research and Information Note, Arboricultural Advisory and Information Service, Farnham, 1995.

Dobson, M.C. and Moffat, A.J. "The potential for woodland establishment on landfill sites. " Department of the Environment, HMSO, London, 1993.

Dunin, F. X., Mcilroy, I. C. and Oloughlin, E. M. "A lysimeter characterization of evaporation by eucalypt forest and its representativeness for the local environment. " Forest–Atmosphere Interaction, 271–291, 1985.

Erie, L.J., French, O.F. and Harris, K. "Consumptive use of water by crops in Arizona. " Tech. Bull. 169, Agric. Exp. Stn., Univ. Arizona, 1965.

Feddes, R. A., Kowalik, P. J., Malink, K. K., and Zaradny, H., "Simulation of field water uptake by plants using a soil water dependent root extraction function." J. Hydro, 31, 13 – 26, 1976.

Feddes, R. A., Kowalik, P. J., and Zaradny, H. "Simulation of field water use and crop yield." Wageningen Center for Agriculture and Documentation, Wageningen, 189, 1978.

Feddes, R. A., Hoff, H., Bruen, M., Dawson, T., Rosnay, P., Dirmeyer, P., Jackson, R. B., Kabat, P., Kleidon, A., Lilly, A. and Pitmank, A. J. "Modeling Root Water Uptake in Hydrological and Climate Models." American Meteorological Society, 82(12), 2797 – 2809, 2001.

Gardner, W. R. "Dynamic aspects of water availability to plants." Soil Sci., 89, 63–73, 1960.

Gardner, W. R. "Relation of root distribution to water uptake and availability." Agronomy J., 56, 41 – 45, 1964.

Gardner, W. R., "Modelling water uptake by roots." Irrig. Sci., 12, 109 -114, 1991.

Gash, J. H. C., and Nobre, C. A. "Climatic effects of Amazonian deforestation: Some results from ABRACOS." American Meteorological Society, 78, 823–830, 1997.

Gong, D., Kang, S., Zhang, L., Du, T. and Yao, L. "A two-dimensional model of root water uptake for single apple trees and its verification with sap flow and soil water content measurements. " Agricultural Water Management, 83, 119 – 129, 2006.

Grayson, R. B. Bloschl, G. and Moore, I. D. "Distributed parameter hydrologic modeling using vector elevation data: Thales and TAPES-C. " Computer models of watershed hydrology, Water Resources Publications, Highlands Ranch, Colo, 669–695, 1995.

Green, S.R., Vogeler, I., Clothier, B.E., Mills, T.M. and Dijssel, C. "Modelling water uptake by a mature apple tree." Aust. J. Soil Res. 41 (3), 365–380, 2003.

Hillel, D., Van Beek, C. G. E. M. and Talpaz, H. "A microscopic scale model of soil water uptake and salt movement to plant roots." Soil Sci., 120, 385–399, 1975.

Homaee, M., Dirksen, C., and Feddes, R. A., "Simulation of root water uptake 1. Non uniform transient salinity using different macroscopic reduction functions." Agricultural Water Management, 57, 89 – 109, 2002.

Hoogland, J. C., Feddes, R. A., and Belmans, C., "Root water uptake model depending on soil water pressure head and maximum extraction rate." Acta Hort, 119, 276 -280, 1981.

Indraratna, B., Fatahi, B. and Khabbaz, H. "Numerical analysis of matric suction effects of tree roots." Geotechnical Engineering, 159, 77 – 90, 2006.

Jaksa, M. B., Kaggwa, W. S. and Woodburn, J. A. "Influence of large gum trees on the soil suction profile in expansive soils." Australian Geomechanics Journal, 37, No. 1, 23–33, 2002.

Jarvis, N. J. "A simple empirical model of root water uptake." J. Hydrol., 107, 57–72, 1989.

Jackson, R. B., Sperry, J. S. and Dawson, T. E. "Root water uptake and transport: using physiological processes in global predictions." Trends in Plant Sci., Nov. 2000, Vol. 5, No.11, p482-488.

Kim, S., Kavvas, M. L. and Chen, Z. Q. "Root-Water Uptake Model at Heterogeneous Soil Fields." Journal of Hydrologic Engineering, 160 – 167, 2005.

Kleidon, A. and Heimann, M. "Optimized rooting depth and its impacts on the simulated climate of an atmospheric general circulation model." Geophysical Research Letters, 25(3), 345 – 348, 1998.

Kramer, P. J. "Plant and Soil Water Relationships: A Modern Synthesis." McGraw-Hill Book Company, New York, 1969.

Lai, C. T. and Katul, G. "The dynamic role of root water uptake in coupling potential to actual transpiration." Advances in Water Resources, 23, 427 – 439, 2000.

Landsberg, J. J., and Fowkes, N. D., "Water movement through plant roots." Ann. Bot., 42, 493 – 508, 1978.

Li, K. Y., Boisvert, J. B. and Jong, R. D. "An exponential root-water-uptake model. " Can. J. Soil Sci., 79, 333–343, 1999.

Li, K. Y., Jong, R. D., and Boisvert, J. B., "An exponential root water uptake model with water stress compensation." Journal of Hydrology, 252, 189 204, 2001.

Li, K. Y., Jong, R. D., Coe, M. T. and Ramankutty, N. "Root-Water-Uptake Based upon a New Water Stress Reduction and an Asymptotic Root Distribution Function. " Earth Interactions, 10(14), 1 – 22, 2006.

Loss Prevention Council. "Subsidence and domestic housing survey: analysis of results, LPR4:1995." Loss Prevention Council Report, Borehamwood, 1995.

Mathur, S. and Rao, S. "Modelling water uptake by plant roots." Journal of Irrigation and Drainage Engineering, 125(3), 159 – 165, 1999.

Meyer, R. E. and Anderson, D. B. "Plant Physiology." Van Nostrand Company, Princeton, 1952.

McCulloch, J. S. G. and Robinson, M. "History of forest hydrology. " Journal of Hydrology, 150, 189–216, 1993.

Molz, F. J., "Models of water transport in the soil-plant system: a review." Water Resour. Res., 17(5), 1245 – 1260, 1981.

Molz, F. J. and Hornberger, G. M. "Water transport through plant tissue in the presence of a diffusible solute." Soil Sci. Soc. Am. Proc., 37, 383–387, 1973.

Molz, F. J. and Remson, I. "Extraction term models of soil moisture use by transpiring plants. " Water Resour. Res., 6(5), 1346–1356, 1970.

Neumann, S. P., Feddes, R. A., and Bresler, E., "Finite Element analysis of two-dimensional flow in soil considering water uptake by roots: I. Theory." Soil Sci. Am. J., 35, 224-230, 1975.

Network Rail. "Network Rail Management Plan 2006." Network Rail Website, http://www.networkrail.co.uk/aspx/4054.aspx, 2006.

Nimah, M. N. and Hanks, R. J. "Model for estimating soil water, plant and atmospheric interrelations: I. Description and Sensitivity." Soil Sci. Soc. Am. Proc. 37, 522–532, 1973.

Nisbet, T. R. "Water Use by Trees." Forestry Commission, Edinburgh, 1 – 8, 2005.

Nobel, P. S. and Alm, D. M. "Root orientation vs. water uptake simulated for monocotyledonous and dicotyledonous desert succulents by root-segment model. " Funct. Ecol., 7, 600 – 609, 1993.

Ojha, C. S. P. and Rai, A. K. "Nonlinear Root-Water Uptake Model. " Journal of Irrigation and Drainage Engineering, 122(4), 198 – 202, 1996.

Pages, L., Jordan, M. O. and Picard, D. "Simulation of the three dimensional architecture of the maize root system. " Plant Soil, 119, 147 – 154, 1989.

Passioura, J. B. and Cowen, I. R. "On solving the nonlinear diffusion equation for the radial flow of water to roots." Agr. Meteorology, 5, 129–134, 1968.

Personne, E., Perrier, A. and Tuzet, A. "Simulating water uptake in the root zone with a microscopic-scale model of root extraction. " Agronomie, 23, 153–168, 2003.

Pitman, A. J., and Co-Authors. "Key results and implications from phase 1(c) of the Project for Intercomparison of Land-surface Parameterization Schemes." Climate Dyn., 15, 673–684, 1999.

Philip, J. R., "The physical principles of water movement during the irrigation cycle." Proc. Int. congress on Irrig. Drain, 8, 124-154, 1957.

Prasad, R., "A linear root water uptake model." J. Hydrology, 99, 297 – 306, 1988.

Protopapas, A.L. and Bras, R.L. "Effects of weather variability and soil parameter uncertainty on the soil-crop-climate system. " Am. Meteorol. Soc., 6, 645 – 656 , 1992.

Raats, P. A. C., "Steady flows of water and salt in uniform soil profiles with plant roots." Soil Sci. Am. Proc., 38, 717-722, 1974.

Rasiah, V. and Kohl, R. A. "Soybean Root Water Uptake in Two Soils." Agricultural Water Management, 15, 387-393, 1989.

Ravina, I. "The influence of vegetation on the swelling and shrinkage of clay." Geotechnique 4th Symposium 33, 151 – 157, 1983.

Roberts J. "Forest Transpiration: A Conservative Hydrological Process." Journal of Hydrology, 66, 133 – 141, 1983.

Roose, T., and Fowler, A. C., "A model for water uptake by plant roots." Journal of Theoretical Biology, 228, 155 171, 2004.

Rowse, H. R., Stone, D. A., and Gerwitz, A. "Simulation of the water distribution in soil." Plant Sci., 49, 534–550, 1978.

Salt, D. E., Blaylock, M., Kumar, N. P.B.A., Dushenkov, V. Ensley, B. D., Chet, I and Raskin, I., " Phytoremediation: A Novel Strategy for the Removal of Toxic Metals from the Environment Using Plants. " Bio/Technology 13, 468 – 474, 1995.

Schelde, K., Thomsen, A., Heidmann, T., Schjonning, P. and Jansson, P.E. "Diurnal fluctuations of water and heat flows in a bare soil. " Water Resour. Res. 34 (11), 2919– 2929, 1998.

Schmidhalter, U., Selim, H. M. and Oertli, J. J. " Measuring and modeling root water uptake based on chloride discrimination in a silt loam soil affected by groundwater. " Soil Sci., 158, 97–105, 1994.

Simunek, J., Vogel, T. and Genuchten, M. T. V. "The SWMS 2D code for simulating water flow and solute transport in two dimensional variably saturated media. " Research Report No. 126, U.S. Salinity Lab, ARS USDA, Riverside, 1992.

Smith, W. R. "Director's Report, 1915-1916." Agricultural Experiment Station, Kansas State Agricultural College, 50, 1917

Somma, F., Hopmans, J.W. and Clausnitzer, V. "Transient three-dimensional modeling of soil water and solute transport with simultaneous root growth, root water and nutrient uptake. " Plant Soil, 202, 281–293, 1998.

Stephenson, G. R. and Freeze, R. A. "Mathematical simulation of subsurface flow contributions to snowmelt and runoff, Reynolds Ck., Watershed, Idaho." Water Resour. Res., 10, 284–294, 1974.

Steudle, E. " Water transport across roots. " Plant Soil, 167, 79 – 90, 1994.

Sung, K., Corapcioglu M. Y. and Drew, M. C. "Heat and mass transfer in the vadose zone with plant roots." Journal of Contaminant Hydrology, 57, 99–127, 2002.

Takagi, K., Harazono, Y., Noguchi, S., Miyata, A., Mano, M.and Komine, M. "Evaluation of the transpiration rate of lotus using the stem heat-balance method. "Aquatic Botany, 2006.

Tiktak, A. and Bouten, W. "Modelling soil water dynamics in a forested ecosystem III: Model description and evaluation of discretization. " Hydrol. Process, 6, 455–465, 1992.

Tyree, M.T. and Zimmermann, M.H. "Xylem Structure and the Ascent of Sap." 2nd Edn., Springer, New York, 2002.

USGS. "The water cycle: Evapotranspiration. " United State Geological Survey, 2005.

Vogel, T., Huang, K., Zhang, R. and Genuchten, M. T. V. "The HYDRUS code for simulating one-dimensional water flow, solute transport and heat movement in variably saturated media. " Research Report No. 140, U.S. Salinity Lab, ARS USDA, Riverside, 1992.

Vrugt, J. A., Hopmans, J. W., and Simunek, J., "Calibration of Two-Dimensional Root Water Uptake Model." Soil Sci. Am. J., 65(4), 1027-1037, 2001a.

Vrugt, J. A., Wijk, M. T. v., Hopmans, J. W., and Simunek, J., "One, two and three-dimensional root water uptake functions for transient modelling." Water Resour. Res., 37(10), 2457-2470, 2001b.

Wallach, R. "Soil water distribution in a nonuniformly irrigated field with root extraction." J. Hydrol., 119, 137–150, 1990.

Walton, B. T. and Anderson. T. A. "Microbial degradation of trichloroethylene in the rhizosphere: Potential application to biological remediation of waste sites." Appl. and Environ. Biol., 56, 1012–1016, 1990.

Warrick, A. W., Lomen, D. O., and Fard, A. A., "Linearized moisture flow with root extraction for three dimensional, steady conditions." Soil Sci. Am. J., 44, 911-914, 1980.

Whisler, F. D., Klute, A. and Millington, R. J. "Analysis of steady state evapotranspiration from a soil column. " Soil Sci. Soc. Am. Proc., 32, 167–174, 1968.

Wise, D.L. and Trantolo, D.J. "Remediation of Hazardous Waste Contaminated Soils." Marcel Dekker, New York, 929, 1994.

WUCOLS. "A Guide to Estimating Irrigation Water Needs of Landscape Plantings in California. " Water Use Classifications of Landscape Species, University of California, 150, 2000.

Wu, J., Zhang, R. and Gui, S. "Modeling soil water movement with water uptake by roots. " Plant and Soil, 215 , 7–17, 1999.

Zeng, X., Dai, Y.J., Dickinson, R.E. and Shaikh, M. "The role of root distribution for climate simulation over land." Geophysical Research Letters, 25(24), 4533 – 4536, 1998.

Zhuang, J., Nakayama, K., Yu, G. R. and Urushisaki, T. "Estimation of root water uptake of maize an ecophysiological perspective." Field Crops Research, 69, 201 – 213, 2001.

CHAPTER THREE

THE THEORETICAL DEVELOPMENT OF THE MOISTURE TRANSFER AND WATER UPTAKE MODEL

3.1 INTRODUCTION

The theoretical basis for describing moisture flow in an unsaturated soil is presented in this chapter. To provide some context for the chosen approach, a brief overview of some of the main issues involved in selecting an appropriate theory are discussed first. This includes some comment on the main types of unsaturated soil flow and the key parameters involved. The fundamental concepts used to describe water-uptake by vegetation are also introduced. These are developed to provide the basis of the model used throughout the remainder of the thesis.

In the approach developed a sink term is included within the moisture transfer model. This term can then be used to facilitate implementation of the chosen water-uptake model. In general, a sink term can be used for one-dimensional, two-

dimensional, two-dimensional axi-symmetric and three-dimensional unsaturated flow. In this work, the model will be employed to represent water-uptake near established trees. Therefore, the theoretical development presented is cast in a two-dimensional axi-symmetric (x r) format. A standard (x z) two-dimensional form of the model can be obtained with minor manipulation of this formulation (as required later in the thesis – see chapter 8). The model can also be easily modified to represent one-dimensional conditions (see - Chapter 5).

3.2 UNSATURATED MOISTURE FLOW

Unsaturated flow is a problem of clear significance to geotechnical engineers and soil scientists. This fact is substantiated by the abundance of literature that has appeared on the subject. Some excellent, comprehensive, cover of the subject can be found elsewhere (see for example, Fredlund, 1979; Justo and Saertersdal, 1979; Schreiner, 1986; Nielsen et al, 1986; Alonso et al, 1987; Fredlund and Rahardjo, 1993). The comments provided below aim only to provide a context for the chosen modelling approach - no attempt is made at providing a full review of the subject here.

The theoretical description of moisture flow in an unsaturated soil can be a complex matter. Assumptions are often made in order to derive appropriate mathematical models that are suitable for particular applications. Ideally the resulting model should be capable of representing the all features of soil behaviour of interest but kept as simple as possible.

3.2.1 Type of Unsaturated Moisture Flow

There are generally two types of unsaturated flow behaviour (Yong, 1974). The first type of flow occurs when there is no significant corresponding change in soil fabric. This typically arises in the low or non-swelling soils. Models of this type are employed when there is little or no change in porosity or where volume change is not of interest. The other type of flow occurs in expansive soils where swelling pressures develop in confined flow or a complete change in fabric and structure occurs in unconstrained flow, i.e. a significant change in porosity occurs. In the current research, the primary interest is related to prediction of moisture content variations. Therefore, it is assumed that a non-deformable soil fabric exists. This assumption is also supported by the fact that the field problems of interest take place in low swelling soils and have been subject to cyclical behaviour over many years.

There are also two different theoretical approaches available to represent moisture flow (in a non-deformable soil). The first approach is a diffusivity based formulation with volumetric moisture content as the independent variable (Philip, 1957). The alternative approach is posed in terms of capillary potential (or pressure head) and is based on Richard's theoretical formulation (Richards, 1931). Both approaches have advantages and disadvantages.

In brief, an approach based on volumetric moisture content is attractive in terms of the immediate practical interpretation of results. It is also generally less prone to difficulties related to the non-linearity of the hydraulic properties of the soil. However, Alonso et al (1987) state that in practice Richard's formulation is preferred since an equation based on volumetric moisture content would not be of use in an analysis containing both saturated and unsaturated zones. Discontinuities in moisture

content may also arise when modelling layered soils - due to differing saturated values of volumetric moisture content at the material interfaces.

Another important aspect regarding the choice of moisture model occurs when the moisture flow analysis is to be linked with a stress analysis. In this respect, capillary potential (or soil suction) is considered to be a more appropriate stress-state variable than volumetric moisture content (Rees, 1990).

Chang and Corapcioglu (1997) claim that nearly all models for the simulation of water flow in unsaturated soils, that include root zone behaviour, use Richard's equation coupled with some model to represent water extraction by the root system. In view of this and the above factors, Richard's formulation will also be employed throughout the current research.

3.2.2 Unsaturated Soils Parameters

The unsaturated hydraulic conductivity, $K(\psi)$, and the specific moisture capacity, $C(\psi)$, are the two most significant parameters to be determined for application of Richard's equation. The unsaturated hydraulic conductivity is known to be strongly related to the moisture content of the soil. It may typically decrease by several orders of magnitude from saturated to dry conditions in a fine grained soil. The specific moisture capacity is a storage term which arises in the unsaturated flow formulation. The term is obtained directly from the slope of the capillary potential – volumetric moisture content relationship or soil-water retention curve. This relationship is non-linear and can be hysteretic.

Reliable estimates of the unsaturated hydraulic conductivity are difficult to obtain, partly because of its extensive variability in the field and partly because

measuring this parameter is time consuming and expensive (Klute, 1972; Genunchten, 1980). Various methods for the measurement of unsaturated hydraulic conductivity have been proposed. In particular, popular methods have been provided by: Childs and Collis, 1950; Millington and Quirk, 1961; Green and Corey, 1971; Gardner, 1974; Mualem, 1976 and Genunchten, 1980. More detail on these methods of measurement have already been provided by other researchers (Klute, 1972; Rees, 1990) and will not be repeated in this Chapter.

Most methods of estimating the unsaturated hydraulic conductivity make use of the corresponding soil-water retention curve - which can be more easily measured. The form of the water retention curve tends to be similar, regardless of soil type, and they are generally 'S' shaped. Some typical examples of this curve are shown in Figure 3.1. The exact shape of the water retention curve varies for different soil types and is primarily dependent on the grain size. The maximum rate of change of slope indicates the dominant void size. As grain size decreases, the water is held more strongly within the pore spaces (Yong and Warkentin, 1974).

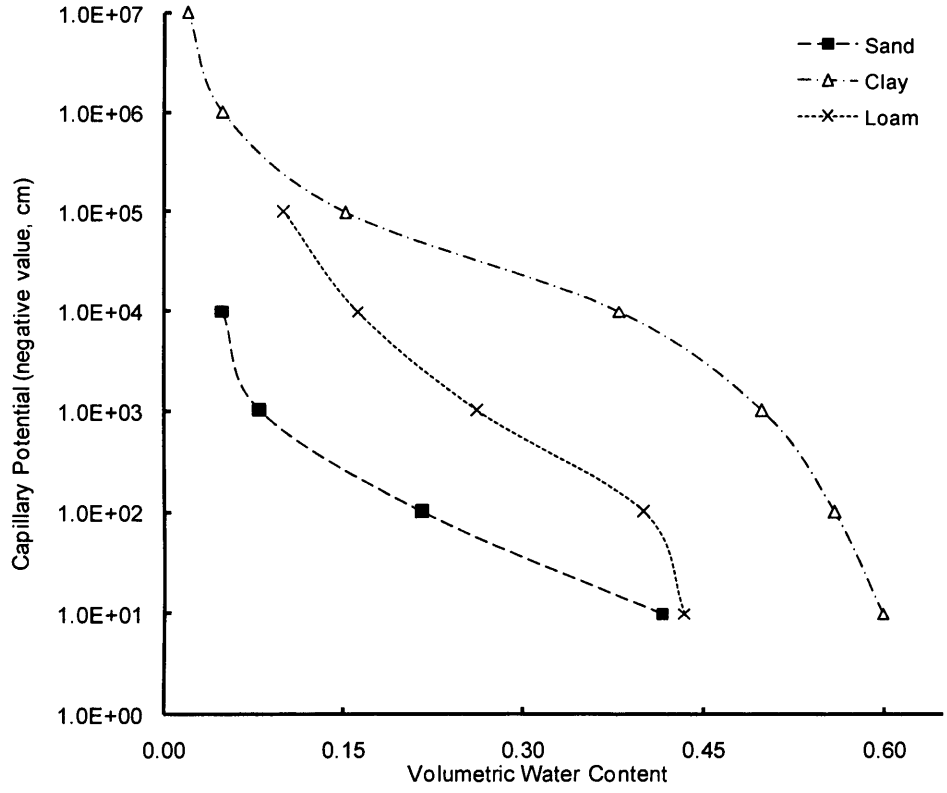

Figure 3.1 Examples of soil-water retention curve for clay, loam and sand, modified after Rees (1990)

There are a number of techniques available for measuring the soil-water retention curve (e.g. Pressure Plate, Centrifuge). Although this relationship is easier to determine than the hydraulic conductivity, the necessary laboratory work usually involves special equipment and can be time consuming and expensive. For these reasons a considerable effort has been made to develop techniques of estimating this relationship from a limited amount of data. One such method was provided by van Genunchten (1980). This method employs a relatively equation to define the soil-water retention curve and it is has been shown to be effective (Mathur and Rao, 1999;

Feddes at al, 2001; Vrugt et al, 2001; Li et al, 2006; Gong et al, 2006). For this reason this approach is also adopted in the current work.

Van Genuchten's model is derived from closed-form analytical expressions for the relative hydraulic conductivity that are substituted in the predictive conductivity model of Mualem (1976). These approaches and the parameters involved will be discussed further in Chapter 6.

3.3 MOISTURE TRANSFER IN UNSATURATED SOILS

3.3.1 Governing Differential Equation Describing Isothermal Moisture Flow

The governing differential equation describing unsaturated moisture flow may be derived from considering conservation of mass in a reference element of soil. Figure 3.2 illustrates a typical control element, in r z co-ordinates. For the axi-symmetric formulation required here, inflow and outflow are shown to occur in both the vertical (z) and radial (r) directions.

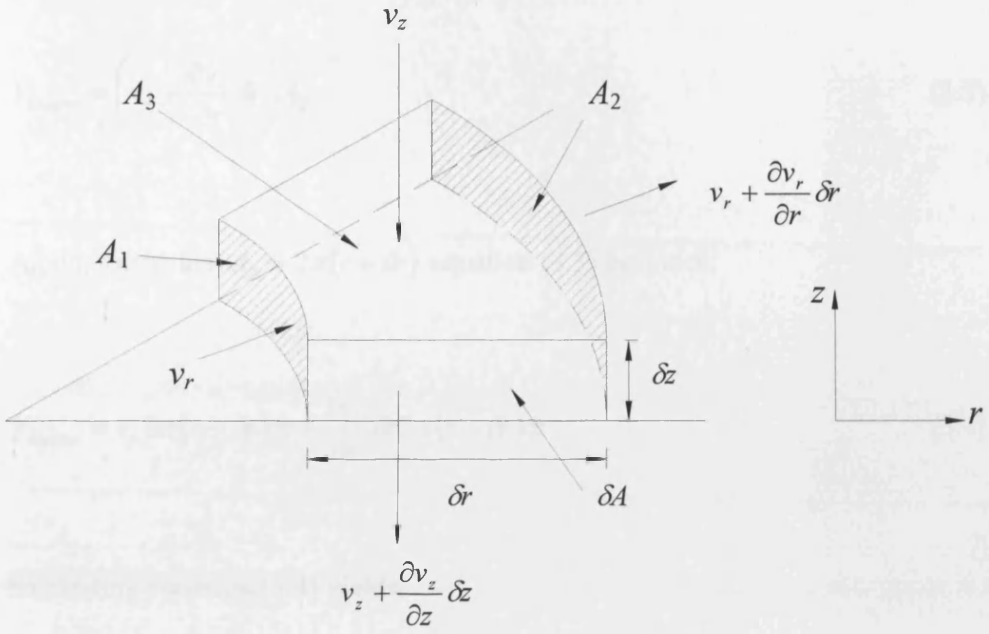

Figure 3.2 3D Flow through a typical control element

Considering first the flow of the moisture in the r direction only. The volume of water entering the system per unit time is given by:

$$V_{Input} = v_r A_1 \tag{3.1}$$

Where v_r is the velocity of water flow in the r direction and A_1 is the area over which this flow occurs. Noting that, $A_1 = 2\pi r \delta z$ equation (3.1) becomes:

$$V_{Input} = v_r 2\pi r \delta z \tag{3.2}$$

Similarly the volume of water leaving the system per unit time is given by:

$$V_{Output} = \left(v_r + \frac{\partial v_r}{\partial r} \delta r \right) A_2 \tag{3.3}$$

Again, toting that $A_2 = 2\pi(r + \delta r)$ equation (3.3) becomes:

$$V_{Output} = v_r 2\pi(r + \delta r)\delta z + \frac{\partial v_r}{\partial r} \delta r 2\pi(r + \delta r)\delta z \tag{3.4}$$

Expanding equation (3.4) yields:

$$V_{Output} = v_r 2\pi r \delta z + v_r 2\pi \delta r \delta z + \frac{\partial v_r}{\partial r} \delta r 2\pi r \delta z + \frac{\partial v_r}{\partial r} \delta r 2\pi \delta r \delta z \tag{3.5}$$

Letting $\delta A = \delta r \delta z$ and substituting into equation (3.5) gives:

$$V_{Output} = v_r 2\pi r \delta z + v_r 2\pi \delta A + \frac{\partial v_r}{\partial r} 2\pi r \delta A + \frac{\partial v_r}{\partial r} 2\pi \delta r^2 \delta z \tag{3.6}$$

The fourth term is relatively small and is therefore eliminated from further consideration. The change in the volume of water stored in the control element is therefore given by difference between inflow and outflow i.e.

$$V_{input} - V_{Output} = v_r 2\pi \delta A + \frac{\partial v_r}{\partial r} 2\pi r \delta A \tag{3.7}$$

The net excess flow in r direction can be equated to the change in the volume of water, V_w in the control element per unit time, t thus:

$$\frac{\partial V_w}{\partial t} = v_r 2\pi\delta A + \frac{\partial v_r}{\partial r} 2\pi r \delta A \tag{3.8}$$

Next considering flow in the z direction. Using a similar approach as above the net outflow in z direction can be written as:

$$\frac{\partial V_w}{\partial t} = \frac{\partial v_z}{\partial z} 2\pi r \delta A \tag{3.9}$$

Now, combining flow from both the r and z directions yields:

$$\frac{\partial V_w}{\partial t} = v_r 2\pi\delta A + \frac{\partial v_r}{\partial r} 2\pi r \delta A + \frac{\partial v_z}{\partial z} 2\pi r \delta A \tag{3.10}$$

Multiplying through by r gives

$$r\frac{\partial V_w}{\partial t} = r v_r 2\pi\delta A + r\frac{\partial v_r}{\partial r} 2\pi r \delta A + r\frac{\partial v_z}{\partial z} 2\pi r \delta A \tag{3.11}$$

Noting from figure 3.2, that the total volume of the element, $V_T = 2\pi r \delta A$ and substituting this into equation (3.11) yields:

$$r\frac{\partial V_w}{\partial t} = v_r V_T + r\frac{\partial v_r}{\partial r}V_T + r\frac{\partial v_z}{\partial z}V_T \tag{3.12}$$

Re-arranging equation (3.12) gives:

$$\frac{1}{V_T}\frac{\partial V_w}{\partial t} = \frac{1}{r}\left(v_r + r\frac{\partial v_r}{\partial r} + r\frac{\partial v_z}{\partial z}\right) \tag{3.13}$$

For constant V_T and volumetric moisture content, $\theta = \partial V_w / V_T$, equation (3.13) may be abbreviated to:

$$\frac{\partial \theta}{\partial t} = \frac{v_r}{r} + \frac{\partial v_r}{\partial r} + \frac{\partial v_z}{\partial z} \tag{3.14}$$

Equation (3.14) is the fundamental governing differential equation describing flow of moisture through an axi-symmetric domain. The equation represents flow under isothermal conditions in non-deformable unsaturated soil. This equation can be further developed by introducing an expression for flow velocity such as Darcy's Law as presented in section 3.2.2 below.

3.3.2 The application of Darcy's Law

In order to develop equation 3.14 to a form that can be applied in practice, a relationship between flow and the appropriate driving force or potential for moisture flow must be established. In practice, Darcy's Law is commonly used to give an average flow velocity through a given cross section of porous medium.

For saturated flow, Darcy's linear flow law provides the following expression for flow velocity,

$$v = -K\nabla i \tag{3.15}$$

Where K is the hydraulic conductivity and i is the hydraulic gradient. The negative sign indicates that flow takes place in the direction of decreasing total head or potential.

In the analysis of saturated flow, K may be reasonably assumed to be constant at the saturated value. However, the finite magnitude of the hydraulic conductivity is known to be dependent on the density and viscosity of the soil water, the turbulence of flow, the porosity of the soil, the shape and arrangement of soil particles and in the case of fine grained soils the thickness of adsorbed layers (Rees, 1990).

For the unsaturated flow, in general, Darcy's Law is valid under the following conditions (Swatzendruber, 1968);

i. That a relatively large sample is used, defined such that its size is at least a few hundred grains in width.

ii. That flow is slow, with an inter-grain Reynolds number of less than unity.

These conditions are generally met for liquid flow due to typical soil water potential gradients.

When applying Darcy's Law to unsaturated flow, the driving force or hydraulic gradient is referred to as the 'total potential' for moisture flow. Soil water may possess kinetic and potential energy, as may any other physical body. However, the kinetic energy is proportional to the square of the velocity and for the case of movement of water through soils, the velocity of flow is usually small enough for the kinetic energy to be assumed negligible.

Total potential may be viewed as the sum of various component potentials. Component potentials that could contribute to the overall driving force for moisture transfer are pressure potential, gravitational potential, osmotic potential and pneumatic potential (Yong and Warkentin, 1974). Osmotic potential is of particular relevance when chemical (e.g. salt) gradients exist and pneumatic potential relates to gas pressure variations. Neither of these contributions were considered to be relevant to the problems in hand, therefore, in this research work the total potential components that are included are pressure potential and gravitational potential only.

Pressure potential is in many cases the most significant of the component potentials listed above. In a saturated soil, the hydrostatic pressure is greater than the atmospheric pressure, here the pressure potential is positive (taking atmospheric pressure as the reference pressure) and water would tend to flow out of the soil into an adjacent free water body.

In contrast, when considering unsaturated soil behaviour, water is attracted to the soil particles by capillary and adsorptive forces. In this case, the potential energy of the system is below that of the reference state creating a negative pressure potential. Here the soil would tend to take in water should it be brought in contact with a free water body. This process is analogous to the way a domestic bathroom sponge takes in bath water or to the way in which blotting paper takes in ink.

The term capillary potential is used in the current work to represent the combined action of adsorption and capillarity. Capillary potential is taken to have the same meaning as negative pressure potential. It can be directly converted to an equivalent negative pore water pressure or soil suction (a positive quantity). In a saturated soil the capillary potential is zero. In a dry clay soil the capillary potential may be up to from -15,000 cm to -20,000 cm (Feddes et al, 1976).

A further component of total potential considered in the current work is the contribution arising from gravitational effects. The inclusion of gravitational potential is important if correct equilibrium moisture content distributions are to be achieved. Gravitational potential may be defined as the work required transferring water from a reference elevation to the soil elevation.

Furthermore, in the analysis of unsaturated flow the dependency of the soil's hydraulic conductivity on the degree of saturation is known to be significant and

should be taken into account. Therefore, defining Darcy's Law for use in the analysis of unsaturated soil yields,

$$v = -K(\phi)\nabla\phi \tag{3.16}$$

Where $K(\phi)$ is the unsaturated hydraulic conductivity and ϕ is the total potential for moisture flow. $K(\phi)$ is written here in this manner to indicate a general dependence of K on total potential.

3.3.3 Capillary Hysteresis

Fundamental to the analysis of flow in partially saturated soils is the relationship between capillary potential and moisture content (i.e. the water retention curve). The specific moisture capacity is obtained directly from the slope of the capillary potential-moisture content relationship for the soil under investigation. However, this relationship is known to be both non-linear and hysteretic.

Hysteresis is apparent in the form of differing wetting and drying curves in capillary potential-moisture content plots. For an initially saturated soil being progressively dried by increasing the capillary potential, the moisture content at any particular capillary potential will generally be higher than that occurring at the same capillary potential for a soil, which is being wetted from an initially unsaturated state.

Kirkham and Powers (1972) clearly illustrated this phenomenon as shown in Figure 3.3 along with corresponding diagrammatic representation of the distribution of soil water in the pore spaces. The failure of the wetting curve to reach the same

value of moisture content at zero capillary potential is sometimes attributed to entrapped air. However, some further concepts are worthy of mention in presenting a general explanation of hysteresis behaviour.

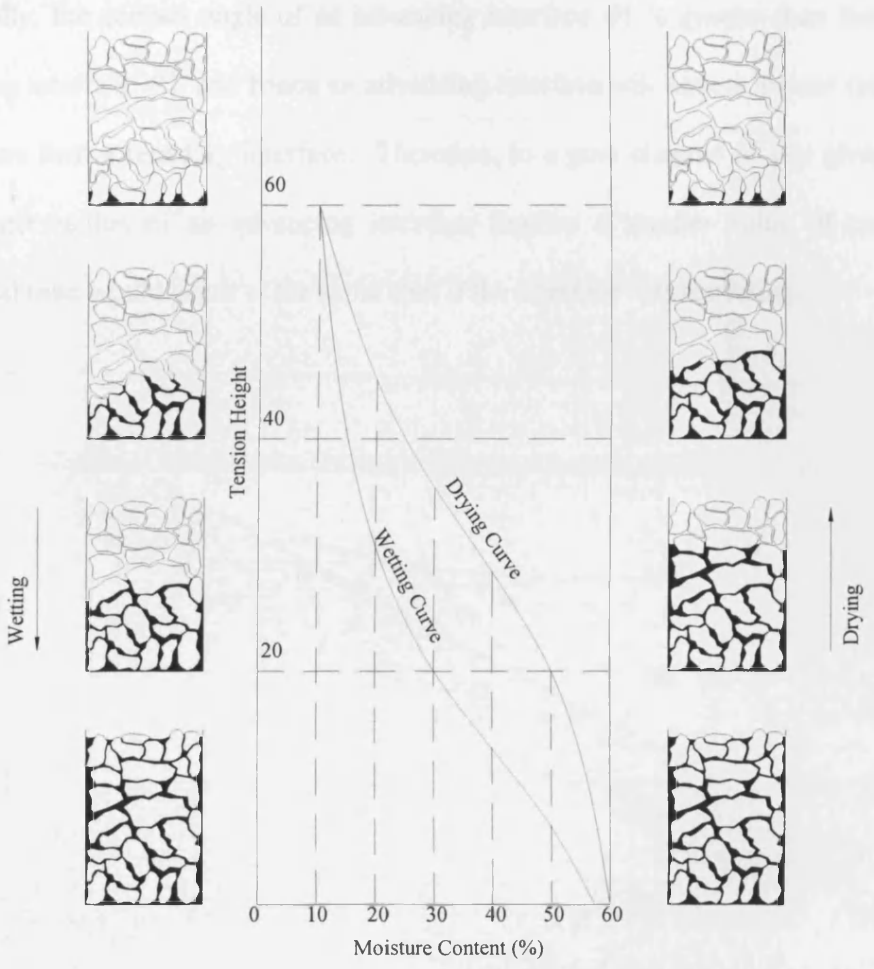

Figure 3.3 Hysteresis effects on moisture retention, modified after Kirkham and Powers (1972)

One concept is known as the 'raindrop effect' which is the term used to describe how an advancing interface has a contact angle that is different to that of a

receding interface between the same two fluids (Bear, 1979). Figure 3.4 shows the effect as a 'raindrop' of water advancing down-slope in an air atmosphere. This phenomenon applies wherever there is an advancing or retreating interface between a wetting and a non-wetting phase, including when such advance is horizontal. Generally, the contact angle of an advancing interface $\theta 1$ is greater than that for a receding interface $\theta 2$ and hence an advancing interface will have a greater radius of curvature than a receding interface. Therefore, in a pore channel of any given size, the larger radius of an advancing interface implies a smaller value of capillary potential than would occur at the same spot if the interface was retreating.

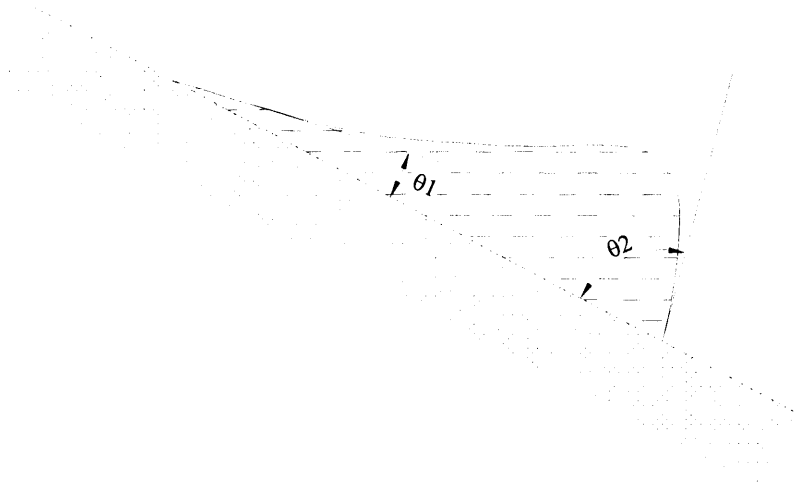

Figure 3.4 Raindrop Effect, modified after Bear (1972)

A further common concept used by Yong and Warkentin (1974) to explain hysteresis in coarse grained soils is the 'ink bottle effect'. This concept suggests that, as in Figure 3.5, for a case where moisture is being extracted from initially full pore

space with a narrow constriction near its top edge, an air pressure, P2 dictated by the smallest pore radius will be required to empty the pore space. Conversely to refill the same pore space, water will not enter the space until a much lower air pressure, P1 is achieved dictated by the largest pore radius.

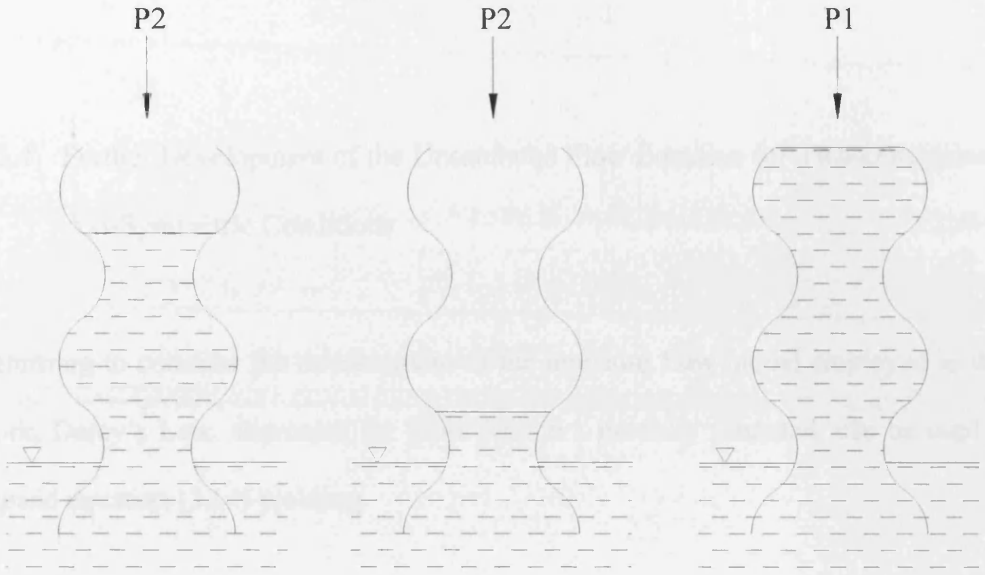

Figure 3.5 A conceptual illustration of the ink bottle effect, modified after Yong and Warkentin (1974)

For the clay soils, hysteresis may be related to some further concepts (Yong and Warkentin, 1974). For example, if initially a clay mass consists of plate particles which are not parallel, the interstices between them will be larger than in an array of parallel plates and the potential energy will be higher. A subsequent increase of capillary potential may not only draw the plates closer together but may also reorientate them into more nearly parallel positions of lower potential energy. A relaxation of capillary potential on rewetting will allow the plates to separate but will

not necessarily cause them to return to their original alignments, so that less water is absorbed than was lost during drying.

In the current work, the soil conditions under consideration include seasonal cycles of drying and wetting. Therefore an attempt is made to assess the significance of hysteresis in these circumstances – this is explained further in Chapter 7.

3.3.4 Further Development of the Unsaturated Flow Equation for Two-Dimensional Axi-Symmetric Conditions

Returning to consider the development of the moisture flow model employed in this work, Darcy's Law, expressed for fluid flow in a partially saturated, can be used to expand equation (3.14) yielding:

$$\frac{\partial \theta}{\partial t} = K_r(\phi)\frac{1}{r}\left(\frac{\partial \phi}{\partial r}\right) + K_r(\phi)\frac{\partial}{\partial r}\left(\frac{\partial \phi}{\partial r}\right) + K_z(\phi)\frac{\partial}{\partial z}\left(\frac{\partial \phi}{\partial z}\right) \qquad (3.17)$$

As discussed above, the total potential for moisture flow is taken as the sum of the pressure or capillary potential and gravitational potential i.e.

$$\phi = \psi + z \qquad (3.18)$$

Therefore, substituting equation (3.18) into equation (3.17) gives:

$$\frac{\partial \theta}{\partial t} = K_r(\psi)\frac{1}{r}\left(\frac{\partial(\psi + z)}{\partial r}\right) + K_r(\psi)\frac{\partial}{\partial r}\left(\frac{\partial(\psi + z)}{\partial r}\right) + K_z(\psi)\frac{\partial}{\partial z}\left(\frac{\partial(\psi + z)}{\partial z}\right) \qquad (3.19)$$

But $\partial z/\partial r = 0$, therefore equation (3.19) becomes:

$$\frac{\partial \theta}{\partial t} = K_r(\psi)\frac{1}{r}\left(\frac{\partial(\psi)}{\partial r}\right) + K_r(\psi)\frac{\partial}{\partial r}\left(\frac{\partial(\psi)}{\partial r}\right) + K_z(\psi)\frac{\partial}{\partial z}\left(\frac{\partial(\psi)}{\partial z}\right) + \frac{\partial K_z(\psi)}{\partial z} \qquad (3.20)$$

As a solution is sought for the variation of capillary potential with time, the unsaturated hydraulic conductivity is known to be dependent on capillary potential. Assuming further that the soil is isotropic and restating the left hand side of equation (3.20) in terms of capillary potential yields,

$$\frac{\partial \theta}{\partial \psi}\frac{\partial \psi}{\partial t} = \frac{\partial}{\partial r}\left[K(\psi)\frac{\partial \psi}{\partial r}\right] + \frac{\partial}{\partial z}\left[K(\psi)\frac{\partial \psi}{\partial z}\right] + \frac{\partial K(\psi)}{\partial z} + \frac{1}{r}K(\psi)\frac{\partial \psi}{\partial r} \qquad (3.21)$$

The term $\partial\theta/\partial\psi$ is called the specific moisture capacity of the soil and is denoted as $C(\psi)$ (Carslaw and Jaeger, 1959)

$$C(\psi)\frac{\partial \psi}{\partial t} = \frac{\partial}{\partial r}\left[K(\psi)\frac{\partial \psi}{\partial r}\right] + \frac{\partial}{\partial z}\left[K(\psi)\frac{\partial \psi}{\partial z}\right] + \frac{\partial K(\psi)}{\partial z} + \frac{1}{r}K(\psi)\frac{\partial \psi}{\partial r} \qquad (3.22)$$

Equation (3.22) is referred to as two-dimensional axi-symmetric Richard's equation (Richards, 1931).

3.4 THE WATER-UPTAKE MODEL

As discussed in Chapter 2, the current work will be based on the development of a macroscopic model. In this approach, a pre-defined root-zone is assumed to be active. Within this zone moisture will be extracted at a rate determined by root density, transpiration demands amongst other factors. This type of behaviour can be conveniently representing by the use of a volumetric sink term included in the unsaturated flow equation. This term can simply be included into equation (3.22) to yield:

$$C(\psi)\frac{\partial \psi}{\partial t} = \frac{\partial}{\partial r}\left[K(\psi)\frac{\partial \psi}{\partial r}\right] + \frac{\partial}{\partial z}\left[K(\psi)\frac{\partial \psi}{\partial z}\right] + \frac{\partial K(\psi)}{\partial z} + \frac{1}{r}K(\psi)\frac{\partial \psi}{\partial r} - S \qquad (3.23)$$

The sink term, S, is expressed as the volume of water per unit volume of soil per unit time (cm^3 water. cm^{-3} soil. sec^{-1}).

However, in order to be able to make use of equation (3.23) to simulate water uptake by roots, this sink term has to be defined in a manner that will adequately reflect the water extraction process throughout the root-zone. A considerable research effort (see Chapter 2) has taken place regard the development of such methods. Before developing a model applicable to 2D axi-symmetric conditions, it is useful to first consider the approach applied to the simpler 1D condition. This is presented below.

3.4.1 One-Dimensional Water Uptake Model

The simplest form of water uptake model assumes a linear variation in water extraction with depth. This is represented in Figure 3.6.

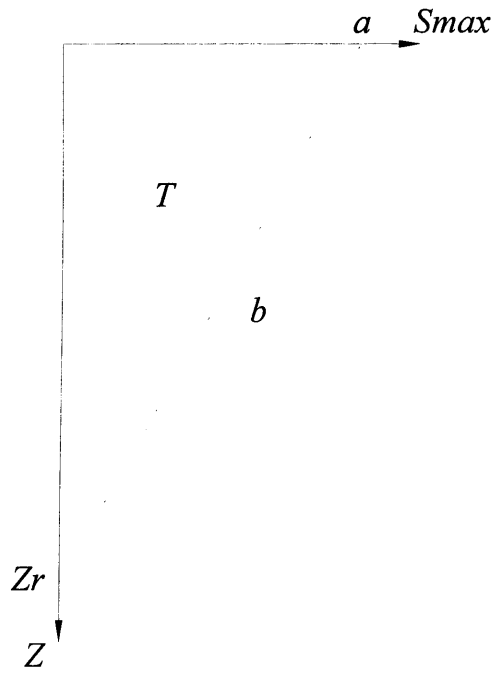

Figure 3.6 Linear variation of extraction rate

It is assumed that for potential transpiration conditions, S_{max} is given by,

$$S_{\max} = a_j - b_j z \tag{3.24}$$

Where S_{max} is the extraction rate, a_j and $-b_j$ are the intercept and slope on the jth day, respectively and z is the rooting depth, z_{rj} is the maximum depth of the root zone. The boundary condition at the bottom of the root zone ($z = z_{rj}$) is $S_{max} = 0$, therefore:

$$a_j - b_j z_{rj} = 0 \tag{3.25}$$

The total transpiration, T_j, across the root zone is then obtained by integrating over the active depth i.e.

$$T_j = \int_0^{z_{rj}} S_{\max} \partial z \tag{3.26}$$

Combining equation (3.24) and (3.26) gives,

$$T_j = \int_0^{z_{rj}} (a_j - b_j z) \partial z \tag{3.27}$$

Integrating Equation (3.27), yields

$$T_j = a_j z_{rj} - \frac{b_j z_{rj}^2}{2} \tag{3.28}$$

At the bottom of root zone equation (3.25) gives:

$$a_j = b_j z_{rj} \tag{3.29}$$

Substituting equation (3.29) into equation (3.28) yields:

$$b_j = \frac{2T_j}{z_{rj}^2} \tag{3.30}$$

Substituting equation (3.30) into equation (3.29) then gives:

$$a_j = \frac{2T_j}{z_{rj}} \tag{3.31}$$

Combining equations (3.24), (3.30) and (3.31) yields:

$$S_{\max} = \frac{2T_j}{z_{rj}} - \frac{2T_j}{z_{rj}^2} z \tag{3.32}$$

This can be re-arranged as:

$$S_{\max} = \frac{2T_j}{z_{rj}} \left(1 - \frac{z}{z_{rj}} \right) \tag{3.33}$$

Equation (3.33) is valid only under optimal soil moisture levels. When the moisture content is low, actual transpiration is lower than the potential value. A model proposed by Feddes et al. (1978) describes the sink term for actual transpiration is as follows:

$$S(\psi) = \alpha(\psi) S_{\max} \tag{3.34}$$

Where $\alpha(\psi)$ (dimensionless) is a prescribed function of the capillary potential referred to as a water-stress function (Figure 3.7). The root water uptake is zero

above the anaerobiosis point, h_1 as well as below the wilting point, h_4 and is constant at its maximum value between h_1 and h_2. A linear variation of $\alpha(\psi)$ with ψ is assumed when the latter is less than h_1 or greater than h_2.

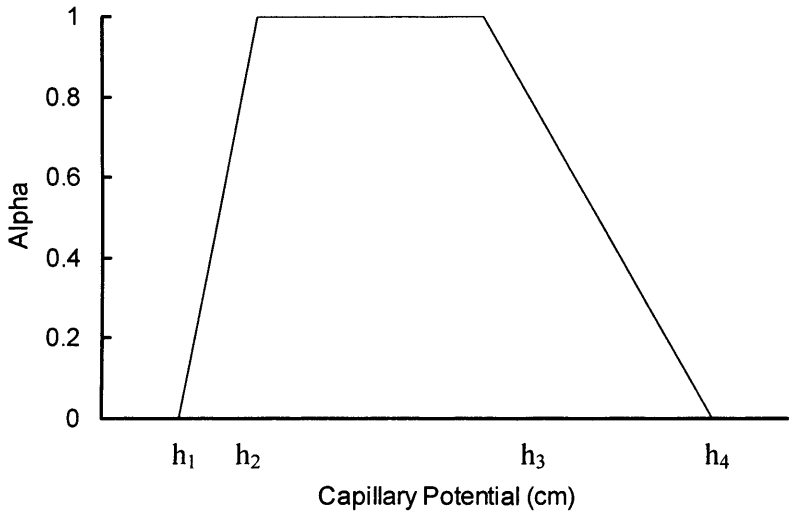

Figure 3.7 General shape of the alpha as a function of the absolute value of the capillary potential, modified after Feddes et al (1978)

For conditions drier than wilting point and wetter than a certain anaerobiosis point, it may be assumed that the water uptake by the roots is zero. It is known that there exists no single wilting point because it varies from -10000 cm to -20000 cm, but for many practical purposes a mean value of about -15000 cm can be regarded as a reasonable estimate (Feddes et al., 1976).

Feddes et al also made two assumptions; i) that no water uptake by the roots take place above anaerobiosis point with a pressure head of -50 cm, and ii) a linear variation of water uptake with ψ is assumed when the pressure head is less than -50 cm. From a review of moisture requirements and the effects of pressure head on yield and quality of various vegetable crops, Feddes et al. (1976) concluded that in general

for these crops the pressure head at which soil water begins to limit plant growth is about -400 cm. Therefore the water uptake by roots is constant and at a maximum rate for -400 cm (h_2) < ψ < -50 cm (h_1). The water uptake for the plant, is assumed to decrease linearly between h_3 = -400 cm and h_4 = -15000 cm. Therefore, when soil moisture is limiting, equation (3.33) becomes:

$$S(\psi, z) = \frac{2T_j}{z_{rj}} \alpha(\psi) \left(1 - \frac{z}{z_{rj}} \right) \tag{3.35}$$

Prasad (1988) first introduced this model to represent one-dimensional water uptake by plant roots. An example hand-calculation to show how this model is applied in practice is shown in Appendix 1. This model provides the basis for the two-dimensional axi-symmetric water uptake model developed in section 3.4.3 below.

3.4.2 Development of Two-Dimensional Axi-Symmetric Water Uptake Equation

Prior to presenting the extension of Prasad's approach, a similar logic is applied here to develop a procedure that is applicable two dimensional axi-symmetric problems. Cutler and Richardson (1989) studied the relationship between root spread and the height of trees. They suggest that root spread for a single tree is approximately similar for both depth and radius. Biddle (1998) measured the water uptake for a range of different trees in the UK. This work shows the moisture migration in the vicinity of trees and clearly shows that as the radial distance from the

trunk of the tree increases, the water extracted by the roots decreases. In view of this work, the follow assumptions have been made here:

i. Root water extraction is maximum directly beneath the tree.
ii. A linear relationship between root water extraction and radial distance is assumed.
iii. Root water extraction becomes zero at some maximum radius.

The relationship between root water extraction and radial distance is then introduced via a simple linear grading of the total transpiration radially over the active root zone. Using similar logic to that employed by Prasad (1998), it is assumed that the distribution of potential transpiration in radial direction, T_j is given by,

$$T_j = c_j - d_j r \tag{3.36}$$

Where c_j and $-d_j$ are the intercept and slope on the jth day, respectively and r is the rooting radial distance. At the end of the root zone (i.e. at $r = r_{rj}$) the boundary condition is $T_j = 0$ and therefore:

$$c_j - d_j r_{rj} = 0 \tag{3.37}$$

The total transpiration, T, across the root zone is then obtained by integrating over the active depth i.e.

$$T = \int_0^{r_{rj}} T_j \partial r \tag{3.38}$$

Combining equation (3.36) and (3.38) gives:

$$T = \int_0^{r_{rj}} (c_j - d_j r) \partial r \tag{3.39}$$

Integrating Equation (3.39) yields:

$$T = c_j r_{rj} - \frac{d_j r_{rj}^2}{2} \tag{3.40}$$

At the end of root zone:

$$c_j = d_j r_{rj} \tag{3.41}$$

Substituting equation (3.41) into equation (3.40), yields

$$d_j = \frac{2T}{r_{rj}^2} \tag{3.42}$$

Substituting equation (3.42) into equation (3.41), then gives

$$c_j = \frac{2T}{r_{rj}} \tag{3.43}$$

Combining equations (3.36), (3.42) and (3.43) gives:

$$T_j = \frac{2T}{r_{rj}} - \frac{2T}{r_{rj}^2} r \tag{3.44}$$

This can be re-arranged as:

$$T_j = \frac{2T}{r_{rj}} \left(1 - \frac{r}{r_{rj}} \right) \tag{3.45}$$

Equation (3.45) is the distribution of transpiration in radial direction across the root zone. The equation for water uptake for two-dimensional axi-symmetry can produce by substituting equation (3.45) into equation (3.35) to gives:

$$S(\psi, z, r) = \frac{4T}{z_{rj} r_{rj}} \alpha(\psi) \left(1 - \frac{z}{z_{rj}} \right) \left(1 - \frac{r}{r_{rj}} \right) \tag{3.46}$$

In the first instance, this model will be applied to simulate water-uptake near established trees. Therefore under these circumstances, it is assumed that the root growth is not important. Thus dropping the subscript j for root growth, equation (3.46) then becomes:

$$S(\psi,z,r)=\frac{4T}{z_r r_r}\alpha(\psi)\left(1-\frac{z}{z_r}\right)\left(1-\frac{r}{r_r}\right) \tag{3.47}$$

This equation permits a simple linear distribution of the total transpiration (T) with both depth and radial distance from the tree. This equation (3.47) can also be re-cast and applied to a standard two-dimensional (x-z) domain - this is shown in Chapter 8. For clarity, hand-calculations illustrating the application of equation (3.47) for some simple examples are shown in Appendix 2 and Appendix 3 respectively.

The actual transpiration from a single tree, linearly over a root zone can be simplified as;

$$T=\int_0^{z_r}\int_0^{r_r}S(\psi,z,r)\partial r\partial z \tag{3.48}$$

Equation (3.45) is applied in a similar manner to equation (3.35) to evaluate the proportion of T_j extracted with depth. The distribution of the total transpiration from a single tree, linearly over a maximum radial root spread (r_r) is clearly a first approximation. The performance of this model is explored in Chapter 6.

Equation (3.47) defines a sink term that can be implemented in equation (3.23) giving;

$$\begin{aligned}C(\psi)\frac{\partial\psi}{\partial t}&=\frac{\partial}{\partial r}\left[K(\psi)\frac{\partial\psi}{\partial r}\right]+\frac{\partial}{\partial z}\left[K(\psi)\frac{\partial\psi}{\partial z}\right]+\frac{\partial K(\psi)}{\partial z}\\&+\frac{1}{r}K(\psi)\frac{\partial\psi}{\partial r}-S(\psi,r,z)\end{aligned} \tag{3.49}$$

Equation (3.49) therefore describes two-dimensional axi-symmetric moisture transfer in an unsaturated. Evaluation of the sink term via application of equation (3.47) provides a mechanism for distributing the extracted value of water over the root zone which is explained in Chapter 4.

3.5 CONCLUSIONS

The theoretical basis for describing moisture flow in an unsaturated soil is presented in this chapter. Some general aspects of the behaviour of unsaturated soils were discussed in the first section of the chapter. Included were brief descriptions of the types of unsaturated moisture flow and introduction of the key hydraulic properties. A brief explanation of the hysteresis phenomenon has also been presented. This feature of behaviour is most prominent in the water retention curves of soils subject to wetting and drying.

The governing differential equation for moisture flow has been derived. the chosen approach is based on Richards equation. In this work, a sink term has been added to Richard's equation to facilitate inclusion of a water uptake model. Since the primary application for the model will be simulation of water uptake near mature trees, the model was presented in a 2D axi-symmetric format. The application of Darcy's Law to unsaturated flow and various components of total potentials also have been presented.

The theoretical development of a water-uptake model has been presented. The model can be applied to two-dimensional axi-symmetric problems and can easily be reduced to operate in 1D mode. The relationship between root-water extraction and

radial distance is introduced via a simple linear grading of the total transpiration over the active root zone. The resulting sink term equation permits a simple linear distribution of the total transpiration with both depth and radial distance from the tree. This new model will be employed for a range of the finite element simulations which are presented later chapters of the thesis.

3.6 REFERENCES

Alonso, E. E., Gens, A. and Hight, D. W. "Special problem soils." Ninth European Conf. on Soil Mechanics and Foundation Engineering: 1087-1146, 1987.

Bear, J . " Hydraulics of Groundwater. " McGraw-Hill, London, 1979.

Biddle, P. G., "Tree Root Damage to Buildings." Willowmead Publishing Ltd, Wantage, 1998.

Carslaw, H. S. and Jaeger, J. C. "Conduction of Heat in Solids. " Oxford University Press, Oxford, 1959.

Chang, Y. Y. and Corapcioglu, M. Y. "Effect of Roots on Water Flow in Unsaturated Soils. " Journal of Irrigation and Drainage Engineering, 202 – 209, 1997.

Chids, E.C. and Collis, G. N. "The Permeability of porous Materials." Proc. Roy. Soc., London, 201, 392 – 405, 1950.

Cutler, D. F., and Richardson, I. B. K., "Tree roots and buildings.", Longman Scientific and Technical, Singapore, 1989.

Feddes, R. A., Kowalik, P. J., Malink, K. K., and Zaradny, H., "Simulation of field water uptake by plants using a soil water dependent root extraction function." J. Hydro, 31, 13 – 26, 1976.

Feddes, R. A., Kowalik, P. J., and Zaradny, H., "Simulation of field water use and crop yield." Wageningen Center for Agriculture and Documentation, Wageningen, 189, 1978.

Feddes, R. A., Hoff, H., Bruen, M., Dawson, T., Rosnay, P., Dirmeyer, P., Jackson, R. B., Kabat, P., Kleidon, A., Lilly, A. and Pitmank, A. J. "Modeling Root Water Uptake in Hydrological and Climate Models." American Meteorological Society, 82(12), 2797 – 2809, 2001.

Fredlund, D. G. "Appropriate concepts and technology for unsaturated soils." Can. Geotech. J., 16, 121 – 139, 1979.

Fredlund, D. G. and Rahardjo, H., "Soil Mechanics of Unsaturated Soils." John Wiley & Sons: New York, 1993.

Gardner, W. R. "The Permeability Problem." Soil Sci. J., 117(5), 243 – 249, 1974.

Genuchten, M. T. V. "A closed form equation for predicting the hydraulic conductivity of unsaturated soils." Soil Sci. Am. J., 44, 892 – 898, 1980.

Gong, D., Kang, S., Zhang, L., Du, T. and Yao, L. "A two-dimensional model of root water uptake for single apple trees and its verification with sap flow and soil water content measurements. " Agricultural Water Management, 83, 119 – 129, 2006.

Green, R. E. and Corey, J. C. "Calculation of Hydraulic Conductivity: A further Evaluation of Some Predictive Methods. " Soil Sci. Soc. Am. J., 35, 3 – 8, 1971.

Justo, J. L. and Saertersdal R. "Design parameters for special soil conditions." General Report, Proc. 7th Eor. Conf. SMFE 4, 181 – 208, 1979.

Kirkham, D., and Powers, W. L. "Advanced Soil Physics." Wiley Interscience, New York, 1972.

Klute, A. "The determination of the hydraulic conductivity and diffusivity of unsaturated soils." Soil Sci. J. 113 (4), 264 – 276, 1972.

Li, K. Y., Jong, R. D., Coe, M. T. and Ramankutty, N. "Root-Water-Uptake Based upon a New Water Stress Reduction and an Asymptotic Root Distribution Function. " Earth Interactions, 10(14), 1 – 22, 2006.

Mathur, S. and Rao, S. "Modelling water uptake by plant roots." Journal of Irrigation and Drainage Engineering, 125(3), 159 – 165, 1999.

Millington, R. J. and Quirk, J. P. "Permeability of Porous Solids." Trans. Faraday Soc., 57, 1200 – 1207, 1961.

Mualem, Y. "A new model for predicting the hydraulic conductivity of unsaturated porous media." Water Resour. Res., 12, 513 – 522, 1976.

Nielsen, D. R., Genuchten, M. T. V. and Biggar, J. W. "Water flow and solute transport processes in the unsaturated zone." Water Resour. Res., 22(9), 89 – 108, 1986.

Philip, J. R., "The theory of infiltration: 1. The infiltration equation and its solution ." Soil Sci., 83, 345 - 357, 1957.

Prasad, R., "A linear root water uptake model." J. Hydrology, 99, 297 – 306, 1988.

Rees, S. W., "Seasonal Ground Movement Effects on Buried Services," PhD, University of Wales, Cardiff, 1990.

Richards, L. A., "Capillary conduction of liquids in porous media." Physics, 1, 318 – 333, 1931.

Schreiner, H. D. "State of the art review of expansive soils for TRRL." Imperial College, London, 1986.

Swatzendruber, D. "The applicability of Dracy's Law." Proc. SSSA, 32, 11 – 18, 1968.

Vrugt, J. A., Hopmans, J. W., and Simunek, J., "Calibration of Two-Dimensional Root Water Uptake Model." Soil Sci. Am. J., 65(4), 1027-1037, 2001.

Yong, R. N., and Warkentin, B. P. "Soil properties and behaviour." Elsevier Publishing Company, Amsterdam, 1974.

CHAPTER FOUR

THE NUMERICAL SOLUTION OF THE MOISTURE TRANSFER MODEL

4.1 INTRODUCTION

An approximate numerical solution of the theoretical model presented in Chapter 3 is now developed. The problem addressed is one in which both spatial and time variations of the unknown variable, capillary potential in this case, are required. The numerical solution is achieved by discretising the two-dimensional axi-symmetric space domain and the time domain.

Spatial discretisation of the governing partial differential equation is achieved by an application of the finite element method. In particular the Galerkin weighted residual approach is adopted. However, a full explanation of the finite element method is not presented here. Such an explanation is beyond the scope of the current

work. Nevertheless, for the clarity of presentation, an introduction to the concepts relevant to the particular finite element formulation adopted is provided.

Discretisation of the time domain is achieved by the application of a finite difference time marching algorithm. A fully implicit mid-interval backward difference algorithm is employed to this end. The technique required to achieve a solution is described along with the chosen convergence criterion.

4.2 SPATIAL DISCRETISATION

4.2.1 Finite Element Concepts

There are many practical engineering problems such as heat conduction, distribution of electrical potential, and water flow in soil that give rise to systems of ordinary or partial differential equations. The mathematical models derived thereof require solution. Often only simple forms of the governing equations with geometrically simple boundaries can be solved exactly by available mathematical methods. With the advent of the digital computer, however, the solution of multiple sets of simultaneous equations is no longer a deterrent. Therefore, methods of obtaining solutions of problems cast in an algebraic form were developed.

Discretisation of the continuum problem is usually necessary and to achieve this end some form of approximation is normally introduced. The particular form of discretisation of the space domain adopted here is known as a trial function approximation. The process of approximating a given function by using trial functions provides a useful introduction to the finite element approach (Rockey et al,

1983). Zienkiewicz and Taylor (1989) clearly illustrate approximation by trial functions and provide the following description.

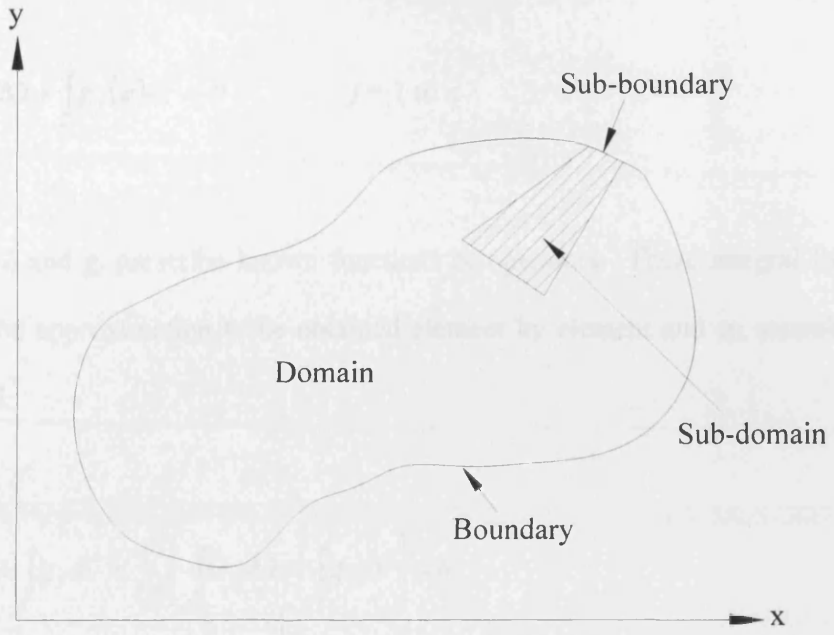

Figure 4.1 Problem domain Ω and boundary Γ, modified after Zienkiewicz and Taylor (1989)

A given function u in some region Ω bounded by closed curve Γ is to be approximated as shown in Figure 4.1. All functions u in Ω may be approximated by:

$$\boldsymbol{u} \approx \hat{\boldsymbol{u}} = \sum_{i=1}^{n} \boldsymbol{N}_i \boldsymbol{a}_i = \boldsymbol{N}\boldsymbol{a} \tag{4.1}$$

Where $\boldsymbol{N}_i$ are shape functions prescribed in terms of independent variables (such as coordinates x, y, etc), $\hat{\boldsymbol{u}}$ are the approximation to the function $\boldsymbol{u}$, i is a point associated

with that element, n is the maximum number of points associated with that element and $\boldsymbol{a}_i$ mostly are unknown. This equation can then be cast in an integral form from which the unknown parameters $\boldsymbol{a}_i$ are to be obtained.

$$\int_{\Omega} \boldsymbol{G}_j(\hat{\boldsymbol{u}})d\Omega + \int_{\Gamma} \boldsymbol{g}_j(\hat{\boldsymbol{u}})d\Gamma = \boldsymbol{0} \qquad j = 1 \text{ to } n \tag{4.2}$$

Which $\boldsymbol{G}_j$ and $\boldsymbol{g}_j$ prescribe known functions or operators. These integral forms will permit the approximation to be obtained element by element and an assembly to be achieved:

$$\int_{\Omega} \boldsymbol{G}_j d\Omega + \int_{\Gamma} \boldsymbol{g}_j d\Gamma = \sum_{e=1}^{m} \left(\int_{\Omega^e} \boldsymbol{G}_j d\Omega + \int_{\Gamma^e} \boldsymbol{g}_j d\Gamma \right) = \boldsymbol{0} \tag{4.3}$$

Where Ω^e is the domain of each element, Γ^e is the boundary, e is the element number and m is the maximum number of elements in the domain.

Two distinct procedures are available for obtaining an approximate solution. These are (Zienkiewicz and Taylor ,1989);

i. The method of weighted residuals (known alternatively as the Galerkin procedure) and,

ii. The determination of variational functionals.

In this study, the method of weighted residuals is used for spatial discretisation. This method is now widely recognised as a useful numerical approach, for the solution of partial differential equation systems subject to appropriate boundary and initial conditions (Taylor and Hughes, 1981; Hinton and Owen, 1989).

4.2.2 The Weighted Residual Approach

The residual or error introduced by the approximation is given by

$$\boldsymbol{R} = \boldsymbol{u} - \hat{\boldsymbol{u}} \tag{4.4}$$

The weighted residual approach attempts to reduce this residual over the entire domain by requiring the integral of the error over the domain, weighted in various ways is equal to zero, i.e.

$$\int_{\Omega} W_1 \boldsymbol{R}_{\Omega} \partial\Omega = 0 \tag{4.5}$$

Where W_1 are the weighting functions required to minimise the error.

This statement leads to a set of simultaneous linear equations for the unknown coefficients $\boldsymbol{a}_i$ (Equation 4.1). Thus when a function is to be approximated in this way, the resulting system of equations may be solved to obtain the unknown coefficients, by using suitable shape and weighting functions.

The type of weighting functions chosen gives rise to different forms of approximation, for example Galerkin, point collocation or least square approximation (Hinton and Owen, 1989). When the chosen weighting functions are the same as the shape functions, N_i then the resulting approximation is known as the Galerkin method. Application of the Galerkin method to the solution of partial differential equations is common in practice. In such cases, the residual $\boldsymbol{R}_\Omega$ is produced by the insertion of the trial function approximation of the unknown variables into the governing equations. The resulting residual is minimised as described above.

The application of this process to achieve spatial discretisation of the governing moisture transfer equation defined in Chapter 3 is presented in the section below.

4.2.3 Spatial Discretisation of the Moisture Transfer

The two-dimensional axi-symmetric form of the governing differential equation (equation 3.44) may be re-arranged to give:

$$\frac{\partial}{\partial r}\left[K(\psi)\frac{\partial \psi}{\partial r}\right]+\frac{\partial}{\partial z}\left[K(\psi)\frac{\partial \psi}{\partial z}\right]+\frac{\partial K(\psi)}{\partial z}+\frac{1}{r}K(\psi)\frac{\partial \psi}{\partial r}$$

$$-S(\psi,z,r)-C(\psi)\frac{\partial \psi}{\partial t}=0 \qquad (4.6)$$

Multiplying through by r, yields:

$$r\frac{\partial}{\partial r}\left[K(\psi)\frac{\partial \psi}{\partial r}\right]+r\frac{\partial}{\partial z}\left[K(\psi)\frac{\partial \psi}{\partial z}\right]+r\frac{\partial K(\psi)}{\partial z}+K(\psi)\frac{\partial \psi}{\partial r}$$
$$-rS(\psi,z,r)-rC(\psi)\frac{\partial \psi}{\partial t}=0 \qquad (4.7)$$

The unknown variable, capillary potential may be approximated using the trial function approach, for an eight node element, to give:

$$\psi \approx \hat{\psi}=\sum_{s=1}^{8} N_s(r,z)\psi_s(t)=N_s\psi_s \qquad (4.8)$$

Replacing ψ by $\hat{\psi}$ in equation (4.7) yields:

$$r\frac{\partial}{\partial r}\left[K(\hat{\psi})\frac{\partial \hat{\psi}}{\partial r}\right]+r\frac{\partial}{\partial z}\left[K(\hat{\psi})\frac{\partial \hat{\psi}}{\partial z}\right]+r\frac{\partial K(\hat{\psi})}{\partial z}+K(\hat{\psi})\frac{\partial \hat{\psi}}{\partial r}$$
$$-rS(\hat{\psi},z,r)-rC(\hat{\psi})\frac{\partial \hat{\psi}}{\partial t}=R_\Omega \qquad (4.9)$$

Where $\boldsymbol{R}_\Omega$ is the residual obtained by introducing the approximation in equation 4.8. Application of the Galerkin weighted residual approach described in section 4.2.2, and making use of the specific moisture capacity, yields:

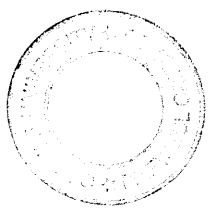

$$\int_{\Omega^e} N_r \begin{bmatrix} r\frac{\partial}{\partial r}\left[K(\hat{\psi})\frac{\partial \hat{\psi}}{\partial r}\right] + r\frac{\partial}{\partial z}\left[K(\hat{\psi})\frac{\partial \hat{\psi}}{\partial z}\right] \\ + r\frac{\partial K(\hat{\psi})}{\partial z} + K(\hat{\psi})\frac{\partial \hat{\psi}}{\partial r} - rS(\hat{\psi},z,r) - rC(\hat{\psi})\frac{\partial \hat{\psi}}{\partial t} \end{bmatrix} \partial\Omega = 0 \qquad (4.10)$$

Hereafter, for the clarity of presentation, the dependency of the unsaturated hydraulic conductivity, the sink term and the specific moisture capacity on capillary potential will be assumed recognised and the notation abbreviated accordingly. Therefore, expanding equation (4.10) and abbreviating the notation yields:

$$\begin{aligned} &\int_{\Omega^e} N_r r\frac{\partial}{\partial r}K\frac{\partial \hat{\psi}}{\partial r}\partial\Omega^e + \int_{\Omega^e} N_r r\frac{\partial}{\partial z}K\frac{\partial \hat{\psi}}{\partial z}\partial\Omega^e + \int_{\Omega^e} N_r r\frac{\partial K}{\partial z}\partial\Omega^e \\ &+ \int_{\Omega^e} N_r K\frac{\partial \hat{\psi}}{\partial r}\partial\Omega^e - \int_{\Omega^e} N_r rS(z,r)\partial\Omega^e - \int_{\Omega^e} N_r rC\frac{\partial \hat{\psi}}{\partial t}\partial\Omega^e = 0 \end{aligned} \qquad (4.11)$$

Using integration by parts, the weak form of equation may be obtained. Considering the first term of equation (4.11) and integrating by parts gives:

$$\int_{\Omega^e} N_r r\frac{\partial}{\partial r}K\frac{\partial \hat{\psi}}{\partial r}\partial\Omega^e = \int_{\Omega^e}\frac{\partial}{\partial r}N_r rK\frac{\partial \hat{\psi}}{\partial r}\partial\Omega^e - \int_{\Omega^e} K\frac{\partial \hat{\psi}}{\partial r}\frac{\partial N_r r}{\partial r}\partial\Omega^e \qquad (4.12)$$

Similarly, for the second term of equation (4.11), repeating the above process yields:

$$\int_{\Omega^e} N_r r\frac{\partial}{\partial z}K\frac{\partial \hat{\psi}}{\partial z}\partial\Omega^e = \int_{\Omega^e}\frac{\partial}{\partial z}N_r rK\frac{\partial \hat{\psi}}{\partial z}\partial\Omega^e - \int_{\Omega^e} K\frac{\partial \hat{\psi}}{\partial z}\frac{\partial N_r r}{\partial z}\partial\Omega^e \qquad (4.13)$$

Substituting equations (4.12) and (4.13) into equation (4.11) yields the weak equation:

$$\int_{\Omega^e}\frac{\partial}{\partial r}N_r rK\frac{\partial\hat{\psi}}{\partial r}\partial\Omega^e - \int_{\Omega^e}K\frac{\partial\hat{\psi}}{\partial r}\frac{\partial N_r r}{\partial r}\partial\Omega^e + \int_{\Omega^e}\frac{\partial}{\partial z}N_r rK\frac{\partial\hat{\psi}}{\partial z}\partial\Omega^e$$

$$-\int_{\Omega^e}K\frac{\partial\hat{\psi}}{\partial z}\frac{\partial N_r r}{\partial z}\partial\Omega^e + \int_{\Omega^e}N_r r\frac{\partial K}{\partial z}\partial\Omega^e + \int_{\Omega^e}N_r K\frac{\partial\hat{\psi}}{\partial r}\partial\Omega^e \qquad (4.14)$$

$$-\int_{\Omega^e}N_r rS(z,r)\partial\Omega^e - \int_{\Omega^e}N_r rC\frac{\partial\hat{\psi}}{\partial t}\partial\Omega^e = 0$$

Noting that:

$$\frac{\partial}{\partial r}N_r r = r\frac{\partial N_r}{\partial r} + N_r \qquad (4.15)$$

and

$$\frac{\partial}{\partial z}N_r r = r\frac{\partial N_r}{\partial z} \qquad (4.16)$$

Substituting equations (4.15) and (4.16) into equation (4.14), gives:

$$\int_{\Omega^e}\frac{\partial}{\partial r}N_r rK\frac{\partial\hat{\psi}}{\partial r}\partial\Omega^e - \int_{\Omega^e}K\frac{\partial\hat{\psi}}{\partial r}\left(r\frac{\partial N_r}{\partial r} + N_r\right)\partial\Omega^e + \int_{\Omega^e}\frac{\partial}{\partial z}N_r rK\frac{\partial\hat{\psi}}{\partial z}\partial\Omega^e$$

$$-\int_{\Omega^e}K\frac{\partial\hat{\psi}}{\partial z}\left(r\frac{\partial N_r}{\partial z}\right)\partial\Omega^e + \int_{\Omega^e}N_r r\frac{\partial K}{\partial z}\partial\Omega^e + \int_{\Omega^e}N_r K\frac{\partial\hat{\psi}}{\partial r}\partial\Omega \qquad (4.17)$$

$$-\int_{\Omega^e}N_r rS(z,r)\partial\Omega^e - \int_{\Omega^e}N_r rC\frac{\partial\hat{\psi}}{\partial t}\partial\Omega^e = 0$$

Expanding equation (4.17) yields:

$$\int_{\Omega^e}\frac{\partial}{\partial r}N_r rK\frac{\partial\hat{\psi}}{\partial r}\partial\Omega^e - \int_{\Omega^e} rK\frac{\partial\hat{\psi}}{\partial r}\frac{\partial N_r}{\partial r}\partial\Omega^e - \int_{\Omega^e}N_r K\frac{\partial\hat{\psi}}{\partial r}\partial\Omega^e$$

$$+\int_{\Omega^e}\frac{\partial}{\partial z}N_r rK\frac{\partial\hat{\psi}}{\partial z}\partial\Omega^e - \int_{\Omega^e} rK\frac{\partial N_r}{\partial z}\frac{\partial\hat{\psi}}{\partial z}\partial\Omega^e + \int_{\Omega^e}N_r r\frac{\partial K}{\partial z}\partial\Omega^e \qquad (4.18)$$

$$+\int_{\Omega^e}N_r K\frac{\partial\hat{\psi}}{\partial r}\partial\Omega^e - \int_{\Omega^e}N_r rS(z,r)\partial\Omega^e - \int_{\Omega^e}N_r rC\frac{\partial\hat{\psi}}{\partial t}\partial\Omega^e = 0$$

By eliminating third and seventh terms equation (4.18) becomes:

$$\int_{\Omega^e}\frac{\partial}{\partial r}N_r rK\frac{\partial\hat{\psi}}{\partial r}\partial\Omega^e - \int_{\Omega^e} rK\frac{\partial\hat{\psi}}{\partial r}\frac{\partial N_r}{\partial r}\partial\Omega^e + \int_{\Omega^e}\frac{\partial}{\partial z}N_r rK\frac{\partial\hat{\psi}}{\partial z}\partial\Omega^e$$

$$-\int_{\Omega^e} rK\frac{\partial N_r}{\partial z}\frac{\partial\hat{\psi}}{\partial z}\partial\Omega^e + \int_{\Omega^e}N_r r\frac{\partial K}{\partial z}\partial\Omega^e - \int_{\Omega^e}N_r rS(z,r)\partial\Omega^e \qquad (4.19)$$

$$-\int_{\Omega^e}N_r rC\frac{\partial\hat{\psi}}{\partial t}\partial\Omega^e = 0$$

Expressing the first and third terms of equation (4.19) in terms of an approximate total potential, $\hat{\phi}$ and since $\frac{\partial}{\partial z}(N_r K) = N_r\frac{\partial K}{\partial z} + K\frac{\partial N_r}{\partial z}$, this equation may be simplified to:

$$\int_{\Omega^e}\frac{\partial}{\partial r}N_r rK\frac{\partial\hat{\phi}}{\partial r}\partial\Omega^e - \int_{\Omega^e}rK\frac{\partial\hat{\psi}}{\partial r}\frac{\partial N_r}{\partial r}\partial\Omega^e + \int_{\Omega^e}\frac{\partial}{\partial z}N_r rK\frac{\partial\hat{\phi}}{\partial z}\partial\Omega^e$$

$$-\int_{\Omega^e}rK\frac{\partial N_r}{\partial z}\frac{\partial\hat{\psi}}{\partial z}\partial\Omega^e - \int_{\Omega^e}N_r r\frac{\partial K}{\partial z}\partial\Omega^e - \int_{\Omega^e}N_r rS(z,r)\partial\Omega^e \qquad (4.20)$$

$$-\int_{\Omega^e}N_r rC\frac{\partial\hat{\psi}}{\partial t}\partial\Omega^e = 0$$

Gauss-Green divergence theorem (Zienkiewicz, 1977) may be used to relate surface integrals to boundary integrals. Application of the divergence formula to the first and third terms in equation (4.20) yields;

$$\int_{\Omega^e}\frac{\partial}{\partial r}N_r rK\frac{\partial\hat{\phi}}{\partial r}\partial\Omega^e = \oint_{\Gamma}N_r rK\frac{\partial\hat{\phi}}{\partial r}\partial\Gamma \qquad (4.21)$$

and

$$\int_{\Omega^e}\frac{\partial}{\partial z}N_r rK\frac{\partial\hat{\phi}}{\partial z}\partial\Omega^e = \oint_{\Gamma}N_r rK\frac{\partial\hat{\phi}}{\partial z}\partial\Gamma \qquad (4.22)$$

Therefore, noting that;

$$\frac{\partial\hat{\phi}}{\partial n} = n_r\frac{\partial\hat{\phi}}{\partial r} + n_z\frac{\partial\hat{\phi}}{\partial z} \qquad (4.23)$$

and also incorporating equations (4.21) and (4.22), equation (4.20) may be re-cast as:

$$-\int_{\Omega^e} rK\frac{\partial\hat{\psi}}{\partial r}\frac{\partial N_r}{\partial r}\partial\Omega^e - \int_{\Omega^e} rK\frac{\partial N_r}{\partial z}\frac{\partial\hat{\psi}}{\partial z}\partial\Omega^e - \int_{\Omega^e} N_r r\frac{\partial K}{\partial z}\partial\Omega^e$$

$$+\int_{\Gamma} N_r rK\frac{\partial\hat{\phi}}{\partial n}\partial\Gamma - \int_{\Omega^e} N_r rS(z,r)\partial\Omega^e - \int_{\Omega^e} N_r rC\frac{\partial\hat{\psi}}{\partial t}\partial\Omega^e = 0 \qquad (4.24)$$

Letting $\lambda = K\frac{\partial\hat{\phi}}{\partial n}$ and noting that;

$$\frac{\partial\hat{\psi}}{\partial r} = \sum_{s=1}^{8}\frac{\partial N_s}{\partial r}\cdot\psi_s \qquad (4.25)$$

and

$$\frac{\partial\hat{\psi}}{\partial z} = \sum_{s=1}^{8}\frac{\partial N_s}{\partial z}\cdot\psi_s \qquad (4.26)$$

Equation (4.24) may be recast as follows:

$$-\int_{\Omega^e} rK\frac{\partial N_s}{\partial r}\frac{\partial N_r}{\partial r}\psi_s\partial\Omega^e - \int_{\Omega^e} rK\frac{\partial N_r}{\partial z}\frac{\partial N_s}{\partial z}\psi_s\partial\Omega^e - \int_{\Omega^e} N_r r\frac{\partial K}{\partial z}\partial\Omega^e$$

$$+\int_{\Gamma} N_r r\lambda\partial\Gamma - \int_{\Omega^e} N_r rS(z,r)\partial\Omega^e - \int_{\Omega^e} N_r N_s rC\frac{\partial\psi_s}{\partial t}\partial\Omega^e = 0 \qquad (4.27)$$

Summing for all elements and re-casting equation (4.27) into concise matrix notation yields;

$$\mathbf{K}\psi_s + \mathbf{C}\frac{\partial \psi_s}{\partial t} + \mathbf{J} + \mathbf{S} = 0 \tag{4.28}$$

where,

$$\boldsymbol{K} = \sum_{e=1}^{m} \int_{\Omega^e} r\left[K\frac{\partial N_s}{\partial r}\cdot\frac{\partial N_r}{\partial r} + K\frac{\partial N_s}{\partial z}\cdot\frac{\partial N_r}{\partial z}\right] \partial\Omega^e \tag{4.29}$$

$$\boldsymbol{C} = \sum_{e=1}^{m} \int_{\Omega^e} r[N_r N_s C]\partial\Omega^e \tag{4.30}$$

$$\boldsymbol{J} = \sum_{e=1}^{m} \int_{\Omega^e} r\left[N_r \frac{\partial K}{\partial z}\right] \partial\Omega^e - \sum_{e=1}^{m} \int_{\Gamma^e} r[N_r \lambda]\partial\Gamma^e \tag{4.31}$$

$$\boldsymbol{S} = \sum_{e=1}^{m} \int_{\Omega^e} r[N_r S(r,z)]\partial\Omega^e \tag{4.32}$$

The matrix representation of the discretised equations is further used in section 4.3.

4.2.4 Boundary Conditions

The above formulation permits the specification of two types of boundary conditions (Feddes et al., 1976). The first, known as Dirichlet type boundary conditions, take the form of prescribed values of capillary potential (in cm of water) at the boundary nodes. The second, known as Neumann or flux type boundary conditions take the form of a moisture flux (specified in cm/sec) set at the boundary nodes. The flux term is represented in the above formulation by the term λ defined after equation (4.24) above.

4.2.5 Root Zone Control

As explained in Chapter 2, typical trees have relatively shallow and wide-spread root systems (Cutler et al, 1990; Dobson and Moffat, 1993; Dobson, 1995). It is unusual for roots to penetrate to a deeper depth. In view of this, the shape of the active root zone implemented in this research is shown in Figure 4.2. The elliptical region is defined by:

i) radial distance a - representing the maximum horizontal spread of the root system, and

ii) depth b – representing the maximum depth of the root system

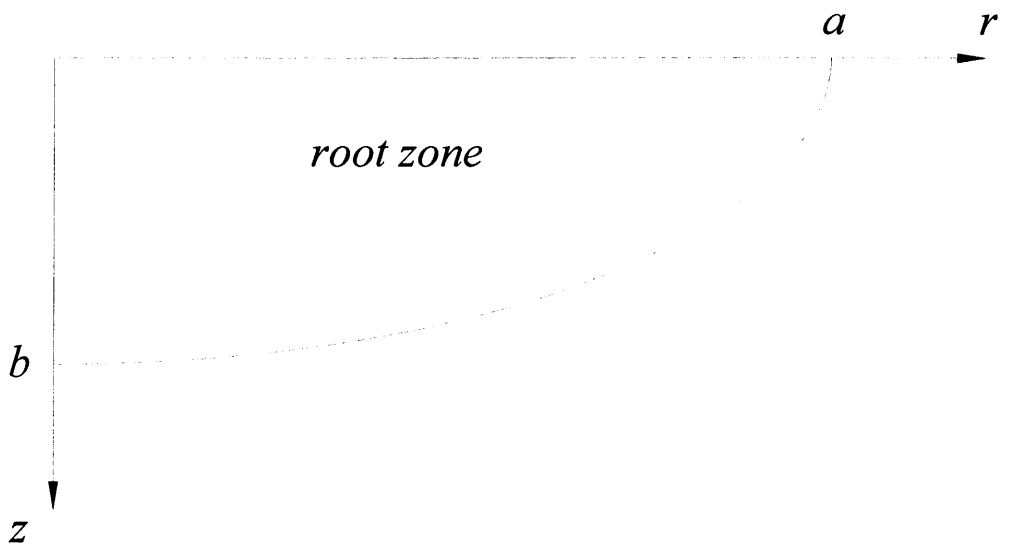

Figure 4.2 Active Root Zone

It is assumed that sink term is active only within this elliptical root zone. The lower boundary line is then defined by a standard equation for an ellipse:

$$\frac{r^2}{a^2}+\frac{z^2}{b^2}=1 \tag{4.33}$$

Re-arranging equation (4.33) gives:

$$z=\sqrt{b^2\left(1-\frac{r^2}{a^2}\right)} \tag{4.34}$$

Equation (4.34) is then used with the finite element code to define if any particular element within the domain falls within the active root zone. It was assumed that there is no active sink term, if the value of the coordinate z in the element is higher than the z value in equation (4.34) at a given radius. Therefore, at any r distance, if

$$z < \sqrt{b^2\left(1-\frac{r^2}{a^2}\right)} \tag{4.35}$$

the sink term is active, and if

$$z > \sqrt{b^2\left(1-\frac{r^2}{a^2}\right)} \tag{4.36}$$

no sink term is applied.

The exact magnitude of the sink operating within any element within the root zone itself is then determined from the water uptake model itself (see equation 3.47, Chapter 3). No sink is applied to any element that is outside of the root zone. However, it should be noted that moisture is, of course, free to migrate across this boundary is response to any hydraulic gradient that occurs during a particular simulation.

4.3 TIME DISCRETISATION

The spatially discretised matrix equation (4.28) is time discretised by the application of a fully implicit mid-interval backward difference algorithm. The chosen scheme is known to be particularly suitable for application to highly non-linear problems such as the one in hand (Neuman, 1973). This scheme has been illustrated by Thomas and Rees (1991) who provided the following description. Equation (4.28) may be approximated by:

$$\boldsymbol{K}^{n+1/2}\boldsymbol{\psi}^{n+1} + \boldsymbol{C}^{n+1/2}\left[\frac{\boldsymbol{\psi}^{n+1} - \boldsymbol{\psi}^{n}}{\Delta t}\right] + \boldsymbol{J}^{n+1/2} + \boldsymbol{S}^{n+1/2} = 0 \qquad (4.37)$$

Re-arranging yields

$$\boldsymbol{\psi}^{n+1} = \left[\mathbf{K}^{n+1/2} + \frac{\mathbf{C}^{n+1/2}}{\Delta t}\right]^{-1} \times \left[\frac{\mathbf{C}^{n+1/2}\boldsymbol{\psi}^{n}}{\Delta t} - \mathbf{J}^{n+1/2} - \mathbf{S}^{n+1/2}\right] \qquad (4.38)$$

Clearly equation (4.38) cannot be solved directly as each calculation of $\boldsymbol{\psi}^{n+1}$ requires the determination of the coefficients at the mid-interval. Therefore, an iterative solution procedure is necessary. In the current work a predictor-corrector approach is used. The method is described as follows.

For a given time interval, a first estimate of $\boldsymbol{\psi}^{n+1}$ is made, this is called the predictor, where the matrices are evaluated using the values of $\boldsymbol{\psi}$ at the start of the time interval. For the first time step these values of $\boldsymbol{\psi}$ clearly represent the initial

conditions of the problem under consideration. Mathematically the predictor is expressed as,

$$\psi_p^{n+1} = \left[\mathbf{K}_0^n + \frac{\mathbf{C}_0^n}{\Delta t}\right]^{-1} \times \left[\frac{\mathbf{C}_0^n \psi_0^n}{\Delta t} - \mathbf{J}_0^n - \mathbf{S}_0^n\right] \tag{4.39}$$

The mid-interval values of ψ are calculated next such that,

$$\psi_1^{n+1/2} = \left(\psi_o^n + \psi_p^{n+1}\right)/2 \tag{4.40}$$

And the first correction is made as:

$$\psi_{1c}^{n+1} = \left[\mathbf{K}_1^{n+1/2} + \frac{\mathbf{C}_1^{n+1/2}}{\Delta t}\right]^{-1} \times \left[\frac{\mathbf{C}_1^{n+1/2} \psi_o^n}{\Delta t} - \mathbf{J}_1^{n+1/2} - \mathbf{S}_1^{n+1/2}\right] \tag{4.41}$$

In equation (4.41) the matrices ***K***, ***C***, ***J*** and ***S*** are evaluated corresponding to the values of ψ given in equation (4.40). The next correction is made based on a new set of values of $\psi^{n+1/2}$ i.e.,

$$\psi_2^{n+1/2} = \left(\psi_o^n + \psi_{1c}^{n+1}\right)/2 \tag{4.42}$$

And therefore,

$$\psi_{2c}^{n+1} = \left[\mathbf{K}_2^{n+1/2} + \frac{\mathbf{C}_2^{n+1/2}}{\Delta t}\right]^{-1} \times \left[\frac{\mathbf{C}_2^{n+1/2} \psi_o^n}{\Delta t} - \mathbf{J}_2^{n+1/2} - \mathbf{S}_2^{n+1/2}\right] \tag{4.43}$$

As the process continues the matrices are evaluated at the last mid-interval estimate. Convergence is monitored between successive correctors and is deemed to have been achieved when,

$$\left|\psi_{ic}^{n+1} - \psi_{(i+1)c}^{n+1}\right| \langle TOLERANCE \qquad \text{For all } \psi \qquad (4.44)$$

The value of *TOLERANCE* is judged for the case in hand, throughout the current work the value adopted is a capillary potential of –l cm of water. The value of i at which the convergence criterion is satisfied, for every node in the flow domain, represents the number of iterations required to obtain solution for the current time step. The iterative process takes place within each time interval. The higher the degree of non-linearity involved, the higher the number of iterations required and consequently the larger the computing cost.

The resulting numerical solution has been coded using FORTRAN. An original code was available at the start of this research programme as developed by Thomas and Rees (1991, 1993). The new axi-symmetric formulation and sink term have been introduced as a result of the current work.

4.4 CONCLUSIONS

An introduction to the basic concepts of the finite element method has been presented in this chapter. The moisture flow model presented in Chapter 3 has been discretised to achieve an approximate numerical solution.

In particular, spatial discretisation has been achieved by application of the finite element method using Galerkin weighted residual approach. This approach is widely recognised as a useful numerical approach, for the solution of partial differential equation systems subject to appropriate boundary and initial conditions.

The resulting model can accommodate two types of boundary conditions: fixed or flux. The water uptake model is applied through the sink term in the governing moisture flow equation. A brief description of how the root zone is defined within the numerical model has also has been presented in this Chapter.

Time discretisation of the model has been achieved by the application of a fully implicit mid-interval backward difference algorithm. The chosen scheme is known to be particularly suitable for application to highly non-linear problems such as the one in hand.

4.6 REFERENCES

Cutler, D.F., Gasson, P.E and Farmer, M.C. "The wind blown tree survey: Analysis of results. " Arboricultural Journal, 14, 265-286, 1990.

Dobson, M.C. "Tree root systems. " Arboriculture Research and Information Note, Arboricultural Advisory and Information Service, Farnham, 1995.

Dobson, M.C. and Moffat, A.J. "The potential for woodland establishment on landfill sites. " Department of the Environment, HMSO, London, 1993.

Feddes, R. A., Kowalik, P. J., Malink, K. K., and Zaradny, H. "Simulation of field water uptake by plants using a soil water dependent root extraction function." J. Hydro, 31, 13 – 26, 1976.

Hinton, E., and Owen, D. R. J. Finite Element Programming, Academic Press, London, 1989.

Neuman, S. P. "Saturated-Unsaturated Seepage by Finite Elements." J.Hydro, 99, 2233 – 2249, 1973.

Rockey, K.C., Evans, H.R., Griffiths, D. W. and Nethercot, D. A. "The Finite Element Method. " Collins, London, 1983.

Taylor, C. and Hughes, T. G. " Finite Element Programming of the Navier-Stokes Equations. " Pineridge, Swansea, 1981.

Thomas, H. R. and Rees, S. W. "A comparison of field monitored and numerically predicted moisture movement in unsaturated soil"; Int. J. for Num. and Anal. Meth. in Geomechanics, 15, 417-431, 1991.

Thomas, H. R. and Rees, S. W. "The numerical simulation of seasonal soil drying in an unsaturated clay soil". Int. J. for Num. and Anal. Meth. in Geomechanics, 17(1), 119-132, 1993.

Zienkiewicz, O. C. The Finite Element Methods, McGraw-Hill, 1977.

Zienkiewicz, O. C., and Taylor, R. L. The Finite Element Method, McGraw-Hill Book Company, London UK, 1989.

CHAPTER FIVE

SIMULATION OF ONE-DIMENSIONAL WATER UPTAKE

5.1 INTRODUCTION

As indicated previously, the primary focus of this research programme is the development of a two-dimensional water-uptake model for application to the simulation of water uptake near trees. However, the development of this model has been approached in a step-by-step manner, starting with implementation of the volumetric sink term within the finite element framework, followed by inclusion of the water-uptake model itself. To help verify these developments, the simplest form of model (1D) was first implemented and tested prior to extension of the formulation to accommodate 2D axi-symmetric conditions. Therefore, this chapter presents some of this initial research and considers

application of the 1D form of the model, as described in Chapter 3, to a number of different practical scenarios. In particular three test cases are considered:

- Case 1 – Linear water-uptake for a loam soil – based on the work of Mathur and Rao (1999)

- Case 2 – Water uptake utilizing a water stress function – based on the work of Feddes et al (1976)

- Case 3 – Water uptake with a non-uniform root distribution – based on the work of Gardner (1964)

5.2 CASE 1 - LINEAR WATER-UPTAKE

5.2.1 Case 1 – Problem Description

Mathur and Rao (1999) developed a finite element model that describes water uptake from soils caused by the roots of transpiring plants. Their study employed Prasad's model with a linear root water extraction term that varies with time (Prasad, 1988). The model also included a sinusoidal root growth function with time. They verified their work by comparing the simulated results with a number of independently published results for both a homogeneous and a layered medium.

One element of Mathur and Rao's work is selected here to provide a first assessment of the new code. In particular they present a 'Test Case' to explore their root-water-extraction model. For this purpose they defined a relatively simple one-dimensional water-uptake problem based on a loamy-sand. The problem they defined was solved with their finite element code and checked via simple mass-balance calculations to confirm that their root extraction procedure was functioning correctly. To the same end, this problem has been re-analysed with the current model, to provide a basic verification of the sink term employed.

5.2.2 Material Properties

Mathur and Rao provided the hydraulic properties for the Berino Loamy Sand. In particular, the water retention curve was obtained using van Genuchten's method (Genuchten, 1980). The resulting relationship was given as:

$$\theta = \theta_r + \frac{(\theta_s - \theta_r)}{\left[1 + (\alpha\psi)^n\right]^m} \tag{5.1}$$

Where θ_r and θ_s are residual and saturated water content respectively, ψ is the capillary potential and α, n and m are the empirical shape parameters. The exact values of these parameters are shown in Table 5.1.

Table 5.1 Basic soil properties, after Mathur and Rao (1999)

θ_r	θ_s	K_s (m/d)	α	l	n	m
0.0286	0.3658	2.5×10^{-4}	0.0280	0.5	2.2390	0.553

The hydraulic conductivity relationship of the soil, was determined by making use of the above water retention curve along with the pore size distribution model of Mualem (1976) to obtain:

$$K = K_s \frac{\left[\left(1+|\alpha\psi|^n\right)^m - |\alpha\psi|^{n-1}\right]^2}{\left(1+|\alpha\psi|^n\right)^{m(l+2)}} \tag{5.2}$$

Where K_s is the saturated hydraulic conductivity and l is a soil specific parameter. Table 5.1 also provides the relevant values of the parameters used in this case. The water retention and hydraulic conductivity relationships are shown in Figures 5.1 and 5.2 respectively.

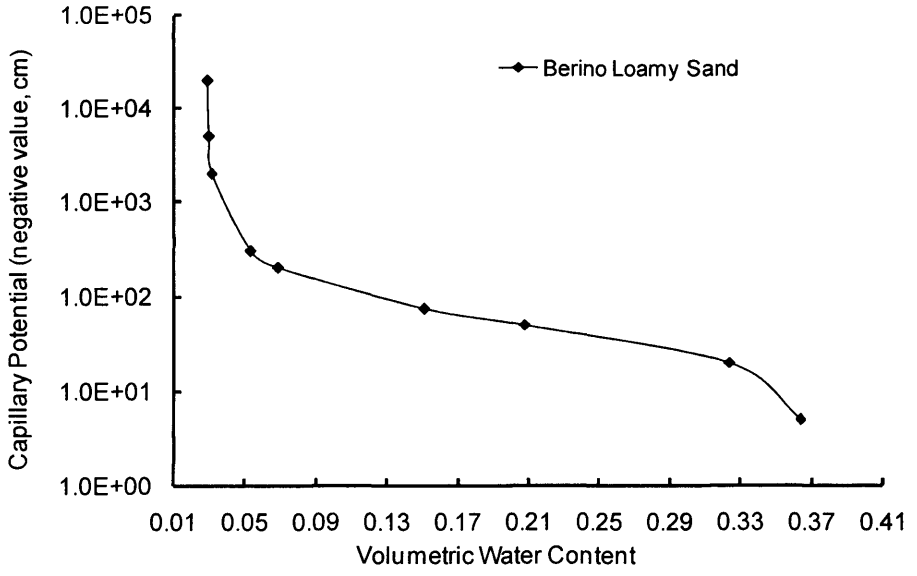

Figure 5.1 Water Retention Curve for Berino Loamy Sand, after Mathur and Rao (1999)

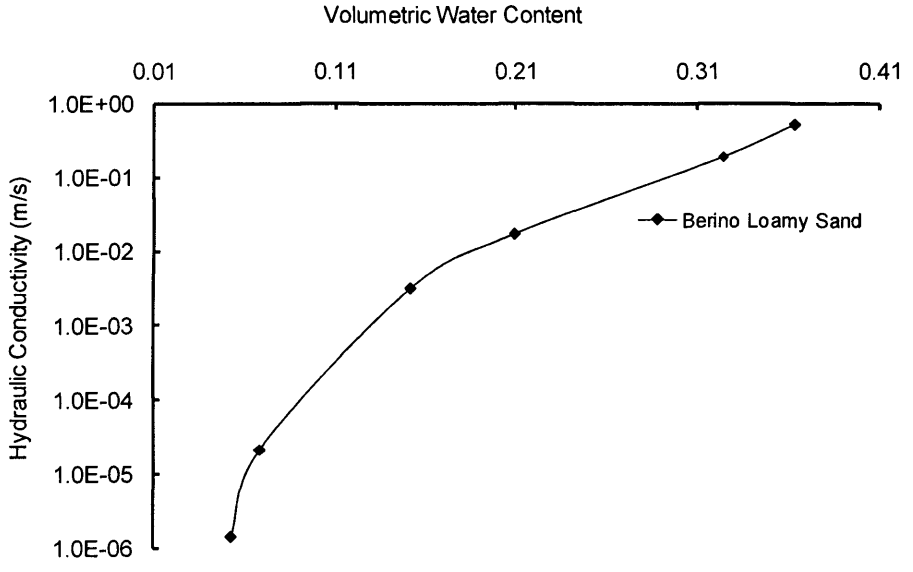

Figure 5.2 Hydraulic Conductivity for Berino Loamy Sand, after Mathur and Rao (1999)

5.2.3 Numerical Simulation

The current simulation employs the same level of discretisation as that used by Mathur and Rao. The domain in this case is a simple column of soil 100 cm in depth. This was represented by a finite element mesh comprising 25 elements each of 4 cm height. The initial moisture content was assumed to be of 0.052625 cm^3 / cm^3. This value corresponds to a degree of saturation of approximately 13 % - a value described by Mathur and Rao as being 'wet' enough to permit water extraction to take place at its potential rate. This corresponds, via equation 5.1, to a pressure head of -300 cm of water.

The simulation employs a time-step size of 21600 seconds, which was held constant for the entire period considered. Preliminary numerical tests were conducted to ensure that the solution for this domain size and a time-step size of 21600 seconds (constant for the entire period considered) is converged.

The boundary conditions at the surface and at the base of the column were assumed to be unconstrained (or natural). The potential transpiration rate applied via the root-extraction model 0.025 cm / day. The maximum root length for the simulation was 13.66 cm and the period analysed covered 4 days. Their numerical result will be presented in the section below.

5.2.4 Results

The results of the current simulation are compared to those presented by Mathur and Rao for days 3 and 4 in Figures 5.3 and 5.4 respectively. In general a good agreement between results has been achieved lending some confidence in the implementation of the new model. The simulated results show that the moisture content of the soil in the root zone progressively decreases with time and depth. The sink term is active within the depth of the root zone (i.e. the upper 13.99 cm of the soil profile – i.e. within the top four elements of the mesh) and it is clear that the majority of the moisture extraction has occurred near the surface. At the end of simulation (day 4 - see Figure 5.4), the volumetric moisture content is reduced to 0.05256 cm^3 / cm^3 at approximately 4 cm depth. The profile is roughly linear (as expected by definition) and the moisture content increases to its initial value of 0.05262 cm^3 / cm^3 at approximately 20 cm below the ground surface.

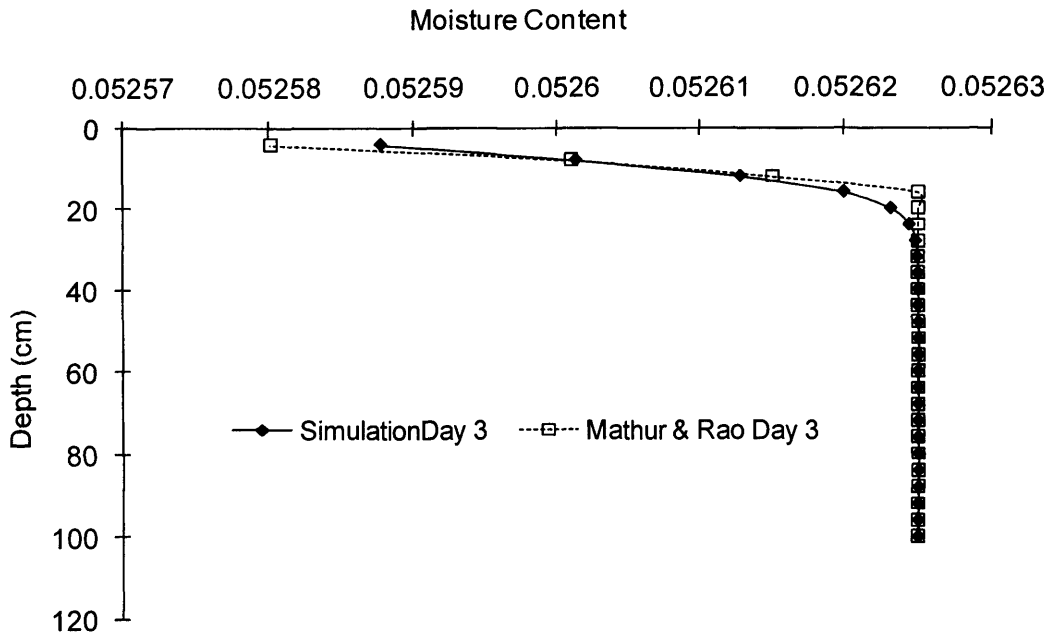

Figure 5.3 Simulated Moisture Profiles at Day 3

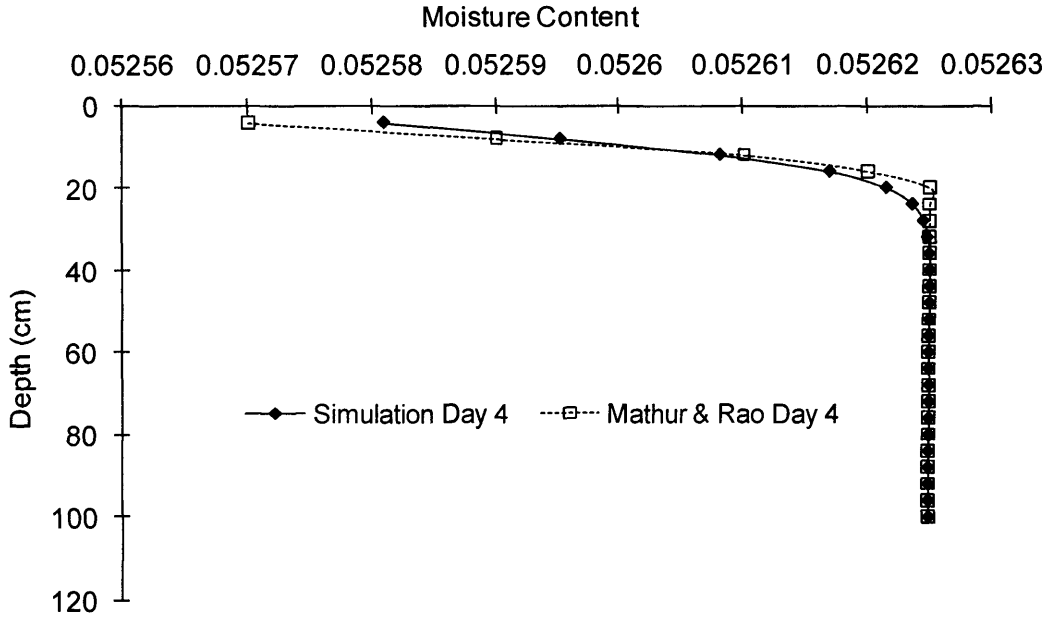

Figure 5.4 Simulated Moisture Profiles at Day 4

It is recognised that the above comparison is limited to a total time period of 4 days. This combined with the extraction rate of only 0.025 cm/day leads to results that show only a small absolute change in moisture content over the simulated period. However, these results serve their purpose in the sense that the case considered would clearly be sensitive to any errors in the implementation of the sink term and the root-extraction model.

5.3 CASE 2 - WATER STRESS FUNCTION

5.3.1 Case 2 – Problem Description

This exercise is based on the study of Feddes et al (1976). In their approach the sink term is considered to be a function of the soil-water content, some detail of this approach has already been presented in section 3.4.1 in Chapter 3. Feddes et al developed their own finite difference model and verified it by comparison to field data obtained from water-balance studies. The field experiment was located at the groundwater-level experimental site at Geestmerambacht, Netherlands (Feddes, 1971). In the experiment, red cabbage (*Brassica oleracea*) was grown on a heavy clay soil (48% < 2 μm) in rows 75 cm wide and spaced 65 cm apart. Water balance studies were carried out by means of a non-weighable lysimeter. Upward and downward flows from and to

the water table were measured daily. Soil water content measurements were performed weekly at 10 cm depth intervals by means of a γ-transmission method.

5.3.2 Material Properties

The soil profile considered by Feddes et al. was a homogeneous clay – described by a single water retention curve. Hydraulic conductivity data from various depths were lumped into a single relationship to represent the entire soil profile. The resulting water retention and hydraulic conductivity relationships, as adopted for this study, are shown in Figures 5.5 and 5.6 respectively.

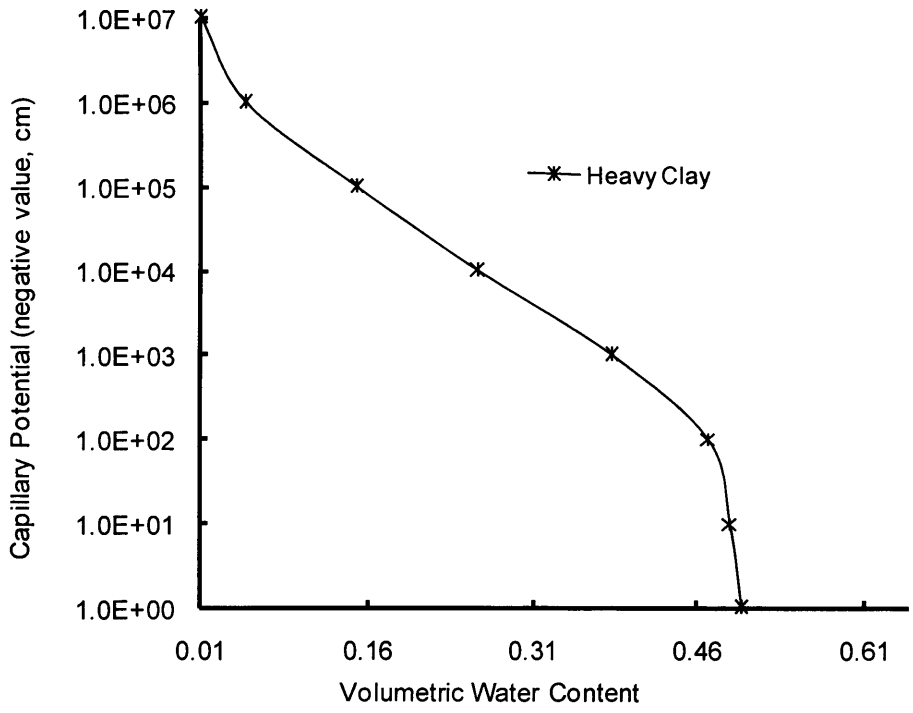

Figure 5.5 Water Retention Curve for Heavy Clay, after Feddes et al (1976)

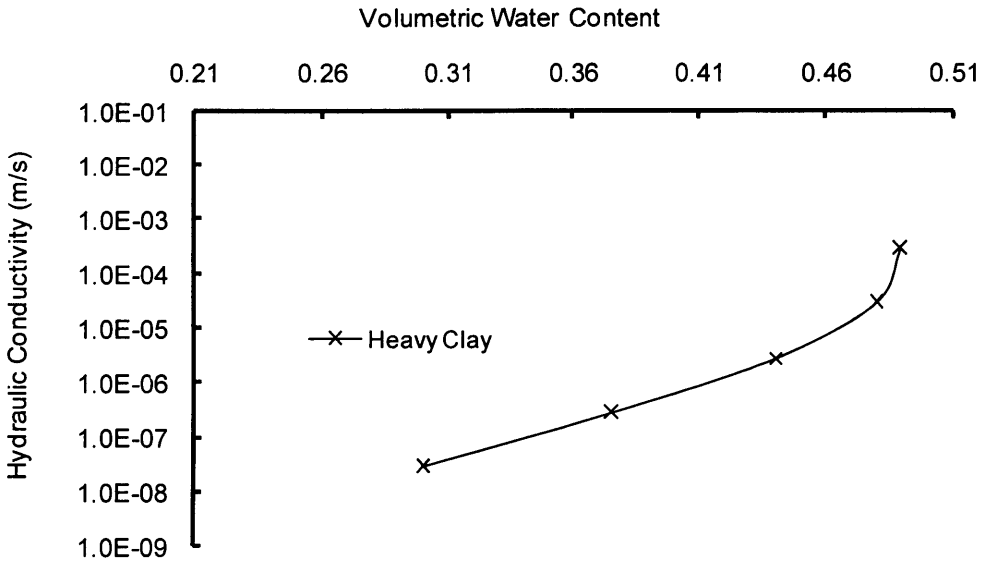

Figure 5.6 Hydraulic Conductivity for Heavy Clay, after Feddes et al (1976)

5.3.3 Numerical Simulation

Feddes et al applied their own (finite difference) model to simulate water-uptake by the red cabbage. Their domain was 100 cm in depth and was represented by elements of 5 cm depth, starting at z = 2.5 cm below ground surface. A time-step size of 2 hours was used and held constant throughout their simulation. The initial moisture content was 0.5 cm^3 / cm^3 throughout the soil column and the boundary conditions at the top and bottom of the column were again unconstrained. The potential transpiration rate was based on the average of 0.025 cm / hour.

The sink term used by Feddes et al was of the form:

$$S(\psi) = \alpha(\psi)\frac{2T}{z} \qquad (23)$$

Where T is the actual transpiration (cm/s), z is the rooting depth (cm) and $\alpha(\psi)$ (dimensionless) is the water stress function as explained in Chapter 3 (see Figure 3.7).

The dimensionless water stress function $\alpha(\psi)$ was defined according to the critical capillary potential values (-50 cm, -400 cm and -15000 cm, see figure 3.7 in Chapter 3). The depth of the effective root zone varied from about 25 cm at the beginning to about 70 cm at the end of the simulation which is 49 days. It is assumed that root growth was uniform throughout the simulation at the rate of 0.038265 cm / hour. Their numerical result will be presented in the section below and this problem has been re-analysed with the current model, to provide a basic comparison of the sink term employed under these conditions.

The current simulation employs the same domain size as used by Feddes et al. The soil column (100 cm depth) has been divided into 25 elements each of 4 cm height and 8 cm width. The elements used for this model are in fact 2D quadratic eight node elements – constrained to 1D behaviour – the element width is essentially arbitrary and has no influence on this problem. The simulation employs a time-step size of 21600 seconds, which was held constant for the entire period considered. Preliminary numerical tests were conducted indicate that the solution for this domain size and a time-step size of 21600 seconds (constant for the entire period considered) is converged.

5.3.4 Results

The results for the current simulation and those presented by Feddes et al (1976) at 34 days and at 49 days are shown in Figures 5.7 and 5.8 respectively. The results show that moisture content in the root zone progressively decreases with time and depth. At the end of simulation, it is clear that the majority of the moisture extraction has occurred near the surface with the volumetric moisture content reducing to 0.2 cm^3 / cm^3. The moisture content increases to its initial value of 0.5 cm^3 / cm^3 at approximately 90 cm below the ground surface. The profile shows some non-linearity due to the varying root depth in the sink term.

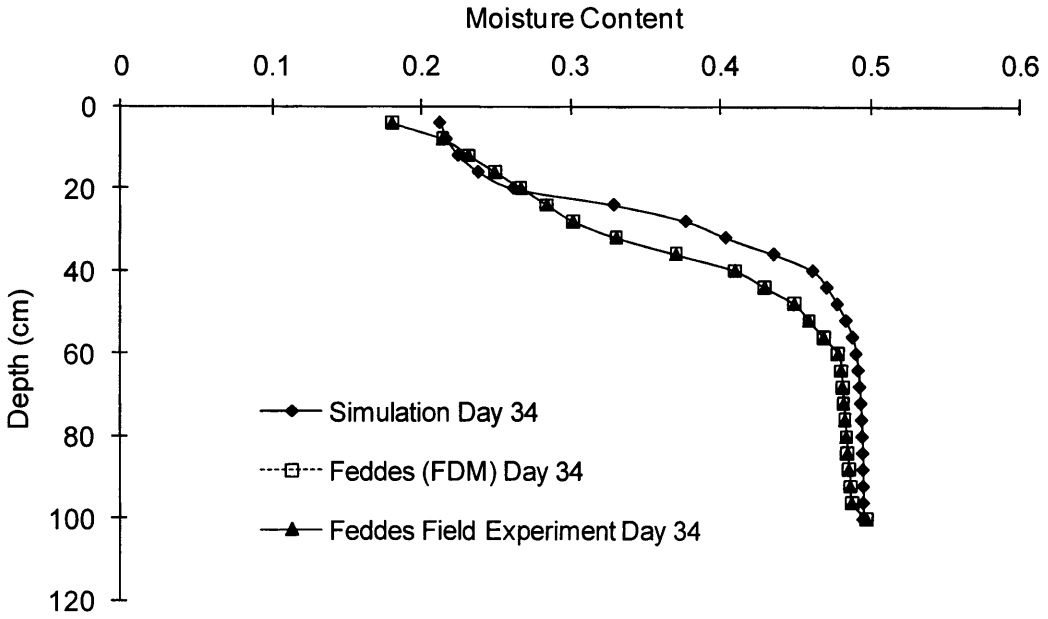

Figure 5.7 Simulated Moisture Profiles at Day 34

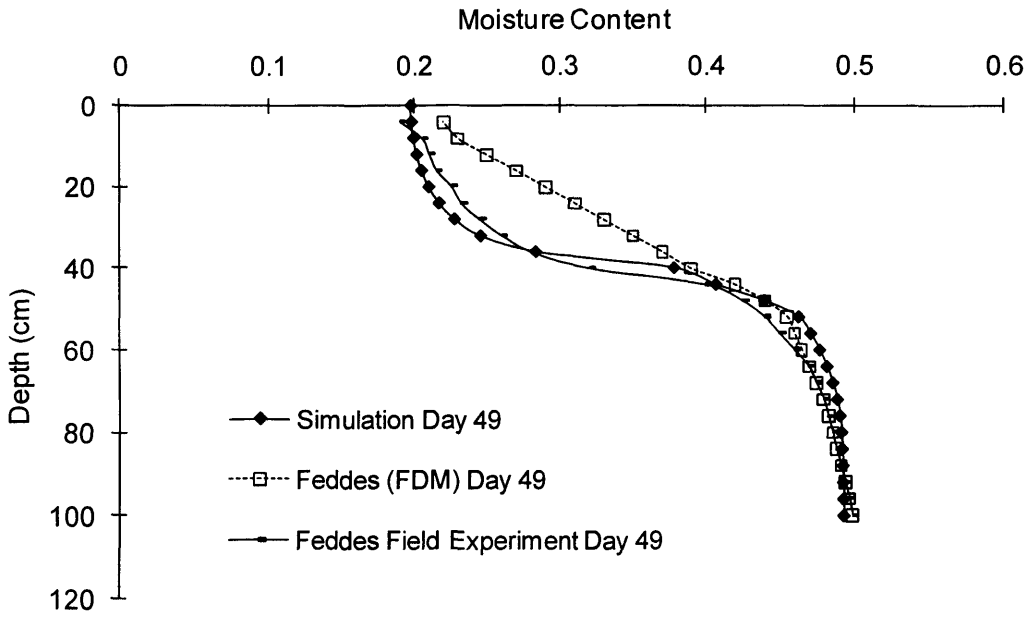

Figure 5.8 Simulated Moisture Profiles at Day 49

These figures also show that simulated results from the current model are in reasonable agreement with Feddes' results at 34 days. However, the new model produces a closer agreement with the experimental data at 49 days than that achieved by Feddes et al using their finite difference model.

5.4 CASE 3 - NON-UNIFORM ROOT MODEL

5.4.1 Case 3 - Problem Description

The final test case presented in this chapter is based on the study of Gardner (1964). Gardner proposed a finite difference model to describe the water uptake by a non-uniform root system. The main thrust of this study was to determine the root distribution associated with each depth increment. Gardner validated the finite difference results by comparison to experimental data for a sorghum plant on Pachappa sandy loam. Gardner's results were based on the following water-uptake equation:

$$q = Bh\sum_{i=1}^{n}(\delta - \eta_i - z_i)K_i L_i \qquad (24)$$

Where q is the total rate of water uptake per unit cross sectional area by summing from $i=1$ to $i=n$ layers, B is a constant, h is the thickness for each layer, δ is the suction or diffusion pressure deficit in the plant roots, η is the average matric suction in the soil, z is the distance from the soil surface to the centre of the layer, K is the unsaturated conductivity of soil and L is the length of roots in the unit volume of soil. The water content in the root zone can thus be obtained as a function of time and depth.

The current model has also been applied to simulate this work and is compared below to the experimental and finite difference results achieved by Gardner. A description of the material properties provided by Gardner is first provided.

5.4.2 Material Properties

The water retention and hydraulic conductivity relationship for Pachappa Sandy Loam are shown in Figures 5.9 and 5.10 respectively.

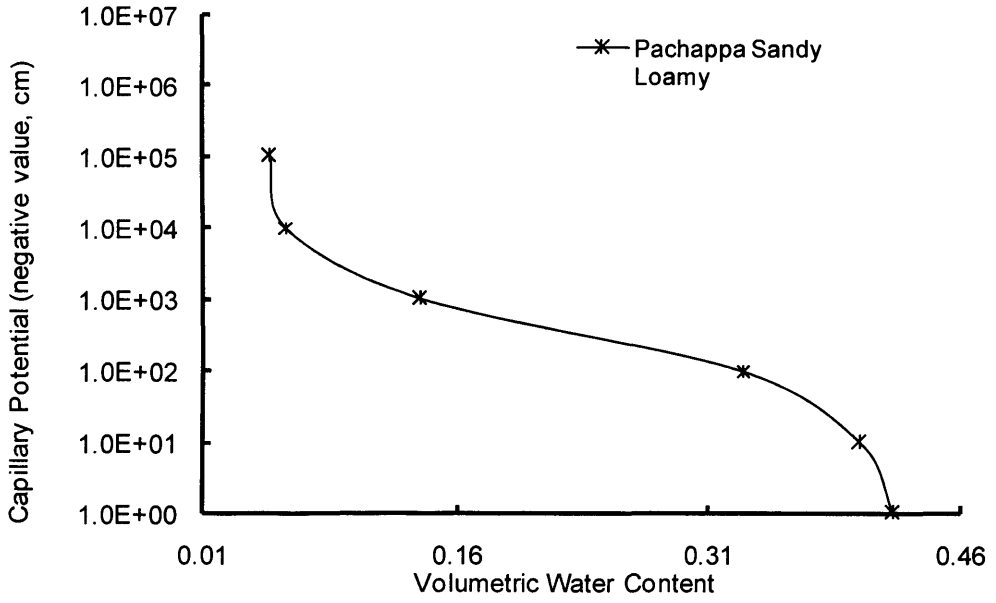

Figure 5.9 Water Retention Curve for Pachappa Sandy Loamy, after Gardner (1964)

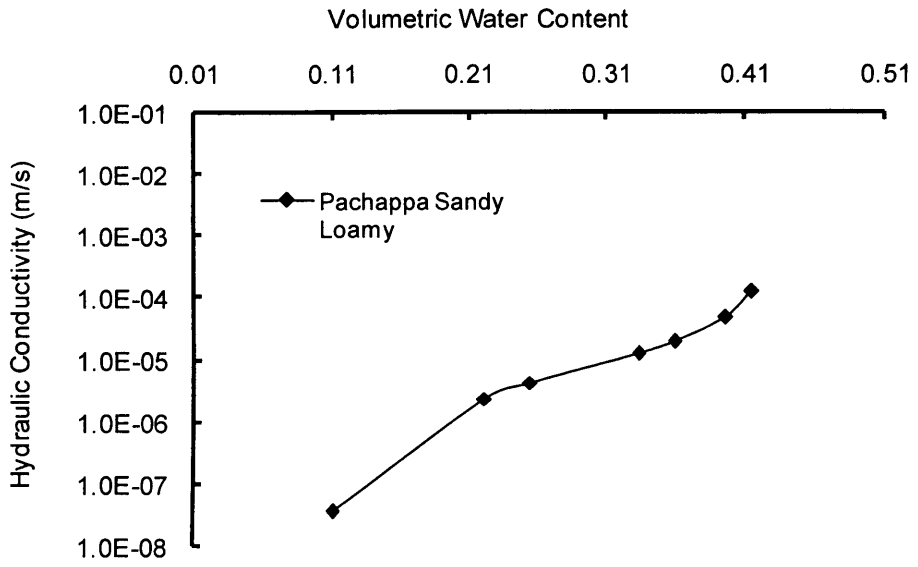

Figure 5.10 Hydraulic Conductivity for Pachappa Sandy Loamy, after Gardner (1964)

5.4.3 Numerical Simulation

Gardner's finite different model was applied to simulate water uptake from a soil column 100 cm in depth. A linear initial moisture content variation was applied. This varied from 0.3 cm^3 / cm^3 at the soil surface and increased to 0.4 cm^3 / cm^3 at 100 cm depth. The boundary condition at the top surface was assumed to be a zero flux. The potential transpiration rate was taken as 2 cm / day. The maximum root length for the simulation was 100 cm and the period analysed covered 4 days

The current model has been used to solve the same problem. Transpiration rate, root depth, initial and boundary conditions were as provided by Gardner. The domain

and finite element mesh is shown in Figure 5.11. The simulation employs a time-step size of 21600 seconds, which was held constant for the entire period considered.

5.4.4 Results

The results for the current simulation and those presented by Gardner (1964) at times of 2 days and 4 days are shown in Figure 5.12 and 5.13 respectively.

.

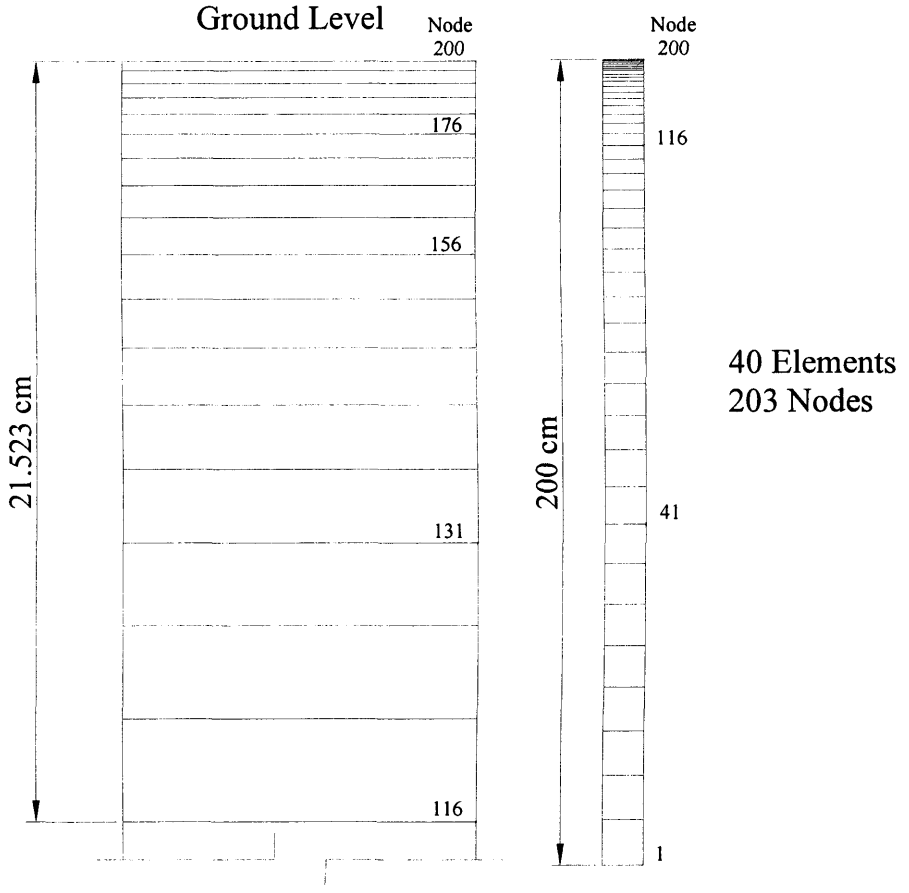

Figure 5.11 1-D Finite Element Mesh

The new results show moisture content in the root zone progressively decreases with time and depth. It is clear that the majority of the moisture extraction has occurred near the surface. At day 4 (see Figure 5.13) the volumetric moisture content has reduced to 0.2 cm^3 / cm^3 at surface. The profile is roughly linear and the moisture content increases to its initial value of 0.4 cm^3 / cm^3 at approximately 120 cm below the ground surface

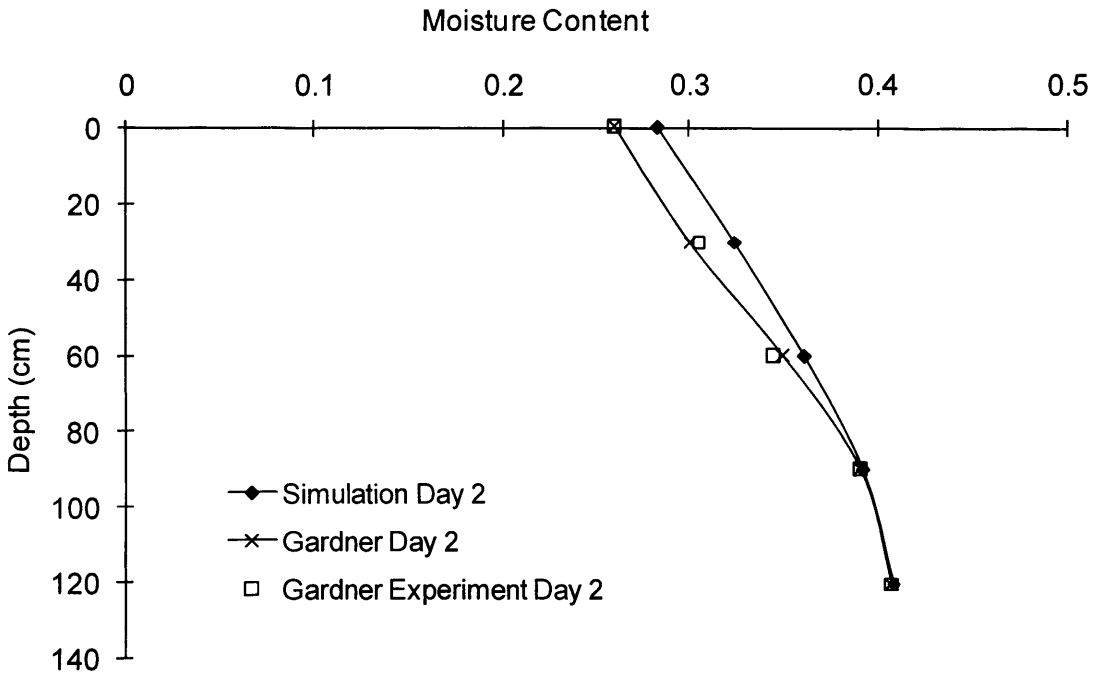

Figure 5.12 Simulated Moisture Profiles at Day 2

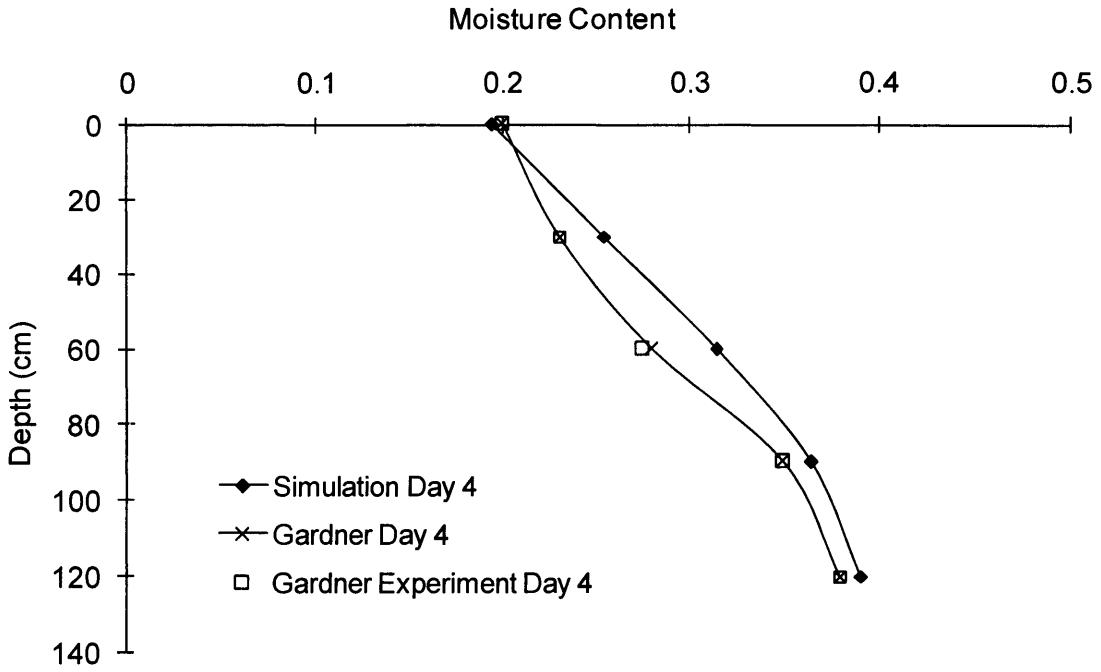

Figure 5.13 Simulated Moisture Profiles at Day 4

As expected by definition, these figures also illustrate that the simulated profile is roughly linear compared to the non-linear profile predicted by Gardner. The difference between the simulated (new) result and Gardner's results is approximately 23.0 % when considering the total volume of water extracted from the soil at day 4. The difference is primarily due to the fact that the current model employs a linear distribution of water uptake, whereas Gardner's approach permits a non-uniform extraction of water to be accommodated. This illustrates a potential shortcoming of the current approach for some applications. For circumstances where the exact form of the moisture content profile is not of great importance, the linear model offers simplicity albeit at the cost of some precision.

5.5 CONCLUSIONS

This chapter has presented some initial applications of the new model, operating in one-dimensional mode. The main aim of this work was to provide some confidence with respect to both the implementation of the volumetric sink term and the basic formulation of the water-uptake model. Three specific case studies have been presented for this purpose. The first case illustrated application of the linear water-uptake model to a simple hypothetical test problem. The new model produced results that were generally within 4.0 % of independently simulated results.

The second problem considered the significance of including a water-stress function for water-uptake modelling. The new model performed adequately for this type of problem. The final case study explored a problem involving a non-uniform root system. This problem served to illustrate the extent to which a simple linear approach could be used to model such a case. The linear model again performed adequately, but was, by definition, not capable of accurately representing a non-uniform extraction process. However, for some practical problems the cumulative water uptake predicted by a simple linear model may be adequate.

Overall, the new model as been shown to be capable of producing results that are comparable with independently published results. The implementation of the water-uptake model and the associated sink term therefore appear to have been successfully undertaken.

5.6 REFERENCES

Feddes, R.A. "Water, Heat and Crop Growth. " Agric. Univ. Wageningen, 71– 12, 184, 1971.

Feddes, R. A., Kowalik, P. J., Malink, K. K., and Zaradny, H., "Simulation of field water uptake by plants using a soil water dependent root extraction function." J. Hydro, 31, 13 – 26, 1976.

Gardner, W. R., "Relation of root distribution to water uptake and availability." Agronomy J., 56, 41 – 45, 1964.

Mathur, S., and Rao, S., "Modelling water uptake by plant roots." Journal of Irrigation and Drainage Engineering, 125(3), 159 – 165, 1999.

Mualem, Y. "A new model for predicting the hydraulic conductivity of unsaturated porous media." Water Resour. Res., 12, 513 – 522, 1976.

Prasad, R., "A linear root water uptake model." Journal of Hydrology, 99, 297 – 306, 1988.

Genuchten, V. M. Th. (1980). "A closed form equation for predicting the hydraulic conductivity of unsaturated soils." Soil. Sci. Soc. Am. J., 44, 892 – 898

CHAPTER SIX

TWO-DIMENSIONAL WATER UPTAKE NEAR TREES: PRELIMINARY ANALYSIS

6.1 INTRODUCTION

This chapter explores issues related to the numerical simulation of moisture migration patterns in the unsaturated zone and in the vicinity of mature trees. The research is based on the development of the unsaturated flow equation to incorporate a sink term and water uptake model. In particular, the axi-symmetric form of the model presented in Chapters 3 and 4 is employed here. The approach adopted utilizes radial symmetry and assumes a linear distribution of water extraction rates with both depth and radius.

The model is validated by direct comparison to field measurements recorded by others. In particular, numerical simulations of two field experiment are presented, namely:

- Simulation 6-1 – Mature Lime tree located on Boulder Clay.
- Simulation 6-2 – Mature Leyland Cypress tree located on Gault Clay.

In both cases, non-linear hydraulic properties have been estimated from independent published data. In recognition of the importance of the soil properties, a parametric sensitivity study has been undertaken for Simulation 6-1. In the first instance, the simulations presented here cover only a spring/summer drying period. Since there is considerable similarity in the approach adopted and the results generated for both simulations, Simulation 6-2 is presented in relatively less detail than Simulation 6-1.

In order to assess the performance of the new model, ideally extensive field data is required. Since the work is aimed at simulation of behaviour in the vicinity o mature trees, field data is needed over a considerable time frame. In this respect, the most comprehensive field experiments found were carried out by Biddle (1998). A brief general description of Biddle's methodology is provided below prior to consideration of each individual field experiment used to assess the performance of the new model.

6.2 BIDDLE'S FIELD EXPERIMENTS

Biddle provides a comprehensive analysis of how the interaction of trees, soils and water can cause foundation movement and damage to buildings. To date, no other publication provides a similar level of detail on this subject. Biddle's work included the measurement of patterns of soil moisture variation, both spatially and with time. A total of 60 trees were studied, covering a range of tree species and soil types. All of these studies were undertaken in simple open field sites, where there were none of the potential complications which occur in the urban situation (i.e. effects of building foundations, water supply, trenches for underground services, drainage systems and hard surfaces). Soil moisture contents were measured using a Neutron Probe or Neutron Soil Moisture Gauge. The probes were based on designs developed at the Institute of Hydrology (Bell, 1976) and are known as Wallingford Neutron Probes.

Typically Biddle measured soil moisture content using around five neutron probe access tubes positioned at various distances from the trees. The field measurements started in 1978 and were completed by 1985. The information obtained from the project was used as the main source of data by the National House Building Council (NHBC) for its Practice Note 3 "Building near Trees".

The resulting two volume publication on Biddle's work provides a comprehensive treatise on the subject. It contains much, but not all, of the field data collected over this period along with many useful insights regarding the observations made. The publication also provides a useful summary of the key relevant hydrological processes involved.

6.3 SIMULATION 6-1 – MATURE LIME TREE ON BOULDER CLAY

6.3.1 Site Description

The particular experimental data set chosen for analysis is based on the field measurements undertaken at a site located at Stacey Hall, Wolverton, England. The case considered here relates to a single mature lime tree, 15 m in height, located on a Boulder Clay sub-soil. Field observations were available for the period January 1979 to April 1980. The Neutron Probe access points for the moisture content measurements were placed in a line to the South West of the tree. Measurements were taken at distances of 1.4 m, 3.0 m, 4.9 m, 10.0 m and 30.0 m from the tree. Details of the soil profile at these locations are shown in Figure 6.1 and Table 6.1. The current work will consider the readings taken at distances of 1.4 m and 4.9 m from the tree in some detail. These measurements were thought to provide reasonable detail for an assessment of the new model. Biddle does not provide all of the data acquired in his publication – therefore some selectivity for this purpose was unavoidable.

Figure 6.1 shows that the ground conditions at the site consist of a layer of topsoil, approximately 0.3 m thick, underlain by a 3 m thick layer of Boulder Clay. Biddle (1998) indicates that for all cases the shallowest reading for soil moisture content is at depth of 0.3 m. Readings at shallower depths than this were not practicable given the dimensions of the probes and disturbance related to inserting the access tubes. No specific information was available on the soil profile below 3 m depth. However, the field measured data indicate that all of the seasonal variation in moisture content of interest here occurred above this depth.

At this site, tree roots were found to be located mostly below 0.3 m depth from the ground surface. Generally, tree roots frequently extend beyond the rooting depth of grasses and crops (Buresh and Tian, 1998, Dawson et al, 2001, Moreno et al, 2005).

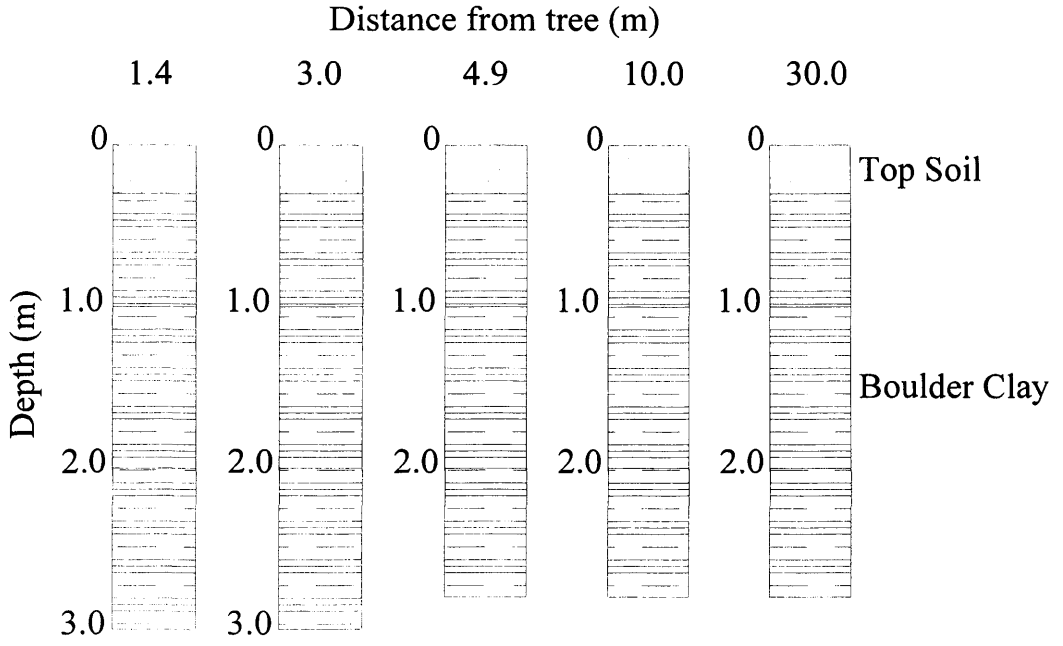

Figure 6.1 Soil Profile at site, modified after Biddle (1998)

Table 6.1 Soil profile detail at 1.4m and 3.0m from tree, modified after Biddle (1998)

Distance from tree (m)	1.4	3.0	3.0	3.0
Depth (m)	2.0	1.0	1.5	2.0
Plastic Limit	29	18	17	17
Liquid Limit	45	36	36	34
Plasticity Index	16	18	19	17

Some grass cover was evident over this particular site. Normally grass roots are shallow in depth ranging from 0.15 m to 0.35 m depth and widespread near the ground level (Karen and Phillip, 1999, Tufekcioglu et al, 1999, Polley et al, 2002). Nisbet (2005) claimed that trees also use more water than most other types of vegetation – including grass. Therefore, no further consideration to the effect of the surrounding grass is given at this stage of the work.

6.3.2 Lime Trees

The Lime Tree under consideration is 15m tall and close to edge of a field grazed by horses. The tree can be considered as a single tree, as the neighbouring trees are sufficiently far away to have negligible effect on local soil moisture patterns. A typical lime tree is shown in Figure 6.2.

Figure 6.2 Typical lime tree, after Derbaum (2005)

The Lime Tree or "*Tilia x europaea*" is a common broadleaved tree which can be found in the United Kingdom. This tree has been selected for consideration here since it has been widely planted in avenues on estates, in streets, parks and large gardens (SAPS, 2007). Figure 6.3 shows that this species of tree can be found throughout much of the United Kingdom.

Figure 6.3 Allocation of Lime Trees in the UK, after SAPS (2007)

Common Lime is a tall, deciduous tree (lose their leaves in autumn), with arching lower branches. It can grow to heights of up to 24 m (Cutler and Richardson, 1989). The old bark (outermost layer of stems and roots) is grey and fissured and

punctuated by irregular bosses. The leaves, which are heart-shaped with a drawn-out pointed tip, are 5-10 cm long. They are dark green and hairless above, but have tufts of white hairs at the junctions of the veins below. The margins have small, sharp teeth, whilst the leaf-stalks are 3-5 cm long. The leaves often have blisters on the upper surface, caused by sap-sucking insects. The leaves are shown in Figure 6.4.

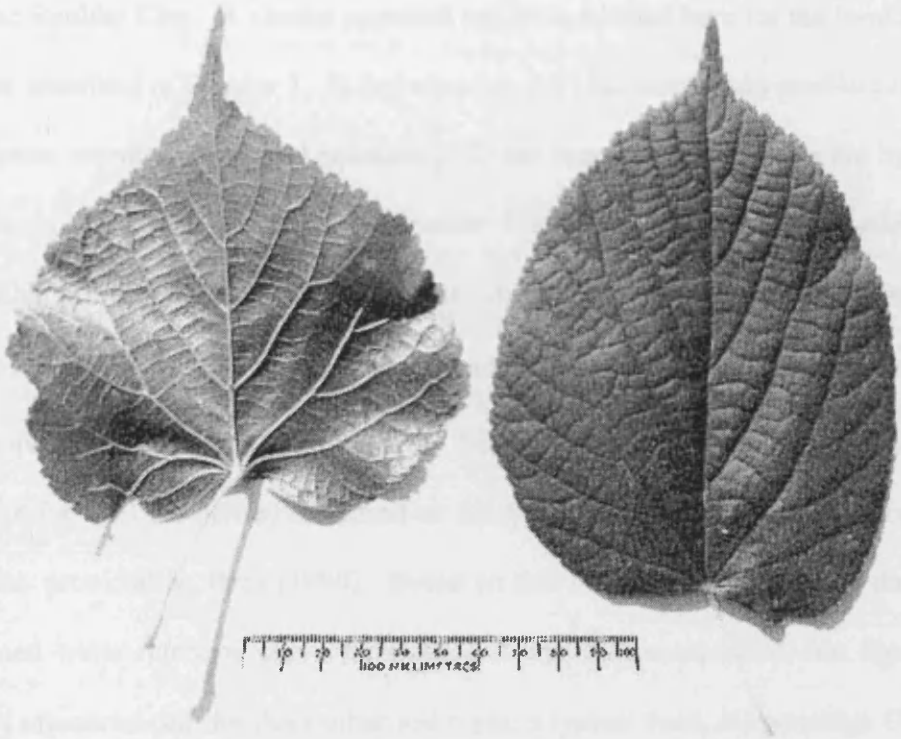

Figure 6.4 Lime Leaves, after SAPS (2007)

6.3.3 Hydraulic Properties of Boulder Clay

In the first instance the soil profile is assumed to be a homogenous layer of Boulder Clay. Although the moisture flow model is capable of representing more than one soil type, an attempt is made to keep the model as simple as possible. This is recognised as a limitation of the following simulation. However, extension of the

work will be attempted later (Chapter 8) to link this type of simulation with slope stability analysis. Therefore, simplification of the soil profile, where acceptable, offers significant advantages at this early stage of the research programme.

Application of the proposed model requires specification of the water retention curve (hence specific moisture capacity) and the hydraulic conductivity relationship for the Boulder Clay. A similar approach has been adopted here for the Boulder clay as that described in Chapter 5. In fact equation (5.1) has been again used to determine the water retention curve and equation (5.2) has been used to estimate the hydraulic conductivity. To apply these for Boulder Clay, reference has been made to the available published data for this material. A summary of the relevant properties is shown in Table 6.2. The values of θ_r and θ_s have been taken directly from the measured moisture profiles provided by Biddle (1998). The remaining parameters (except for K_s – see below) are based on the typical shape of a water retention curve for clay provided by Rees (1990). Based on this information, Figure 6.5 shows the assumed water retention curve for Boulder Clay. For comparison, the figure also shows measured data for three other soil types: a typical Sand, Kimmeridge Clay and typical Loam (Rees, 1990). The overall set of results would appear to suggest that the assumed relationship for Boulder Clay is within the range of previously published data for this soil type.

Table 6.2 Assume soil properties for Boulder Clay

θ_r	θ_s	K_s (m/s)	α	l	n	m
0.1	0.4	1×10^{-6}	0.0280	0.5	1.4	0.29

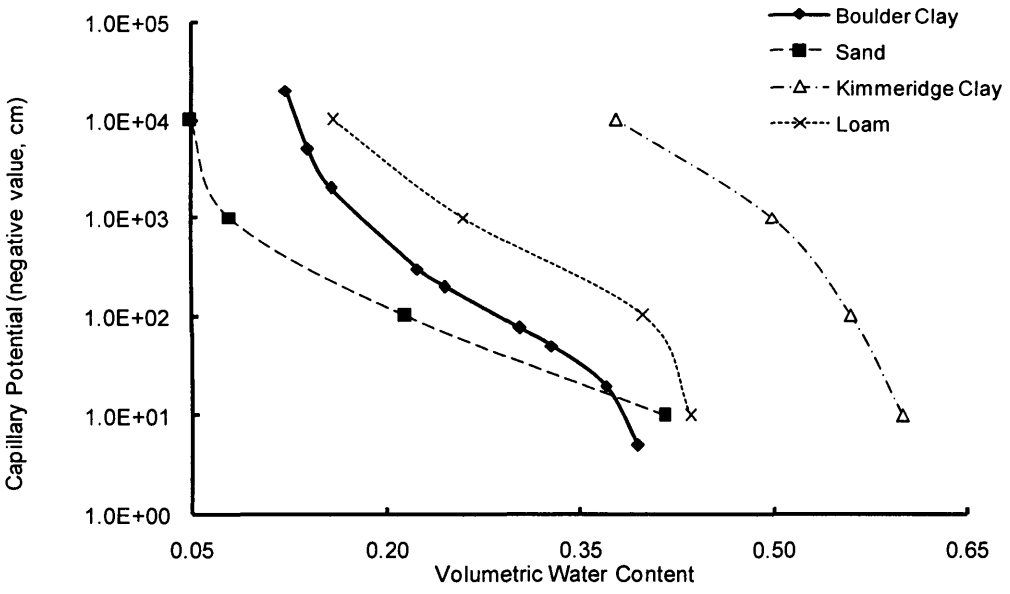

Figure 6.5 Water Retention Curve for Boulder Clay

Figure 6.6, shows that a similar approach has been adopted to approximate the hydraulic conductivity of Boulder Clay. The saturated hydraulic conductivity, K_s for Boulder Clay can range from 1 x 10^{-6} m/s to 1 x 10^{-9} m/s based on independent data published in the literature as shown in Table 6.3. In this study, the saturated hydraulic conductivity of the Boulder clay was taken as 1 x 10^{-6} m/s since this was the value that Biddle viewed as most representative of this location.

Table 6.3 Saturated Hydraulic Conductivity for Boulder Clay

Authors	Hydraulic conductivity, K_s (m/s)
Wilcock and Essery (1984)	1.6×10^{-7}
Jackson and Rushton (1987)	1×10^{-9}
Bouma et al (1989)	3.475×10^{-8}
Biddle (1998)	1×10^{-6}

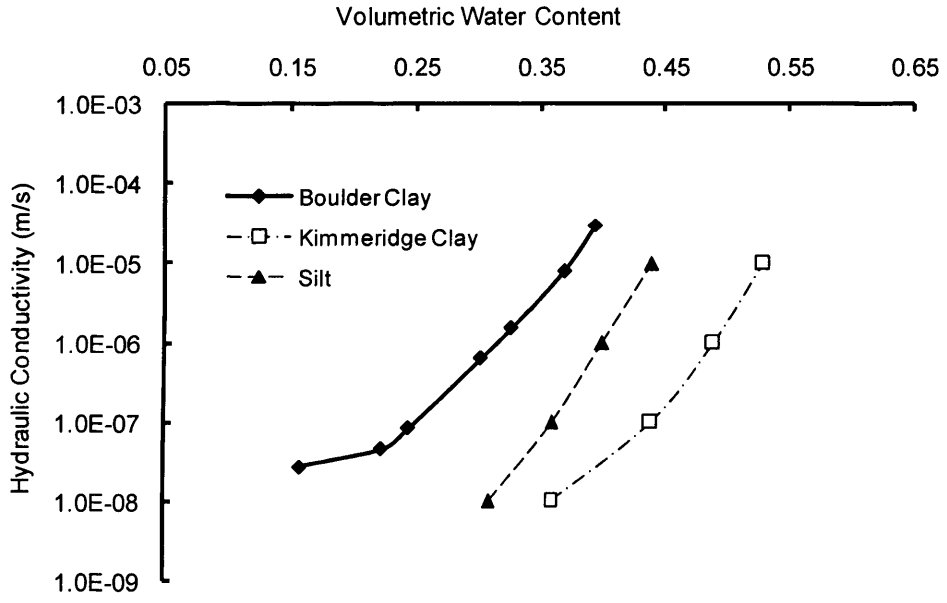

Figure 6.6 Hydraulic Conductivity for Boulder Clay

The first problem under consideration is one of soil drying only. Therefore any hysteresis that may occur in the water retention characteristics of the Boulder clay will be not be significant in this case. However, this aspect of soil behaviour is given some consideration in Chapter 7. Furthermore, the sensitivity of the results to the assumed relationships above is considered further in section 6.3.6 of this Chapter.

6.3.4 Discretisation, Boundary Conditions and Initial Conditions

Figure 6.7 shows a diagrammatic representation of the tree, the extent of the root zone and the domain size employed. Based on the field observations, the root zone is assumed to extend a depth of 2 m and a radial distance of 5 m. The overall size of the finite element domain is 10 m x 10 m.

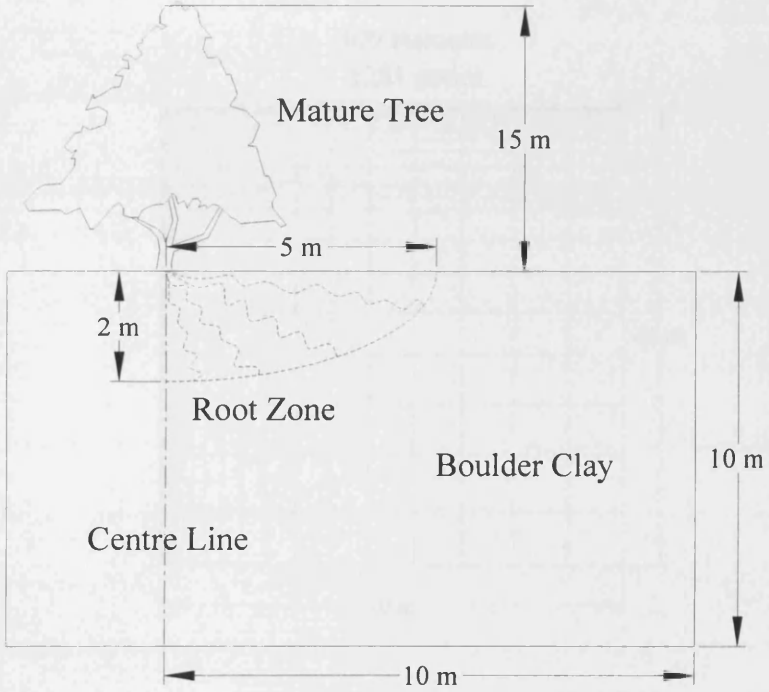

Figure 6.7 Axi-symmetric Domain

Spatial discretisation has been achieved via the finite element mesh shown in Figure 6.8. The mesh consists of four hundred, eight-node isoparametric elements with 1281 nodes. The mesh was configured to offer some refinement within the root zone area since this is the region where the most significant moisture content variations were expected to occur. Preliminary numerical tests were conducted to

ensure for this domain size, the outer boundaries do not significantly influence the simulated results within the region of interest. The simulation employs a time-step size of 21600 seconds, which was held constant for the entire period considered. Preliminary checks were made to ensure that the solution is both time-step and spatially converged.

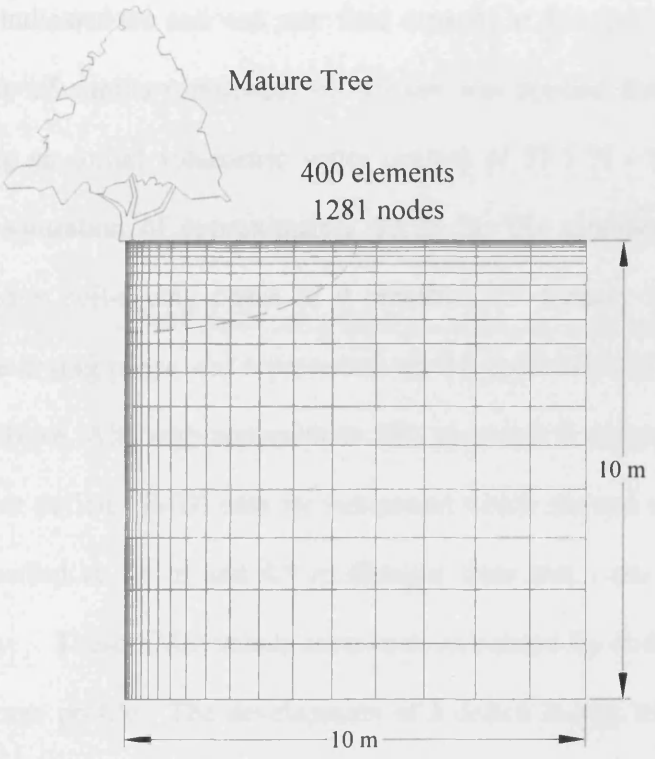

Figure 6.8 Finite Element Mesh

Biddle's work indicated that for a mature tree in Southern England, the transpiration rate can typically reach 5 mm/day. This value has therefore been used to define the transpiration rate employed in this simulation. The information previously presented in Chapter 2, Table 2.3, would appear to suggest that 5 mm/day is within the range of previously published data. This value was distributed throughout the

root-zone via application of the water-uptake model described in Chapter 3. The pressure head dependent reduction factor $\alpha(\psi)$ was assumed to be constant at a value of 1.0 (see Figure 3.7). This value ensures that optimal water extraction was possible throughout the simulation period (Feddes et al., 1978).

The initial conditions employed for the simulation were based on the measured moisture content profile for the start date of the period considered. In fact the profile indicated the soil was near field capacity at this time. Therefore a uniform initial value of capillary potential of -20 cm was applied throughout the domain, representing an initial volumetric water content of 37.5 % - this corresponds to a degree of saturation of approximately 93.75 %. The simulated period covered a spring/summer soil-drying phase of 9 months (23rd January 1979 to 24th October 1979). The drying phase was represented via the application of the transpiration rate described above. Although approximate, this approach is supported by the available soil moisture deficit (SMD) data for this period which showed a continuous decrease over this period at 1.4 m and 4.9 m distance from tree - see Figure 6.9 and 6.10 respectively. These SMD values have been calculated by Biddle by reference to a spring average profile. The development of a deficit during the season is shown to occur at depths of 0.3 m, 1.0 m and 2.0 m below ground level.

In Figure 6.9, the soil moisture deficit at 0.3 m below ground level indicated that there was wetting period in the soil between July 1979 and August 1979. This profile indicates some seasonality in the soil profile. This aspect of behaviour is considered in more detail in Chapter 7. The lower boundary of the domain and the far-field vertical boundary were unconstrained (natural) throughout the simulation.

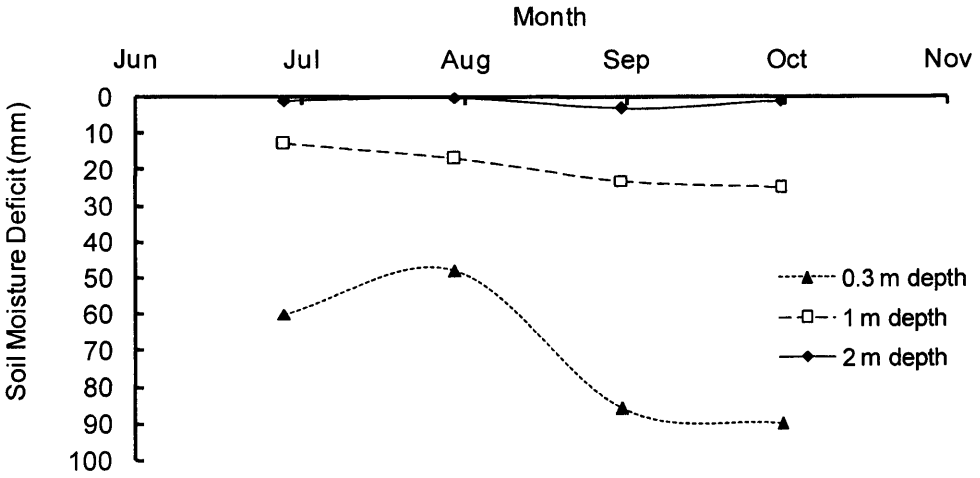

Figure 6.9 Soil Moisture Deficit at 1.4 m distance from tree

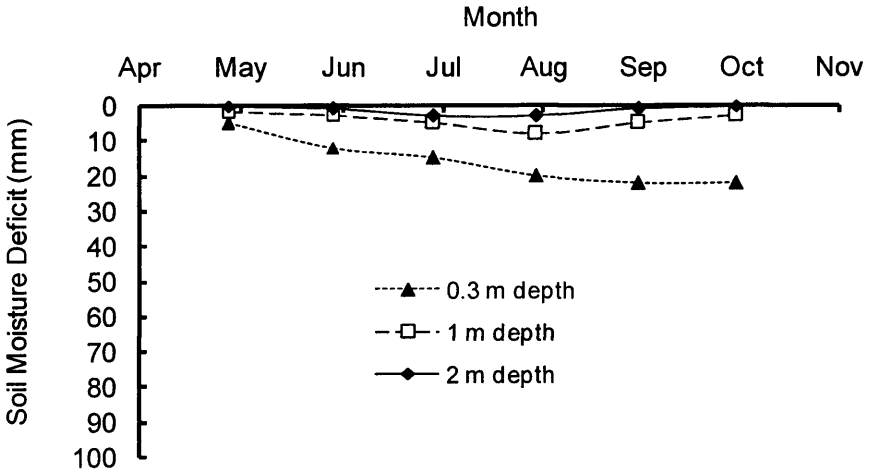

Figure 6.10 Soil Moisture Deficit at 4.9 m distance from tree

6.3.5 Results

The numerical model, presented in Chapter 4, produces results in terms of capillary potential (with respect to space and time). It is believe that formulating the moisture flow equation in this manner is important since it maintains compatibility with deformation models and also avoids possible discontinuity problems that may arise when a moisture content based formulation is employed for more than one soil type. However, for ease of discussion and to facilitate direct comparison between simulated and field measured data, the results of the simulation have been converted to volumetric moisture content. This was done making use of the mathematical equation for the water retention curve for Boulder Clay, presented above in Figure 6.5 (i.e. equation 5.1 – employing the parameters given in Table 6.2).

Figures 6.11, 6.12 and 6.13 show predicted and measured moisture content profiles at a radial distance of 1.4 m from the centre-line of the tree, and at times of 190 days, 238 days and 270 days respectively. These times relate to the specific dates of 02/08/79, 21/09/79 and 24/10/79 respectively. Field data was only available at a limited number of dates; however, the results shown serve to illustrate the overall behaviour at the site. Figures 6.14 to 6.16 show the corresponding moisture content profiles at a distance of 4.9 m from the tree. The results achieved are also plotted as direct transient variations in Figure 6.17 to 6.22. Finally, two typical contour plots are shown in Figure 6.23 and 6.24. These results are considered in some detail below.

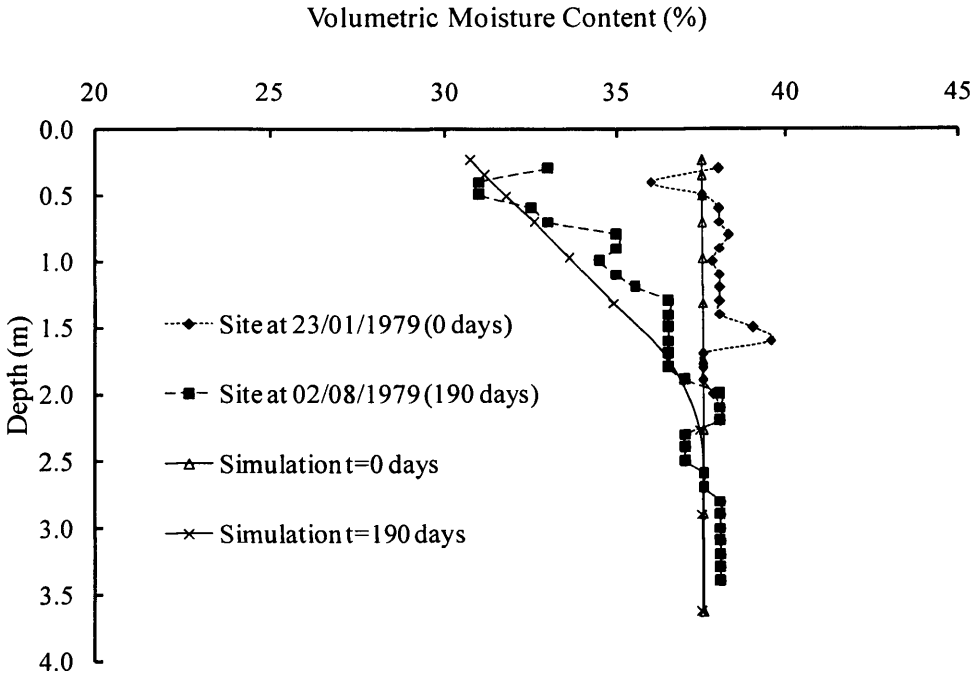

Figure 6.11 Simulated and Measured Moisture Content Profiles (Time 190 days, Radial Distance 1.4 m)

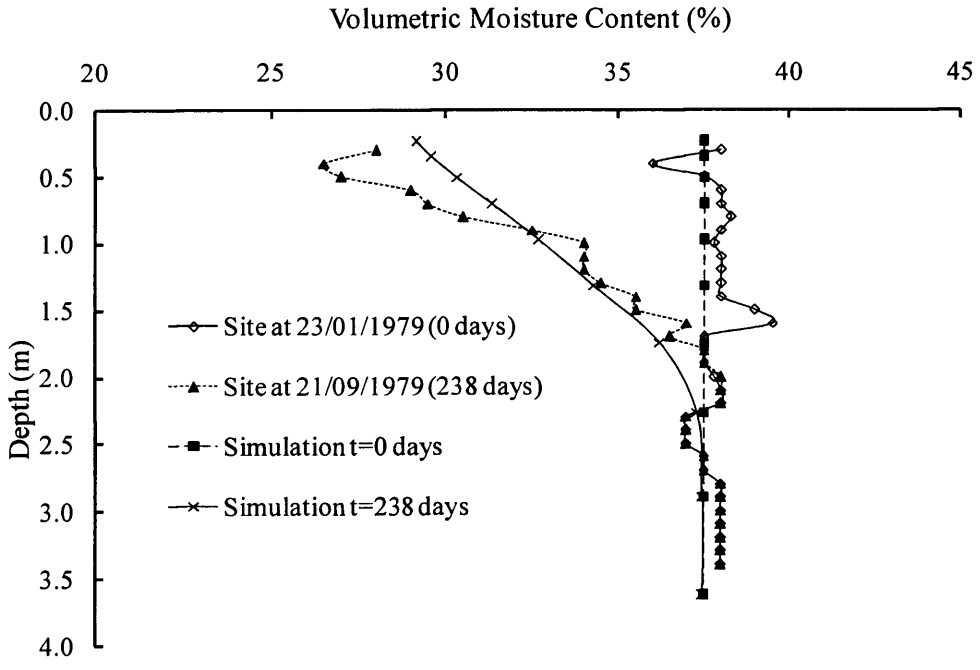

Figure 6.12 Simulated and Measured Moisture Content Profiles (Time 238 days, Radial Distance 1.4 m)

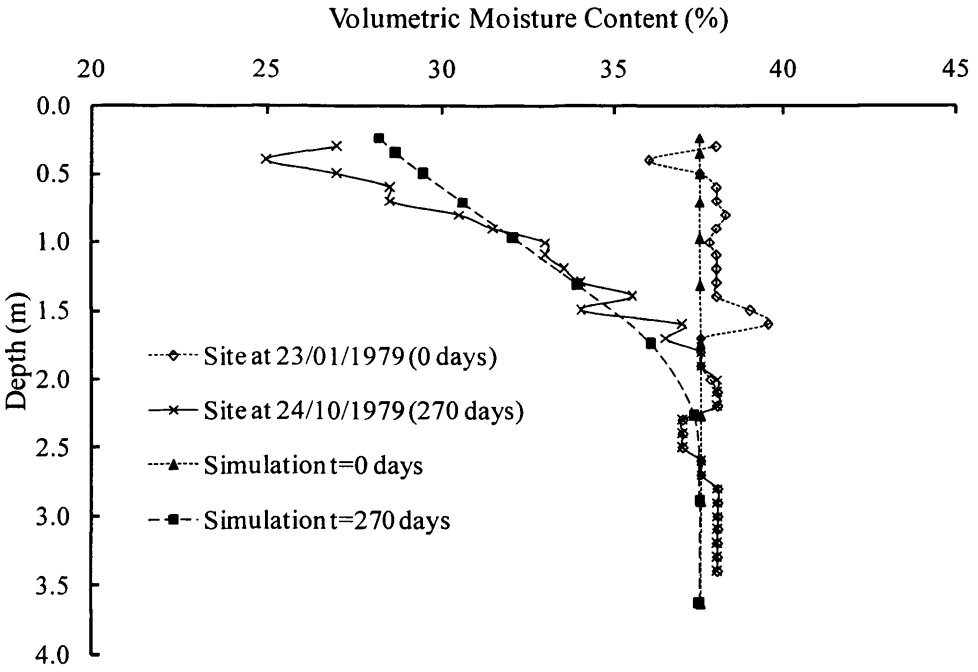

Figure 6.13 Simulated and Measured Moisture Content Profiles (Time 270 days, Radial Distance 1.4 m)

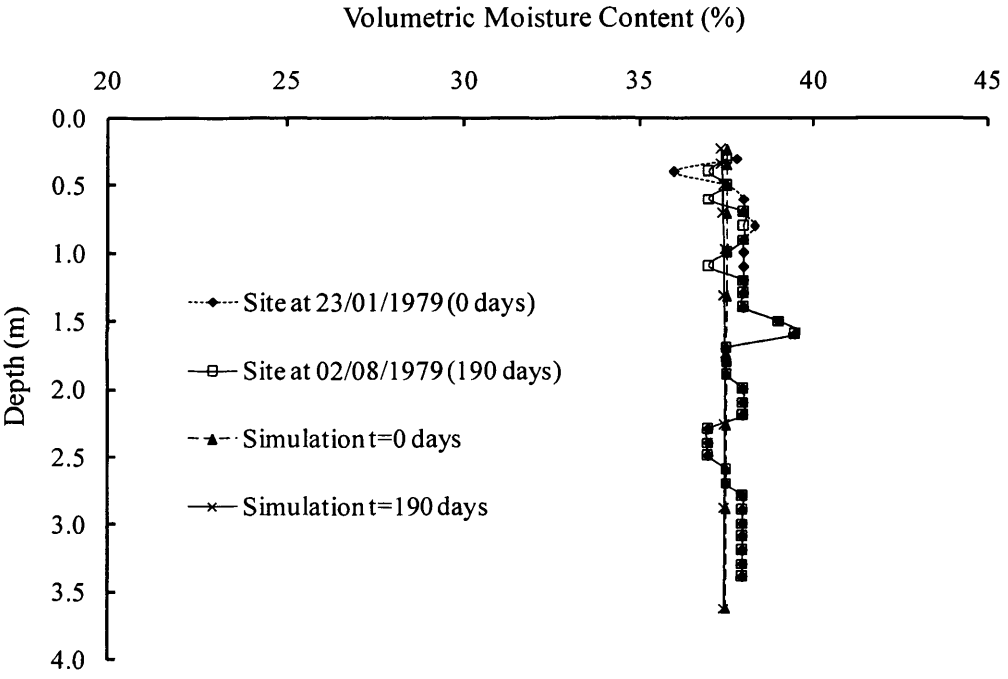

Figure 6.14 Simulated and Measured Moisture Content Profiles (Time 190 days, Radial Distance 4.9 m)

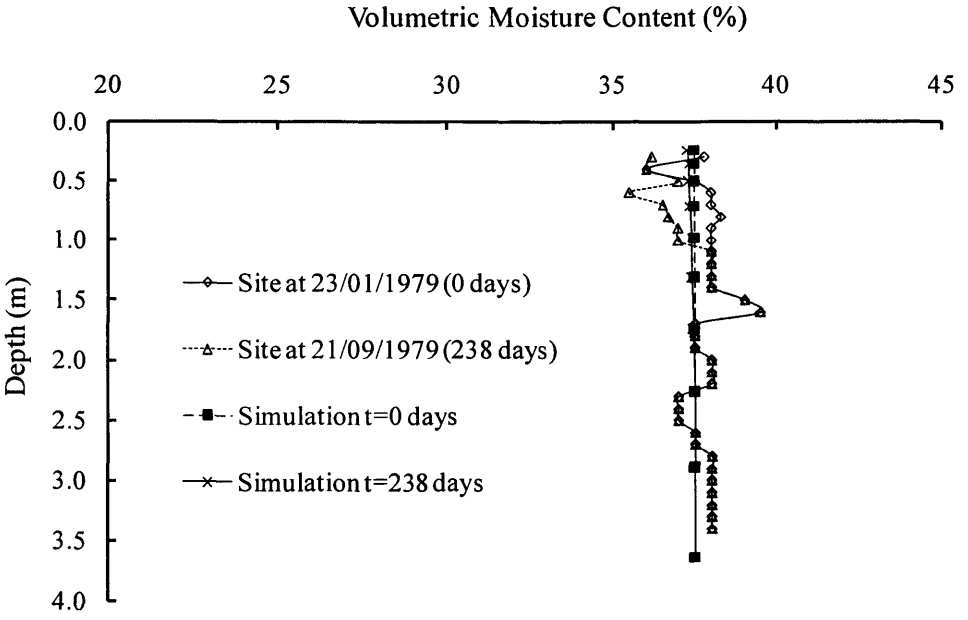

Figure 6.15 Simulated and Measured Moisture Content Profiles (Time 238 days, Radial Distance 4.9 m)

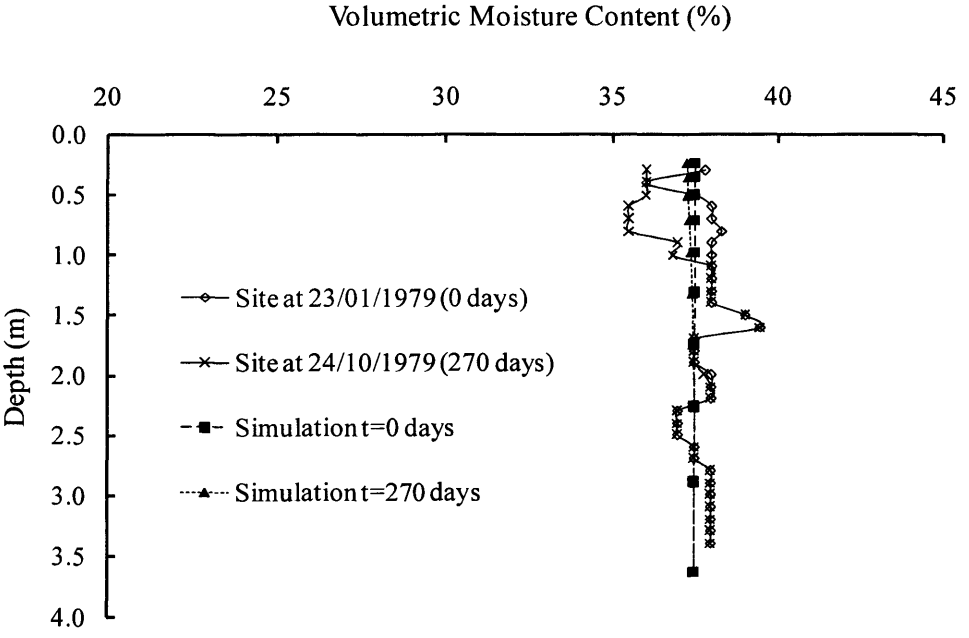

Figure 6.16 Simulated and Measured Moisture Content Profiles (Time 270 days, Radial Distance 4.9 m)

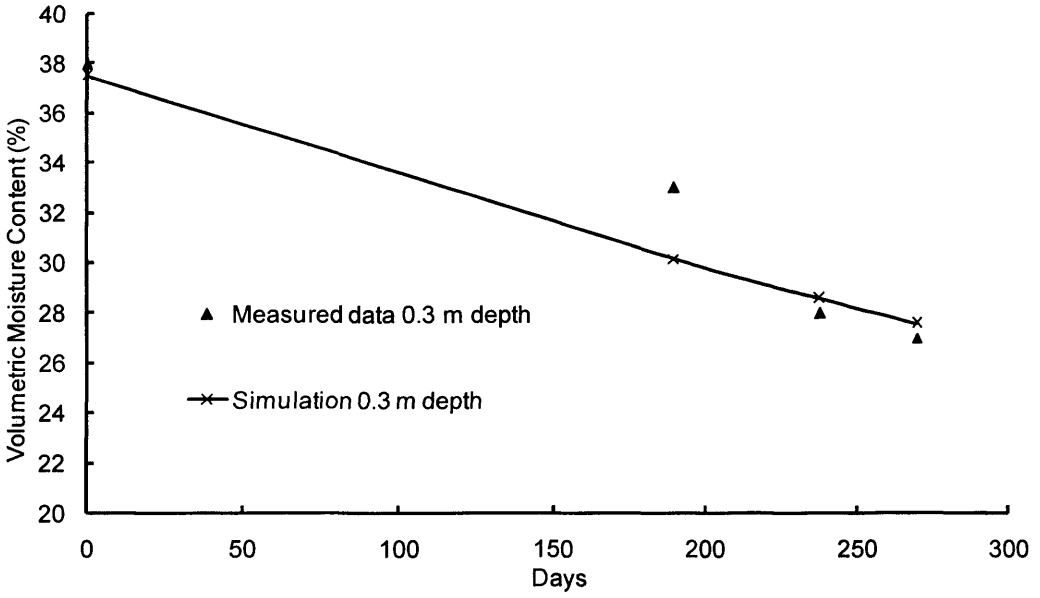

Figure 6.17 Simulated and Measured Transient Moisture Content Variation (Depth 0.3 m, Radial Distance 1.4 m)

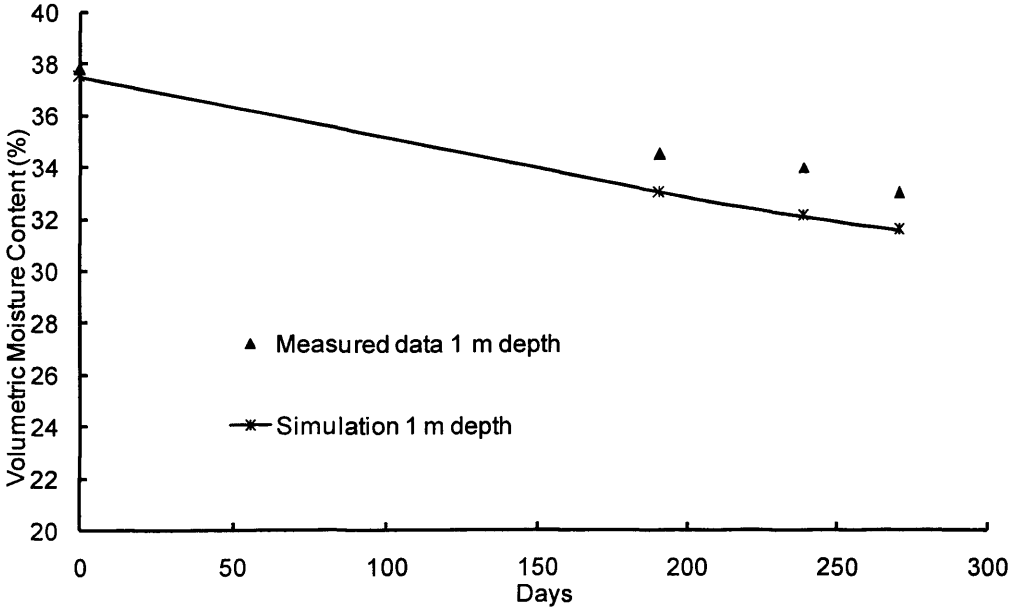

Figure 6.18 Simulated and Measured Transient Moisture Content Variation (Depth 1 m, Radial Distance 1.4 m)

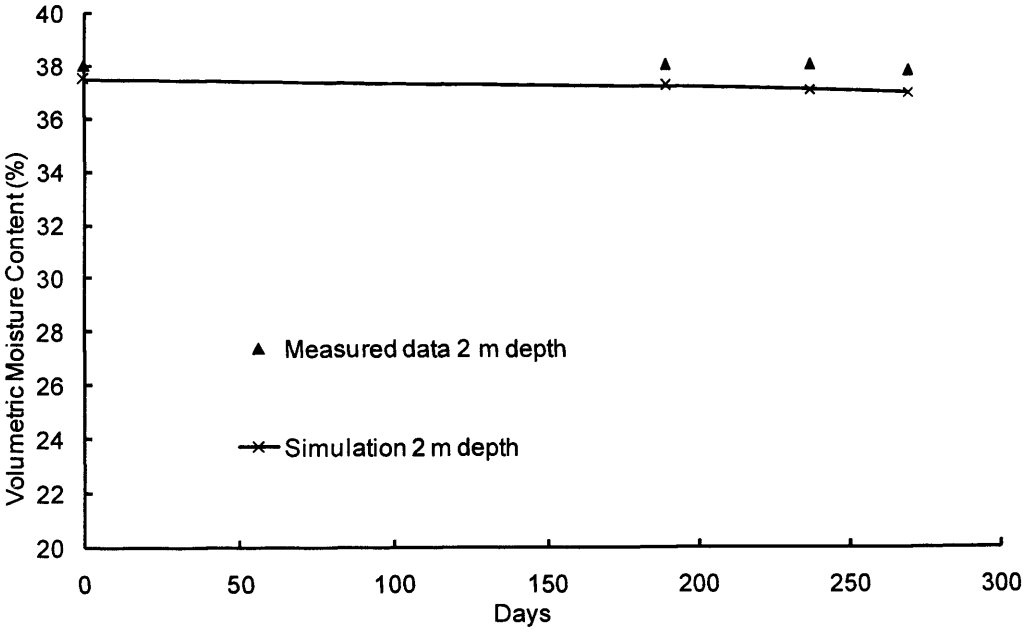

Figure 6.19 Simulated and Measured Transient Moisture Content Variation (Depth 2 m, Radial Distance 1.4 m)

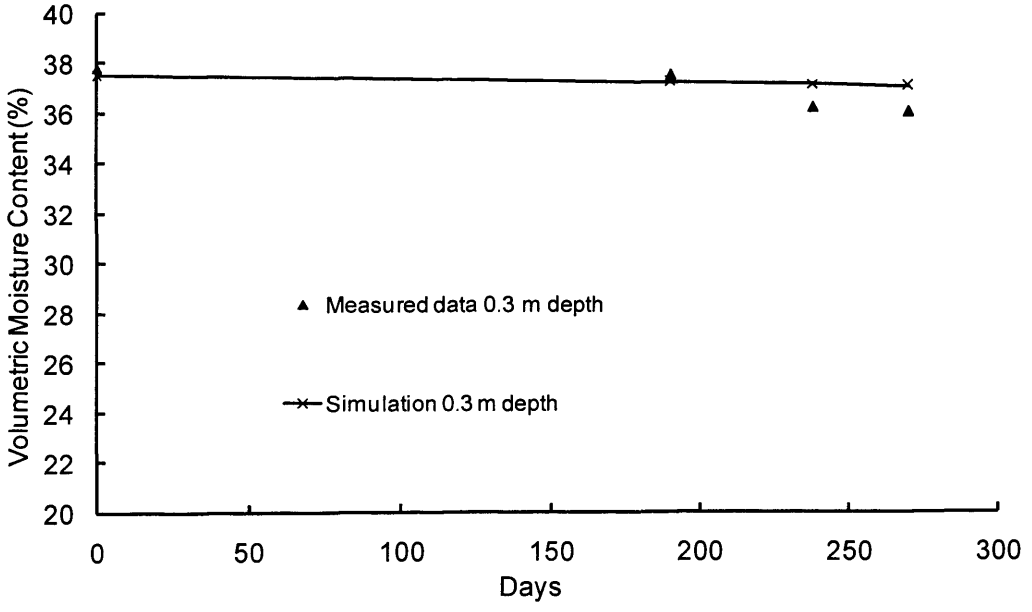

Figure 6.20 Simulated and Measured Transient Moisture Content Variation (Depth 0.3 m, Radial Distance 4.9 m)

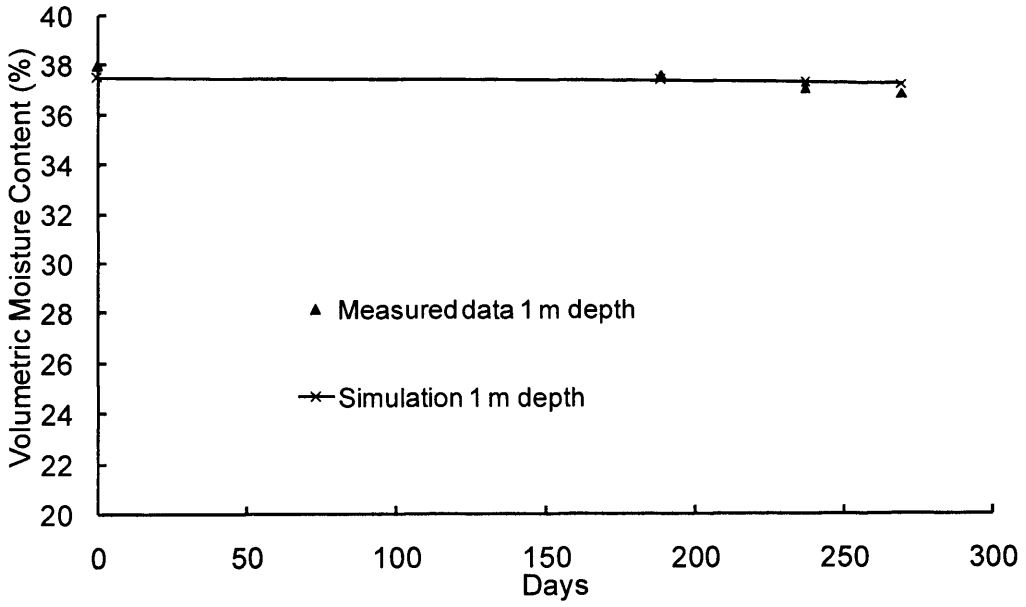

Figure 6.21 Simulated and Measured Transient Moisture Content Variation (Depth 1 m, Radial Distance 4.9 m)

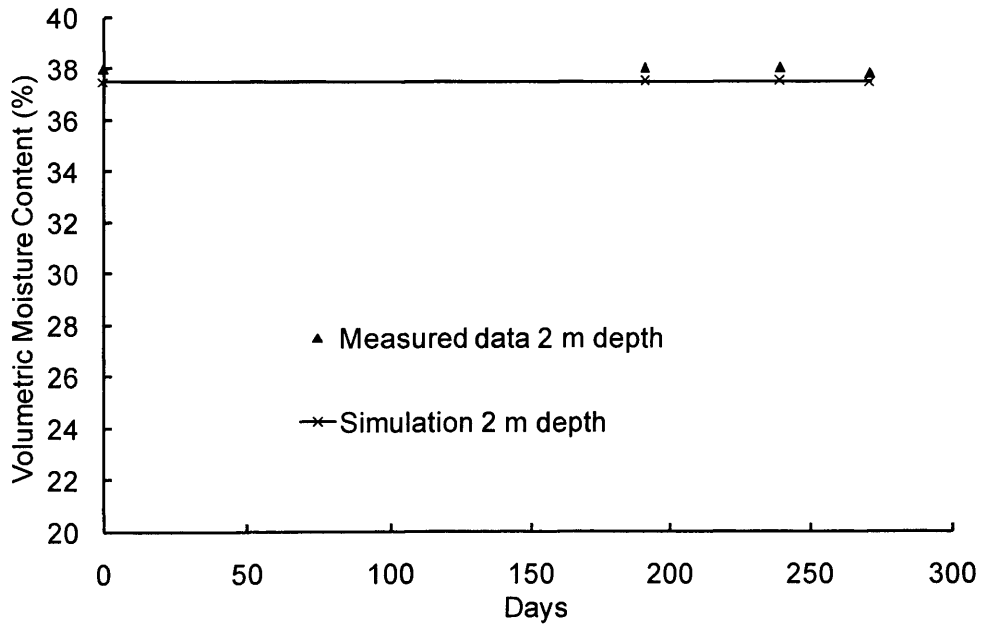

Figure 6.22 Simulated and Measured Transient Moisture Content Variation (Depth 2 m, Radial Distance 4.9 m)

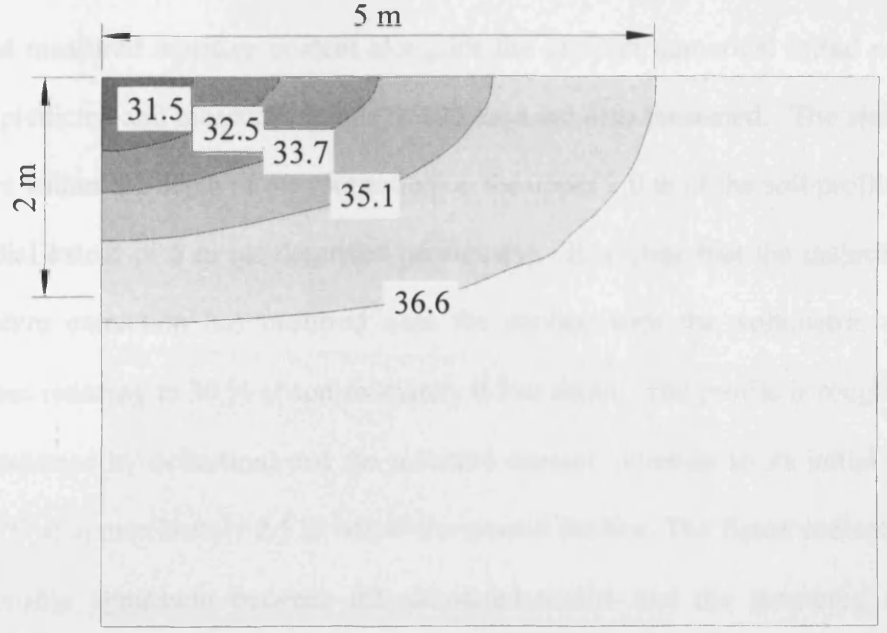

Figure 6.23 Volumetric moisture content (%) Contours at 190 days

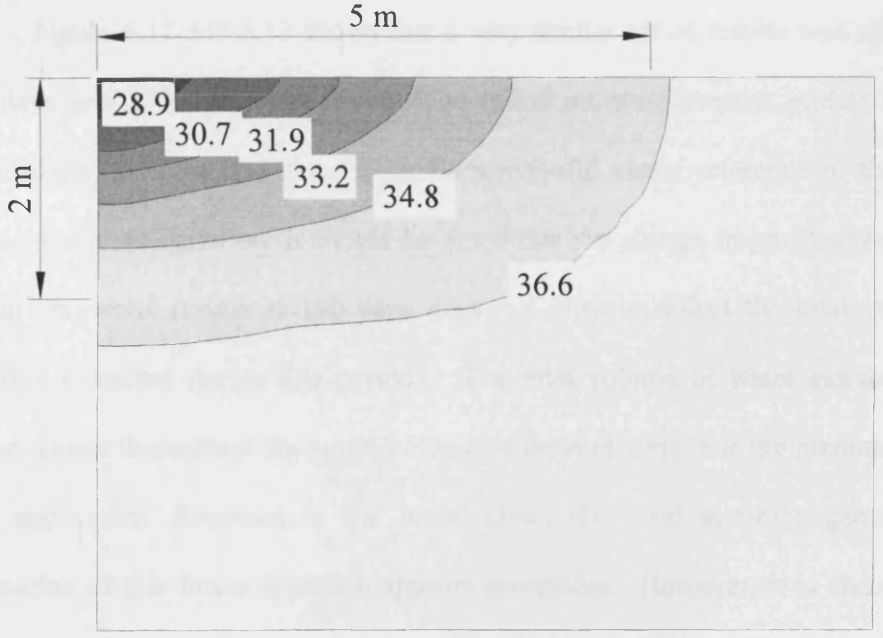

Figure 6.24 Volumetric moisture content (%) Contours at 270 days

First considering predicted moisture content profiles. Figure 6.11 shows the initial measured moisture content alongside the uniform numerical initial condition. The predicted and measured results at 190 days are also presented. The sink term is active within the depth of the root zone (i.e. the upper 2.0 m of the soil profile) and to a radial extent of 5 m (as described previously). It is clear that the majority of the moisture extraction has occurred near the surface with the volumetric moisture content reducing to 30 % at approximately 0.3 m depth. The profile is roughly linear (as expected by definition) and the moisture content increases to its initial value of 37.5 % at approximately 2.5 m below the ground surface. The figure indicates that a reasonable agreement between the simulated results and the measured moisture profiles has been achieved. It was found that the difference between the two set of results was generally less than 5 %.

Figure 6.12 and 6.13 shows that a very similar set of results was obtained at 238 days and 270 days respectively. The initial moisture content profile has been included on this plot also since it provides a useful visual reference of the overall moisture content variation. It should be noted that the change in profiles shown here and the previous results at 190 days does not directly reflect the total volume of moisture extracted during this period. The total volume of water extracted is of course spread throughout the entire volume of the root-zone. For the medium to long term application discussed in the introduction, the level accuracy generated by application of this linear approach appears acceptable. However, it is clear that the linear model does not precisely distribute moisture content in exactly the same manner observed in the field. Figures 6.14 to 6.16 show the corresponding set of results achieved remote from the tree. At a radial distance of 4.9 m it is clear that the tree roots have relatively little effect on the seasonal moisture depletion. In general, a

good agreement between simulated and measured profiles is also achieved at this distance, with errors ranging between 0.9 % and 1.7 %.

Figures 6.17 to 6.19 show the moisture content variation plotted directly against time at depths 0.3 m, 1.0 m and 2.0 m below the surface and at a radial distance of 1.4 m from the tree. The measured data is simply plotted as discrete data points at the times when measurements were recorded on site. Numerical results can be output at any number of time intervals hence a continuous variation has been plotted for comparison. Figure 6.19 is consistent with the moisture content profiles shown previously and indicates that relatively little moisture variation occurred at (and below) a depth of 2.0 m. The overall predicted trend appears to be in fair agreement with the measured data. Figures 6.20 to 6.22 show a corresponding set of results at a radial distance of 4.9 m from the trees. At this distance from the tree very little change in moisture content occurred. These results serve to show that the geometry of the root-zone assumed in the simulation appears reasonable.

Figures 6.23 to 6.24 present the simulated contours of volumetric moisture content (%) generated by the simulation at 190 days and 270 days respectively. These figures provide further illustration that the approach adopted has produced an overall moisture pattern similar to that observed in the field.

6.3.6 Parameter Sensitivity Study

The water retention curve in Figure 6.5 and hydraulic conductivity in Figure 6.6 were based on a number of assumptions as explained in section 6.3.3 of this Chapter. Given the importance of these parameters on the results generated, a sensitivity check has been made to ensure the assumptions made were reasonable. To do this, an alternate water retention curve relationship was considered. This is shown in Figure 6.25. Figure 6.26 indicates that there are no significant changes in hydraulic conductivity relationship if the alternate water retention curve is employed. Therefore, this sensitivity study only considers changes in water retention curve and still employs the original hydraulic conductivity relation based on Figure 6.6.

The above simulation has been re-run employing this alternative set of material properties and the results achieved (time at 270 days and radial distance at 1.4 m) are shown in Figure 6.27. From this figure, the percentage of error is 9 % when comparing the results based on the initial assumptions with the results from the alternate material properties. The alternate material properties were simply chosen to show sensitivity of the simulation to the exact form of the parameters used. The resulting variation is not particularly drastic, indicating that the initial assumptions are reasonably robust and that the accuracy of results achieved are not overly influenced by parameter selection.

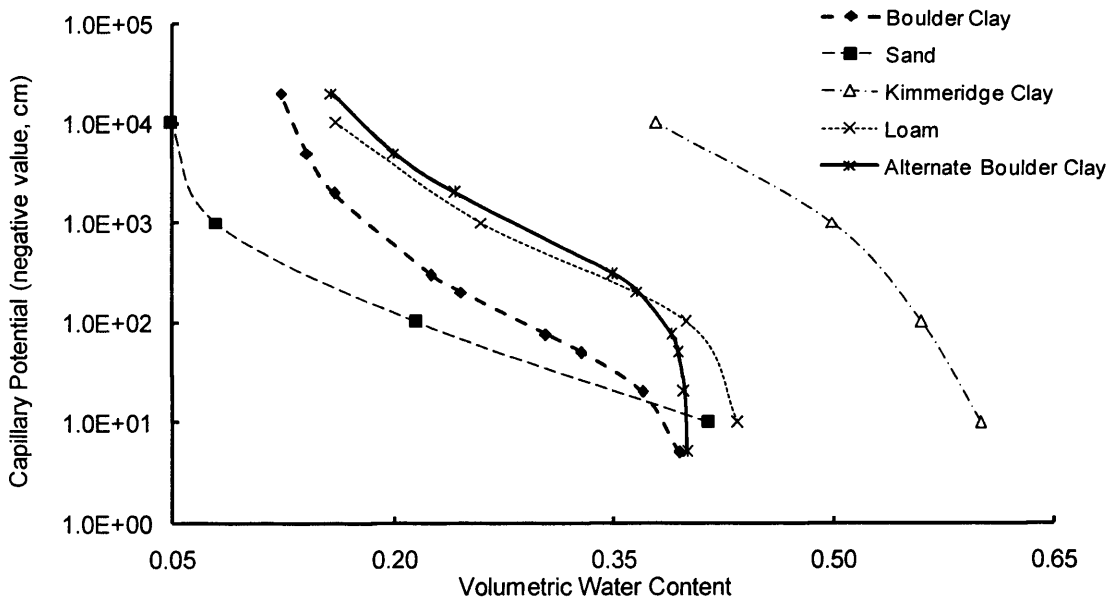

Figure 6.25 Water Retention Curve for Alternate Boulder Clay

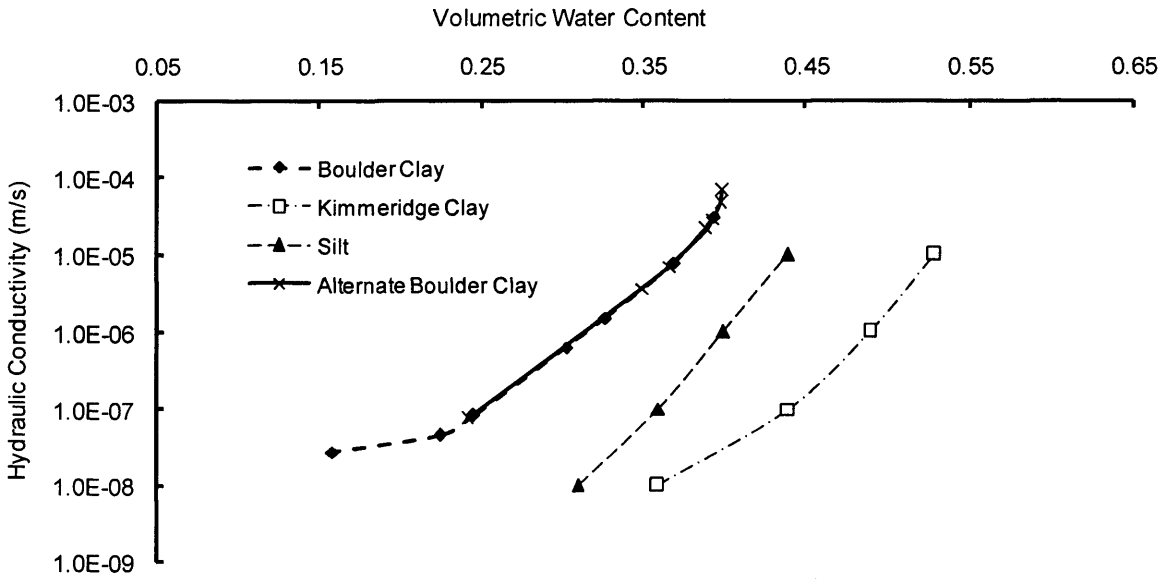

Figure 6.26 Hydraulic Conductivity for Alternate Boulder Clay

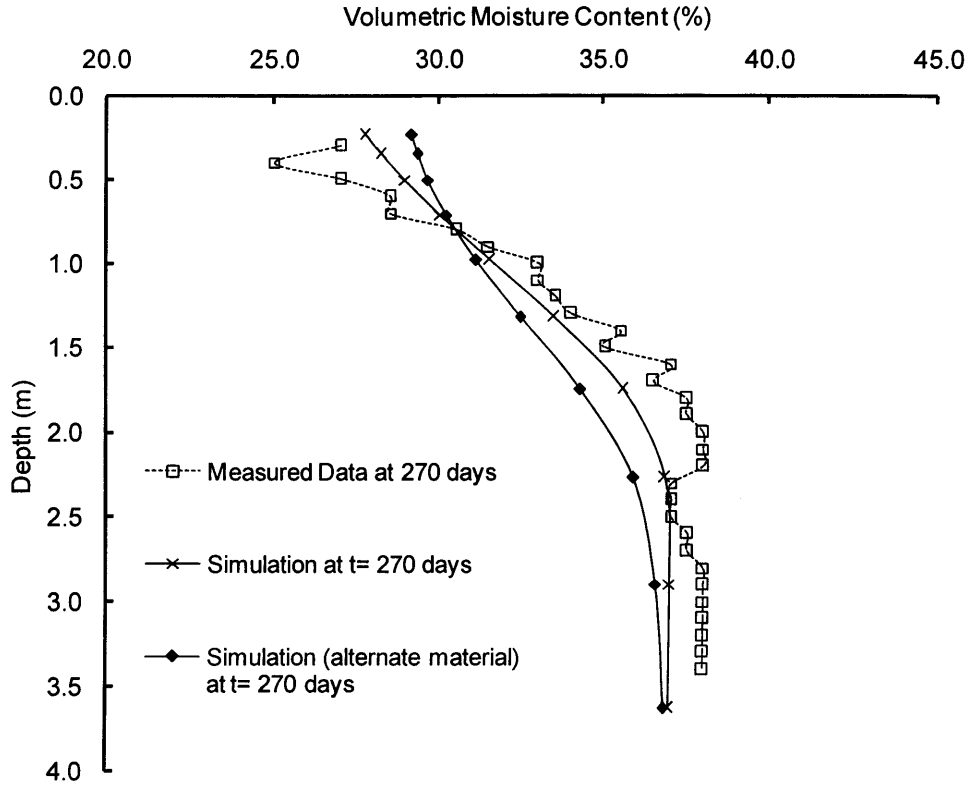

Figure 6.27 Comparison using alternate material properties (Time 270 days, Radial Distance 1.4 m)

6.4 NUMERCAL SIMULATION 6-2 – LEYLAND CYPRESS ON GAULT CLAY

6.4.1 Site Description

The particular experimental data set chosen for second analysis is based on the field measurements undertaken at a site located at Corpus Christi College, Cambridge, England. The data was recorded in the vicinity of a single Leyland Cypress tree (a conifer) 10 m in height and located on a Gault Clay sub-soil. Field observations were available from February 1981 to October 1981. The Neutron Probe access points for the moisture content measurements were placed in the lush mown grass of the playing field in a line to the South East of the tree. Measurements were taken at distances of 1.5 m, 3.0 m, 5.0 m, 7.5 m and 20.0 m from the tree. The current work will only consider the readings taken at distances of 1.5 from the tree in some detail. Biddle does not provide all of the data acquired in his publication – therefore some selectivity for this case was unavoidable.

6.4.2 Leyland Cypress Trees

Leyland Cypress or "*Cupressocyparis leylandii*" is a large evergreen tree that forms a graceful pyramid, with dense pendulous branches and fine, feathery foliage. This tree will grow 18 to 21 m tall and 4 to 6 m wide (CLEMSON, 2007). This foliage, on flattened branches and is dark green or blue-green in colour. This is a fast-

growing evergreen when young and will quickly outgrow its space in small landscapes. This tree has been selected for consideration here since it has been widely planted for quick screens, hedges and groupings, especially on large properties. Although Leyland cypress can be sheared into a tall screen on small lots, it is most effective when allowed to develop into its natural shape. Regular trimming is necessary to retain a formal hedge, screen or windbreak. It grows well in clay soil and tolerates poor drainage for only a short period of time. The typical Leyland Cypress tree is shown in Figure 6.28.

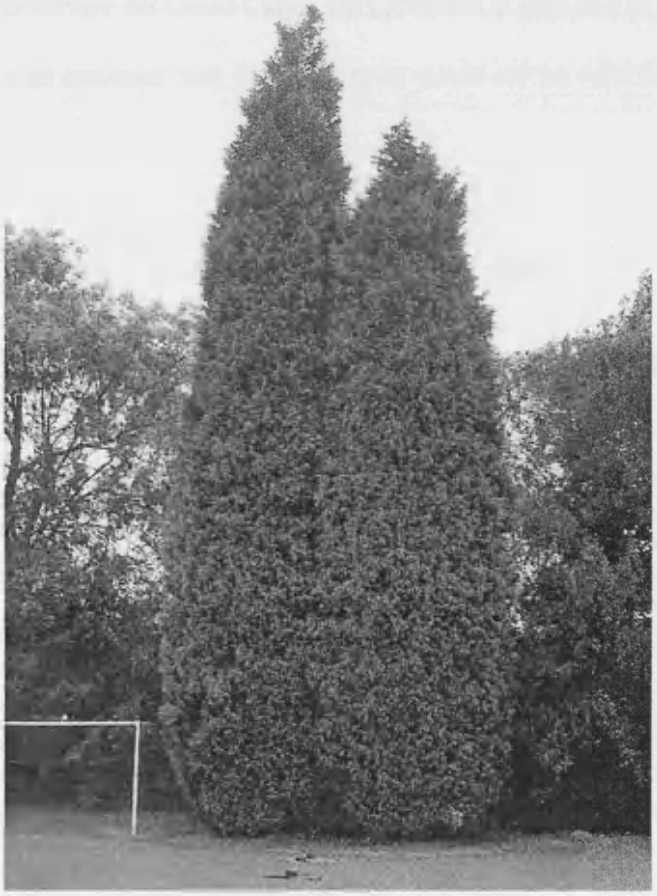

Figure 6.28 Typical Leyland Cypress tree, after Biddle (1998)

6.4.3 Hydraulic Properties of Gault Clay

This simulation also used equation (5.1) and equation (5.2) for estimation of the water retention curve and the hydraulic conductivity relationship for Gault Clay. The values of θ_r and θ_s are approximated from the measured moisture profiles. The remaining parameters (except for K_s) are based on the typical shape of a water retention curve for this clay provided by Croney (1977). The saturated hydraulic conductivity, K_s of the Gault clay was taken as 1 x 10^{-6} m/s based on Biddle's data. Figure 6.29 and 6.30 show the assumed water retention curve and hydraulic conductivity respectively for Gault Clay. This problem is also one of seasonal drying; therefore it was also assumed here that hysteresis would not be relevant.

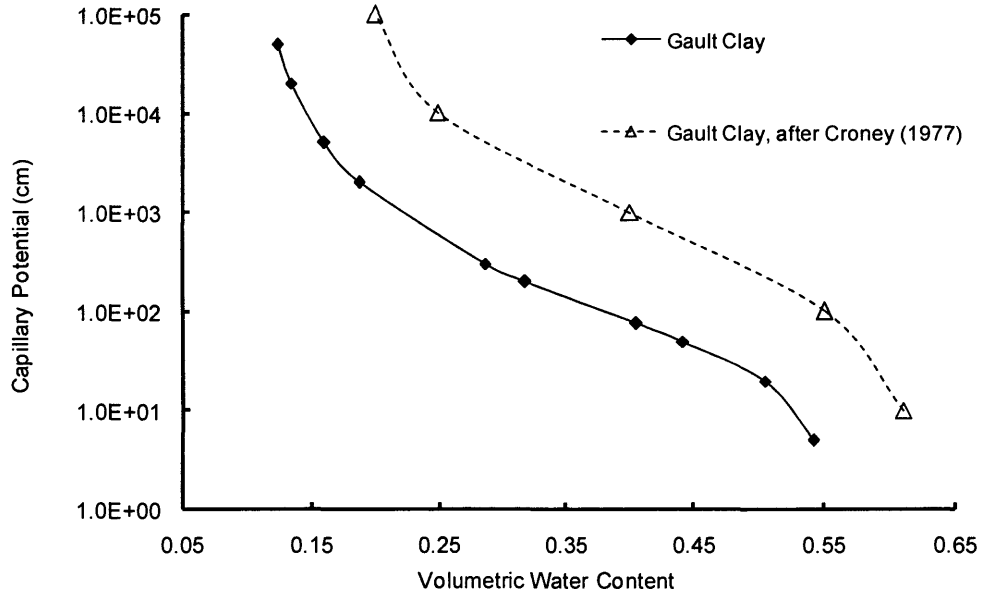

Figure 6.29 Water Retention Curve for Gault Clay

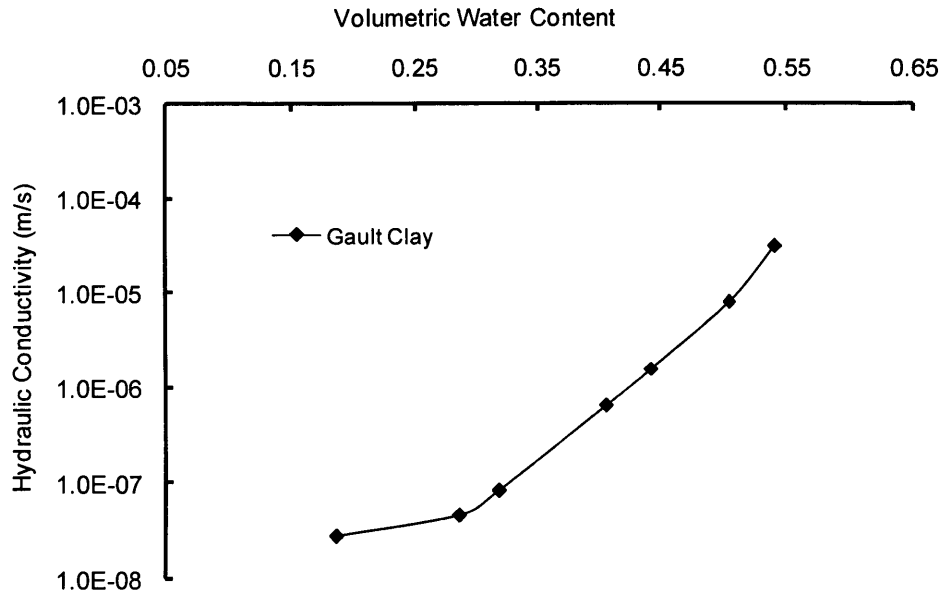

Figure 6.30 Hydraulic Conductivity for Gault Clay

6.4.5 Discretisation, Initial Conditions and Boundary Conditions

Based on the field observations provided by Biddle (1998), the root zone is assumed to extend a depth of 1.0 m and a radial distance of 5.0 m. A similar finite element mesh as used in Simulation 6-1 (see Figure 6.8) is employed here. The overall size of the finite element domain is again 10 m x 10 m. The mesh analyzed consisted of four hundred, eight-node isoparametric elements with 1281 nodes. Once again, preliminary numerical tests were conducted to ensure for this domain size, the outer boundaries do not significantly influence the simulated results within the region of interest.

The simulation also employs a time-step size of 21600 seconds, which was held constant for the entire period considered. Again, a preliminary check has been

made to ensure that the solution is time-step converged. As in first case, the transpiration rate was assumed to be 5 mm/day. For the reason explained in section 6.3, the pressure head dependent reduction factor, $\alpha(\psi)$ was assumed constant at a value of 1.0.

The initial conditions employed for the simulation were based on the experimental moisture profile at the start of the period considered. The non-uniform initial values of capillary potential were applied throughout the domain as shown in the results section below (see Figure 6.31). The simulated period covered a spring/summer soil-drying phase of 8 months (7th February 1981 to 8th October 1981). The drying phase was represented via the application of the transpiration rate described above. The lower boundary of the domain and the far-field vertical boundary remained unconstrained (natural) throughout the simulation.

6.4.6 Results

Figure 6.31 shows the initial measured moisture content alongside the numerical initial condition. The predicted and measured results at the end of drying period (240 days) at a radial distance of 1.5 m from the centre-line of the tree are also presented.

It is clear that the majority of the moisture extraction at 240 days has occurred near the surface with the volumetric moisture content reducing to 22 % at approximately 0.3 m depth. The moisture content increases to its initial value of 50 % at approximately 1.5 m below the ground surface.

The figure indicates that a reasonable agreement between the simulated results and the measured moisture profiles has been achieved. It was found that the difference between the two set of results was generally less than 5 %, yielding further confidence in the implementation of the approach.

Field data was only available at the start and at the end of simulation period; therefore, transient variations cannot be presented here.

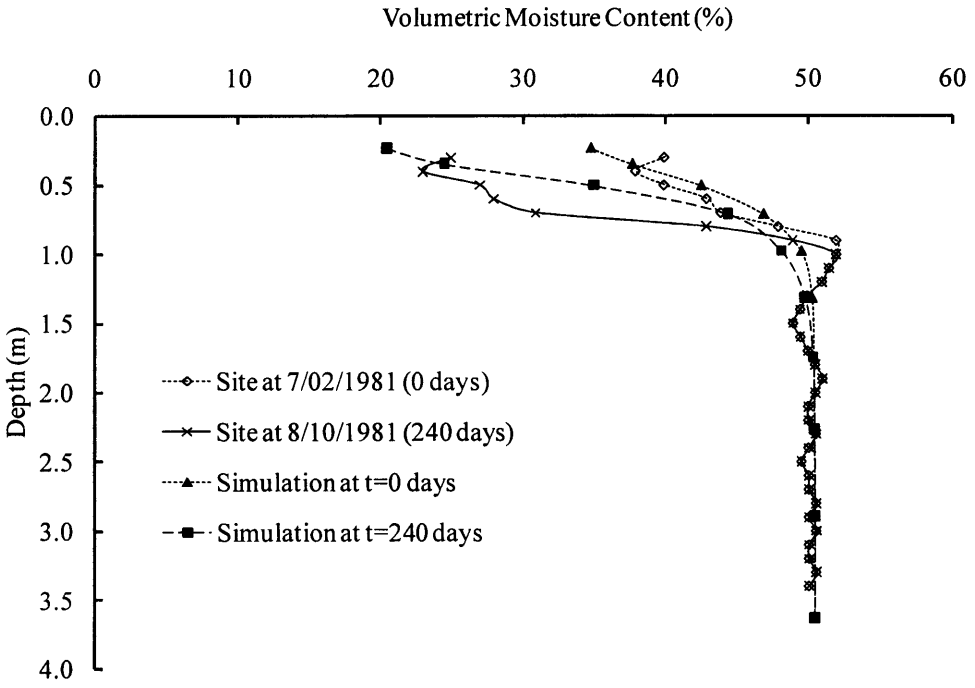

Figure 6.31 Simulated and Measured Moisture Content Profiles (Time 240 days, Radial Distance 1.5 m)

Figures 6.32 present the simulated contours of volumetric moisture content generated at the end of simulation (240 days). This figure provides further illustration that the approach adopted has produced an overall moisture pattern that appears similar to that observed in the field.

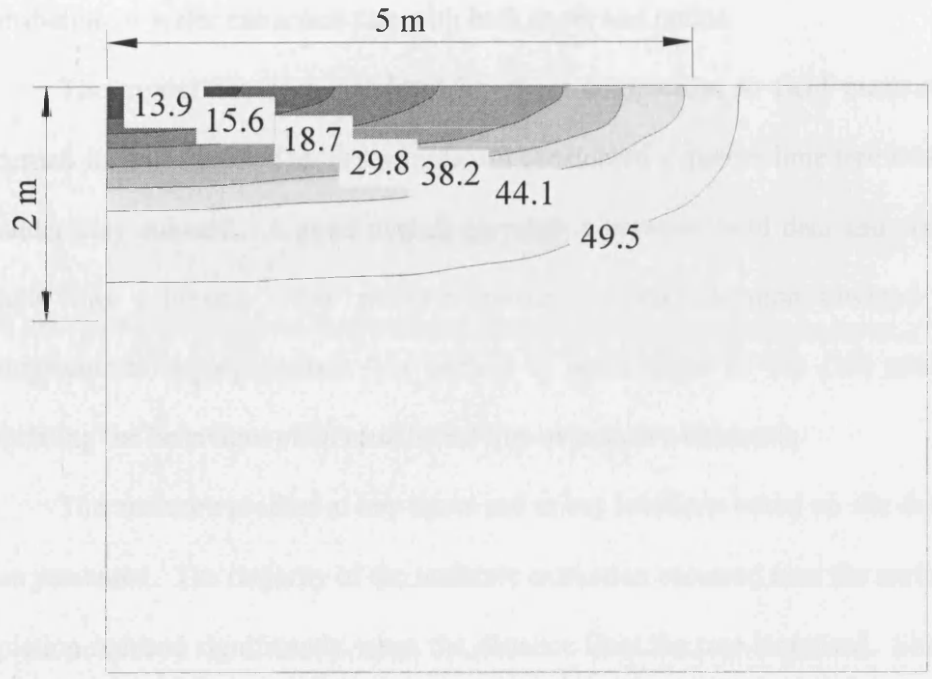

Figure 6.32 Volumetric moisture content (%) Contours at 240 days

6.5 CONCLUSIONS

The application of the new model for the simulation of moisture migration patterns near trees has been presented in this chapter. Particular attention is given to prediction of moisture content variations in the unsaturated zone and in the vicinity of a single mature tree. The approach proposed utilizes radial symmetry and a linear distribution of water extraction rate with both depth and radius.

The model has been validated by direct comparison to field measurements recorded for two cases. The first simulation considered a mature lime tree located on Boulder clay sub-soil. A good overall correlation between field data and simulated results was achieved. The problem chosen for consideration covered a full spring/summer drying period. As such it is believed to be the first attempt at simulating the behaviour of an established tree over such a timescale.

The moisture profiles at key times and at key locations based on site data have been presented. The majority of the moisture extraction occurred near the surface and depletion reduced significantly when the distance from the tree increased. Simulated contours of volumetric moisture content generated were also presented. These served to illustrate that an overall moisture pattern similar to that observed in the field was produced by the proposed approach.

A second numerical simulation has also been presented to show application of the model for a different tree species and soil type. In this case, a mature Leyland Cypress tree located on Gault clay was analysed. Although the results were presented in less detail than the first simulation, overall quite good agreement with the available field data was also achieved in this case.

A sensitivity check has been made in this Chapter to ensure the assumptions made in relation to the water retention and hydraulic conductivity relationships were reasonable. The simulation was re-run with alternate material properties to investigate this issue. The difference in results was found to be relatively small (9 %). Therefore, the assumed material properties were thought to be acceptable for use in this simulation work.

To provide some confidence in the implementation of the approach, the model also has been validated by a second comparison to field measurements recorded for a mature Leyland cypress tree located on Gault clay soil. The problem chosen for consideration covered a full spring/summer drying period. A good overall correlation between field data and simulated results has been achieved where the difference between the two set of results was less than 5 %. Simulated contours of volumetric moisture content generated by the simulation were presented that produced an overall moisture pattern similar to that observed in the field.

6.6 REFERENCES

Bell, J. P. "Neutron Probe Practice." Institute of Hydrology, Wallingford, 1976.

Biddle, P. G., "Tree Root Damage to Buildings." Willowmead Publishing Ltd, Wantage, 1998.

Buresh, R. J. & Tian, G. "Soil improvement by trees in sub-Saharan Africa. " Agroforestry Systems, 38: 51–76, 1998.

Bouma, J., Jongmans, A. G., Stein, A., and G. Peek, "Characterising Spatially Variable Hydraulic Properteis of a Boulder Clay Deposit in the Netherlands." Geoderma, 45, p19-29, 1989.

CLEMSON. "Home & Garden Information Center - Leyland Cypruss. " http://hgic.clemson.edu/factsheets/hgic1013.htm. Clemson University cooperating with U.S. Department of Agriculture, South Carolina, 2007.

Cutler, D. F., and Richardson, I. B. K., "Tree roots and buildings.", Longman Scientific and Technical, Singapore, 1989.

Croney, D. " The design and performance of road pavements. " Pub. London, HMSO, 647, 1977.

Dawson, L.A., Duff, E.I., Campbell, C.D. & Hirst, D.J. "Depth distribution of cherry (Prunus avium L.) tree roots as influenced by grass root competition." Plant and Soil, 231: 11–19, 2001.

Derbaum. " Lime." http://www.flickr.comphotos/derbaum/15318101. Flickr Blog, 2005.

Feddes, R. A., Kowalik, P. J., and Zaradny, H., "Simulation of field water use and crop yield." Wageningen Center for Agriculture and Documentation, Wageningen, 189, 1978.

Jackson, D. and Rushton, K.R. "Assessment Of Recharge Components For A Chalk Aquifer Unit. "Journal of Hydrology, 92, 1 – 15, 1987.

Karen, J. E. & Philip, W. R. " Comparative patterns of phenology and growth form diversity in two winter rainfall deserts: the Succulent Karoo and Mojave Desert ecosystems." Plant Ecology, 142: 97–104, 1999.

Moreno, G., Obrador, J.J., Cubera, E. & Dupraz, C. "Fine root distribution in Dehesas of Central-Western Spain." Plant and Soil, 277:153–162, 2005.

Nisbet, T. R. " Water Use by Trees." Forestry Commission, Edinburgh, 1 – 8, 2005.

Polley, H.W., Hyrum B. J. and Charles R. T. " Woody invasion of grasslands: evidence that CO2 enrichment indirectly promotes establishment of Prosopis glandulosa." Plant Ecology, 164: 85–94, 2002.

Rees, S. W., "Seasonal Ground Movement Effects on Buried Services," PhD, University of Wales, Cardiff, 1990.

SAPS (Science and Plants for Schools). "Common Lime (Tilia x europaea)." Homerton College, Cambridge UK, 2007.

Tufekcioglu, A., Raich, J. W., Isenhart, T. M. and Schultz, R. C. " Fine root dynamics, coarse root biomass, root distribution,and soil respiration in a multispecies riparian buffer in Central Iowa, USA." Agroforestry Systems, 44: 163–174, 1999.

Wilcock, D. N. and Essery, C. I. "Infiltration Measurement in a Small Lowland Catchment." Journal of Hydrology, 74, p 191-204, 1984.

CHAPTER SEVEN

SEASONAL EFFECTS ON WATER UPTAKE NEAR TREES

7.1 INTRODUCTION

This chapter explores some of the issues that arise in relation to seasonal climate variation on moisture migration patterns near mature trees. In Chapter 6, a relatively straightforward simulation was considered to provide a first assessment of the model for a spring/summer drying period only. In this chapter, the work presented previously in Chapter 6 is now extended and developed to explore application of the model to simulate a full annual cycle starting from field capacity in winter, extending through a full spring/summer drying period and including the subsequent autumn recharge.

Section 7.2 considers a simple method of representing time dependent variations in boundary conditions based on daily rainfall patterns. Data from the nearest Meteorological Station to the site under consideration has been used to estimate behaviour at the soil surface. In addition, since the period now considered includes both drying and wetting some consideration is given to the influence of possible hysteresis in the soil water retention curve. Section 7.3 considers this aspect of behaviour. The final section of this chapter attempts to provide an assessment of the refinements undertaken.

Table 7.1 provides a summary of the new simulations presented in this chapter and indicates which particular features are included in each case in comparison with the previous work presented in Chapter 6.

Table 7.1 Summary of the Numerical Simulations

Simulation No	Drying period	Wetting Period	Variation of Boundary Condition	Hysteresis
Simulation 6-1 (see Chapter 6)	Yes	No	No	No
Simulation 7-1	Yes	Yes	Yes	No
Simulation 7-2	Yes	Yes	Yes	Yes

7.2 TIME DEPENDENT BOUNDARY CONDITIONS

7.2.1 Soil Moisture Deficit (SMD)

The particular period now considered for simulation is from 23rd January 1979 to 21st April 1980. The field problem is as previously considered in Chapter 6 (Simulation 6 – 1). For this location, Biddle (1998) provided an estimate of the soil moisture deficit (SMD) variation at distances of 1.4 m and 4.9 m from the tree as shown in Figures 7.1 and 7.2 respectively. The estimate of SMD at 1.4 m from tree was only available from June 1979 to April 1980 whereas at 4.9 m from tree data was available from April 1979 to April 1980. Biddle estimated SMD by comparison with a 3-year averaged spring profile as a control. This approach was claimed to help eliminate random counting errors and the variations which can occur near the surface as a result of the weather conditions immediately prior to readings being taken.

Returning to Figure 7.1, the resulting variation in SMD during the season is shown for depths of 0.3 m, 1.0 m and 2.0 m below ground surface level. Overall, the soil profile appears to have undergone a period of drying up to October 1979. The data for 0.3 m depth shows some fluctuation. This may indicate a short period of wetting near the surface of the profile. However, Biddle commented that reliability of this reading may have been influenced by the fact that readings started mid-summer, giving rise to some uncertainty regarding the initial state of the soil profile.

Although SMD data is available from the Meteorological Office it was thought that Biddle's direct estimates for this particular site were likely to provide a more representative estimate of SMD.

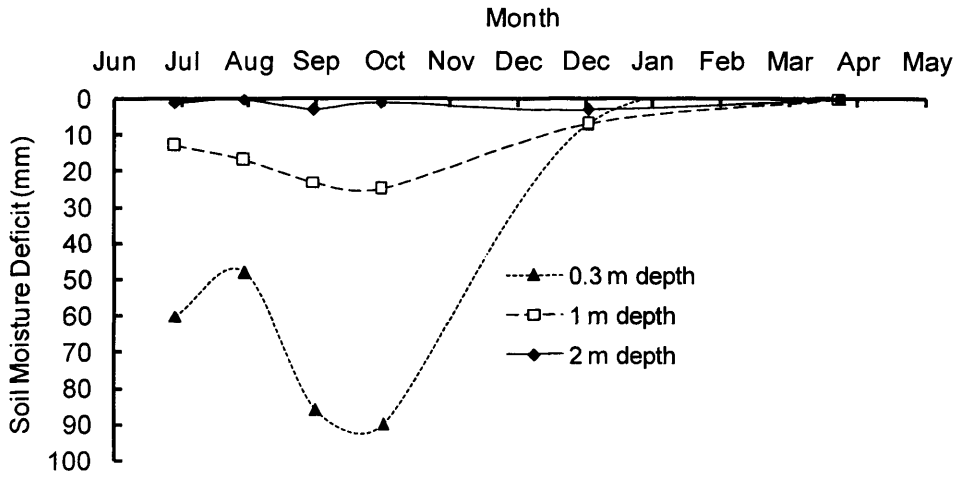

Figure 7.1 Soil Moisture Deficit at 1.4 m distance from tree

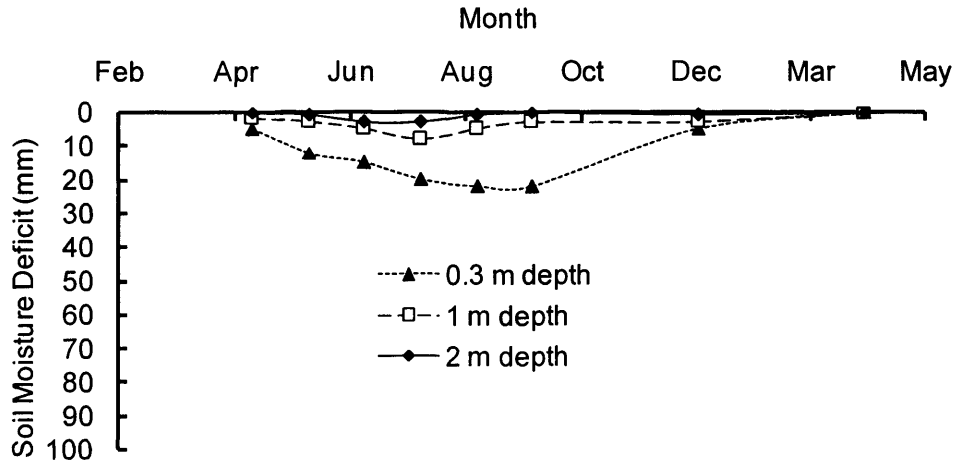

Figure 7.2 Soil Moisture Deficit at 4.9 m distance from tree

7.2.2 Rainfall Data

Rainfall data provided by the Meteorological Office (2006) has been acquired for the nearest weather station to the site (Wolverton Hampshire). Figure 7.3 shows the location of the nearest station at Wotton House which is some 6.5 Km away from the site under consideration.

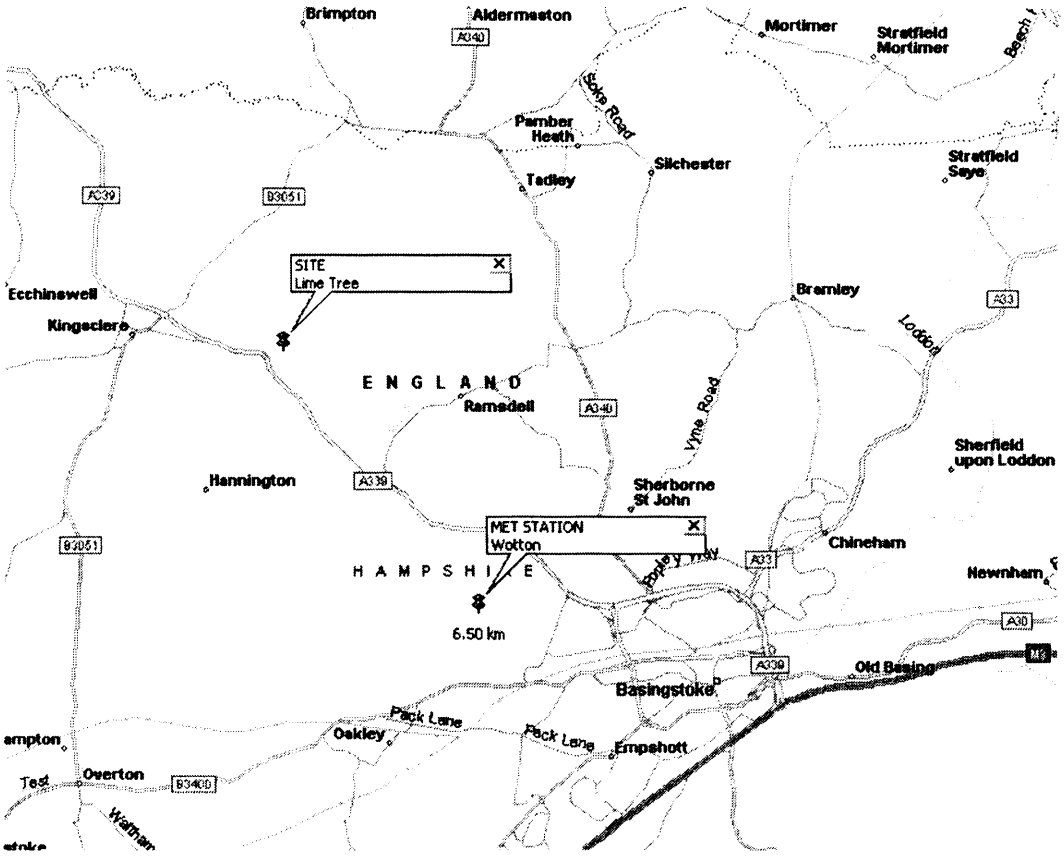

Figure 7.3 Study Site and Meteorological Office Station (using Microsoft AutoRoute, 2006)

Figure 7.4 shows the rainfall data recorded at Wotton House for the period under consideration here (23rd January 1979 to 21st April 1979). Figure 7.4 also shows a 'cut-off' line at 2.7 mm/day - this is explained in section 7.2.3 below.

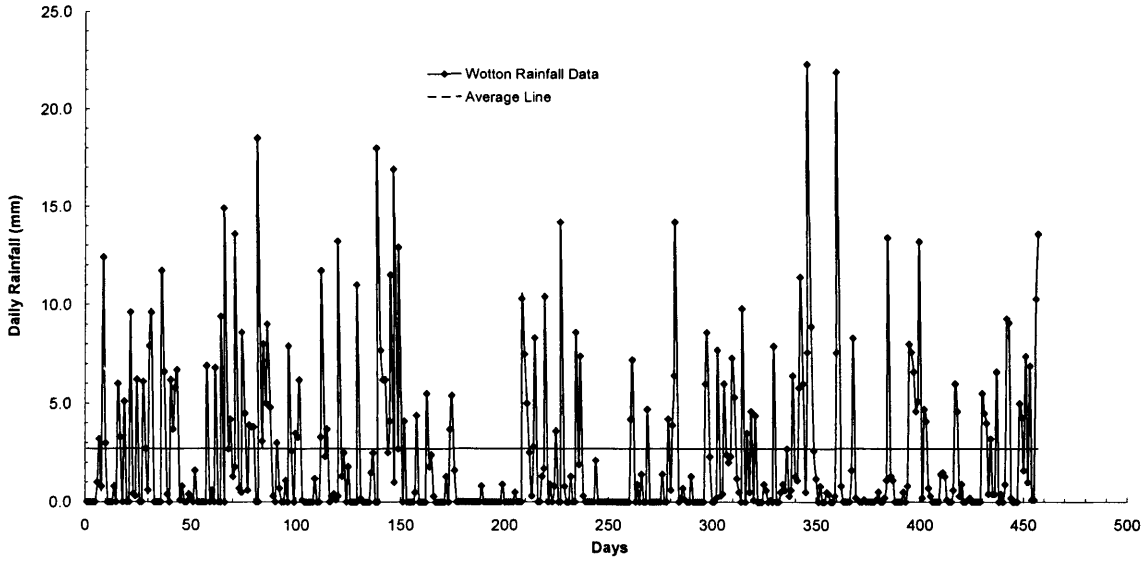

Figure 7.4 Wooton Rainfall Data and the evaporation cut off line

The SMD data and rainfall data presented above provide a general indication of the seasonal weather patterns and soil moisture variations that took place at the site of the field experiment. The following numerical simulation utilizes some of this information in an attempt to include a more representative surface boundary condition than was previously adopted in Chapter 6. From a numerical point of view, two basic forms of boundary condition can be applied; fixed or flux. Flux boundary conditions offer the attraction of directly controlling the quantity of water entering or leaving the system. However, when incorporated within a highly non-linear flow simulation, flux boundary conditions can give rise to significant numerical instability problems. In the first instance, therefore, an attempt is made below to approximate surface conditions using fixed boundary conditions only. The water-uptake aspect of the problem is, of course, dealt with by the sink-term based model described previously.

7.2.3 SIMULATION 7-1 Time Dependent Boundary Conditions

Simulation 7-1 employs time varying boundary conditions based on the above rainfall data. Apart from the time-scale and boundary conditions, the model is otherwise the same as described for Simulation 6-1 for water-uptake near a lime tree (see Chapter 6). The simulated period now covers a spring/summer soil-drying phase of 9 months followed by an autumn/winter 6 month recharge phase.

In this simulation, the sink term was activated, to represent water uptake by transpiration, during spring/summer soil-drying phase and deactivated during the autumn/winter recharge phase. Although approximate, this approach is supported by the available soil moisture deficit data for this period which showed a continuous decrease over this period as shown in Figure 7.1 and 7.2.

The daily rainfall data, presented above, has been used to specify a variation in fixed (Dirichlet) boundary conditions at the soil surface. During the simulation, it has been assumed that the soil surface was saturated when the daily rainfall exceeded evaporation demand from the grass cover. At all other times, the surface boundary was unconstrained. Blight (2003) suggested that the maximum evaporation from an open grassy site is approximately 2.7 mm/day. Therefore, in the simulation, all available water from the precipitation up to 2.7 mm/day (as shown in Figure 7.4 as a 'cut-off' line) was assumed to be used by the grass and evaporated back to the atmosphere. During the simulation, saturation of the soil surface was simulated via application of a fixed boundary condition of zero capillary potential prescribed at the surface nodes. The saturated boundary condition was only applied to the surface at times when the rate of the rainfall was found to be more than the cut-off line shown in

Figure 7.4. Therefore, in the simulation, the surface boundary is switching between a fixed saturated state and a free state (un-prescribed). Figure 7.5 provides an extract of the data shown in Figure 7.4. In particular the period from 0 day (23rd January 1979) to 30 days (22nd February 1979) in shown here in some detail to indicate the process more clearly.

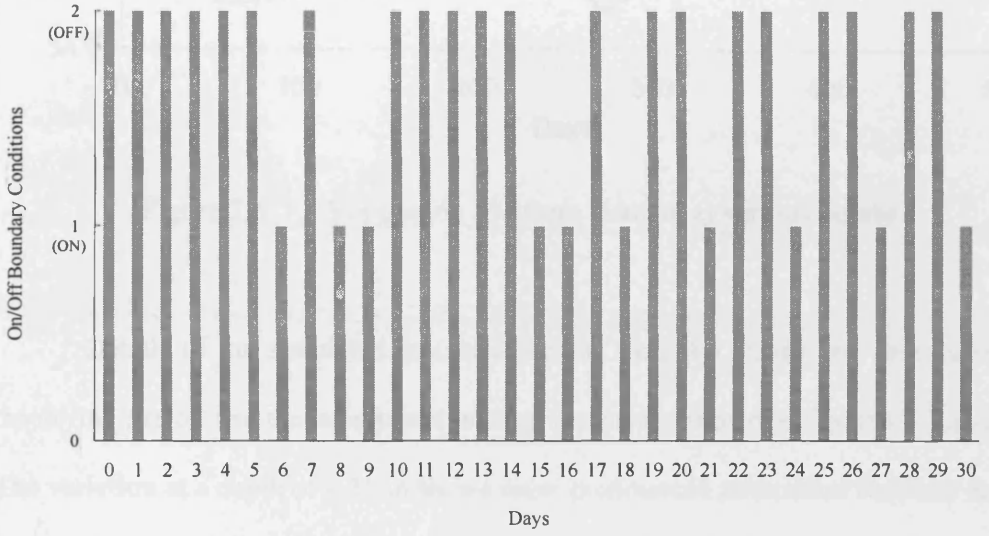

Figure 7.5 Example Switch On/Off periods for boundary conditions

Figure 7.6 shows the variation of moisture content from 0 day (23rd January 1979) to 450 days (21st April 1980) at various depths. The effect of the time varying boundary conditions is clearly visible in these results. This figure also shows that a full drying period and full wetting period are now simulated.

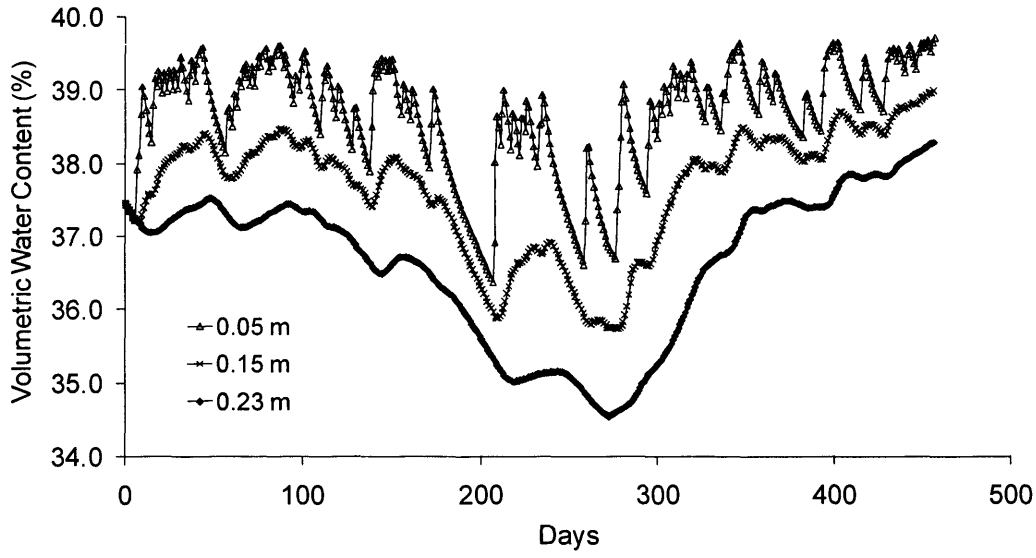

Figure 7.6 Volumetric Moisture Content at various depths

Details of the simulated moisture content variation during the first month of the drying period and the subsequent wetting period are shown in Figures 7.7 and 7.8. The variation at a depth of 0.15 m shows more pronounced alternation between drying and wetting when compared to the results at a depth of 0.23 m. Unfortunately, the field data was insufficiently detailed to compare with these results.

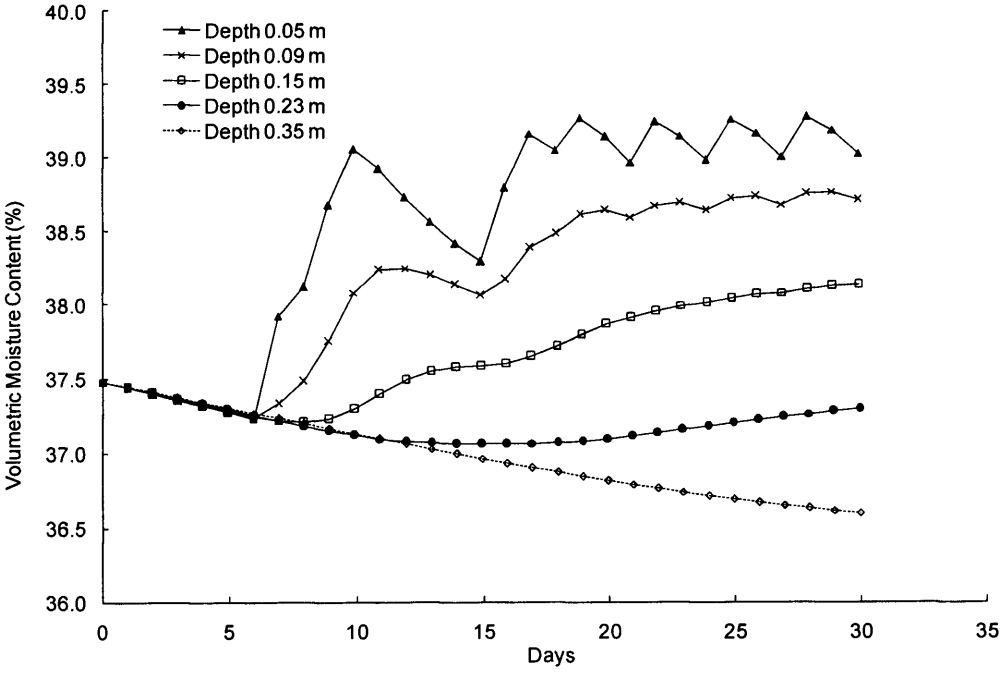

Figure 7.7 Volumetric Moisture Content at various depths from 0 to 30 days

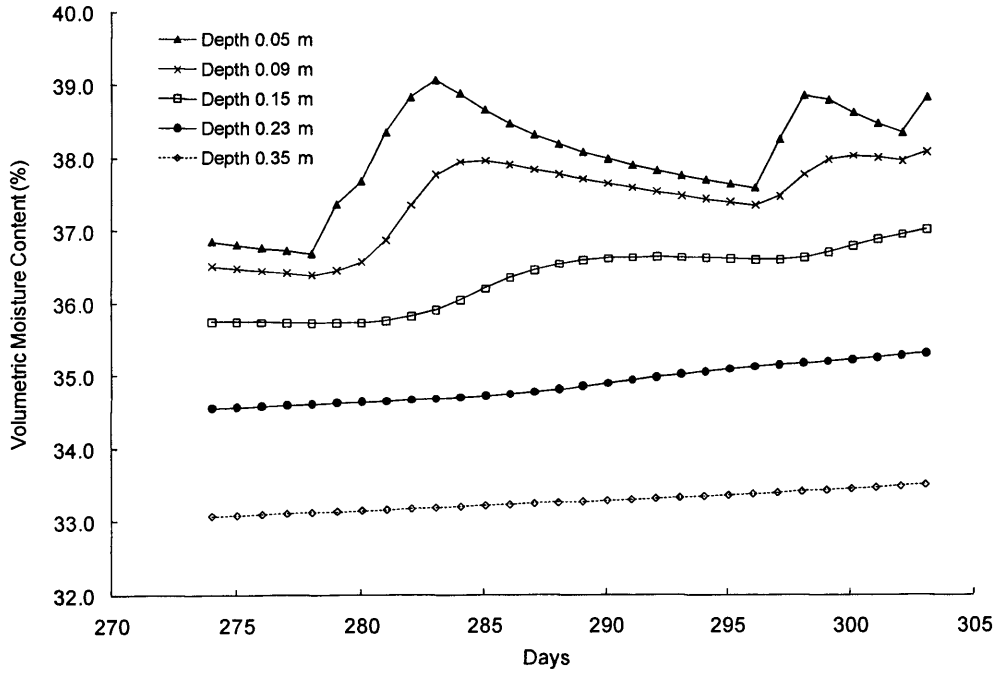

Figure 7.8 Volumetric Moisture Content at various depths from 274 to 303 days

The problem simulated above clearly involves both drying and wetting phases. Therefore, it is likely that some hysteresis may arise in the water retention characteristics of the soil. The site of the field experiment is likely to have been subjected to repeated wetting and drying over many years. It is therefore, reasonable to assume that any such hysteresis is likely to be of a closed-loop form (Yong and Warkentin, 1974). This aspect of the problem is considered in the following sections of this Chapter.

7.3 HYSTERESIS

It is generally recognised that hysteresis is most pronounced in the water retention curve of soils. Background detail on the theory of hysteresis has already been discussed in Chapter 3. The hydraulic conductivity/water content relationship shows only minor hysteresis (Van Dam et al, 1996). Therefore in this work a single hydraulic conductivity function is used here for both wetting and drying phases of the simulation. The particular relationship employed was as presented in the previous Chapter, see Figure 6.6. Only hysteresis in the water retention curve will therefore be considered.

In Chapter 6, the water retention curve for Boulder Clay was estimated using Van Genutchen's method (Van Genuchten, 1980). This curve was based on a typical drying response of the clay. In Van Genutchen's equation, there are four parameters $(\alpha, n, \theta_r, \theta_s)$ which describe the $\theta(\psi)$ relation. Ultimately the difference between wetting and drying curves can be achieved by varying the α parameter (Van Genutchen, 1980, Van Dam et al, 1996). Yong and Warkentin (1974) illustrate the

shape of typical wetting and drying curves for a clay, a loam and a sand as shown in Figure 7.9. This basic form of the water retention curve has also been adopted here for the Boulder Clay.

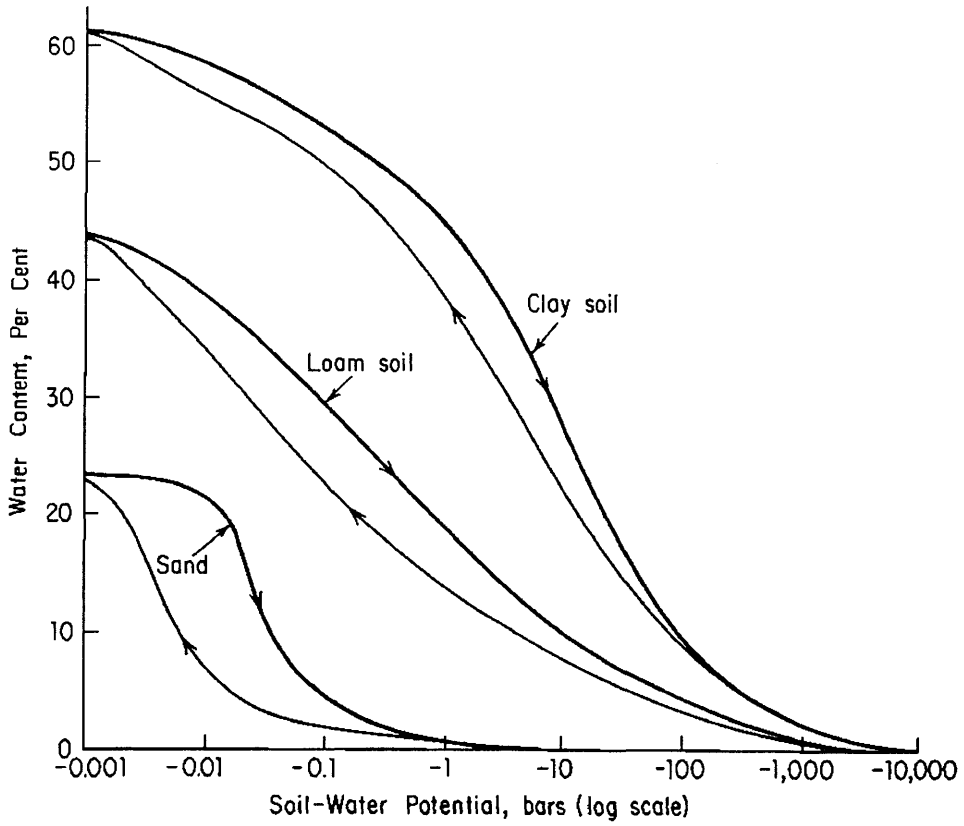

Figure 7.9 Typical hysteresis curves for a clay, loam and sand (Yong and Warkentin 1974)

7.3.1 Hysteresis - Sensitivity Study

In order to explore the significance of hysteresis on the simulated moisture migration patterns a sensitivity study has been undertaken. This was achieved using the range of α values shown in Table 7.2, and taking guidance from Figure 7.9.

Table 7.2 Assumed Soil Properties for Hysteresis Study

Parameters	θ_r	θ_s	K_s *(m/s)*	α	l	n	m
Drying Curve	0.1	0.4	1×10^{-6}	0.0280	0.5	1.4	0.29
Wetting Curve 1	0.1	0.4	1×10^{-6}	0.05	0.5	1.4	0.29
Wetting Curve 2	0.1	0.4	1×10^{-6}	0.07	0.5	1.4	0.29
Wetting Curve 3	0.1	0.4	1×10^{-6}	0.1	0.5	1.4	0.29

Three trial wetting curves, shown in Figure 7.10, were generated and included in separate re-runs of the previous simulation. As mentioned in Chapter 3, the specific moisture capacity $C(\psi)$ is a storage term which arises in the unsaturated flow formulation. The term is obtained directly from the slope of the capillary potential – volumetric moisture content relationship or soil-water retention curve. Therefore, the magnitude of this parameter is fundamentally linked to the shape of the water retention curve employed.

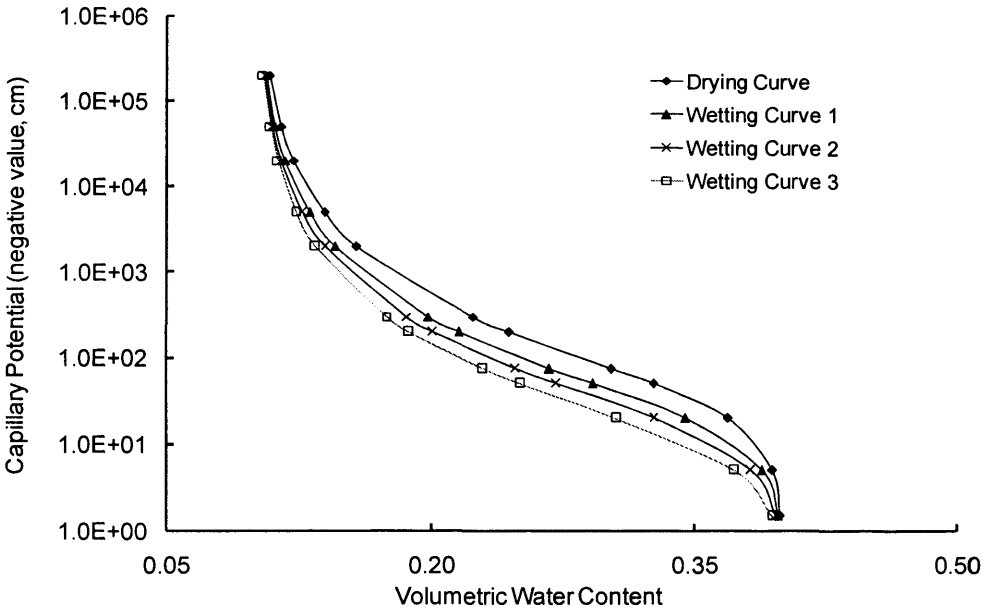

Figure 7.10 Water retention curve for Boulder Clay

From Figure 7.10, it is clear that the specific moisture capacity will take on different values depending if the soil is drying or wetting. Table 7.3 shows the variation in specific moisture capacity for these curves.

Table 7.3 Variations of Specific Moisture Capacity, $C(\psi)$

	Drying Curve	*Wetting Curve 1*	*Wetting Curve 2*	*Wetting Curve 3*
Capillary (cm)	$C(\psi)$ (cm^{-1})	$C(\psi)$ (cm^{-1})	$C(\psi)$ (cm^{-1})	$C(\psi)$ (cm^{-1})
2000	1.3861843E-05	1.0994053E-05	9.6007011E-06	8.3123174E-06
300	1.1327101E-04	9.3174478E-05	8.2284816E-05	7.1772399E-05
200	3.0539227E-04	2.6175208E-04	2.3429456E-04	2.0623347E-04
75	8.1365079E-04	7.8788237E-04	7.3552010E-04	6.6654207E-04
50	1.1411552E-03	1.2379275E-03	1.2092868E-03	1.1333659E-03
20	1.6552996E-03	2.4957982E-03	2.9072666E-03	3.1929622E-03
5	1.4308934E-03	2.9335775E-03	4.2766939E-03	6.0821221E-03

The additional simulations performed to explore hysteresis utilised a simple monitoring procedure within the finite element code to indicate if any particular node in the domain was either drying or wetting. In effect, the capillary potential, ψ for each node was monitored and compared to the previous capillary potential for every time step. This comparison indicated whether the soil was drying or wetting. The appropriate $\psi(\theta)$ curve was then used, depending on these comparisons.

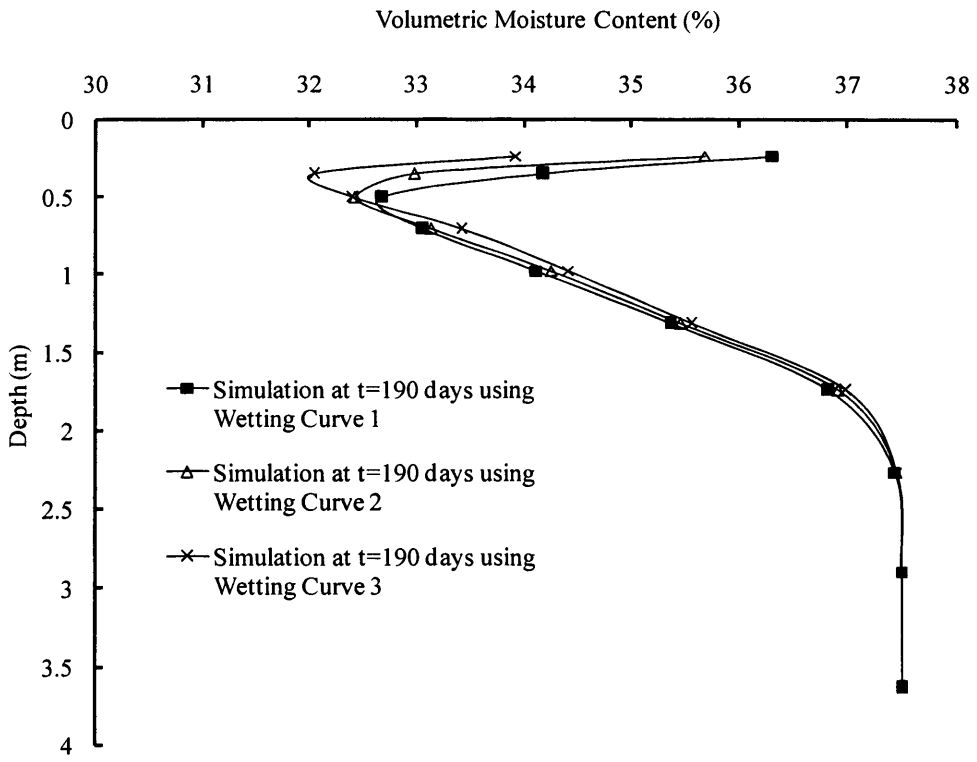

Figure 7.11 Volumetric Moisture Content at 1.4 m distance from tree using different Wetting Curve

Figure 7.11 shows three simulated moisture profiles at a distance of 1.4 m from the tree while Figure 7.12 shows the simulated moisture content variations with time at a depth of 1.0 m when using the three different wetting curves. These figures provide an overall indication of the effect of including the three different water retention curves. Whereas the overall patterns remain similar, differences in water uptake patterns are evident. Direct comparison with the available field data is presented in section 7.3.2 below. For this comparison, Wetting Curve 3 is considered since it provides the most significant difference between the simulations that excludes hysteresis.

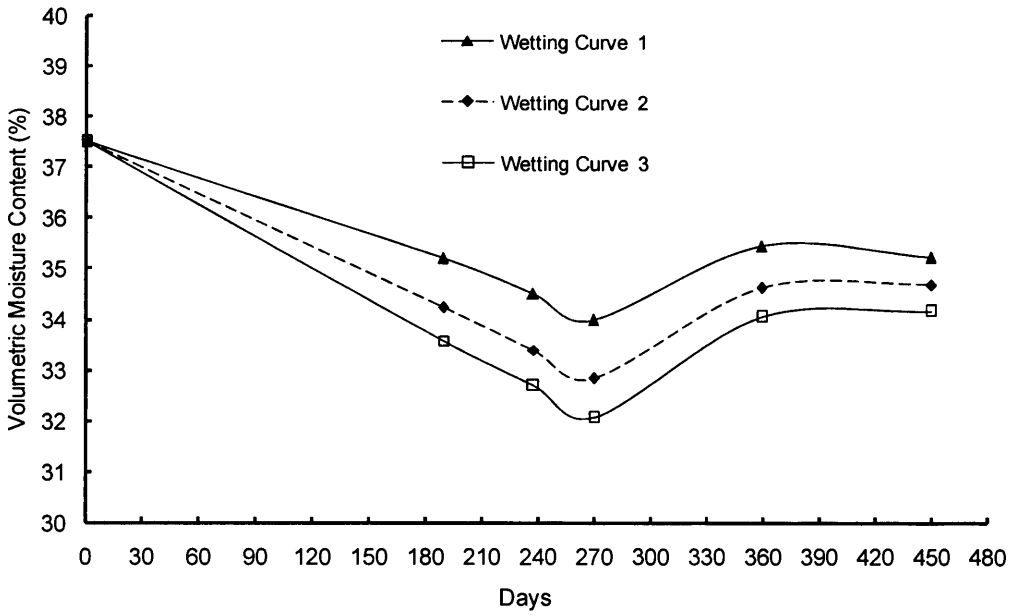

Figure 7.12 Volumetric Moisture Content at 1 m depth using different Wetting Curve

7.3.2 SIMULATION 7-2 Time Dependent Boundary Conditions and Hysteresis

Simulation 7-2 extends the above work to examine the effect of hysteresis (using Wetting Curve 3 in previous section 7.3.1). Apart from the alternate wetting curve now employed, this simulation is otherwise the same as Simulation 7-1.

A comparison has been made to explore the extent to which the alternative wetting curve may influence the overall water uptake process. Figure 7.13 provides a comparison of the moisture profiles, at 190 days at 1.4 m from tree, for the each case considered.

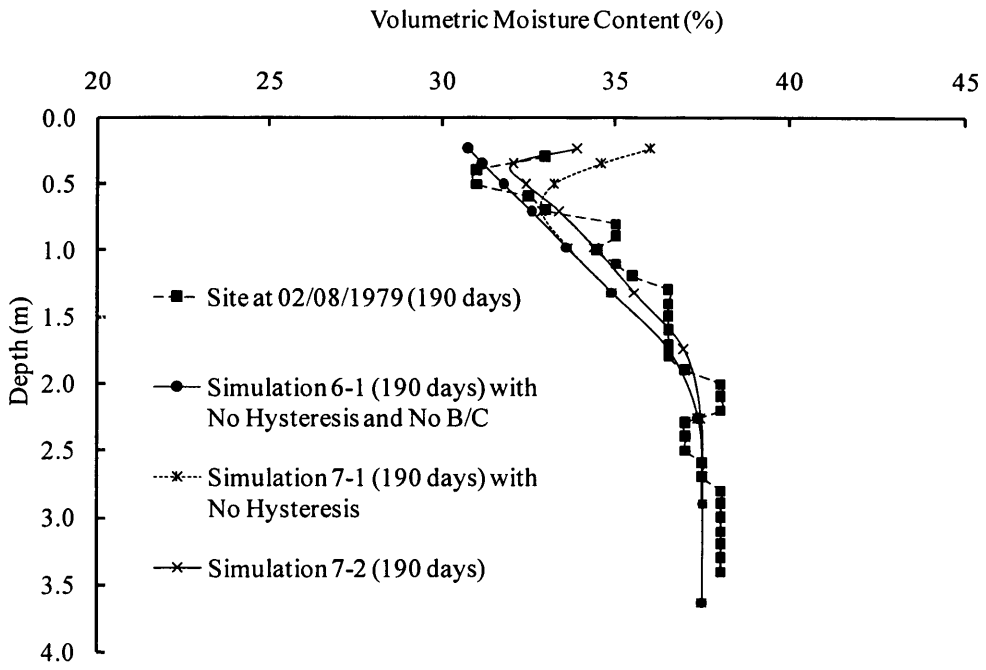

Figure 7.13 Comparison of Moisture Content Profiles (Time 190 days, Radial Distance 1.4 m)

This comparison indicates that the moisture profiles predicted by Simulation 7-2 provide a better match with the field data than the other two simulations. This gives an indication of the significance of both the inclusion of time varying boundary conditions and the specification of the water retention curve (including hysteresis) have on the prediction of water uptake.

7.3.3 Simulation 7-2 - Transient Variations

The results of Simulation 7-2 are presented more fully below to reveal the overall predicted patterns over the full annual cycle. Figures 7.14 and 7.15 illustrate predicted and measured moisture content profiles at a radial distance of 1.4 m from the centre-line of the tree, and at times of 238 days and 270 days respectively.

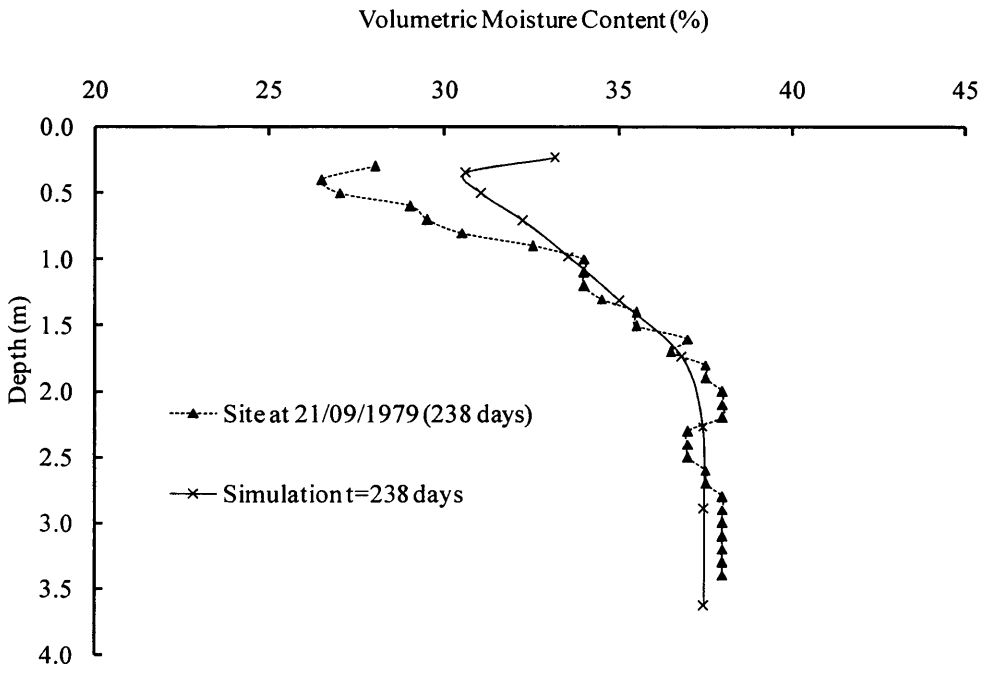

Figure 7.14 Simulated and Measured Moisture Content Profiles (Time 238 days, Radial Distance 1.4 m)

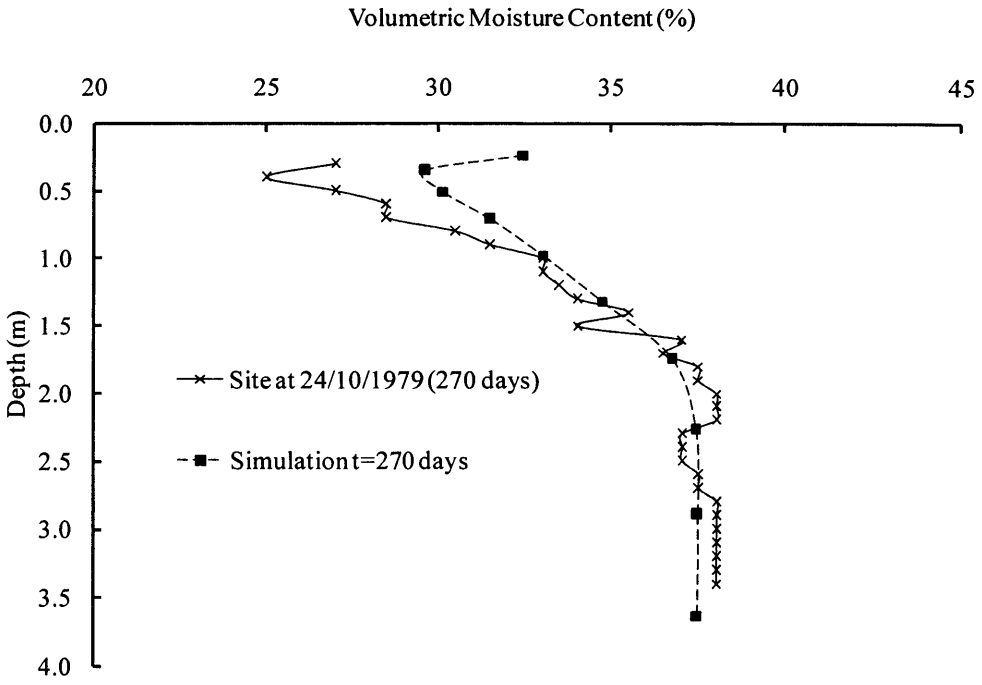

Figure 7.15 Simulated and Measured Moisture Content Profiles (Time 270 days, Radial Distance 1.4 m)

From these figures, it is clear that the maximum moisture extraction has occurred approximately at 0.4 m depth below the ground surface. The moisture content increases near to the surface due to the effect of the time varying boundary condition. The figure indicates that a reasonable agreement between the simulated results and the measured moisture profiles has been achieved. The simulated profile also produced a better match with the field data compared to the results presented in Chapter 6. At a radial distance of 4.9 m, the tree roots had relatively little effect on the seasonal moisture depletion.

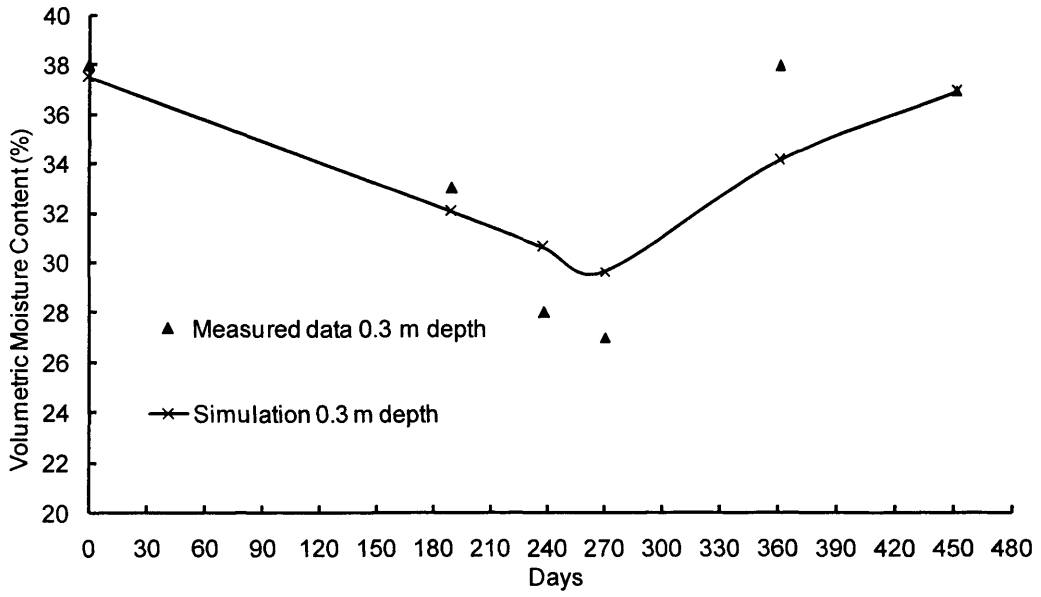

Figure 7.16 Simulated and Measured Transient Moisture Content Variation (Depth 0.3 m, Radial Distance 1.4 m)

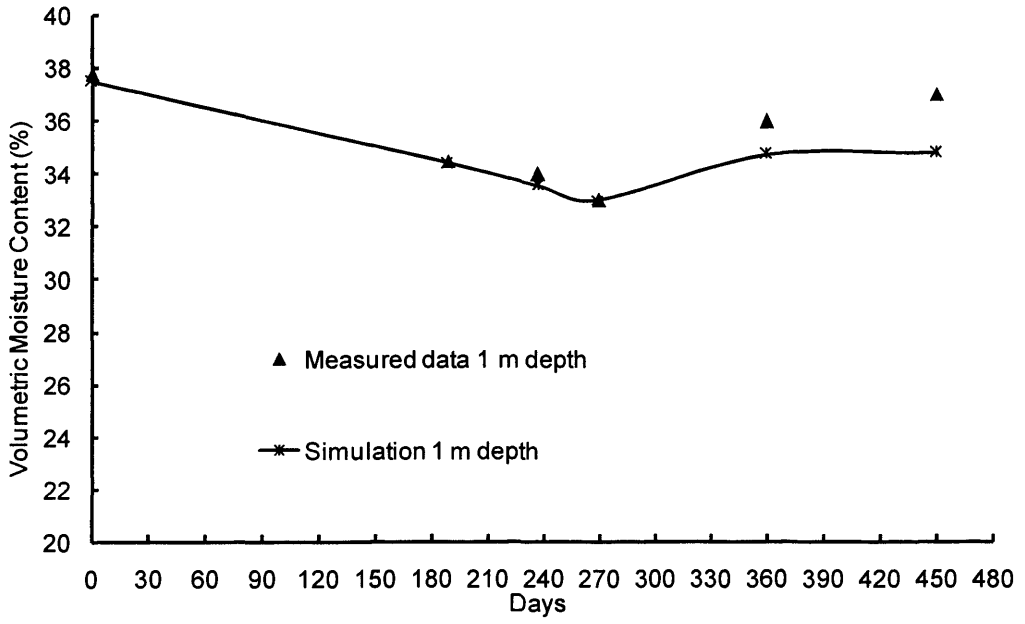

Figure 7.17 Simulated and Measured Transient Moisture Content Variation (Depth 1 m, Radial Distance 1.4 m)

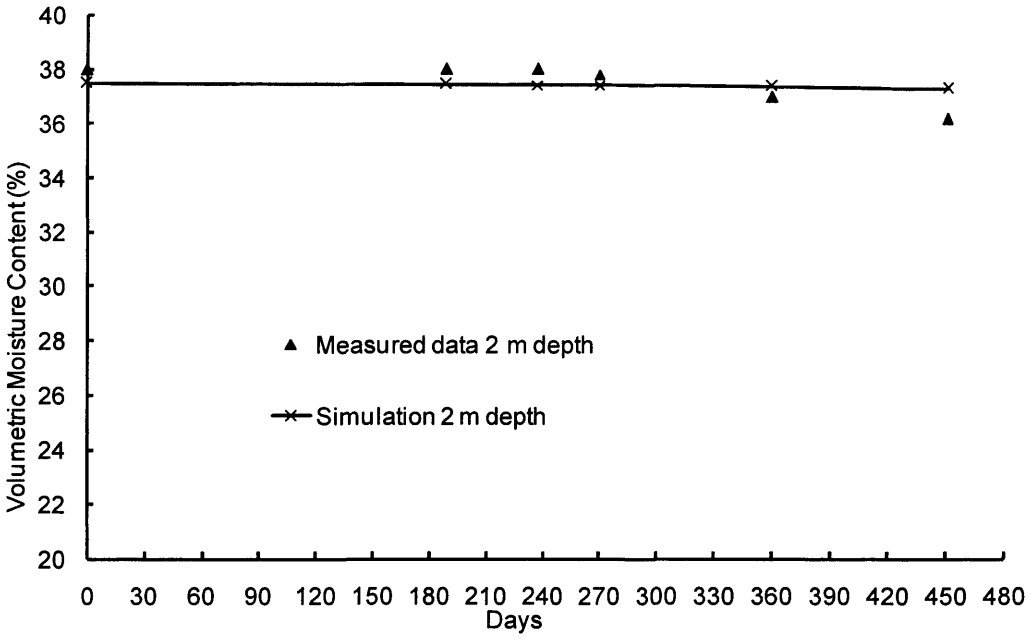

Figure 7.18 Simulated and Measured Transient Moisture Content Variation (Depth 2 m, Radial Distance 1.4 m)

Figures 7.16 to 7.18 show the moisture content variation plotted directly against time at depths 0.3 m, 1.0 m and 2.0 m below the surface and at a radial distance of 1.4 m from the tree. The measured data is simply plotted as discrete data points at the times when measurements were recorded on site. Since there was no field data available at intermediate times, no extrapolation has been undertaken. Numerical results can be output at any number of time intervals hence a continuous variation has been plotted for comparison.

Figure 7.18 is consistent with the moisture content profiles shown previously and indicates that relatively little moisture variation occurred at (and below) a depth of 2.0 m. The overall predicted trend appears to be in fair agreement with the measured data. At the distance 4.9 m far from the tree very little change in moisture content occurred.

7.4 CONCLUSIONS

This chapter has presented an extended approach for the simulation of water-uptake patterns, over a full seasonal cycle, in the unsaturated zone and in the vicinity of mature trees. In particular, the simulation presented starts from field capacity in winter and extends through a full spring/summer drying period and subsequent autumn recharge. Time varying boundary conditions and hysteresis effects have also been considered in the simulation.

Determination of boundary conditions was based on data recorded at the nearest Meteorological Station to the field experiment. Daily cumulative rainfall data and SMD data have been used top indicate the surface conditions that were likely to have occurred during the period analysed. From this data, a cut off line was introduced to estimate time at which the soil surface was likely to have been in a near saturated condition.

In the simulation, the sink term was activated, to represent water uptake by transpiration, during spring/summer soil-drying phase and deactivated during the autumn/winter recharge phase. Although approximate, this approach is supported by the available soil moisture deficit data over this period.

To explore the effect of hysteresis, the simulation was re-run employing a basic method of including the relevant wetting or drying water retention curves. Inclusion of this aspect of behaviour was shown to yield a moderate improvement in the overall quality of the results in comparison with the field data.

In summary, the overall simulation strategy has been successful extended to provide a more realistic representation of boundary conditions at the soil surface and to provide a simple method of including hysteresis in the water retention characteristics of the soil.

7.5 REFERENCES

Biddle, P. G., "Tree Root Damage to Buildings." Willowmead Publishing Ltd, Wantage, 1998.

Blight, G. E., "The vadose zone soil-water balance and transpiration rates of vegetation." Geotechnique, 53(1), 55 64, 2003.

Meteorological Rainfall Data (1979-1980), Met Office, Exeter, United Kingdom, 2006.

Microsoft AutoRoute, Microsoft Corporation, United State, 2006.

Van Dam, J. C., Wosten, J.H.M. & Nemes, A. "Unsaturated soil water movement in hysteresis and water repellent field soils." Hydrology, 184: 153 – 173, 1996.

Van Genuchten, M. T. "A closed form equation for predicting the hydraulic conductivity of unsaturated soils." Soil Sci. Am., 44, 892 – 898, 1980.

Yong, R. N., and Warkentin, B. P. "Soil properties and behaviour." Elsevier Publishing Company, Amsterdam, 1974.

CHAPTER EIGHT

PRELIMINARY ANALYSIS OF WATER UPTAKE ON SLOPE STABILITY

8.1 INTRODUCTION

From the numerical simulations presented in the preceding chapters it is clear that significant variations in soil suction may occur in the presence of vegetation. This chapter aims to examine the influence of such variations within the context of slope stability assessment. This is a problem that is exacerbated by climate change and increasingly intense rainfall events. Design, repair, maintenance and operation of railway and road earthworks are particular areas where this is an important issue.

Previous experience in Malaysia illustrated that removal of vegetation can be the main cause of the failure of a slope (The Collapse of Highland Towers Condominium, 1994). In this tragedy, one block of a 14 storey building of the Highland Towers Condominium suddenly toppled over and collapsed and killed 48

people. Investigation of the substructure and the surroundings revealed that clearing of trees on the adjacent slope led to the water level in soil to rise, thus causing the instability of slope.

Some researchers (Thorne, 1990; Simon and Darby, 1999; Simon et al, 2000; MacNeil, 2001) claim that vegetation is widely believed to increase the stability of a slope. Simon and Collison (2002) suggested that the impact of vegetation can be generally categorised as either mechanical or hydrological. Mechanical effects arise from the tensile strength of roots and the weight of vegetation. Hydrological effects are related to the soil moisture variations that are predominantly driven by transpiration. Hydrological effects are almost entirely subsurface processes when canopy interception is negligible. Seasonal variation (winter/early spring when the deciduous trees are dormant) and the intensity of rainfall influence overall behaviour. A key finding of Simon and Collison's work was that the hydrological effects were found to be as important as mechanical effects and in certain cases, providing a more significant increase in the stability of a slope.

Ridley et al (2004) discussed the relationship between climate, in the form of soil moisture deficit, the presence of trees and pore water pressures in embankments. The study showed that most embankment failures in London were due to an increase in soil moisture content. An increase in soil moisture content occurred when there was no water uptake from trees during winter time (no transpiration for deciduous trees during this period). These findings further clarify of the importance of tree-water uptake in increasing the stability of slopes.

Recently Greenwood (2006) considered the potential engineering influences of vegetation and how it can be characterised on site within a geotechnical framework for slope stability assessments. Greenwood's software, SLIP4EX is based on

equilibrium of forces and may be used for estimating the factor of safety (FOS) against slope failure. The software includes a number of key vegetation effects. It includes; vegetation mass, groundwater regime, enhanced cohesion due to fine roots, wind forces and the anchoring effects of larger roots. Changes in ground water table due to vegetation are included however the changes in ground water table employed in their work were taken directly from piezometer readings - no numerical simulation of this process was involved. The study was based on the effective stress approach and as such is valid only for saturated soils. Greenwood et al (2004) provide a full description.

Further evidence of the importance of soil suction changes on shear strength is also available in the literature. For example, Smith (2003) indicated that a loss of matric suction is followed by a loss of shear strength which can be responsible for shallow landslides or initiation of debris flow with a failure surface created within the unsaturated zone.

This chapter explores the application of the water uptake model described previously to provide a preliminary assessment of the significance of water content (and therefore suction) changes on the stability of unsaturated soil slopes. This research only considers hydrological effects (i.e. water uptake) at this stage. The work presented employs a typical slope geometry. A range of initial conditions and tree locations have been considered.

In summary, the overall problem is intrinsically complicated by the many factors that can influence the stability of any particular slope in the presence of trees. In relation to the tree; species, age, weight, height, growth status, root strength, root geometry, canopy and leaf area will influence behaviour. In relation to the soil: permeability, pore structure, density, porosity, plasticity, swelling potential

(mineralogy) and water content will all have some influence. The overall site characteristics: slope geometry, cutting/embankment/natural-slope, soil profile, history, exposure (wind-throw) and climate are relevant. In addition, the precise location of trees in relation to the slope (e.g. at toe, on slope, at crest) and in relation to each other (grouping) may also need consideration.

Set against this background, the work presented here must be viewed as a preliminary assessment aimed at illustrating the potential value of the developed water uptake modelling approach. The following section discusses some of the issues that arise in relation to any attempt to describe the above via theoretical models for slope stability.

8.2 UNSATURATED SOIL SLOPE STABILITY

Slope stability analyses have become a common analytical tool for assessing the factor of safety of natural and man made slopes. The limiting equilibrium method of slices is widely used for its simplicity particularly when compared to the finite element method (Fredlund and Rahardjo, 1993; Renaud et al, 2003; Griffiths and Lu, 2005). The limiting equilibrium method assumes 2-D plane-strain conditions and is based upon the principles of static equilibrium of forces and moments. The heart of the problem lies in finding the critical failure surface and its corresponding (minimum) factor of safety (FOS). A range of well established methods use this principle, for example; Ordinary Swedish or Fellenius's method (1936), Bishop's Simplified method (1955), Janbu's Simplified method (1956), Morgenstern and Price's method (1965) and Spencer's method (1967).

When a soil is saturated, there are two main types of stability analysis considered; total stress analysis and effective stress analysis (Lambe and Whitman, 1969). Total stress analysis is normally applied to the case of a newly cut or constructed slope (i.e. short-term period) and it is assumed that the water pressure in the slope has had no time to dissipate. The strength parameters are defined using Mohr-Coulomb failure envelope in terms of total stresses and pore water pressures are not required.

Alternatively, effective stress analysis is generally used when performing long term slope stability calculations. The strength parameters are described using Mohr-Coulomb failure envelope and the effective shear strength concept provided by Terzaghi (1936). This concept requires measurement (or knowledge) of the positive pore water pressures that occur below the ground water table. The contribution to shear strength from negative pore water pressures above the ground water table is usually ignored. Difficulties related to the measurement of negative pore water pressures and the incorporation of this information within a suitable theoretical framework are the primary reasons for this practice.

Of course, it will be a reasonable assumption to ignore negative pore water pressures for many situations where the major portion of the slip surface is below the ground water table and the weakest (saturated) condition is of primary concern. However, for the situations where the ground water table is deep and perhaps where tree root activity is involved, negative pore water pressure become more significant. As indicated earlier in the thesis, condition assessment of earth-works is now a recognised task facing the rail and highway agencies. An evaluation of slope strength in the presence of trees is clearly of value in this context. Pruning and possible removal of vegetation is a routine part of the decision making process in these

industries. A clear understanding of the consequence of various actions in terms of stability and strength change is recognised to be of importance (Russell et al 2000, McGinnity et al, 1998). In order to make progress in this respect, one approach is to attempt to perform slope stability analyses which include the contributions of vegetation to shear strength. One of these contributions will arise from soil suction generated in the vicinity of trees. To this end, the approach adopted here is to utilize a modified form of the Mohr-Coulomb equation. Further detail is provided in section 8.2.2.

Fredlund and Rahardjo (1993) define total suction of soil as being made up of two components, matric suction and osmotic suction. The matric suction component is commonly associated with the capillary phenomenon arising from the surface tension of water. Osmotic suction is related to the salt content in the pore water and if the salt content changes in a soil, there will be a change in the volume and shear strength of the soil.

In this Chapter, the stability of an unsaturated soil slope is considered in relation to soil suction created by the plant water-uptake process. These changes primarily affect the matric suction component only. In this situation, osmotic suction changes are generally less significant and as explained in Chapter 3, it is therefore assumed that the soil has the same chemical properties throughout the profile. Hence only matric suction is considered in this Chapter.

Fredlund and Rahardjo (1993) defined matric suction as the difference between the pore-air and the pore-water pressures, $(u_a - u_w)$. In this work, the pore air pressure is assumed to be constant at its atmospheric value. Therefore, only changes in pore water pressure are considered. As described previously, the numerical solution of the water-uptake model yields raw output in terms of capillary

potential (with respect to space and time). However, for ease of discussion and to facilitate direct calculation for the FOS, the results of the model have been converted to matric suction. This has been achieved directly from the water retention curve for the soils considered.

8.2.1 Shear Strength of Unsaturated Soils

A detailed discussion of unsaturated shear strength, stress path analysis and the variety strength tests available can be found elsewhere (Fredlund and Rahardjo, 1993). A very useful update on this area of work is also available in current conference proceedings in UNSAT, 2006.

In the current work, a reasonably simple framework has been sought that will permit a first assessment of the influence of soil suction changes on soil shear strength. For this purpose, the following relationship provided by (Fredlund et al 1978) appears suitable:

$$\tau = c' + (\sigma_n - u_a)\tan\phi' + (u_a - u_w)\tan\phi^b \qquad (8.1)$$

Where $(u_a - u_w)$ is the matric suction and ϕ^b is the angle indicating the rate of increase in shear strength relative to matric suction. $(\sigma_n - u_a)$ is the net normal stress, c' is the effective cohesion and ϕ' is angle of friction.

In equation (8.1) two stress state variables, the net normal stress and the matric suction are used to describe unsaturated shear strength while only one stress state variable, effective normal stress is required for a saturated soil. To calculate the FOS for a slope, as described below in section 8.2.2, these two stress state variables must

be specified, however, the only new strength parameter introduced is ϕ^b. Fredlund et al (1978) described ϕ^b as the angle indicating the rate of increase in shear strength relative to the matric suction. This parameter is always less than or equal to ϕ', the saturated angle of friction.

Fredlund and Rahardjo (1993) showed how matric suction, net normal stress and shear strength interrelate to give a three dimensional failure surface, as shown in Figure 8.1. This figure shows a planar failure surface that has a slope angle ϕ^b with respect the matric suction axis. This angle depends on many factors, for example; density, void ratio, degree of saturation, mineral composition, stress history and strain rate of the soil. The experimental determination of this parameter is clearly complex and is beyond the scope of the current work. In summary, the increase in shear strength caused by an increase in matric suction is described by the angle, ϕ^b.

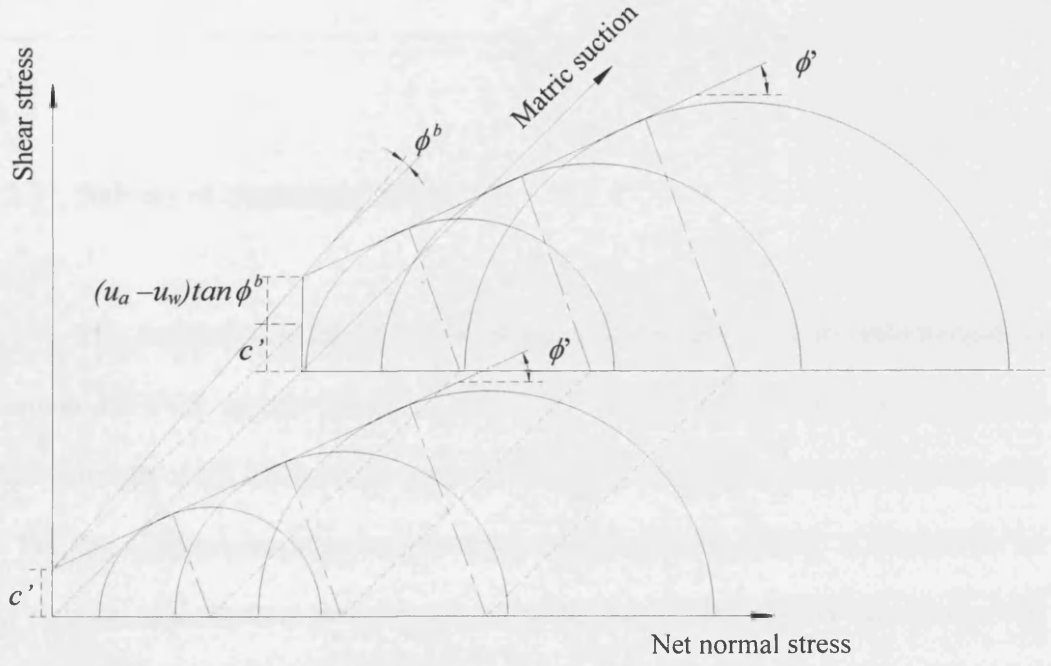

Figure 8.1 Extended Mohr-Coulomb failure envelope for unsaturated soils, modified after Fredlund and Rahardjo (1993)

Fredlund and Rahardjo (1993) presented some typical values for ϕ^b for various soils worldwide, as shown here in Table 8.1.

Table 8.1 Experimental Values of ϕ^b, modified after Fredlund and Rahardjo (1993)

Soil Type	c' (kPa)	ϕ' (degrees)	ϕ^b (degrees)
Compacted shale	15.8	24.8	18.1
Boulder clay	9.6	27.3	21.7
Dhanauri clay	37.3	28.5	16.2
Madrid grey clay	23.7	22.5	16.1
Tappen-Notch Hill silt	0	35.0	16.0
Compacted glacial till	10.0	25.3	25.0

8.2.2 Stability of Unsaturated Slopes

This research uses the theory of limiting equilibrium of forces and moments to compute the FOS against failure. The FOS is defined as that factor by which the shear strength of the soil must be reduced in order to bring the mass of soil into a state of limiting equilibrium along a selected slip surface (Krahn, 2004). Calculations for the stability of a slope are performed by dividing the soil mass above the circular slip surface into vertical slices (i.e. method of slices). The limiting equilibrium formulation assumes that the factor of safety is to be equal for all soils involved and for all slices.

Since the current work aims to explore the importance of suction changes on slope stability, in the example considered, the water table is assumed to be below the zone of interest. In addition, tension cracks are excluded from the current work. It is also assumed that there are no interslice shear forces involved in the equation for both horizontal and vertical forces. This assumption has been made on the following basis;

a. Vertical interslice forces are assumed equal and opposite (Bishop, 1955).
b. It is assumed that the resultant of the interslice forces acting on a slice act parallel to the base of the slice. The interslice forces are eliminated by resolving forces normal to the base of the slice,

The forces acting on a slice within the sliding soil mass are shown in Figure 8.2.

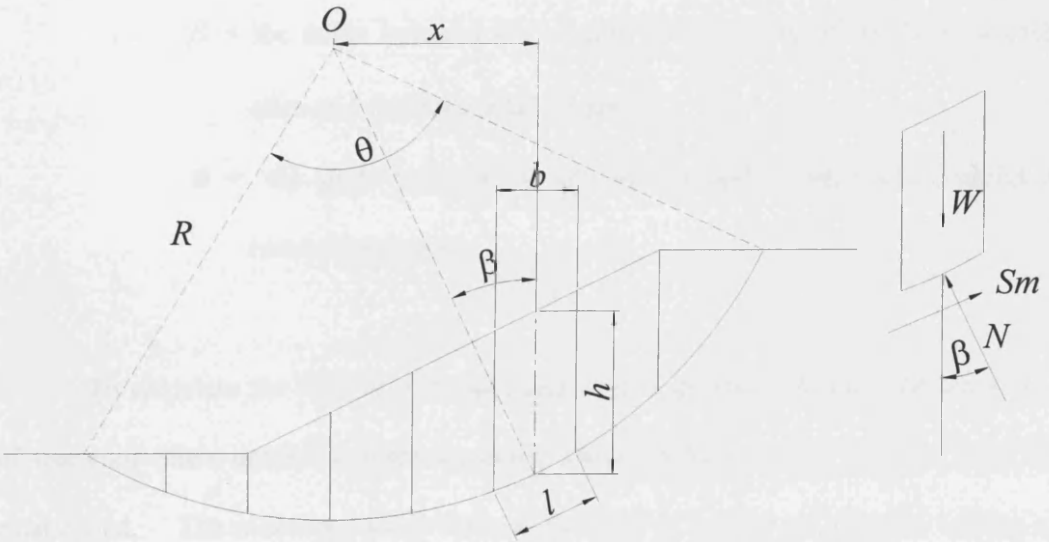

Figure 8.2 Forces acting on a slice through a sliding mass with a circular slip surface, modified after Fredlund and Rahadjo (1993)

The variables in Figure 8.2 are defined as follows:

W = the total weight of a slice (kN)

N = the total normal force on the base of the slice (kN)

S_m = the shear force mobilized on the base of each slice (kN)

O = the centre of rotation

x = the horizontal distance from the centreline of each slice to the centre of rotation, O (m)

l = the length of the each slice (m)

b = the width of the each slice (m)

h = the vertical distance from the centre of the base of each slice to the uppermost line in the geometry (m)

R = the radius for a circular slip surface (m)

β = the angle between the tangent to the centre of the base of each slice and the horizontal (*degrees*)

θ = the angle between the slip surface and a centre about which it rotates (*degrees*)

To calculate the FOS in an unsaturated soil slope and link this with the effect of tree-root-water uptake, a force equation which includes matric suction must be established. The mobilized shear force at the base of a slice can then be written as (Lambe and Whitman, 1969)

$$S_m = \frac{\tau l}{F} \tag{8.2}$$

Where τ is shear strength of unsaturated soil as defined previously in equation (8.1).

Combining equation (8.1) and (8.2), gives,

$$S_m = \frac{l\left[c' + (\sigma_n - u_a)\tan\phi' + (u_a - u_w)\tan\phi^b\right]}{F} \tag{8.3}$$

From Figure 8.2, (taking point O as centre of the moments) the summation of moments in the slope, yields:

$$\sum Wx - \sum S_m R = 0 \tag{8.4}$$

Substituting equation (8.3) into (8.4) yields

$$\sum Wx = \frac{\sum Rl\left[c' + (\sigma_n - u_a)\tan\phi' + (u_a - u_w)\tan\phi^b\right]}{F} \tag{8.5}$$

Rearranging equation (8.5) then produces:

$$F = \frac{\sum c' lR + (N - u_a l)R\tan\phi' + (u_a - u_w)Rl\tan\phi^b}{\sum Wx} \tag{8.6}$$

Substituting $(u_a - u_w) = S$ and assuming that the air pore pressure is constant (atmospheric) then $u_a = 0$ and equation (8.6) becomes:

$$F = \frac{\sum c'lR + NR\tan\phi' + SRl\tan\phi^b}{\sum Wx} \tag{8.7}$$

Where N is total normal force on the base of the slice, and β is the angle between the tangent to the centre of the base of each slice and the horizontal, therefore

$$N = W\cos\beta \tag{8.8}$$

Substituting equation (8.8) into (8.7) gives the FOS for the unsaturated soil slope:

$$F = \frac{\sum c'lR + (W\cos\beta)R\tan\phi' + SRl\tan\phi^b}{\sum WR\sin\beta} \tag{8.9}$$

Equation (8.9) forms the basis for the following exploration of the influence of vegetation induced suction changes on slope strength. It should be noted that if the matric suction becomes zero, then the soil is saturated and equation (8.9) defaults to the standard Fellenius's method (Fellenius, 1936).

8.2.3 Verification of the Stability Model

To provide a basic check on the implementation of above slope analysis a simple comparison to the results generated from commercial software is first explored. SLOPEW Version 6.17 (2004) has been used for this purpose. For this initial test case, the behaviour of a slope on saturated Boulder clay, in the absence of any trees, was considered. The material properties employed are as shown in Table 8.2. For the initial check on the routine, a fully saturated slope was considered (i.e. $S = 0$ and $\phi^b = 0$).

Table 8.2 Material Properties (Bishop et al, 1960)

Soil Type	γ (kN/m^3)	c' (kPa)	ϕ' (degrees)	ϕ^b (degrees)
Boulder Clay	22	9.6	27.3	21.7

Determining the position of the critical slip surface still remains one of the key issues in a stability analysis (Krahn, 2004). In this study, location of the critical slip surface has been determined using SLOPEW. The result is shown in Figure 8.3. To find the critical slip surface, some 147 possible failure surfaces were examined. To implement equation (8.9) the mass of soil bounded by the critical slip surface was then divided into 8 slices. The slope geometry, the critical slip surface and the location of each slice are shown in Figure 8.4. Detailed calculations are summarised in Appendix 6.

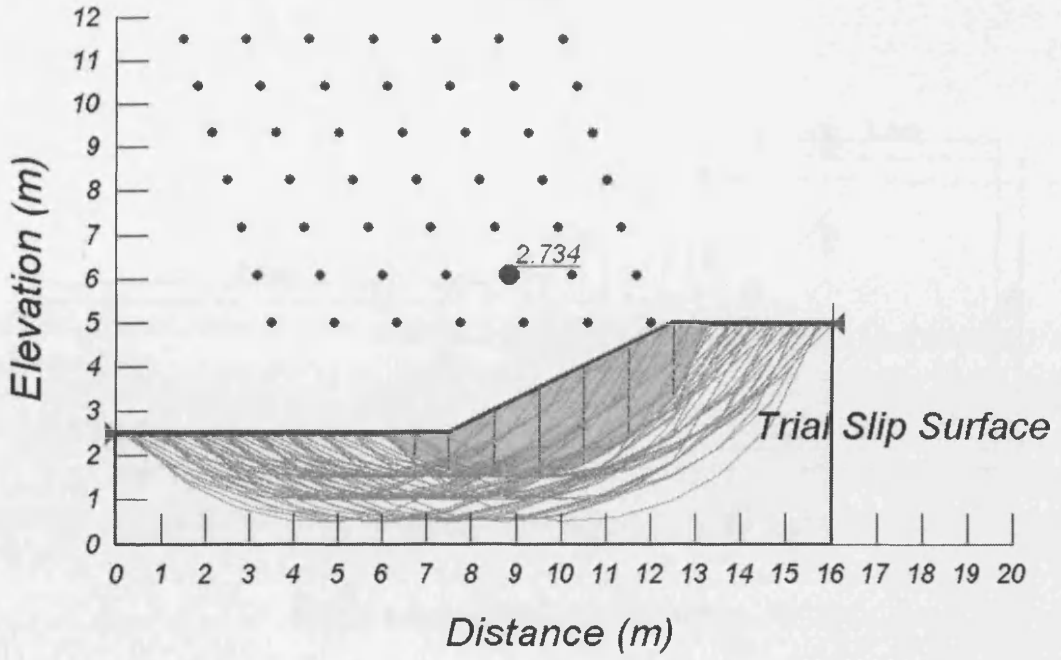

Figure 8.3 Identification of the Critical Slip Surface, using SLOPEW (2004)

A minimum FOS of 2.734 was calculated from SLOPEW using the conventional method of slices. This corresponded to a slip surface of radius 5.83 m and of origin x = 8.5 m, z = 7.5 m. Table 8.3 provides the result obtained for this particular slip surface employing equation (8.9) in comparison with the various methods available using SLOPEW.

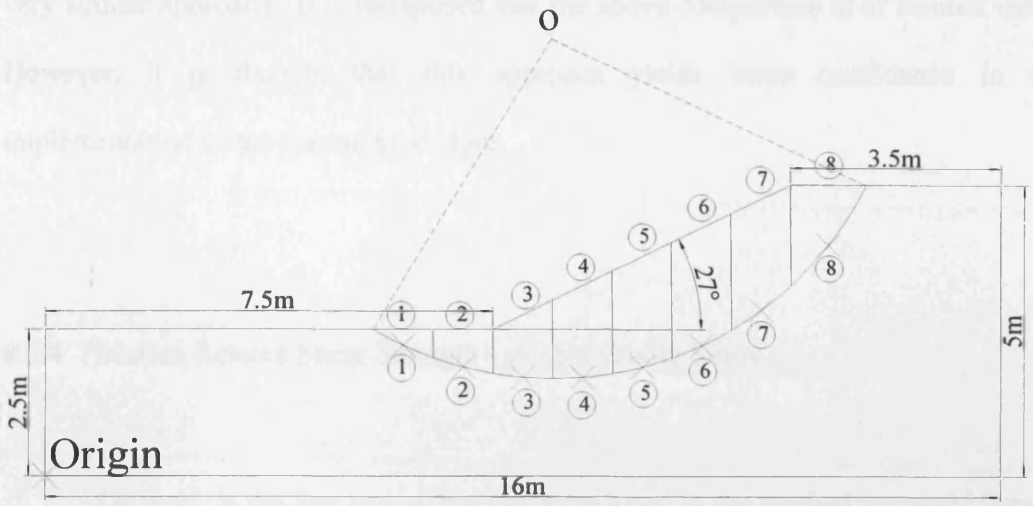

Figure 8.4 Test Slope Geometry

Table 8.3 Comparison of FOS by various methods of analysis

Type of Analysis	FOS	Percentage Difference (%)
Manual Calculation using Equation (8.9) – Ordinary Method	2.742	0
SLOPEW using Ordinary Method	2.734	0.29
SLOPEW using Bishop Method	3.087	12.58
SLOPEW using Janbu Method	2.569	6.31
SLOPEW using Morgenstern – Price Method	3.074	12.11

Table 8.3 shows that the differences between methods are in the range 0.3 % and 13 % when compared to the manual calculation. As expected, the difference between the use of equation (8.9) and the Ordinary Method (SLOPEW) is small due

to the fact that these two methods, when applied to analyse a saturated slope, adopt a very similar approach. It is recognised that the above comparison is of limited value. However, it is thought that this approach yields some confidence in the implementation of the current procedure.

8.2.4 Suction Related Shear Strength - ϕ^b Sensitivity Study

Since ϕ^b is the key new parameter introduced in the method proposed here, a sensitivity study has been undertaken to illustrate its importance on the overall calculation of the FOS for the slope defined in Figure 8.4 above. Referring back to Table 8.1, it can be seen that the magnitude of ϕ^b varies between 50 % and 100 % of the value of ϕ' for a given soil type. For example, for a compacted shale $\phi^b = 18.1^\circ$ and $\phi' = 24.8^\circ$ - therefore ϕ^b is approximately 73% of ϕ' for this soil type. Based on this information, a sensitivity study has been undertaken for the Boulder Clay. The study employs ϕ^b values of 13.6°, 16.4°, 19.1°, 21.8°, 24.6° and 27.3°. These values represent 50%, 60%, 70%, 80%, 90% and 100% of ϕ' for Boulder clay (given as 27.3° in Table 8.2).

Figure 8.5 shows how the FOS varies with matric suction for this range of ϕ^b values. The FOS increases as ϕ^b and matric suction increase. Figure 8.6 shows the variation of FOS with respect to the value of ϕ^b at a suction of 10 kPa. The result indicates that every 1° change of ϕ^b will cause the FOS to change by 0.026. However, as mentioned by Fabius et al (2004), the change in FOS is relatively small, showing that the overall results are not particularly sensitive to the value of ϕ^b. The

form of equation 8.9 requires that an increase in the value of ϕ^b will linearly increase both the shear strength and the FOS.

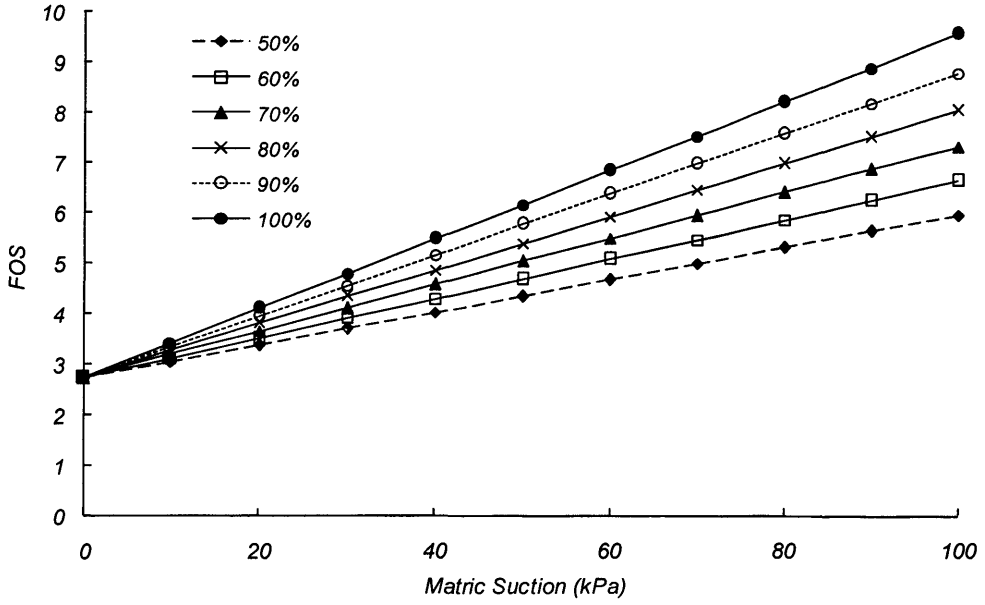

Figure 8.5 Variation of FOS with matric suction

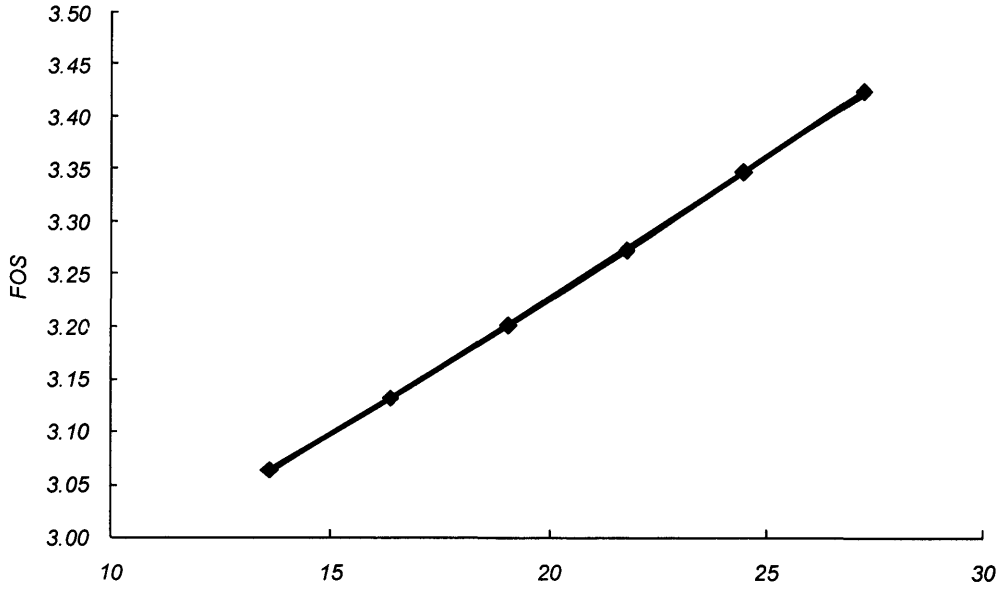

Figure 8.6 Variation of FOS with ϕ^b

8.3 COMBINED WATER-UPTAKE MODELLING AND UNSATURATED SLOPE ANALYSIS

This section attempts to bring together the slope stability approach discussed above and the water-uptake model presented in Chapters 6 and 7. The traditional slope stability problem is formulated as a two-dimensional (2-D) plane problem. However the previous simulation work presented in Chapter 6 and 7 was undertaken within a 2-D axi-symmetric framework. In order to obtain some compatibility between the two formats, the moisture flow simulation undertaken here is also conducted in 2D plane geometry. The necessary modifications to the moisture transfer equations are explained further in section 8.3.1 below.

8.3.1 Water Uptake and Moisture Flow in a 2-D Plane Domain

To deal with 2-D plane problem, modification of the flow equation from Chapter 3 has been made. The sink term must now be based on the x co-ordinate in place of the previous radial co-ordinate, r used for the axi-symmetric form. Therefore:

$$S(\psi,x,z)=\frac{4T}{z_r x_r}\alpha(\psi)\left(1-\frac{z}{z_r}\right)\left(1-\frac{x}{x_r}\right) \tag{8.10}$$

Combining the standard two-dimensional Richard's equation (Appendix 4 provides the full derivation) and the modified sink term equation (8.10) provides the 2D plane form of the water uptake model:

$$C(\psi)\frac{\partial\psi}{\partial t}=\frac{\partial}{\partial x}\left[K(\psi)\frac{\partial\psi}{\partial x}\right]+\frac{\partial}{\partial z}\left[K(\psi)\frac{\partial\psi}{\partial z}\right]+\frac{\partial K(\psi)}{\partial z}-S(\psi,x,z) \tag{8.11}$$

A solution of equation (8.11) was obtained via application of the numerical techniques described in Chapter 4. The necessary changes to the numerical formulation are provided in Appendix 5.

8.3.2 Numerical Simulation

The simulation now attempted employs the slope geometry from Figure 8.4. The shear strength properties are as above (Table 8.2). The water retention curve and the hydraulic conductivity relationships for this material have been described previously (see Figures 6.5 and 6.6 in Chapter 6). The problem considered is a typical drying period and the moisture migration caused by a single tree. Therefore the same approach to simulate water uptake described in Chapter 6 is again employed here. Figure 8.7 shows the domain and location of the tree. A larger domain size is now adopted in order to include the slope geometry.

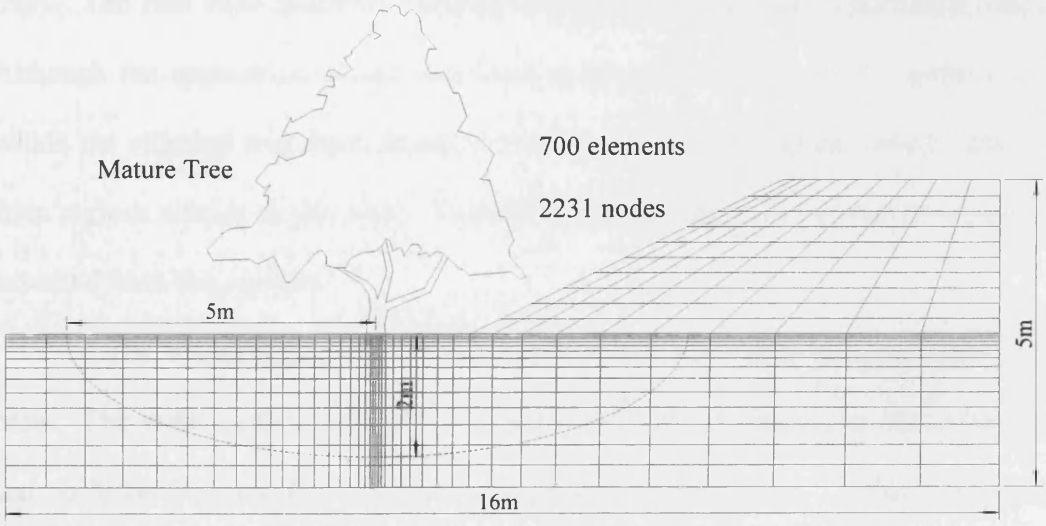

Figure 8.7 Finite Element Mesh

The mesh consists of seven hundred, eight-node isoparametric elements with 2231 nodes. The mesh was configured to offer some refinement within the root zone area since this is the region where the most significant moisture content variations were expected to occur. Numerical tests were conducted to ensure that for this domain size, the outer boundaries do not significantly influence the simulated results within the region of interest. The simulated period covered a spring/summer soil-drying phase of 9 months. The simulation employs a time-step size of 21600 seconds, which was held constant for the entire period considered. Again, a check has been made to ensure that the solution is time-step converged.

The root zone is assumed to extend to a depth of 2 m and a radial distance of 5 m both left and right of the centre line of the tree (assumed root zone based on a lime tree). The root zone therefore extends beneath the toe of the embankment slope. Although the application of the sink term in the water uptake model applies only within the elliptical root zone, moisture is of course free to migrate towards the tree from regions outside of this zone. Therefore some drying of the embankment can be expected from this scenario.

The transpiration rate for the tree has been converted to a per metre run basis. The water-uptake simulation undertaken effectively represents the behaviour that could be expected from a linear source (i.e. a line of trees). Initial conditions employed for the simulation were again based on the experimental moisture profiles shown in Chapter 6.

The drying phase was represented via the application of the water-uptake model described below for this domain. In effect the transpiration rate is therefore distributed through the root zone via use of the sink term. No flux boundary is therefore specified at the soil surface. The lower boundary of the domain and the far-field vertical boundary remained unconstrained (natural) throughout the simulation.

8.3.3 Results

Figure 8.8 presents the simulated contours of matric suction generated at the end of the simulation (at 270 days). This figure shows that clear moisture content variations within the slope have taken place. For clarity, the position of critical slip surface with the slices also has been shown in this figure.

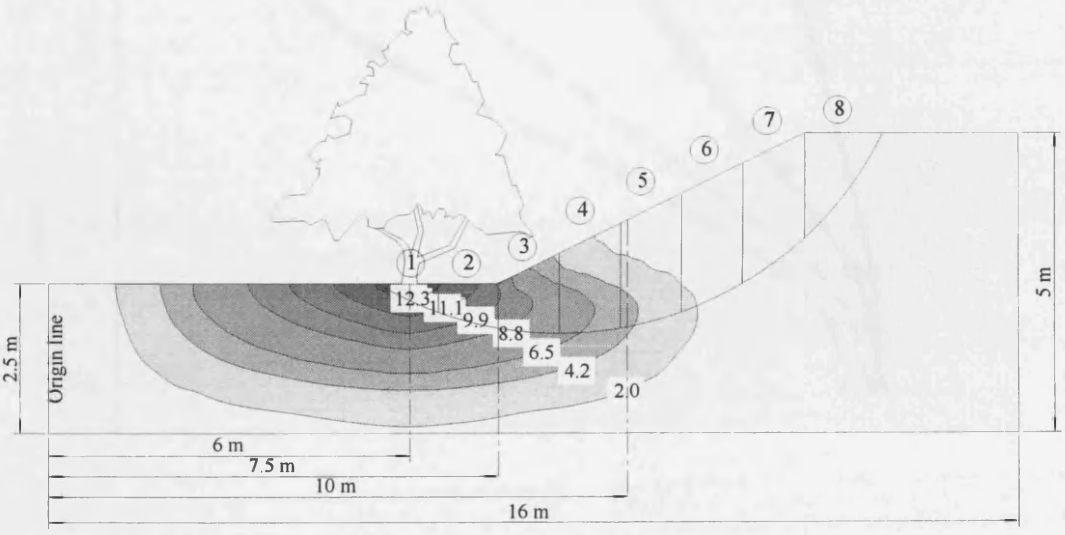

Figure 8.8 Matric suction (kPa) contours at 270 days (Tree near the toe of slope)

The finite element results provide a means for estimating the suction change generated by the drying process at the base of each slice used in the slope analysis (equation 8.9). Details of this calculation and the conversion of the basic data given in terms of capillary potential are shown in Appendix 6.

Figure 8.9 shows the predicted moisture content profiles at a distance of 6.0 m from the origin line (located at the left hand edge of the domain as shown in Figure 8.8) at times of 30 days, 90 days, 180 days and 270 days. These results are produced for the soil profile directly beneath the centreline of the tree. It is clear that the majority of the moisture extraction has occurred near the surface with the volumetric moisture content reducing to 24.0 % at surface. The moisture content profile increases to its initial value of 37.5 % at approximately 2.5 m below the ground surface.

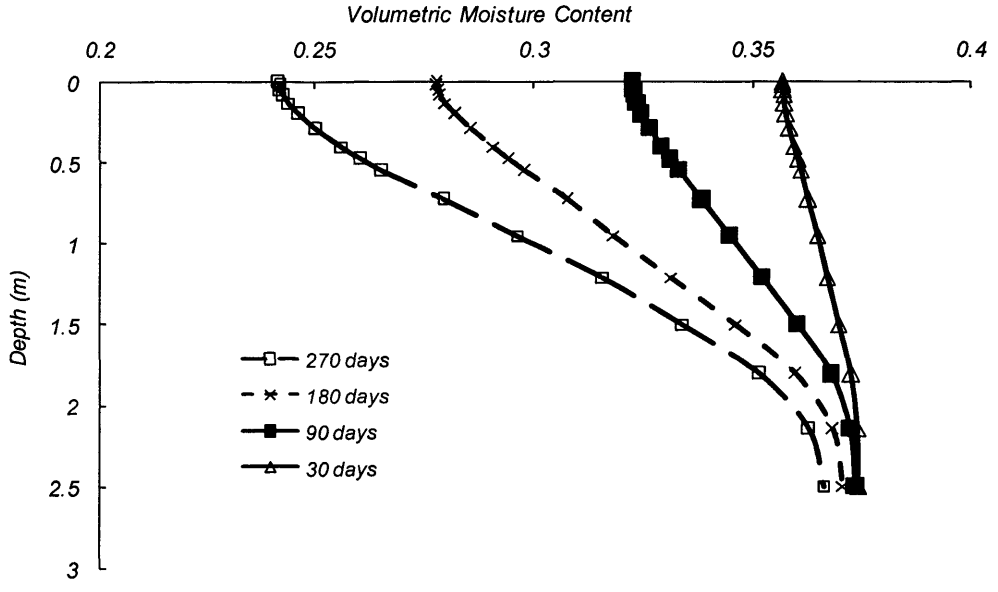

Figure 8.9 Simulated Moisture Content Profiles at distance 6.0 m (Tree near the toe of slope)

Figure 8.10 and 8.11 shows that a very similar set of results was obtained at 7.5 m and 10.0 m from origin line respectively. It should be noted that the change in profiles show relatively little moisture depletion compared those at a distance of 6.0 m. At a distance of 10.0 m, Figure 8.11 shows that the maximum moisture extraction occurred at depth of approximately 1.65 m from the slope surface - the volumetric moisture content reduced to 35.0 % at this point. This moisture profile can be expected since this depth is roughly at the same level as the point at which the tree meets the soils surface - at a distance 6.0 m. This level is where the main source of water extraction takes place.

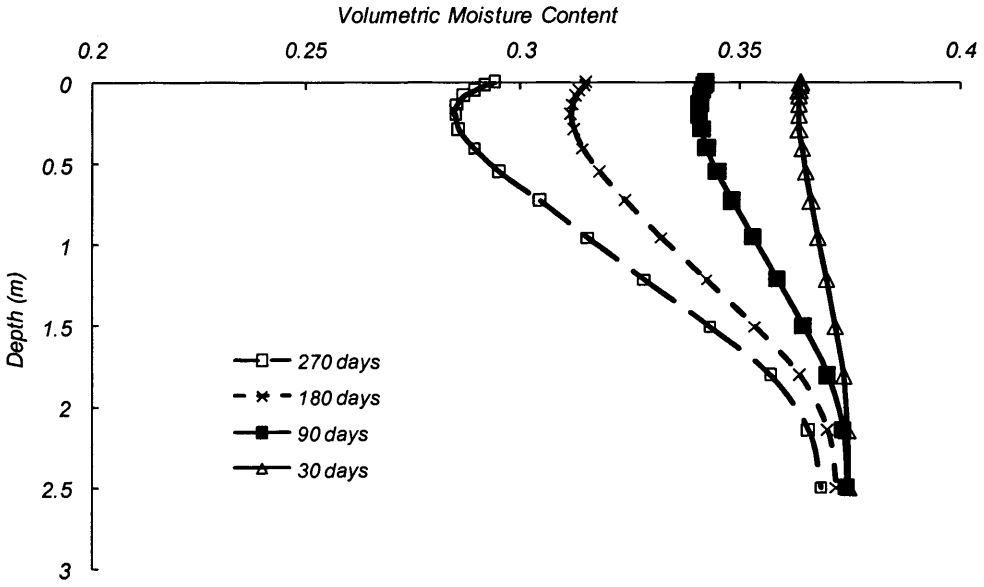

Figure 8.10 Simulated Moisture Content Profiles at distance 7.5 m (Tree at toe of slope)

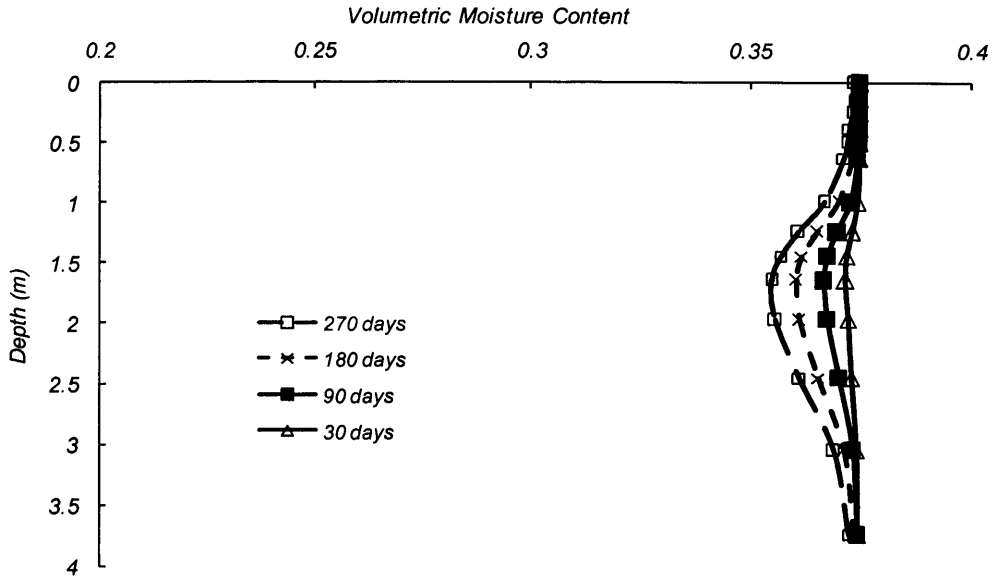

Figure 8.11 Simulated Moisture Content Profiles at distance 10.0 m (Tree at toe of slope)

Figure 8.12 shows the predicted matric suction at a distance of 6.0 m from the origin (refer Figure 8.8) at times of 30 days, 90 days, 180 days and 270 days. The maximum matric suction has occurred near the surface with matric suction increase to 12 kPa at surface. Figure 8.13 and 8.14 shows corresponding results in term of matric suction obtained at 7.5 m and 10.0 m from the origin respectively. It should be noted that the changes in matric suction shown here are relatively small when remote from the tree.

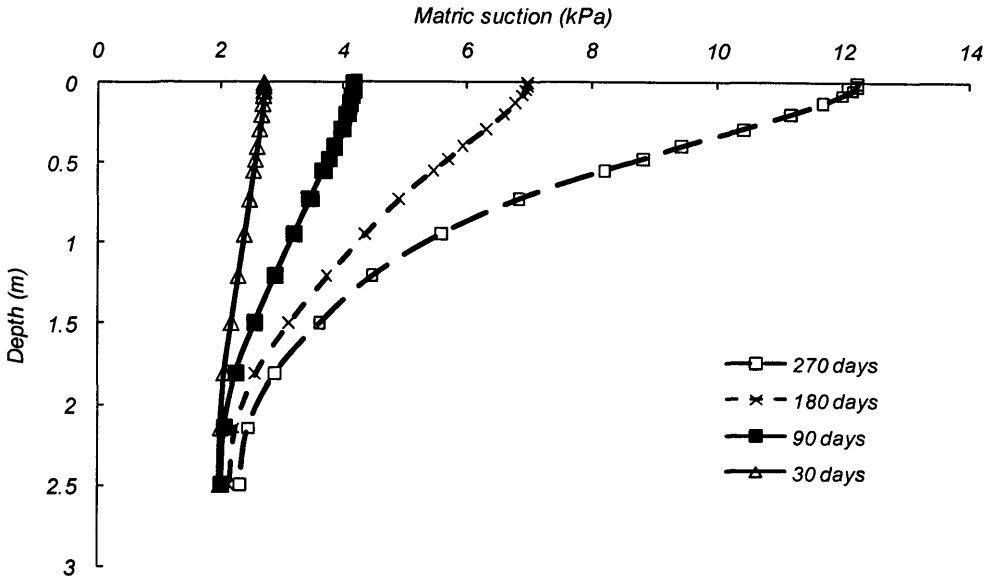

Figure 8.12 Matric Suction at distance 6.0 m (Tree at toe of slope)

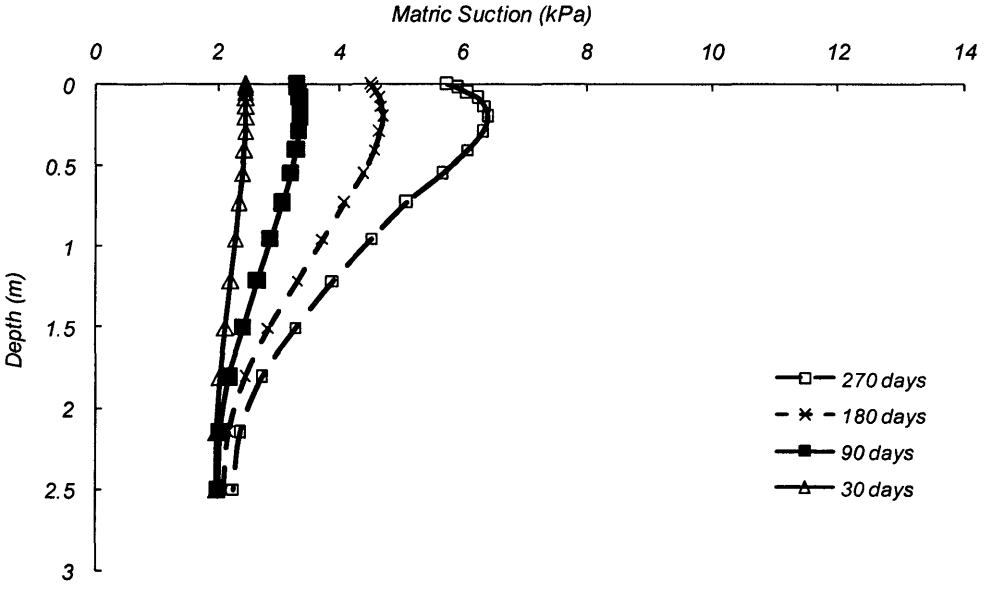

Figure 8.13 Matric Suction at distance 7.5 m (Tree at toe of slope)

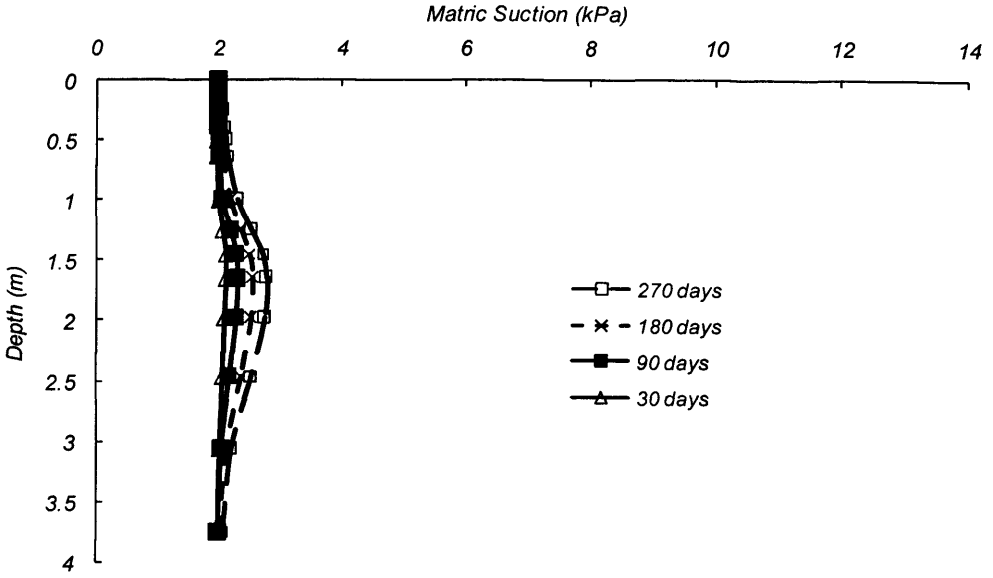

Figure 8.14 Matric Suction at distance 10.0 m (Tree at toe of slope)

Figure 8.15 shows the change in suction at the centre-node located at the base of a selection of slices (defined in Figure 8.3). As expected, significant changes in suction occur near to the centre of the tree (i.e. Slice 1). This change reduces at a distance away from the centre of tree (Slice 2 > Slice 4 > Slice 8). For completeness, Figure 8.16 shows the changes in terms of volumetric moisture content at these locations.

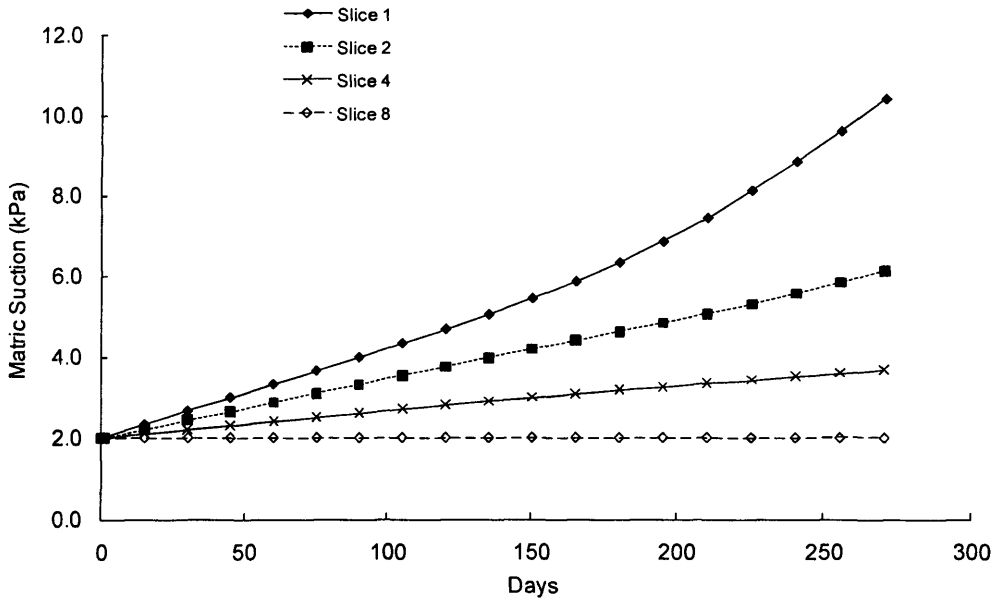

Figure 8.15 Matric Suction (kPa) profile history at the base of the slice (Refer to Figure 8.3)

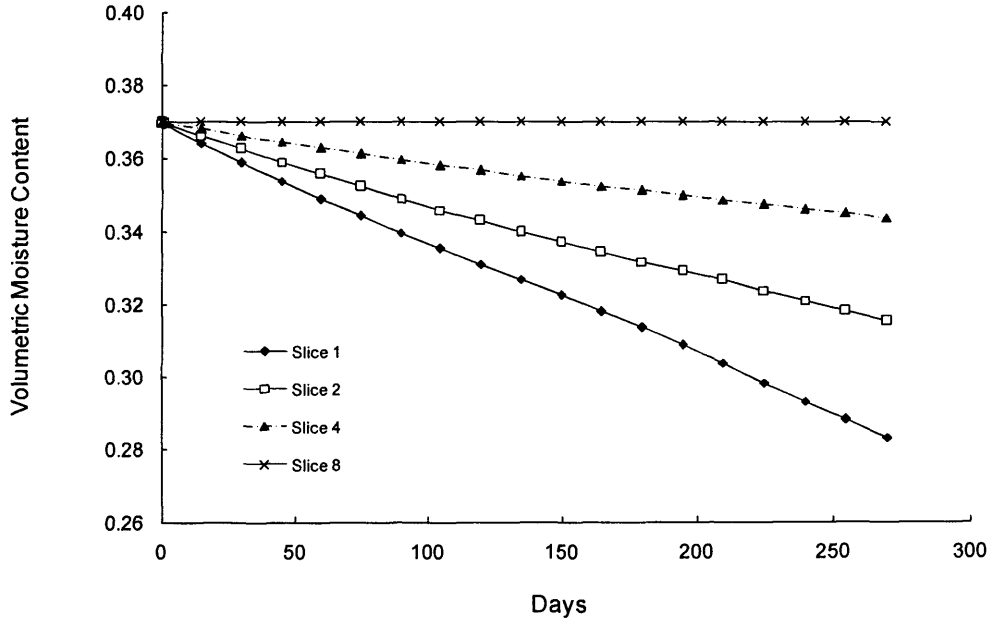

Figure 8.16 Volumetric moisture content (%) profile history at the base of the slice (Refer to Figure 8.3)

Figure 8.17 shows the resulting changes in the FOS against slope failure during the drying period. This figure shows that the FOS varies with time and increases as the suction increases in the soil. The initial FOS is 2.847 at the beginning of the simulation. This increased to 2.952, an increase of 3.7 %, at the end (270 days) of the simulation.

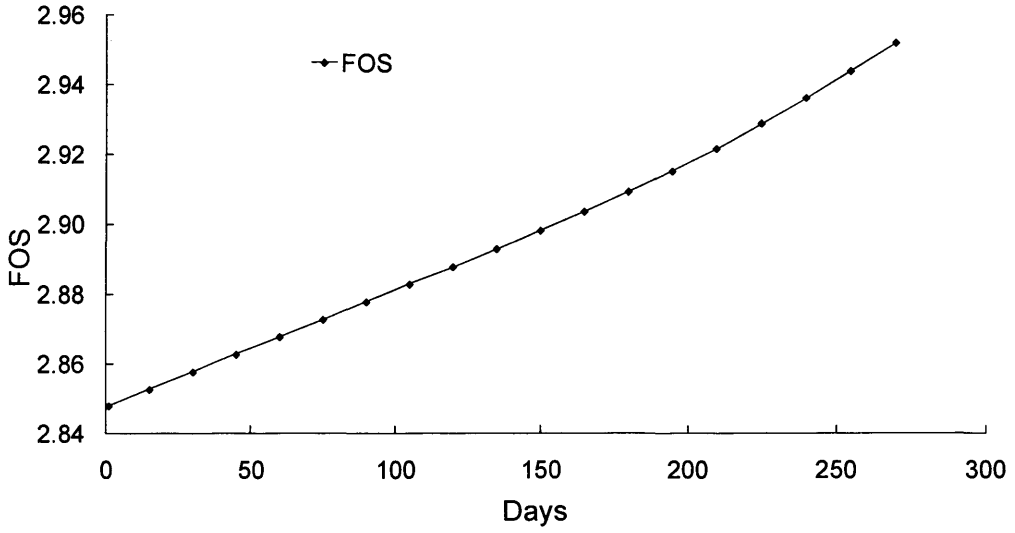

Figure 8.17 Variation of FOS in time (Tree near toe of slope)

The results also show that the percentage increase in shear strength leads to similar percentage increase in FOS. For example, the average shear strength at the slip surface varies from 1 day to 15 day from 207.421 kPa to 207.785 kPa (an increase of 0.17 %). This leads to an increase in the FOS from 2.847 to 2.852 (also an increase of 0.17 %). Again this response is dictated by the mathematical form of equation 8.9.

8.3.4 Influence of location of tree in slope stability

Two new simulations have been undertaken where the position of the tree has been relocated to; i) the centre of the slope, and ii) to the top of the slope. Material properties, transpiration rate, root zone, boundary condition, initial condition and slip failure surface all remain unchanged from the previous simulation. However several modifications (i.e. geometric control) in the FORTRAN code have been made to ensure that the water uptake model functions correctly when the tree is positioned anywhere along the slope surface. The new simulations employ a similar finite element mesh to that shown previously and a time-step size of 21600 seconds, which was held constant for the entire period considered. The simulated period also covered a spring/summer soil-drying phase of 9 months.

8.3.4.1 Tree at centre of slope

The simulated contours of matric suction now generated at the end of the simulation at 270 days for a tree located at the mid-height of the slope is shown in Figure 8.18. For clarity, the position of critical slip surface along with location of the slices also is shown in this figure.

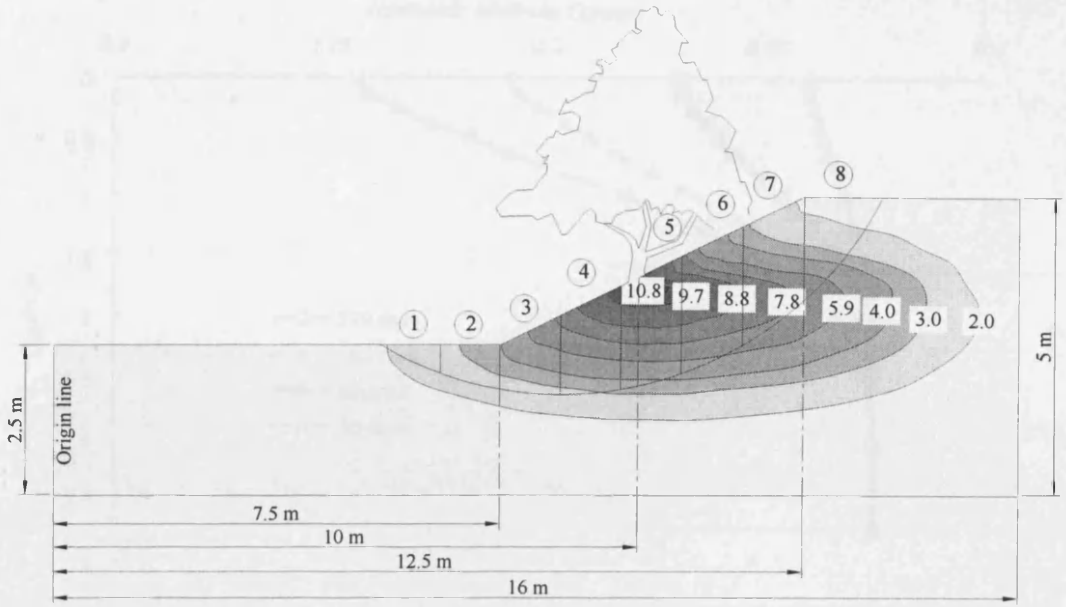

Figure 8.18 Matric suction (kPa) contours at 270 days (Tree at centre of slope)

Figure 8.19 shows the predicted moisture content profiles at a distance of 10.0 m from the origin (located at left line of the domain as shown in Figure 8.18) at times of 30 days, 90 days, 180 days and 270 days. It is clear that the majority of the moisture extraction has occurred near the slope surface with the volumetric moisture content reducing to 26.0 %. The profile is roughly linear and the moisture content increases to its initial value of 37.5 % at approximately 3.0 m below the slope surface.

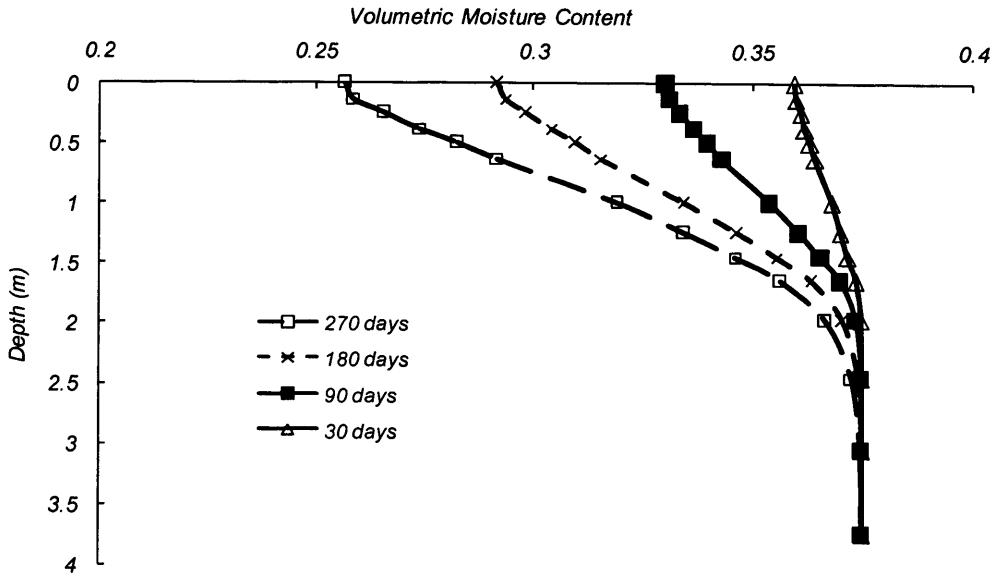

Figure 8.19 Simulated Moisture Content Profiles at a distance of 10 m (Tree at centre of slope)

Figures 8.20 and 8.21 show that a very similar set of results was obtained remote from the tree at 12.5 m and 7.5 m from the origin respectively. It should be noted that the change in moisture content shown here is small compared to that near the centre of tree. Figure 8.20, shows the maximum moisture extraction at 12.5 m from the origin occurred at depth 1.5 m below the slope surface. The volumetric moisture content reduced to 32.0 % at this position. Again, this moisture profile pattern can be explained due to the fact that the depth of 1.5 m from soil surface is approximately at the same level as the tree. Figure 8.21 shows that less moisture depletion occurred at a distance of 7.5 m.

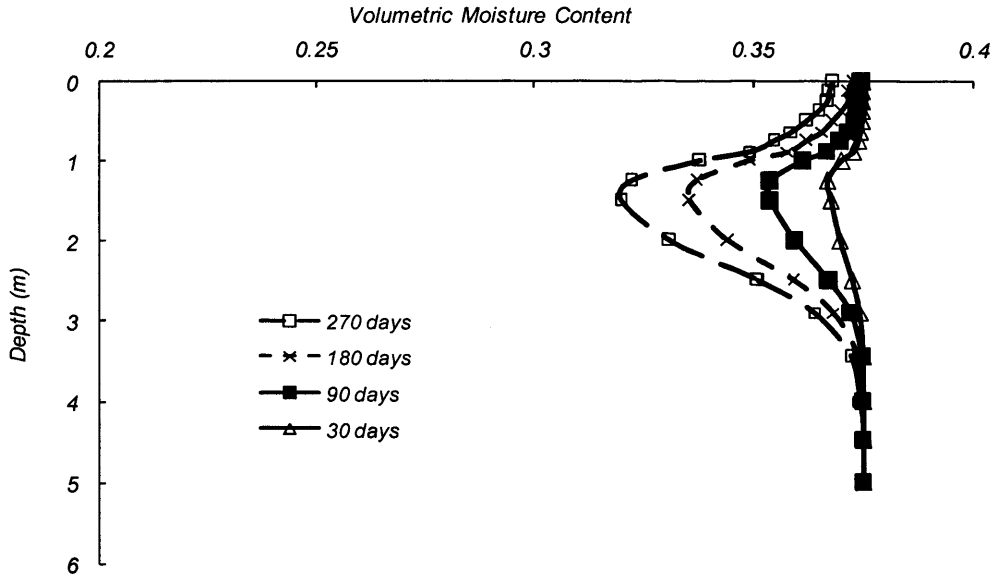

Figure 8.20 Simulated Moisture Content Profiles at distance 12.5 m (Tree at centre of slope)

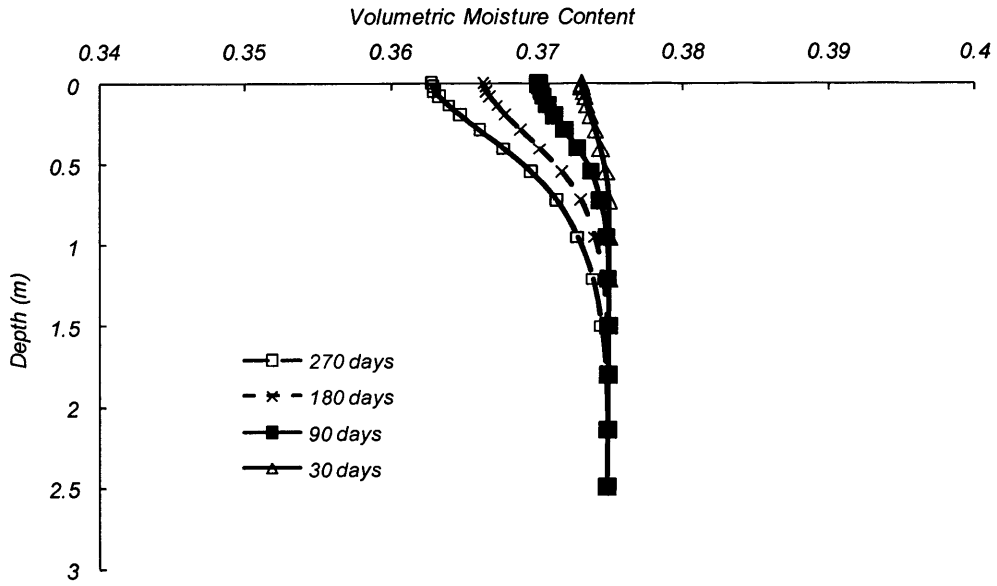

Figure 8.21 Simulated Moisture Content Profiles at distance 7.5 m (Tree at centre of slope)

Figure 8.22 shows the predicted matric suction at a distance of 10.0 m from the origin at times of 30 days, 90 days, 180 days and 270 days. The maximum matric suction has occurred near the surface with matric suction increase to 9.4 kPa at surface.

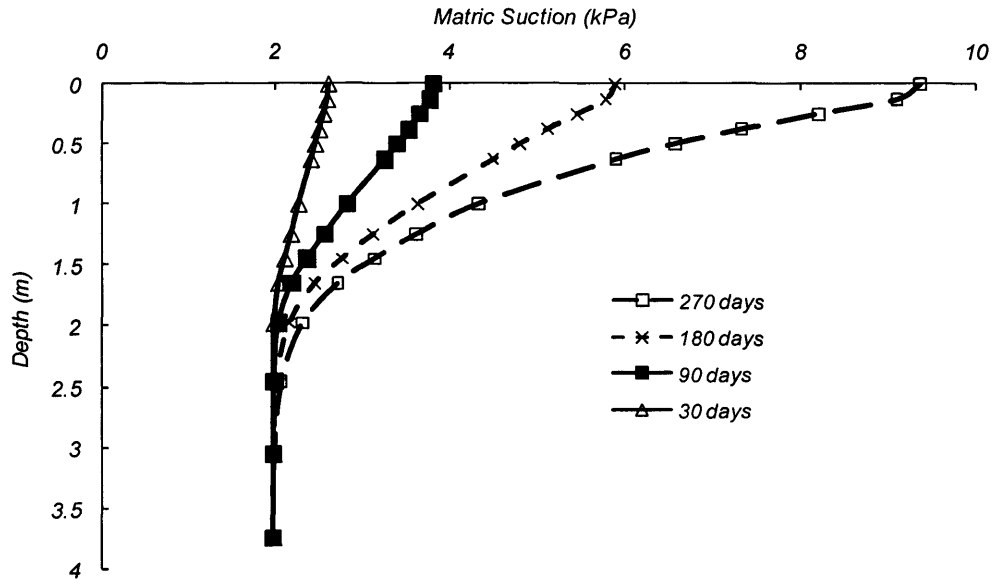

Figure 8.22 Matric Suction at distance 10 m (Tree at centre of slope)

Figures 8.23 and 8.24 show the change in matric suction obtained at 12.5 m and 7.5 m from the origin respectively. The results are similar to those explained above.

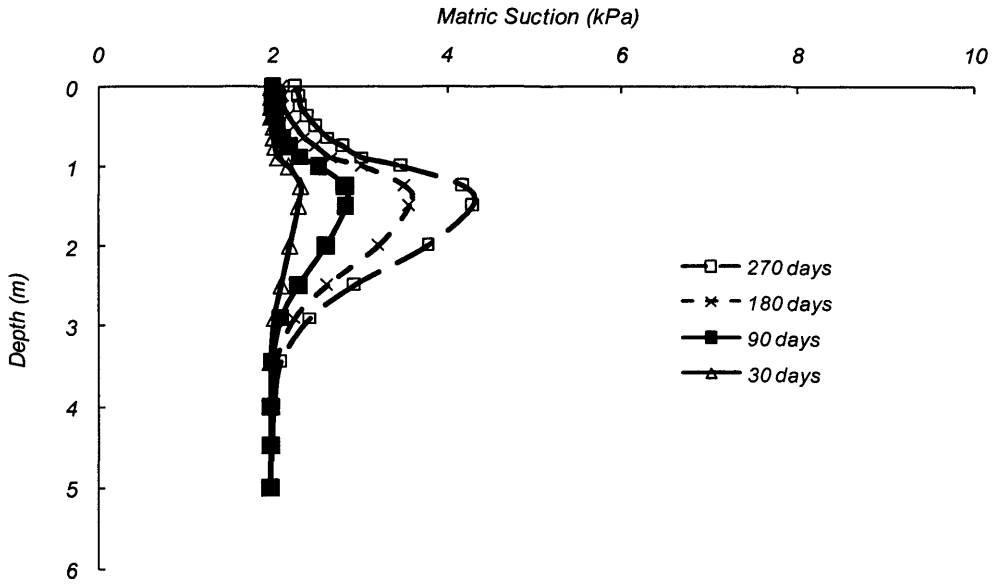

Figure 8.23 Matric Suction at distance 12.5 m (Tree at centre of slope)

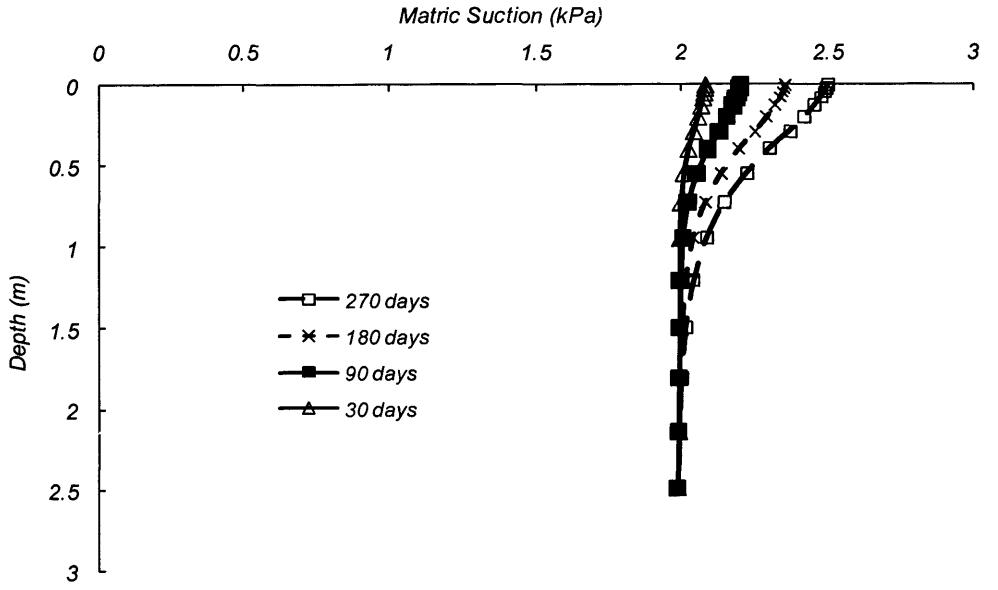

Figure 8.24 Matric Suction at distance 7.5 m (Tree at centre of slope)

Figure 8.25 shows the change in FOS against slope failure (refer Figure 8.18). As expected, this figure shows that the FOS varies with time and increases as the suction increased in the soil. The initial FOS is 2.847 at the beginning of the simulation. This increased to 2.887, an increase of 1.4 %, at the end (270 days) of the simulation.

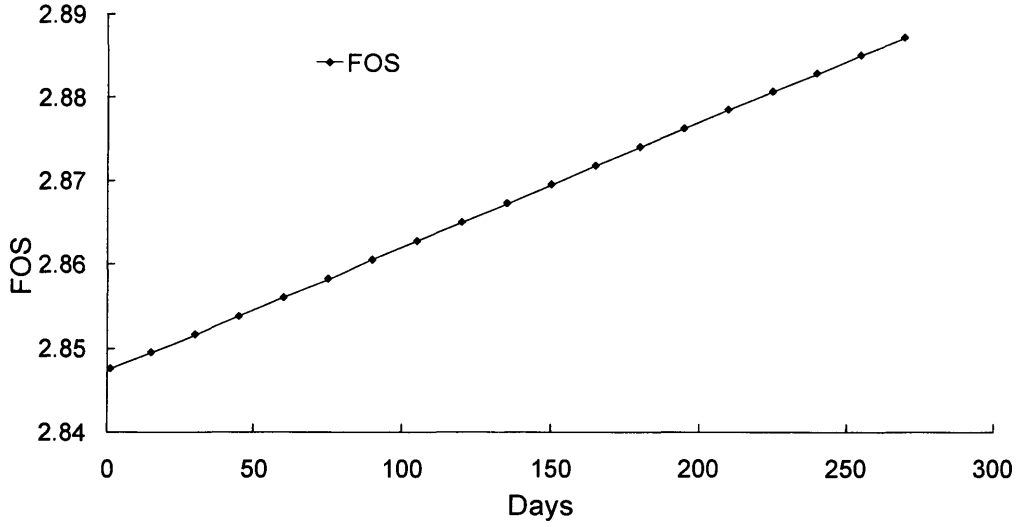

Figure 8.25 Variation of FOS in time (Tree at centre of slope)

8.3.4.2 Tree at the top of slope

Figure 8.26 shows the simulated contours of matric suction generated at the end of the simulation at 270 days for a tree at the top of slope. Again, for clarity, the position of critical slip surface along with location of the slices is shown in this figure.

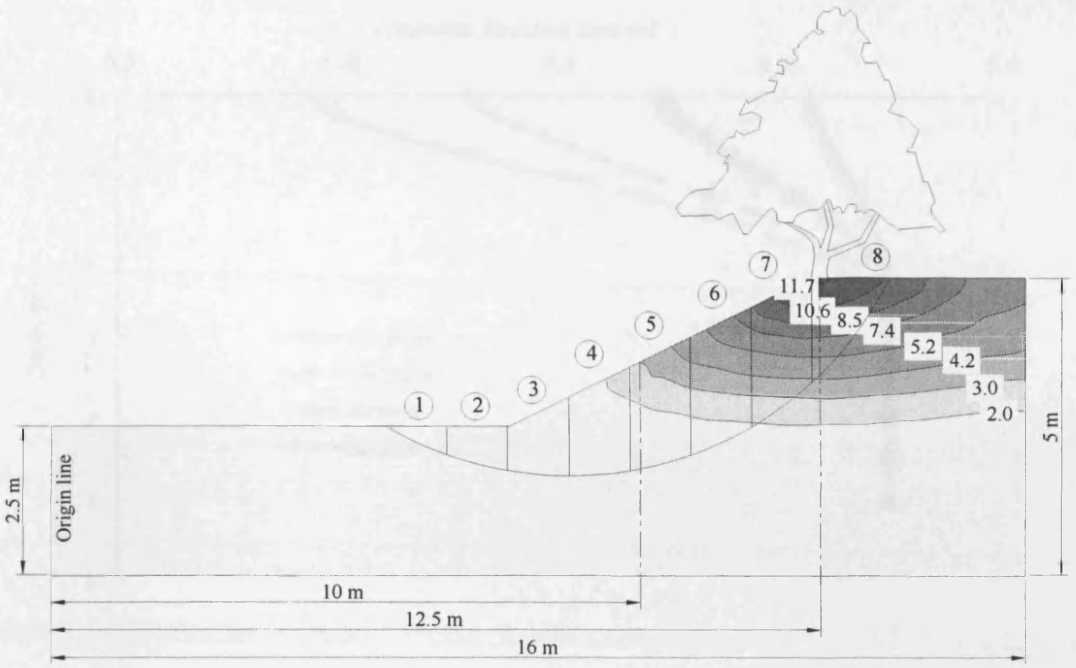

Figure 8.26 Matric suction (kPa) contours at 270 days (Tree at the top of slope)

Figure 8.27 shows the predicted moisture content profiles at a distance of 12.5 m from the origin at times of 30 days, 90 days, 180 days and 270 days. The majority of the moisture extraction has occurred near the slope surface with the volumetric moisture content reducing to 24.0 % at slope surface. The moisture content profile increases to its initial value of 37.5 % at approximately 2.9 m below the slope surface.

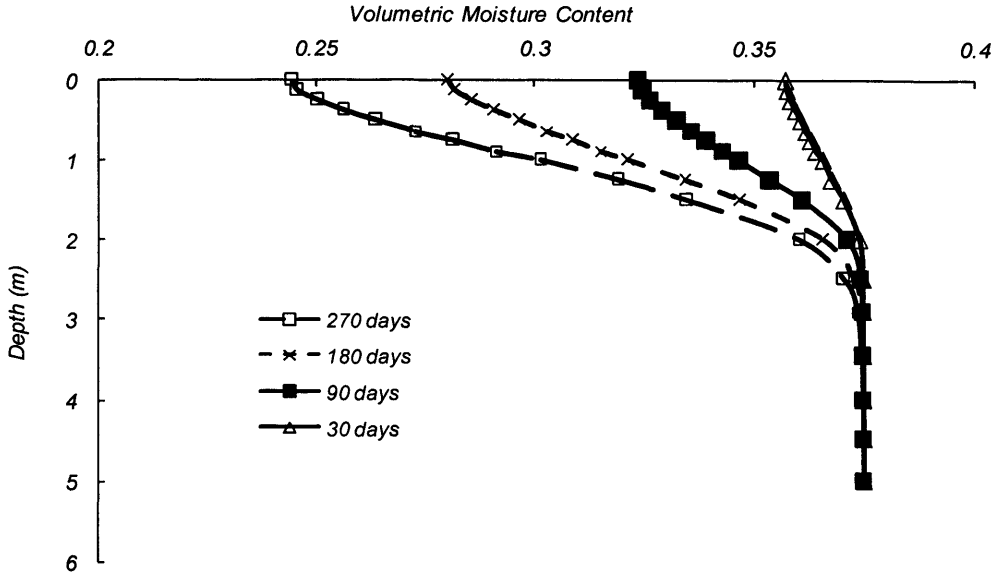

Figure 8.27 Simulated Moisture Content Profiles at distance 12.5 m (Tree at the top of slope)

Figure 8.28 shows that a less significant variation was obtained remote from the tree at 10.0 m from the origin. Figure 8.29 shows the predicted matric suction at a distance of 12.5 m from the origin at times of 30 days, 90 days, 180 days and 270 days. The maximum matric suction of 11.6 kPa occurred near the surface. Figure 8.30 shows the change in matric suction at 10.0 m from the origin.

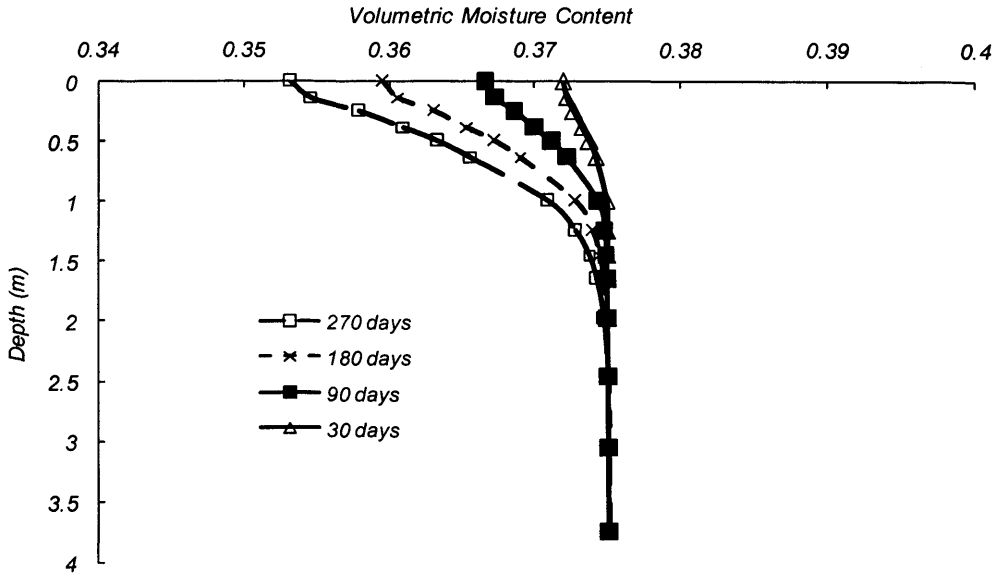

Figure 8.28 Simulated Moisture Content Profiles at distance 10 m (Tree at the top of slope)

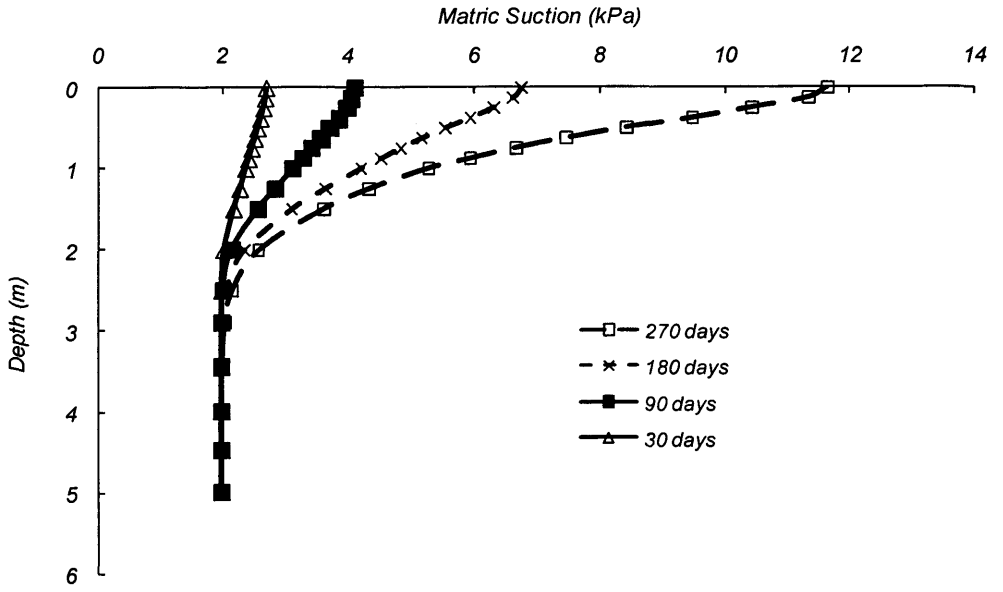

Figure 8.29 Matric Suction at distance 12.5 m (Tree at the top of slope)

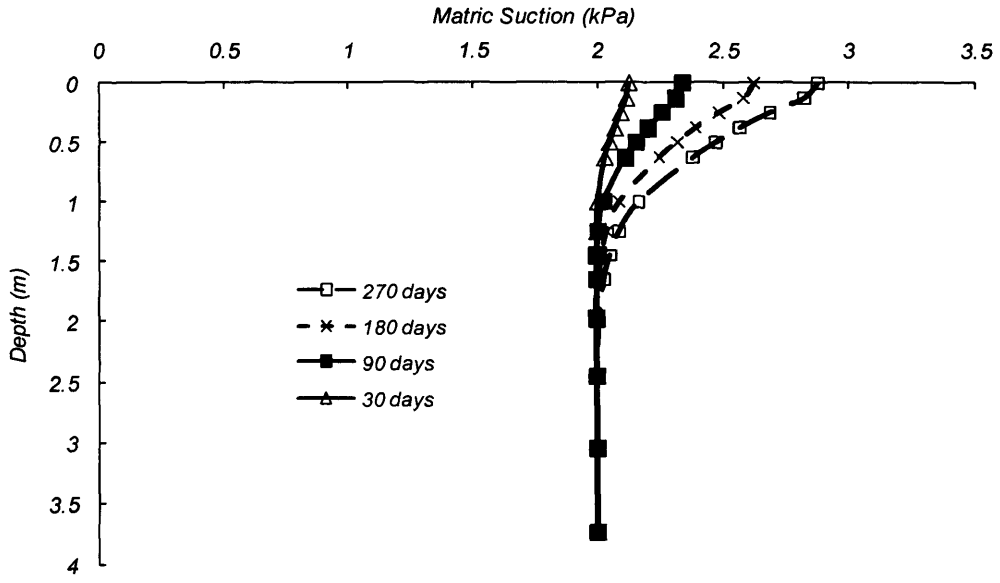

Figure 8.30 Matric Suction at distance 10 m (Tree at the top of slope)

Figure 8.31 shows the change in FOS against slope failure plotted against time. The initial FOS is 2.847 at the beginning of the simulation. This increases to 2.887, an increase of 1.4 %, at the end (270 days) of the simulation.

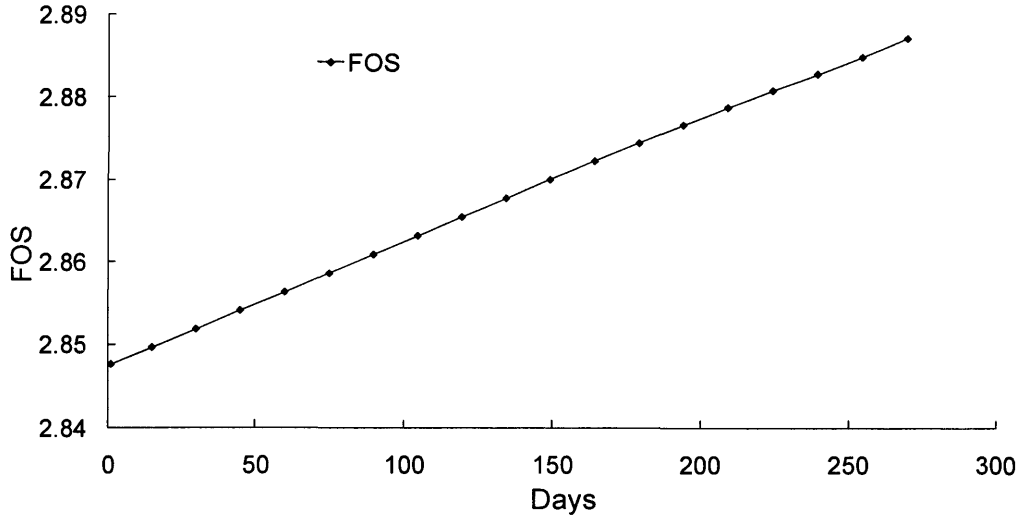

Figure 8.31 Variation of FOS in time (Tree at the top of slope)

8.3.5 Summary of FOS Variations

Table 8.4 shows a comparison of the FOS at the end of each simulation and the percentage difference when compare to a fully saturated slope. This table shows the various conditions considered, the position of tree in terms of coordinates and the values of the FOS. The coordinates are given in metres and are based on an origin located at lower left corner of the domain shown in Figure 8.2.

Table 8.4 Comparison of FOS at various conditions

Conditions	Description	FOS	Percentage difference (%)
1. Fully Saturated	Trial slope with no tree water uptake	2.74	0
2. Unsaturated	No tree water uptake and assumed capillary potential at -20 cm	2.85	4
3. Tree at toe (Figure 8.8)	Position of tree; Coordinate x = 6.0 m, Coordinate y = 2.5 m	2.95	7.7
4. Tree at centre of slope (Figure 8.18)	Position of tree; Coordinate x = 10.0 m, Coordinate y = 4.0 m	2.89	5.47
5. Tree at the top of slope (Figure 8.26)	Position of tree; Coordinate x = 12.5 m, Coordinate y = 5.0 m	2.89	5.47

In Table 8.4, the FOS for the slope geometry (referring back to Figure 8.4) when fully saturated is 2.74. This value is used as reference to compute the percentage difference of FOS for other conditions.

The first comparison is made when the slope is unsaturated and without tree. As a first illustration, the value of capillary potential of -20 cm was assumed throughout the domain. This value has been employed as an initial condition for all tree water uptake cases considered. The results indicate that the FOS against slip failure increases by 4.0 % from 2.74 to 2.85 when the slope is unsaturated at capillary potential -20 cm.

Other FOS comparisons have been made according to the presence of a tree at various locations on the slope. From these results it can be seen that changes in matric

suction due to tree water uptake can increase the FOS in the range 5.47 % to 7.7 %. It is clear that the FOS for a tree located near at the toe shows the most significant increase of 7.7 % (from 2.74 to 2.95). This is due to the fact that the slip failure surface for this case coincides with the main root zone where the majority of the suction increase occurs.

8.4 CONCLUSIONS

The application of a numerical model for the simulation of moisture migration patterns due to tree water uptake in a typical soil slope has been presented in this chapter. The approach was utilized to provide a preliminary assessment of the significance of water content (and therefore suction) changes on the stability of unsaturated soil slopes.

This research used the theory of limit equilibrium of forces and moment to compute the FOS against failure. A FOS equation which included matric suction in an unsaturated soil slope was developed and used throughout the work. In the study, the location of the critical slip surface was determined using SLOPEW. A comparison of FOS calculations by various methods of analysis has been presented.

A sensitivity study of the angle indicating the rate of increase in shear strength relative to matric suction, ϕ^b has been undertaken to illustrate its importance on the overall calculation of the FOS against failure. It has been shown that the FOS increases as ϕ^b increases. The results indicated that every 1° change of ϕ^b may change the FOS by 0.026 for the specific case considered. Therefore the results do

not appear to be particularly sensitive to small variations in the magnitude of ϕ^b. It is also clear that the change in FOS is linearly related to the value of ϕ^b.

For a typical slope geometry, a range of initial conditions and tree locations have been considered. These include both fully saturated and unsaturated conditions. Three locations of a tree on the slope have been considered. These were, i) a tree located near at the toe of the slope, ii) a tree located at the centre of the slope, and iii) a tree located and at the top of slope.

The moisture profiles and matric suction profiles at key times and at key locations have been presented. A comparison of the FOS for different the three tree locations was made. The results indicated that for all cases, the FOS increased as the suction increased in the soil. The percentage change in FOS was shown to depend, to some extent, on the precise position of the tree. The study indicated that the suction generated by a tree may increase the FOS up to 7.7 % above the value at saturation.

The FOS calculations presented here only consider hydrological effects which are related to soil moisture variations driven by transpiration. Mechanical effects that arise from the tensile strength of roots and the weight of vegetation have been ignored. Although beyond the scope of this study, Greenwood et al (2004) claim that the FOS can increase by 10 % from mechanical effects. Combining both effects, the presence of trees may increase the FOS by as much as 15.0 % to 17.0 %. Clearly this magnitude of effect suggests careful consideration is needed for practical cases when vegetation is to be used or removed from slopes. It is hoped that these findings enhance our overall understanding of the beneficial role of trees in increasing the stability of a slope.

8.5 REFERENCES

Bishop, A.W., "The use of the slip circle in the stability analysis of earth slopes." Geotechnique, 5 (1), 7 – 17, 1955.

Bishop, A. W., Alphan I., Blight, G. E. and Donald, I. B., "Factors Controlling the Shear Strength of Partly Saturated Cohesive Soils." ASCE, Colorado, 503 – 532, 1960.

Fabius, K., Fabius, M., Vanapalli, S and Maki, G. "Slope hazard management with the cautionary zone approach: a case history." 57th Canadian Geotechnical Conference, Canada 1 – 8, 2004.

Fellenius, W., "Calculation of the Stability of Earth Dams." Trans. 2nd Int. Cong. Large Dams, Washington, 445 – 459, 1936.

Fredlund, D.G., Morgenstern, N. R. and Widger, R. A., "The shear strength of unsaturated soils." Canadian Geotechnical Journal, 15, 313 – 321, 1978.

Fredlund, D. G. and Rahardjo, H., "Soil Mechanics of Unsaturated Soils." John Wiley & Sons: New York, 1993.

Greenwood, J. R., "SLIP4EX – A program for routine slope stability analysis to include the effects of vegetation, reinforcement and hydrological changes." Geotechnical and Geological Engineering, 24, 449–465, 2006.

Greenwood, J. R. BSc, Norris, J. E. and Wint, J., "Assessing the contribution of vegetation to slope stability." Geotechnical Engineering, 157, 199–207, 2004.

Griffiths, D. V. and Lu, N. "Unsaturated slope stability analysis with steady infiltration or evaporation using elasto-plastic finite elements." Int. J. Numer. Anal. Meth. Geomech., 29, 249–267, 2005.

Janbu, N., Bjerrum, L. and Kjaernsli, B. "Soil mechanics applied to some engineering problems. " Norwegian Geotechnical Institute Publication, 16, 1956.

Krahn, J., "Stability modelling with SLOPEW." GEO-SLOPE/W International Ltd, Canada, 2004.

Lambe, T. W. and Whitman, R. V., "Soil Mechanics." Wiley, New York, 363–365, 1969.

MacNeil, D. J., Steele, D. P., McMahoii, W. and Carder, D. R. "Vegetation for slope stability." Prepared for Quality Services, Civil Engineering, Highways Agency, 48, 2001.

McGinnity, B. T., Fitch T. and Rankin, W. J. "A systematic and cost-effective approach to inspecting, prioritising and upgrading London Underground Earth Structures. " ICE Proceedings of Seminar, "Value of Geotechnics in Construction". 309-332, 1998.

Morgenstern, N. R. and Price, V. E., "The analysis of the Stability of General Slip Surfaces." Geotechnique, 15, 79 – 93 , 1965.

Renaud, J. P., Anderson, M. G., Wilkinson, P. L., Lloyd, D. M. and Wood, D. M. "The importance of visualisation of results from slope stability." Geotechnical Engineering, 156 (1), 27–33, 2003.

Ridley, A., Ginnity, M. and Vaughan, P., "Role of pore water pressures in embankment stability." Geotechnical Engineering, 157, 193–198, 2004.

Russell, D., Ellis E. O'Brien A. S. & McGinnity B. "Role of vegetation on the stability and serviceability of railways embankments. " 1st Int. Conf. on Railway Engineering, London, UK, 2000.

SLOPEW ver. 6.17 Software, GEO-SLOPE International Ltd, Calgary Alberta, Canada, 2004.

Smith, P. G. C. "Numerical analysis of infiltration into partially saturated soil slopes." PhD, Imperial College of Science, London, 2003.

Simon, A. and Collison, A. J., "Quantifying the mechanical and hydrologic effects of Riparian vegetation on streambank stability." Earth Surface Processes and Landforms, 27, 527–546, 2002.

Simon, A., Curini, A., Darby, S. E. and Langendoen, E. J., "Bank and near-bank processes in an incised channel." Geomorphology, 35, 193–217, 2000.

Simon, A. and Darby, S. E., "The nature and significance of incised river channels." In Incised River Channels: Processes, Forms, Engineering and Management, John Wiley and Sons, 3 – 18, 1999.

Spencer, E., "A Method of Analysis of the Stability of Embankments Assuming Parallel Interslice Forces." Geotechnique, 17, 11 – 26, 1967.

Technical Committee of Investigation, "The Collapse of Block 1 and the Stability of Blocks 2 and 3 Highland Towers Condominium." Report of the Technical Committee, Hulu Klang, Malaysia, 1994.

Terzaghi, K., "The Shear Resistence of Saturated Soils." Proc. Conf. Soil Mech. Found. Eng., Cambridge, 54 – 56, 1936.

Thorne, C. R., "Effects of vegetation on riverbank erosion and stability." In Vegetation and Erosion: Processes and Environments, John Wiley and Sons, 125–144, 1990.

UNSAT. "Proceedings of the Fourth International Conference on Unsaturated Soils. " Carefree, Arizona, 147, 2006.

CHAPTER NINE

CONCLUSIONS

9.1 OVERALL CONCLUSION

The overall objectives and limitations of the current investigation were defined in Chapter 1. In summary, the major objectives of the research programme were to:

i. Introduce a volumetric sink term into the governing equation for unsaturated moisture flow and subsequent finite element code.

ii. Identify a theoretical model for one-dimensional water-uptake by vegetation.

iii. Implement the selected 1D water-uptake model within the finite element framework.

iv. Verify and validate the new 1D model.

v. Develop a theoretical model for two-dimensional axi-symmetric water uptake processes associated with an established tree.

vi. Implement the 2D axi-symmetric model within the finite element formulation.

vii. Incorporate the root zone geometry and control routines related to the water uptake models within the finite element code.

viii. Validate the 2D axi-symmetric model by comparison with experimental data.

ix. Investigate water-uptake from an established tree over a seasonal time frame.

x. Investigate the influence of hysteresis in the water retention characteristics on seasonal wetting/drying trends.

xi. Provide a preliminary assessment of the role of vegetation in slope stability analysis.

It is claimed that each of these objectives have been successfully achieved. Inevitably, further work is required in relation to some of these developments. Suggestions for further development and refinement of the research are made at the end of this chapter.

The main achievement for this research was to develop a new two-dimensional axi-symmetric model to simulate moisture migration near established trees. This has been achieved. The approach adopted utilized radial symmetry and assumed a linear distribution of water extraction rate with both depth and radius. The model was validated by direct comparison to field measurements recorded (by others) for mature trees located on a clay sub-soil. Furthermore, the model has been shown to be capable of representing water-uptake over a full-annual cycle. Time dependent boundary conditions, based on rainfall data, and hysteresis effects have also been

explored. Overall, a good correlation between field data and simulated results has been achieved. It is believed that this is the first attempt at predicting moisture migration near trees over an annual time frame in this manner. The research also provides a preliminary assessment of the significance of tree induced water content (and therefore suction) changes on the stability of unsaturated soil slopes. Further detail of specific achievements is discussed below.

Chapter 2 of the thesis presented an overview of the literature. The complexity of the problem in hand was illustrated along with the significance of vegetation effects. The various approaches suggested by other researchers were discussed. These ranged from simple one-dimensional models to more complex multi-dimensional models.

Chapters 5 to 8 presented the work performed to achieve the main objectives of the research programme. The conclusions drawn from the work reported in these chapters is therefore summarised in more detail below.

An introduction to the fundamental concepts and the derivation of general partial differential equations describing water flow in an unsaturated soil was presented in Chapter 3. This included brief descriptions of the application of Darcy's Law to unsaturated flow, the concept of hysterisis and the theoretical basis of the chosen water uptake model. The key outcome of this work was the development of a two-dimensional axi-symmetric model for the simulation of water uptake from trees. The relationship between root water extraction and radial distance was introduced via a simple linear grading of the total transpiration over the active root zone.

Chapter 4 presented an approximate numerical solution of the unsaturated flow equation, modified to include a volumetric sink term and the water-uptake model. An introduction to the concepts relevant to the particular finite element

formulation used was also provided. Spatial discretisation was achieved by application of the Galerkin weighted residual approach. Time discretisation of the model was achieved by the application of a fully implicit mid-interval backward difference algorithm.

Chapter 5 presented some initial applications of the new model, operating in one-dimensional mode. This work provided some confidence with respect to both the implementation of the volumetric sink term and the basic formulation of the water-uptake model. Three specific case studies were considered. The first case illustrated application of the linear water-uptake model to a simple hypothetical test problem. The second problem considered the significance of including a water-stress function for water-uptake modelling. The final case study explored a problem involving a non-uniform root system. Overall, the new model, operating in 1D-mode, was shown to be capable of producing results that were comparable with independently published results.

The first applications of the new model for the simulation of moisture migration patterns near trees were presented in Chapter 6. In the first instance, attention was given to the prediction of moisture content variations in the vicinity of a single mature tree. The model was validated by direct comparison to field measurements recorded for two cases. The first simulation considered a mature lime tree located on Boulder clay sub-soil. A good overall correlation between field data and simulated results was achieved. A second numerical simulation was also presented to show application of the model for a different tree species and soil type. In this case, a mature Leyland Cypress tree located on Gault clay was analysed. These problems spanned a typical spring/summer drying period only. A sensitivity check was also presented in relation to the assumed hydraulic properties.

Chapter 7 presented an extended approach for the simulation of water-uptake patterns, over a full seasonal cycle, in the unsaturated zone and in the vicinity of mature trees. Time varying boundary conditions and hysteresis effects were considered at this stage. Determination of boundary conditions was based on data recorded at the nearest Meteorological Station to the field experiment. To explore the effect of hysteresis, the simulation was re-run employing a basic method of including the relevant wetting or drying water retention curves. Inclusion of this aspect of behaviour was shown to yield a moderate improvement in the overall quality of the results in comparison with the field data.

In Chapter 8, the water-uptake model was applied to investigate how suctions generated by a tree may contribute to the overall stability of a typical soil slope. The research used an equilibrium method that included the contribution of suction to soil shear strength. For typical slope geometry, a range of initial conditions and tree locations were considered. The results indicated that for all cases, slope stability increased as the soil suction increased. Stability was also shown to depend, to some extent, on the precise position of the tree. Overall, the study indicated that the suction generated by a tree may increase stability by approximately 8 % above the value obtained for a saturated slope. The stability calculations presented here only considered hydrological effects related to soil moisture variations driven by transpiration. Mechanical effects that arise from the tensile strength of roots and the weight of vegetation were not considered in this work.

9.2 FUTURE RESEARCH

The current approach has been shown to be capable of producing encouraging results for the range of problems considered. However, some clear limitations of the current approach arise if application to a wider range of problems is considered.

Firstly, the model was developed in a number of differing formats, starting with 1D representation used to establish the basis of the approach required. The two-dimensional axi-symmetric form of water uptake model then developed appears to function acceptably for the particular cases considered. However, in the field 3D moisture transfer will occur in a number of cases and extension of the model to accommodate this behaviour may be a useful future step. The theoretical extension of the water uptake model to 3D form is not a particularly onerous task in itself. However, implementation of this within a 3D finite element framework and the required verification and validation of such a model are significant undertakings. A shortage of adequate field measurement also limits this kind of development.

The current work was developed for potential application to a range of geo-engineering problems mentioned in Chapter 1. Therefore, simplicity was thought to be an attractive feature of any model developed. In this work water-uptake was assumed to vary linearly with depth and radial distance. However, field data is available that suggest a more sophisticated non-linear approach may prove a valuable further refinement – depending on the degree of precision required. Furthermore, since the current work was focused on the behaviour of established trees, root growth was excluded from the model. Root growth functions can be included within this type of water-uptake model and may be useful for future applications.

Field soils will often exhibited a variation with depth of soil properties. The current simulations have assumed a homogenous soil profile. Although in the cases considered this did not appear to be particularly significant, in other cases more detailed consideration of the soil profile will be necessary.

The moisture transfer simulations presented here were based on a constant volume soil model - no deformation was included in the current framework. However, for some swelling clays, analysis of the problem accounting for a volume change dependency on soil suction may be required. This would be useful, for example, in the assessment of the influence of trees in relation to foundation movements which damage domestic buildings.

Geometric simplification is standard practice in slope analysis and any deviation from this would give rise to a number of issues. For this reason the work presented here maintained the traditional 2D-plane simplification of the slope. However, this would give rise to an apparent geometric inconsistency if one were to attempt to link a slope analysis with, for example, the axi-symmetric simulations presented in Chapters 6 and 7. For this reason the example slope calculations presented here were based on an assumption that a line-source of moisture extraction applied. Although this provides some indication of the influence of vegetation on stability, a much more complex moisture migration may exist in a number of field problems. Mechanical effects that arise from the tensile strength of roots and the weight of vegetation have not been considered here. Independent research indicates that slope stability can be increased in the order of 10 % from mechanical effects. However, it is also clear that some mechanical effects can also reduce stability; therefore careful consideration of the overall problem will be needed in practice.

APPENDIX 1

EXAMPLE CALCULATION FOR A ONE-DIMENSIONAL PROBLEM

1-D PROBLEM

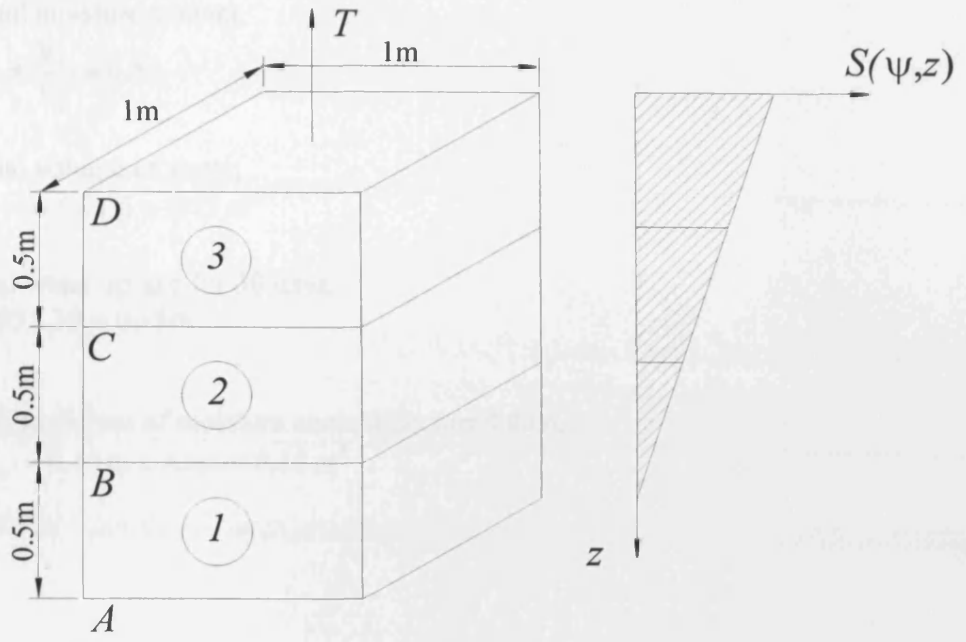

Consider test problem above,

Area,	$A = 1m \times 1m = 1m^2$
Total Volume,	$V_T = 1m \times 1.5m = 1.5m^3$
Initial moisture content,	$\theta_{sat} = 0.5$
Transpiration rate,	$T = 0.005$ m/day
Total time,	$t = 30$ days
Maximum root depth,	$z_r = 1.5m$

Manual Solution

Initial moisture content,

$$\theta_{sat} = \frac{V_w}{V_T} = 0.5$$

Initial volume of water,

$V_{wi} = 0.5 \times 1.5 = 0.75\ m^3$

Total water uptake for 30 days,

$0.005 \times 30 = 0.15m$

If uniform loss of moisture content occurred then,

$\Delta V_w = 0.15\ m \times Area = 0.15\ m^3$

Sink Term

Application of linear variation in equation (3.35) in chapter 3, $S(\psi, z) = \frac{2T_j}{z_{rj}} \alpha(\psi) \left(1 - \frac{z}{z_{rj}} \right)$ would apply for this 3 element problem,

Assuming $\alpha(\psi) = 1$,

Element no 1,

$$\int_{z=1.0}^{z=1.5} \frac{2T}{z_r}\left(1-\frac{z}{zr}\right)\partial z$$

$$=\frac{2T}{z_r}\int_{z=1.0}^{z=1.5}\left(1-\frac{z}{zr}\right)\partial z$$

$$=\frac{(2)(0.005)}{1.5}\int_{z=1.0}^{z=1.5}\left(1-\frac{z}{1.5}\right)\partial z$$

$$=\frac{(2)(0.005)}{1.5}\left[z-\frac{z^2}{3.0}\right]_{1.0}^{1.5}$$

$$=\frac{(2)(0.005)}{1.5}\left[\left(1.5-\frac{1.5^2}{3.0}\right)-\left(1.0-\frac{1.0^2}{3.0}\right)\right]$$

=0.00056 m/d

Water uptake rate for element no 1,

0.00056 m/d x 1 m^2 area

$= 0.00056\ m^3/d$

For 30 days,
$0.00056 \times 30 = 0.0168\ m^3$

Element no 2,

$$\int_{z=0.5}^{z=0.1} \frac{2T}{z_r}\left(1-\frac{z}{zr}\right)\partial z$$

$$=\frac{2T}{z_r}\int_{z=0.5}^{z=1.0}\left(1-\frac{z}{zr}\right)\partial z$$

$$=\frac{(2)(0.005)}{1.5}\int_{z=0.5}^{z=1.0}\left(1-\frac{z}{1.5}\right)\partial z$$

$$=\frac{(2)(0.005)}{1.5}\left[z-\frac{z^2}{3.0}\right]_{0.5}^{1.0}$$

$$=\frac{(2)(0.005)}{1.5}\left[\left(1.0-\frac{1.0^2}{3.0}\right)-\left(0.5-\frac{0.5^2}{3.0}\right)\right]$$

=0.00166 m/d

Water uptake rate for element no 2,

=0.00166 m/d x 1m^2 area

=0.00166 m^3/d

For 30 days,
0.00166 x 30 = 0.0498 m^3

Element no 3,

$$\int_{z=0}^{z=0.5} \frac{2T}{z_r}\left(1-\frac{z}{zr}\right)\partial z$$

$$=\frac{2T}{z_r}\int_{z=0}^{z=0.5}\left(1-\frac{z}{zr}\right)\partial z$$

$$=\frac{(2)(0.005)}{1.5}\int_{z=0}^{z=0.5}\left(1-\frac{z}{1.5}\right)\partial z$$

$$=\frac{(2)(0.005)}{1.5}\left[z-\frac{z^2}{3.0}\right]_0^{0.5}$$

$$=\frac{(2)(0.005)}{1.5}\left[\left(1.0-\frac{0.5^2}{3.0}\right)-\left(0.5-\frac{0^2}{3.0}\right)\right]$$

$$=0.00277\,\text{m/d}$$

Water uptake rate for element no 3,

=0.00277m/d x $1m^2$ area

$=0.00277\,m^3/d$

For 30 days,
$0.00277 \times 30 = 0.0833\,m^3$

Therefore, total volume of water depletion in all elements for 30 days,

$0.0168 + 0.0498 + 0.0833 = 0.15\,m^3$

APPENDIX 2

EXAMPLE CALCULATION
FOR STANDARD TWO-DIMENSIONAL PROBLEM

2-D PROBLEM

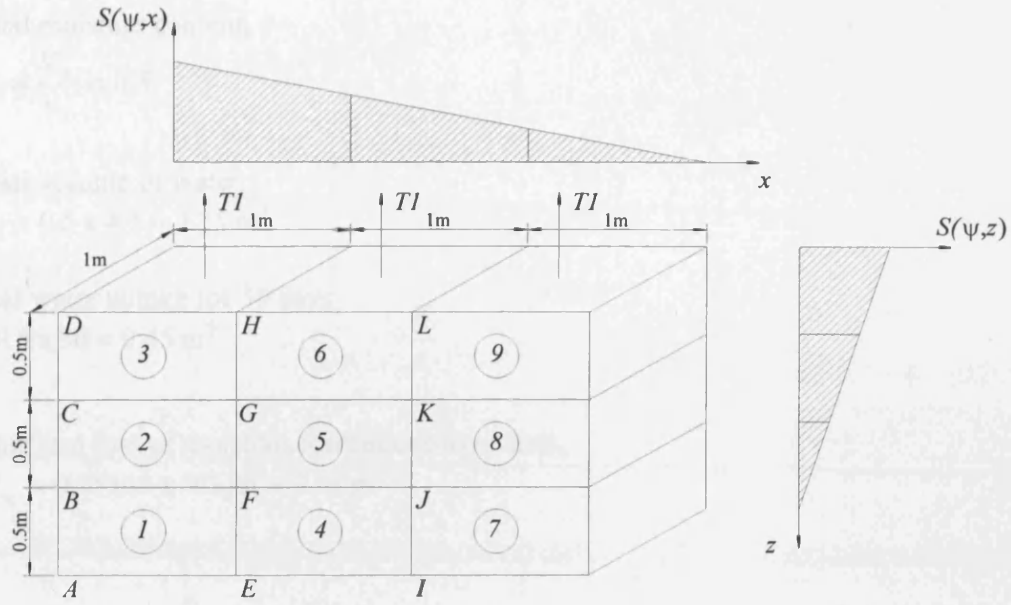

Consider test problem above,

Total Volume,	$V_T = 3m \times 1.5m = 4.5\ m^3$
Initial moisture content,	$\theta_{sat} = 0.5$
Transpiration rate,	$T1 = 0.005$ m/day
Total time,	$t = 30$ days
Maximum root depth,	$z_r = 1.5m$
Maximum length of root distance	$x_r = 3.0m$

Note that the total transpiration rate,
T = T1 x Length

$T = 0.005 \times 3 = 0.015\ m^2/day$

Manual Solution

Initial moisture content,

$$\theta_{sat} = \frac{V_w}{V_T} = 0.5$$

Initial volume of water,

$V_{wi} = 0.5 \times 4.5 = 2.25\ m^3$

Total water uptake for 30 days

$0.015 \times 30 = 0.45\ m^2$

If uniform loss of moisture content occurred then,

$\Delta V_w = 0.45\ m^2 \times \text{Width} = 0.45\ m^3$

Sink Term

Application of linear variation in equation (3.47) in chapter 3, $S(\psi,z,r) = \frac{4T}{z_r r_r}\alpha(\psi)\left(1-\frac{z}{z_r}\right)\left(1-\frac{r}{r_r}\right)$ can be re-cast in a standard two-dimensional format as follows:

$$S(\psi,z,x) = \frac{4T}{z_r x_r}\alpha(\psi)\left(1-\frac{z}{z_r}\right)\left(1-\frac{x}{x_r}\right)$$

The example will assume $\alpha(\psi) = 1$

Element no 1,

$$\int_{z=1.0}^{z=1.5}\int_{x=0}^{x=1.0}\frac{4T}{z_r}\left(1-\frac{z}{z_r}\right)\left(1-\frac{x}{x_r}\right)\partial x\partial z$$

$$=\frac{4T}{z_r x_r}\int_{z=1.0}^{z=1.5}\int_{x=0}^{x=1.0}\left(1-\frac{z}{z_r}\right)\left(1-\frac{x}{x_r}\right)\partial x\partial z$$

$$=\frac{(4)(0.015)}{1.5x3.0}\int_{z=1.0}^{z=1.5}\int_{x=0}^{x=1.0}\left(1-\frac{z}{1.5}\right)\left(1-\frac{x}{3.0}\right)\partial x\partial z$$

$$=0.0133\int_{z=1.0}^{z=1.5}\int_{x=0}^{x=1.0}\left(1-\frac{x}{3.0}-\frac{z}{1.5}+\frac{xz}{4.5}\right)\partial x\partial z$$

$$=0.0133\int_{z=1.0}^{z=1.5}\left[x-\frac{x^2}{6}-\frac{xz}{1.5}+\frac{x^2z}{9}\right]_0^{1.0}\partial z$$

$$=0.0133\int_{z=1.0}^{z=1.5}\left[\left(1-\frac{1}{6}-\frac{z}{1.5}+\frac{z}{9}\right)-(0)\right]\partial z$$

$$=0.0133\int_{z=1.0}^{z=1.5}[0.8333-0.555z]\partial z$$

$$=0.0133\left[0.8333z-\frac{0.555z^2}{2}\right]_{1.0}^{1.5}$$

$$=0.0133\left[\left(0.8333\,\text{x}\,1.5-\frac{0.555\,\text{x}\,1.5^2}{2}\right)-\left(0.8333\,\text{x}\,1.0-\frac{0.555\,\text{x}\,1.0^2}{2}\right)\right]$$

$$=0.0133(0.069)$$

$=0.0009\ \text{m}^2/\text{d}$

Water uptake rate for element no 1,

$0.0009\ \text{m}^2/\text{d}$ x 1m width
$=0.0009\ \text{m}^3/\text{d}$

For 30 days,
$=0.0003$ x $30 = 0.027\ \text{m}^3$

Element no 2,

$$= 0.0133 \int_{z=0.5}^{z=1.0} \int_{x=0}^{x=1.0} \left(1 - \frac{x}{3.0} - \frac{z}{1.5} + \frac{xz}{4.5}\right) \partial x \partial z$$

$$= 0.0133 \int_{z=0.5}^{z=1.0} \left[x - \frac{x^2}{6} - \frac{xz}{1.5} + \frac{x^2 z}{9} \right]_0^{1.0} \partial z$$

$$= 0.0133 \int_{z=1.0}^{z=1.5} \left[\left(1 - \frac{1}{6} - \frac{z}{1.5} + \frac{z}{9}\right) - (0) \right] \partial z$$

$$= 0.0133 \int_{z=0.5}^{z=1.0} [0.8333 - 0.555z] \partial z$$

$$= 0.0133 \left[0.8333z - \frac{0.555z^2}{2} \right]_{0.5}^{1.0}$$

$$= 0.0133 \left[\left(0.8333 \text{ x } 1.0 - \frac{0.555 \text{ x } 1.0^2}{2} \right) - \left(0.8333 \text{ x } 0.5 - \frac{0.555 \text{ x } 0.5^2}{2} \right) \right]$$

$$= 0.0133(0.2085)$$

$=0.0027 m^2/d$

Water uptake rate for element no 2,

$0.0027 m^2/d$ x 1m width

$=0.0027 m^3/d$

For 30 days,
$=0.0027 \text{ x } 30 = 0.081 \text{ } m^3$

Element no 3,

$$= 0.0133 \int_{z=0}^{z=0.5} \int_{x=0}^{x=1.0} \left(1 - \frac{x}{3.0} - \frac{z}{1.5} + \frac{xz}{4.5}\right) \partial x \partial z$$

$$= 0.0133 \int_{z=0}^{z=0.5} \left[x - \frac{x^2}{6} - \frac{xz}{1.5} + \frac{x^2 z}{9}\right]_0^{1.0} \partial z$$

$$= 0.0133 \int_{z=0}^{z=0.5} \left[\left(1 - \frac{1}{6} - \frac{z}{1.5} + \frac{z}{9}\right) - (0)\right] \partial z$$

$$= 0.0133 \int_{z=0}^{z=0.5} [0.8333 - 0.555z] \partial z$$

$$= 0.0133 \left[0.8333z - \frac{0.555z^2}{2}\right]_0^{0.5}$$

$$= 0.0133 \left[\left(0.8333 \text{ x } 0.5 - \frac{0.555 \text{ x } 0.5^2}{2}\right) - (0)\right]$$

=0.0133(0.3473)

=0.0046 m^2/d

Water uptake rate for element no 3,

0.0046 m^2/d x 1m width

=0.0046 m^3/d

For 30 days,
=0.0046 x 30 = 0.138 m^3

Element no 4,

$$= 0.0133 \int_{z=1.0}^{z=1.5} \int_{x=1.0}^{x=2.0} \left(1 - \frac{x}{3.0} - \frac{z}{1.5} + \frac{xz}{4.5}\right) \partial x \partial z$$

$$= 0.0133 \int_{z=1.0}^{z=1.5} \left[x - \frac{x^2}{6} - \frac{xz}{1.5} + \frac{x^2 z}{9} \right]_{1.0}^{2.0} \partial z$$

$$= 0.0133 \int_{z=1.0}^{z=1.5} \left[\left(2 - \frac{4}{6} - \frac{2z}{1.5} + \frac{4z}{9}\right) - \left(1 - \frac{1}{6} - \frac{z}{1.5} + \frac{z}{9}\right) \right] \partial z$$

$$= 0.0133 \int_{z=1.0}^{z=1.5} [0.5 - 0.333z] \partial z$$

$$= 0.0133 \left[0.5z - \frac{0.333z^2}{2} \right]_{1.0}^{1.5}$$

$$= 0.0133 \left[\left(0.5 \text{ x } 1.5 - \frac{0.333 \text{ x } 1.5^2}{2}\right) - \left(0.5 \text{ x } 1.0 - \frac{0.333 \text{ x } 1.0^2}{2}\right) \right]$$

$=0.0133(0.0418)$

$=0.0006 \text{ m}^2/\text{d}$

Water uptake rate for element no 4,

$0.0006 \text{ m}^2/\text{d}$ x 1m width

$=0.0006 \text{ m}^3/\text{d}$

For 30 days,
$=0.0006 \text{ x } 30 = 0.018 \text{ m}^3$

Element no 5,

$$= 0.0133 \int_{z=0.5}^{z=1.0} \int_{x=1.0}^{x=2.0} \left(1 - \frac{x}{3.0} - \frac{z}{1.5} + \frac{xz}{4.5}\right) \partial x \partial z$$

$$= 0.0133 \int_{z=0.5}^{z=1.0} \left[x - \frac{x^2}{6} - \frac{xz}{1.5} + \frac{x^2 z}{9} \right]_{1.0}^{2.0} \partial z$$

$$= 0.0133 \int_{z=0.5}^{z=1.0} \left[\left(2 - \frac{4}{6} - \frac{2z}{1.5} + \frac{4z}{9}\right) - \left(1 - \frac{1}{6} - \frac{z}{1.5} + \frac{z}{9}\right) \right] \partial z$$

$$= 0.0133 \int_{z=0.5}^{z=1.0} [0.5 - 0.333z] \partial z$$

$$= 0.0133 \left[0.5z - \frac{0.333z^2}{2} \right]_{0.5}^{1.0}$$

$$= 0.0133 \left[\left(0.5 \text{ x } 1.0 - \frac{0.333 \text{ x } 1.0^2}{2}\right) - \left(0.5 \text{ x } 0.5 - \frac{0.333 \text{ x } 0.5^2}{2}\right) \right]$$

$=0.0133(0.125)$

$=0.0016 \text{ m}^2/\text{d}$

Water uptake rate for element no 5,

$0.0016 \text{ m}^2/\text{d}$ x 1m width

$=0.0016 \text{ m}^3/\text{d}$

For 30 days,
$=0.0016 \text{ x } 30 = 0.048 \text{ m}^3$

Element no 6,

$$= 0.0133 \int_{z=0}^{z=0.5} \int_{x=1.0}^{x=2.0} \left(1 - \frac{x}{3.0} - \frac{z}{1.5} + \frac{xz}{4.5}\right) \partial x \partial z$$

$$= 0.0133 \int_{z=0}^{z=0.5} \left[x - \frac{x^2}{6} - \frac{xz}{1.5} + \frac{x^2 z}{9}\right]_{1.0}^{2.0} \partial z$$

$$= 0.0133 \int_{z=0}^{z=0.5} \left[\left(2 - \frac{4}{6} - \frac{2z}{1.5} + \frac{4z}{9}\right) - \left(1 - \frac{1}{6} - \frac{z}{1.5} + \frac{z}{9}\right)\right] \partial z$$

$$= 0.0133 \int_{z=0}^{z=0.5} [0.5 - 0.333z] \partial z$$

$$= 0.0133 \left[0.5z - \frac{0.333z^2}{2}\right]_0^{0.5}$$

$$= 0.0133 \left[\left(0.5 \text{ x } 0.5 - \frac{0.333 \text{ x } 0.5^2}{2}\right) - (0)\right]$$

=0.0133(0.2084)

=0.0027 m^2/d

Water uptake rate for element no 6,

0.0027 m^2/d x 1m width

=0.0027 m^3/d

For 30 days,
=0.0027 x 30 = 0.081 m^3

Element no 7,

$$= 0.0133 \int_{z=1.0}^{z=1.5} \int_{x=2.0}^{x=3.0} \left(1 - \frac{x}{3.0} - \frac{z}{1.5} + \frac{xz}{4.5}\right) \partial x \partial z$$

$$= 0.0133 \int_{z=1.0}^{z=1.5} \left[x - \frac{x^2}{6} - \frac{xz}{1.5} + \frac{x^2 z}{9}\right]_{2.0}^{3.0} \partial z$$

$$= 0.0133 \int_{z=1.0}^{z=1.5} \left[\left(3 - \frac{9}{6} - \frac{3z}{1.5} + \frac{9z}{9}\right) - \left(2 - \frac{4}{6} - \frac{2z}{1.5} + \frac{4z}{9}\right)\right] \partial z$$

$$= 0.0133 \int_{z=1.0}^{z=1.5} [0.1666 - 0.111z] \partial z$$

$$= 0.0133 \left[0.1666z - \frac{0.111z^2}{2}\right]_{1.0}^{1.5}$$

$$= 0.0133 \left[\left(0.1666 \text{ x } 1.5 - \frac{0.111 \text{ x } 1.5^2}{2}\right) - \left(0.1666 \text{ x } 1.0 - \frac{0.111 \text{ x } 1.0^2}{2}\right)\right]$$

=0.0133(0.014)

=0.0002 m^2/d

Water uptake rate for element no 7,

0.0002 m^2/d x 1m width

=0.0002 m^3/d

For 30 days,
=0.0002 x 30 = 0.006m^3

Element no 8,

$$= 0.0133 \int_{z=0.5}^{z=1.0} \int_{x=2.0}^{x=3.0} \left(1 - \frac{x}{3.0} - \frac{z}{1.5} + \frac{xz}{4.5}\right) \partial x \partial z$$

$$= 0.0133 \int_{z=0.5}^{z=1.0} \left[x - \frac{x^2}{6} - \frac{xz}{1.5} + \frac{x^2 z}{9}\right]_{2.0}^{3.0} \partial z$$

$$= 0.0133 \int_{z=0.5}^{z=1.0} \left[\left(3 - \frac{9}{6} - \frac{3z}{1.5} + \frac{9z}{9}\right) - \left(2 - \frac{4}{6} - \frac{2z}{1.5} + \frac{4z}{9}\right)\right] \partial z$$

$$= 0.0133 \int_{z=0.5}^{z=1.0} [0.1666 - 0.111z] \partial z$$

$$= 0.0133 \left[0.1666z - \frac{0.111z^2}{2}\right]_{0.5}^{1.0}$$

$$= 0.0133 \left[\left(0.1666 \text{ x } 1.0 - \frac{0.111 \text{ x } 1.0^2}{2}\right) - \left(0.1666 \text{ x } 0.5 - \frac{0.111 \text{ x } 0.5^2}{2}\right)\right]$$

$=0.0133(0.042)$

$=0.0006 \text{ m}^2/\text{d}$

Water uptake rate for element no 8,

$0.0006 \text{ m}^2/\text{d}$ x 1m width

$=0.0006 \text{ m}^3/\text{d}$

For 30 days,
$=0.0006 \text{ x } 30 = 0.018 \text{ m}^3$

Element no 9,

$$= 0.0133 \int_{z=0}^{z=0.5} \int_{x=2.0}^{x=3.0} \left(1 - \frac{x}{3.0} - \frac{z}{1.5} + \frac{xz}{4.5}\right) \partial x \partial z$$

$$= 0.0133 \int_{z=0}^{z=0.5} \left[x - \frac{x^2}{6} - \frac{xz}{1.5} + \frac{x^2 z}{9}\right]_{2.0}^{3.0} \partial z$$

$$= 0.0133 \int_{z=0}^{z=0.5} \left[\left(3 - \frac{9}{6} - \frac{3z}{1.5} + \frac{9z}{9}\right) - \left(2 - \frac{4}{6} - \frac{2z}{1.5} + \frac{4z}{9}\right)\right] \partial z$$

$$= 0.0133 \int_{z=0}^{z=0.5} [0.1666 - 0.111z] \partial z$$

$$= 0.0133 \left[0.1666z - \frac{0.111z^2}{2}\right]_0^{0.5}$$

$$= 0.0133 \left[\left(0.1666 \text{ x } 0.5 - \frac{0.111 \text{ x } 0.5^2}{2}\right) - (0)\right]$$

$=0.0133(0.069)$

$=0.0009 \text{ m}^2/\text{d}$

Water uptake rate for element no 9,

$0.0009 \text{ m}^2/\text{d}$ x 1m width

$=0.0009 \text{ m}^3/\text{d}$

For 30 days,
$=0.0009 \text{ x } 30 = 0.027 \text{ m}^3$

Therefore, total volume of water depletion in all elements for 30 days,

$0.027 + 0.081 + 0.138 + 0.018 + 0.048 + 0.081 + 0.006 + 0.018 + 0.027 = 0.45 \text{ m}^3$

APPENDIX 3

EXAMPLE CALCULATION FOR A TWO-DIMENSIONAL AXI-SYMMETRIC PROBLEM

2-D AXI-SYMMETRIC PROBLEM

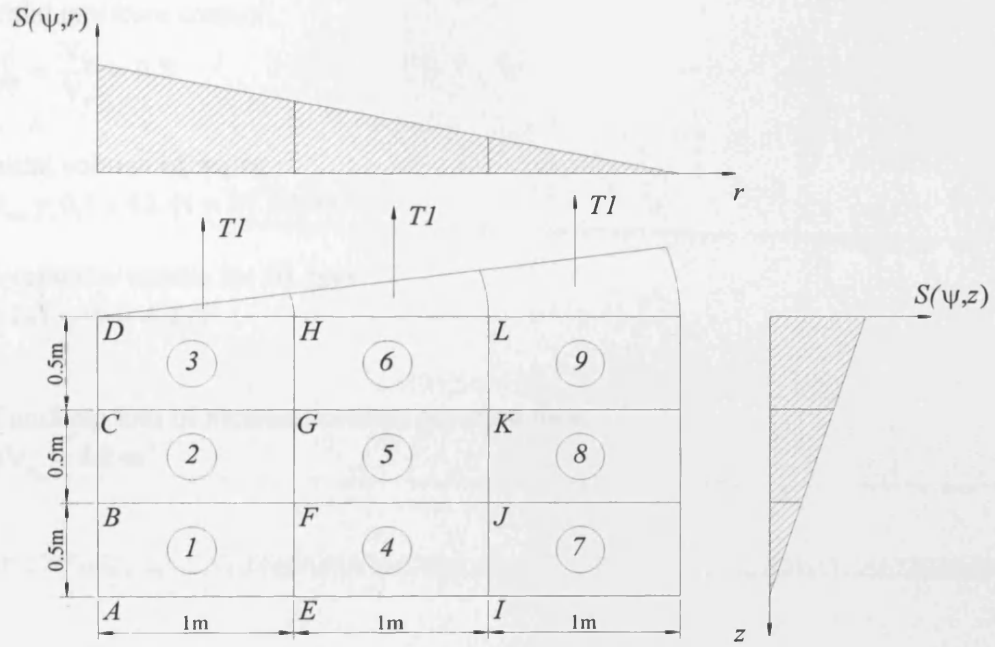

Consider test problem above,

Total Volume,	$V_T = \pi \times 3^2 \times 1.5 = 42.41\,m^3$
Initial moisture content,	$\theta_{sat} = 0.5$
Transpiration rate,	$T1 = 0.005$ m/day
Total time,	$t = 30$days
Maximum root depth,	$z_r = 1.5$m
Maximum radial root distance	$r_r = 3.0$m

Note that the total transpiration rate,
$T = T1 \times$ Area
$T = 0.005 \times \pi \times 3^2 = 0.141\,m^3$/day

Manual Solution

Initial moisture content,

$$\theta_{sat} = \frac{V_w}{V_T} = 0.5$$

Initial volume of water,

$V_{wi} = 0.5 \times 42.41 = 21.205\ m^3$

Total water uptake for 30 days

$0.141 \times 30 = 4.2\ m^3$

If uniform loss of moisture content occurred then,

$\Delta V_w = 4.2\ m^3$

Sink Term

Application of linear variation in equation (3.47) in chapter 3, $S(\psi, z, r) = \frac{4T}{z_r r_r}\alpha(\psi)\left(1-\frac{z}{z_r}\right)\left(1-\frac{r}{r_r}\right)$ would apply for this 9 element problem,

Assuming $\alpha(\psi) = 1$,

Element no 1,

$$\int_{z=1.0}^{z=1.5}\int_{r=0}^{r=1.0}\frac{4T}{z_r}\left(1-\frac{z}{z_r}\right)\left(1-\frac{r}{r_r}\right)\partial r\partial z$$

$$=\frac{4T}{z_r r_r}\int_{z=1.0}^{z=1.5}\int_{r=0}^{r=1.0}\left(1-\frac{z}{z_r}\right)\left(1-\frac{r}{r_r}\right)\partial r\partial z$$

$$=\frac{(4)(0.141)}{1.5x3.0}\int_{z=1.0}^{z=1.5}\int_{r=0}^{r=1.0}\left(1-\frac{z}{1.5}\right)\left(1-\frac{r}{3.0}\right)\partial r\partial z$$

$$=0.125\int_{z=1.0}^{z=1.5}\int_{r=0}^{r=1.0}\left(1-\frac{r}{3.0}-\frac{z}{1.5}+\frac{rz}{4.5}\right)\partial r\partial z$$

$$=0.125\int_{z=1.0}^{z=1.5}\left[r-\frac{r^2}{6}-\frac{rz}{1.5}+\frac{r^2z}{9}\right]_0^{1.0}\partial z$$

$$=0.125\int_{z=1.0}^{z=1.5}\left[\left(1-\frac{1}{6}-\frac{z}{1.5}+\frac{z}{9}\right)-(0)\right]\partial z$$

$$=0.125\int_{z=1.0}^{z=1.5}[0.8333-0.555z]\partial z$$

$$=0.125\left[0.8333z-\frac{0.555z^2}{2}\right]_{1.0}^{1.5}$$

$$=0.125\left[\left(0.8333\,\text{x}\,1.5-\frac{0.555\,\text{x}\,1.5^2}{2}\right)-\left(0.8333\,\text{x}\,1.0-\frac{0.555\,\text{x}\,1.0^2}{2}\right)\right]$$

$$=0.125(0.069)$$

$=0.0086\ \text{m}^3/\text{d}$

For 30 days,
$0.0086\,\text{x}\,30 = 0.26\ \text{m}^3$

Element no 2,

$$= 0.125 \int_{z=0.5}^{z=1.0} \int_{r=0}^{r=1.0} \left(1 - \frac{r}{3.0} - \frac{z}{1.5} + \frac{rz}{4.5}\right) \partial r \partial z$$

$$= 0.125 \int_{z=0.5}^{z=1.0} \left[r - \frac{r^2}{6} - \frac{rz}{1.5} + \frac{r^2 z}{9} \right]_0^{1.0} \partial z$$

$$= 0.125 \int_{z=1.0}^{z=1.5} \left[\left(1 - \frac{1}{6} - \frac{z}{1.5} + \frac{z}{9}\right) - (0) \right] \partial z$$

$$= 0.125 \int_{z=0.5}^{z=1.0} [0.8333 - 0.555z] \partial z$$

$$= 0.125 \left[0.8333z - \frac{0.555z^2}{2} \right]_{0.5}^{1.0}$$

$$= 0.125 \left[\left(0.8333 \text{ x } 1.0 - \frac{0.555 \text{ x } 1.0^2}{2} \right) - \left(0.8333 \text{ x } 0.5 - \frac{0.555 \text{ x } 0.5^2}{2} \right) \right]$$

$$= 0.125(0.2085)$$

$=0.026 \text{ m}^3/\text{d}$

For 30 days,
$=0.026 \text{ x } 30 = 0.78 \text{ m}^3$

Element no 3,

$$= 0.125 \int_{z=0}^{z=0.5} \int_{r=0}^{r=1.0} \left(1 - \frac{r}{3.0} - \frac{z}{1.5} + \frac{rz}{4.5}\right) \partial r \partial z$$

$$= 0.125 \int_{z=0}^{z=0.5} \left[r - \frac{r^2}{6} - \frac{rz}{1.5} + \frac{r^2 z}{9} \right]_0^{1.0} \partial z$$

$$= 0.125 \int_{z=0}^{z=0.5} \left[\left(1 - \frac{1}{6} - \frac{z}{1.5} + \frac{z}{9}\right) - (0) \right] \partial z$$

$$= 0.125 \int_{z=0}^{z=0.5} [0.8333 - 0.555z] \partial z$$

$$= 0.125 \left[0.8333z - \frac{0.555z^2}{2} \right]_0^{0.5}$$

$$= 0.125 \left[\left(0.8333 \text{ x } 0.5 - \frac{0.555 \text{ x } 0.5^2}{2} \right) - (0) \right]$$

$=0.125(0.3473)$

$=0.043 \text{ m}^3/\text{d}$

For 30 days,
$=0.043 \text{ x } 30 = 1.29 \text{ m}^3$

Element no 4,

$$= 0.125 \int_{z=1.0}^{z=1.5} \int_{r=1.0}^{r=2.0} \left(1 - \frac{r}{3.0} - \frac{z}{1.5} + \frac{rz}{4.5}\right) \partial r \partial z$$

$$= 0.125 \int_{z=1.0}^{z=1.5} \left[r - \frac{r^2}{6} - \frac{rz}{1.5} + \frac{r^2 z}{9} \right]_{1.0}^{2.0} \partial z$$

$$= 0.125 \int_{z=1.0}^{z=1.5} \left[\left(2 - \frac{4}{6} - \frac{2z}{1.5} + \frac{4z}{9}\right) - \left(1 - \frac{1}{6} - \frac{z}{1.5} + \frac{z}{9}\right) \right] \partial z$$

$$= 0.125 \int_{z=1.0}^{z=1.5} [0.5 - 0.333z] \partial z$$

$$= 0.125 \left[0.5z - \frac{0.333z^2}{2} \right]_{1.0}^{1.5}$$

$$= 0.125 \left[\left(0.5 \times 1.5 - \frac{0.333 \times 1.5^2}{2}\right) - \left(0.5 \times 1.0 - \frac{0.333 \times 1.0^2}{2}\right) \right]$$

$=0.125(0.0418)$

$=0.0052\ m^3/d$

For 30 days,
$=0.0052 \times 30 = 0.156\ m^3$

Element no 5,

$$= 0.125 \int_{z=0.5}^{z=1.0} \int_{r=1.0}^{r=2.0} \left(1 - \frac{r}{3.0} - \frac{z}{1.5} + \frac{rz}{4.5}\right) \partial r \partial z$$

$$= 0.125 \int_{z=0.5}^{z=1.0} \left[r - \frac{r^2}{6} - \frac{rz}{1.5} + \frac{r^2 z}{9} \right]_{1.0}^{2.0} \partial z$$

$$= 0.125 \int_{z=0.5}^{z=1.0} \left[\left(2 - \frac{4}{6} - \frac{2z}{1.5} + \frac{4z}{9}\right) - \left(1 - \frac{1}{6} - \frac{z}{1.5} + \frac{z}{9}\right) \right] \partial z$$

$$= 0.125 \int_{z=0.5}^{z=1.0} [0.5 - 0.333z] \partial z$$

$$= 0.125 \left[0.5z - \frac{0.333z^2}{2} \right]_{0.5}^{1.0}$$

$$= 0.125 \left[\left(0.5 \text{ x } 1.0 - \frac{0.333 \text{ x } 1.0^2}{2}\right) - \left(0.5 \text{ x } 0.5 - \frac{0.333 \text{ x } 0.5^2}{2}\right) \right]$$

$=0.125(0.125)$

$=0.0156 \text{ m}^3/\text{d}$

For 30 days,
$=0.0156 \text{ x } 30 = 0.468 \text{ m}^3$

Element no 6,

$$= 0.125 \int_{z=0}^{z=0.5} \int_{r=1.0}^{r=2.0} \left(1 - \frac{r}{3.0} - \frac{z}{1.5} + \frac{rz}{4.5}\right) \partial r \partial z$$

$$= 0.125 \int_{z=0}^{z=0.5} \left[r - \frac{r^2}{6} - \frac{rz}{1.5} + \frac{r^2 z}{9} \right]_{1.0}^{2.0} \partial z$$

$$= 0.125 \int_{z=0}^{z=0.5} \left[\left(2 - \frac{4}{6} - \frac{2z}{1.5} + \frac{4z}{9}\right) - \left(1 - \frac{1}{6} - \frac{z}{1.5} + \frac{z}{9}\right) \right] \partial z$$

$$= 0.125 \int_{z=0}^{z=0.5} [0.5 - 0.333z] \partial z$$

$$= 0.125 \left[0.5z - \frac{0.333z^2}{2} \right]_0^{0.5}$$

$$= 0.125 \left[\left(0.5 \text{ x } 0.5 - \frac{0.333 \text{ x } 0.5^2}{2} \right) - (0) \right]$$

$=0.125(0.2084)$

$=0.026 \text{ m}^3/\text{d}$

For 30 days,
$=0.026 \text{ x } 30 = 0.78\text{m}^3$

Element no 7,

$$= 0.125 \int_{z=1.0}^{z=1.5} \int_{r=2.0}^{r=3.0} \left(1 - \frac{r}{3.0} - \frac{z}{1.5} + \frac{rz}{4.5}\right) \partial r \partial z$$

$$= 0.125 \int_{z=1.0}^{z=1.5} \left[r - \frac{r^2}{6} - \frac{rz}{1.5} + \frac{r^2 z}{9} \right]_{2.0}^{3.0} \partial z$$

$$= 0.125 \int_{z=1.0}^{z=1.5} \left[\left(3 - \frac{9}{6} - \frac{3z}{1.5} + \frac{9z}{9}\right) - \left(2 - \frac{4}{6} - \frac{2z}{1.5} + \frac{4z}{9}\right) \right] \partial z$$

$$= 0.125 \int_{z=1.0}^{z=1.5} [0.1666 - 0.111z] \partial z$$

$$= 0.125 \left[0.1666z - \frac{0.111z^2}{2} \right]_{1.0}^{1.5}$$

$$= 0.125 \left[\left(0.1666 \text{ x } 1.5 - \frac{0.111 \text{ x } 1.5^2}{2}\right) - \left(0.1666 \text{ x } 1.0 - \frac{0.111 \text{ x } 1.0^2}{2}\right) \right]$$

$=0.125(0.014)$

$=0.0018 \text{ m}^3/\text{d}$

For 30 days,
$=0.0018 \text{ x } 30 = 0.054 \text{ m}^3$

Element no 8,

$$= 0.125 \int_{z=0.5}^{z=1.0} \int_{r=2.0}^{r=3.0} \left(1 - \frac{r}{3.0} - \frac{z}{1.5} + \frac{rz}{4.5}\right) \partial r \partial z$$

$$= 0.125 \int_{z=0.5}^{z=1.0} \left[r - \frac{r^2}{6} - \frac{rz}{1.5} + \frac{r^2 z}{9} \right]_{2.0}^{3.0} \partial z$$

$$= 0.125 \int_{z=0.5}^{z=1.0} \left[\left(3 - \frac{9}{6} - \frac{3z}{1.5} + \frac{9z}{9}\right) - \left(2 - \frac{4}{6} - \frac{2z}{1.5} + \frac{4z}{9}\right) \right] \partial z$$

$$= 0.125 \int_{z=0.5}^{z=1.0} [0.1666 - 0.111z] \partial z$$

$$= 0.125 \left[0.1666z - \frac{0.111z^2}{2} \right]_{0.5}^{1.0}$$

$$= 0.125 \left[\left(0.1666 \text{ x } 1.0 - \frac{0.111 \text{ x } 1.0^2}{2} \right) - \left(0.1666 \text{ x } 0.5 - \frac{0.111 \text{ x } 0.5^2}{2} \right) \right]$$

$=0.125(0.042)$

$=0.0052 \text{ m}^3/\text{d}$

For 30 days,
$=0.0052 \text{ x } 30 = 0.156 \text{ m}^3$

Element no 9,

$$= 0.125 \int_{z=0}^{z=0.5} \int_{r=2.0}^{r=3.0} \left(1 - \frac{r}{3.0} - \frac{z}{1.5} + \frac{rz}{4.5}\right) \partial r \partial z$$

$$= 0.125 \int_{z=0}^{z=0.5} \left[r - \frac{r^2}{6} - \frac{rz}{1.5} + \frac{r^2 z}{9} \right]_{2.0}^{3.0} \partial z$$

$$= 0.125 \int_{z=0}^{z=0.5} \left[\left(3 - \frac{9}{6} - \frac{3z}{1.5} + \frac{9z}{9}\right) - \left(2 - \frac{4}{6} - \frac{2z}{1.5} + \frac{4z}{9}\right) \right] \partial z$$

$$= 0.125 \int_{z=0}^{z=0.5} [0.1666 - 0.111z] \partial z$$

$$= 0.125 \left[0.1666z - \frac{0.111z^2}{2} \right]_0^{0.5}$$

$$= 0.125 \left[\left(0.1666 \text{ x } 0.5 - \frac{0.111 \text{ x } 0.5^2}{2} \right) - (0) \right]$$

$=0.125(0.069)$

$=0.0086 \text{ m}^3/\text{d}$

For 30 days,
$0.0086 \text{ x } 30 = 0.26 \text{ m}^3$

Therefore, total volume of water depletion in all elements for 30 days,

$0.26 + 0.78 + 1.29 + 0.156 + 0.468 + 0.78 + 0.054 + 0.156 + 0.26 = 4.2 \text{ m}^3$

APPENDIX 4

DERIVATION OF RICHARD'S EQUATION FOR TWO DIMENSIONAL CONDITIONS

Governing Differential Equation Describing Isothermal Moisture Flow

Figure 3.1 illustrates a typical control element with inflow and outflow occurring in three dimensions x, y and z.

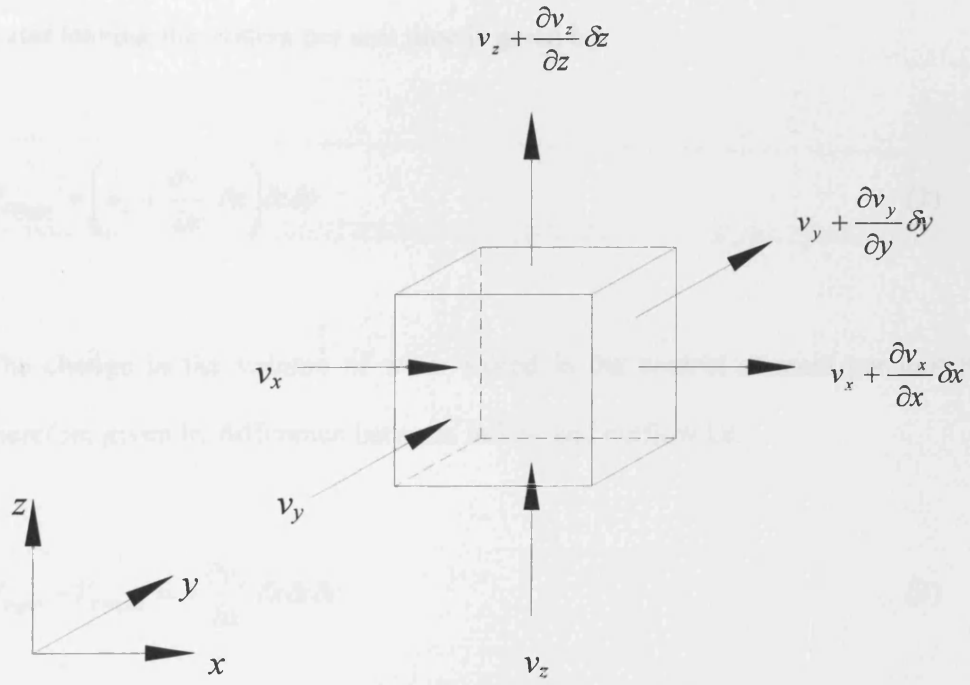

Figure 1 3D Flow through a typical control element, modified after Yong and Warkentin (1974)

Considering first the flow of the moisture in the x direction only. The volume of water entering the system per unit time in the x direction is given by

$$V_{Input} = v_x \delta z \delta y \tag{1}$$

Where v_x is the velocity of water flow in the x direction. Similarly the volume of water leaving the system per unit time is given by

$$V_{Output} = \left(v_x + \frac{\partial v_x}{\partial x} \delta x \right) \delta z \delta y \tag{2}$$

The change in the volume of water stored in the control element per unit time is therefore given by difference between inflow and outflow i.e.

$$V_{Input} - V_{Output} = -\frac{\partial v_x}{\partial x} \delta x \delta z \delta y \tag{3}$$

By symmetry the change in volume of water stored under three-dimensional conditions is given by

$$V_{Input} - V_{Output} = -\left(\frac{\partial v_x}{\partial x} + \frac{\partial v_y}{\partial y} + \frac{\partial v_z}{\partial z} \right) \delta x \delta y \delta z \tag{4}$$

For the cases of flow through a saturated soil, assuming steady conditions exist, the change in storage of water in the control element must be equal to zero i.e.

$$\left(\frac{\partial v_x}{\partial x}+\frac{\partial v_y}{\partial y}+\frac{\partial v_z}{\partial z}\right)\delta x\delta y\delta z=0 \qquad (5)$$

And since $\delta x\delta y\delta z \neq 0$ then

$$\left(\frac{\partial v_x}{\partial x}+\frac{\partial v_y}{\partial y}+\frac{\partial v_z}{\partial z}\right)=0 \qquad (6)$$

Alternatively, for an unsaturated soil the net excess flow is equated to the change in the volume of water in the control element per unit time, thus

$$\left(\frac{\partial v_x}{\partial x}+\frac{\partial v_y}{\partial y}+\frac{\partial v_z}{\partial z}\right)\delta x\delta y\delta z=-\frac{\partial \theta}{\partial t}\delta x\delta y\delta z \qquad (7)$$

Where θ is the volumetric moisture content. Equation (7) may be abbreviated to

$$-\frac{\partial \theta}{\partial t}=\nabla v \qquad (8)$$

Equation (8) can be expressed as follows for two-dimensional flow only,

$$-\frac{\partial \theta}{\partial t}=\frac{\partial v_x}{\partial x}+\frac{\partial v_z}{\partial z} \qquad (11)$$

Introducing Darcy's Law expressed for fluid flow in a partially saturated soil yields,

$$\frac{\partial \theta}{\partial t} = \frac{\partial}{\partial x}\left[K_x(\phi)\frac{\partial \phi}{\partial x}\right] + \frac{\partial}{\partial z}\left[K_z(\phi)\frac{\partial \phi}{\partial z}\right] \tag{12}$$

The total potential for moisture flow is taken as the sum of the pressure or capillary potential and gravitational potential i.e.

$$\phi = \psi + z \tag{13}$$

Therefore, substituting equation (13) into equation (12) gives,

$$\frac{\partial \theta}{\partial t} = \frac{\partial}{\partial x}\left[K_x(\psi)\frac{\partial \psi}{\partial x}\right] + \frac{\partial}{\partial z}\left[K_z(\psi)\frac{\partial \psi}{\partial z}\right] + \frac{\partial K_z(\psi)}{\partial z} \tag{14}$$

Assuming that the soil is isotropic and restating the left hand side of equation (14) in terms of capillary potential yields,

$$\frac{\partial \theta}{\partial \psi}\frac{\partial \psi}{\partial t} = \frac{\partial}{\partial x}\left[K(\psi)\frac{\partial \psi}{\partial x}\right] + \frac{\partial}{\partial z}\left[K(\psi)\frac{\partial \psi}{\partial z}\right] + \frac{\partial K(\psi)}{\partial z} \tag{15}$$

The term $\partial\theta/\partial\psi$ is called the specific moisture capacity of the soil and is denoted as $C(\psi)$.

$$C(\psi)\frac{\partial \psi}{\partial t} = \frac{\partial}{\partial x}\left[K(\psi)\frac{\partial \psi}{\partial x}\right] + \frac{\partial}{\partial z}\left[K(\psi)\frac{\partial \psi}{\partial z}\right] + \frac{\partial K(\psi)}{\partial z} \qquad (16)$$

Equation (16) is often referred to as two-dimensional Richard's equations (Richard, 1931).

References

Richards, L. A., "Capillary conduction of liquids in porous media." Physics, 1, 318 – 333, 1931.

Yong, R. N., and Warkentin, B. P. "Soil properties and behaviour." Elsevier Publishing Company, Amsterdam, 1974.

APPENDIX 5

DISCRETISATION OF STANDARD TWO-DIMENSIONAL MOISTURE TRANSFER

Two-dimensional moisture transfer in an unsaturated soil is derived by combining standard two-dimensional Richard's equation and sink term equation

$$C(\psi)\frac{\partial \psi}{\partial t} = \frac{\partial}{\partial x}\left[K(\psi)\frac{\partial \psi}{\partial x}\right] + \frac{\partial}{\partial z}\left[K(\psi)\frac{\partial \psi}{\partial z}\right] + \frac{\partial K(\psi)}{\partial z} - S(\psi, x, z) \qquad (1)$$

A solution of equation (1) is obtained via a finite element spatial discretisation procedure and a finite difference time-stepping scheme. In particular, adopting a Galerkin weighted residual approach yields:

$$\int_{\Omega^e} N_r \left[\begin{array}{l} \frac{\partial}{\partial x}\left[K(\hat{\psi})\frac{\partial \hat{\psi}}{\partial x}\right] + \frac{\partial}{\partial z}\left[K(\hat{\psi})\frac{\partial \hat{\psi}}{\partial z}\right] \\ + \frac{\partial K(\hat{\psi})}{\partial z} - S(\hat{\psi}, z, x) - C(\hat{\psi})\frac{\partial \hat{\psi}}{\partial t} \end{array} \right] \partial\Omega = 0 \qquad (2)$$

Using, Green's formula and introducing boundary terms leads to the final disctretised form:

$$\begin{array}{l} -\int_{\Omega^e} K \frac{\partial N_s}{\partial x}\frac{\partial N_r}{\partial x}\psi_s \partial\Omega^e - \int_{\Omega^e} K \frac{\partial N_r}{\partial z}\frac{\partial N_s}{\partial z}\psi_s \partial\Omega^e - \int_{\Omega^e} N_r \frac{\partial K}{\partial z}\partial\Omega^e \\ + \int_{\Gamma} N_r \lambda \partial\Gamma - \int_{\Omega^e} N_r S(z, x)\partial\Omega^e - \int_{\Omega^e} N_r N_s C \frac{\partial \psi_s}{\partial t}\partial\Omega^e = 0 \end{array} \qquad (3)$$

Summing for all elements and re-casting equation (3) into concise matrix notation yields;

$$K\psi_s + C\frac{\psi_s}{\partial t} + J + S = 0 \tag{4}$$

Where

$$K = \sum_{e=1}^{m} \int_{\Omega^e} \left[K\frac{\partial N_s}{\partial x}\cdot\frac{\partial N_r}{\partial x} + K\frac{\partial N_s}{\partial z}\cdot\frac{\partial N_r}{\partial z} \right] \partial\Omega^e \tag{5}$$

$$C = \sum_{e=1}^{m} \int_{\Omega^e} [N_r N_s C] \partial\Omega^e \tag{6}$$

$$J = \sum_{e=1}^{m} \int_{\Omega^e} \left[N_x \frac{\partial K}{\partial x} \right] \partial\Omega^e - \sum_{e=1}^{m} \int_{\Gamma^e} [N_x \lambda] \partial\Gamma^e \tag{7}$$

$$S = \sum_{e=1}^{m} \int_{\Omega^e} [N_x S(x,z)] \partial\Omega^e \tag{8}$$

The time dependent nature of equation (3) is dealt with via a mid-interval backward difference technique, yielding:

$$K^{n+1/2}\psi^{n+1} + C^{n+1/2}\left[\frac{\psi^{n+1} - \psi^n}{\Delta t}\right] + J^{n+1/2} + S^{n+1/2} = 0 \tag{9}$$

APPENDIX 6

SLOPE STABILITY ANALYSIS CALCULATIONS

FOS for Saturated Soils

c (kPa)	ϕ' (°)	ϕb (°)	γ (kN/m3)
9.6	27.3	21.7	22

Slice No	z (cm)	b (m)	W (kN)	α (°)	$\sin\alpha$	W sin α (kN) (4)	l (m)	ψ (kPa)	$\tan\phi'$	$\tan\phi b$	c'l (kN) (1)	W cos α (m)	W cos α tan ϕ' (kN) (2)	ψ tan ϕb (kN) (3)
1	26.78	1	5.9	-25.0	-0.423	-2.490	1.103	0	0.516	0.398	10.593	5.340	2.756	0.000
2	63.47	1	14.0	-15.0	-0.259	-3.614	1.035	0	0.516	0.398	9.939	13.488	6.961	0.000
3	105.95	1	23.3	-5.0	-0.087	-2.032	1.004	0	0.516	0.398	9.637	23.220	11.985	0.000
4	155.95	1	34.3	5.0	0.087	2.990	1.004	0	0.516	0.398	9.637	34.178	17.641	0.000
5	188.47	1	41.5	15.0	0.259	10.732	1.035	0	0.516	0.398	9.939	40.051	20.672	0.000
6	201.78	1	44.4	25.0	0.423	18.761	1.103	0	0.516	0.398	10.593	40.232	20.766	0.000
7	191.37	1	42.1	37.0	0.602	25.337	1.252	0	0.516	0.398	12.021	33.624	17.354	0.000
8	103.93	1.268	29.0	53.0	0.799	23.154	2.107	0	0.516	0.398	20.230	17.448	9.006	0.000
Total						72.839					92.588		107.140	0.000

FOS = 2.7420621

FOS for Unsaturated Soils, initial $\psi = -20cm$

c (kPa)	ϕ' (°)	ϕb (°)	γ (kN/m3)
9.6	27.3	21.7	22

Slice No	z (cm)	b (m)	W (kN)	α (°)	$\sin\alpha$	W sin α (kN) (4)	l (m)	ψ (kPa)	$\tan\phi'$	$\tan\phi b$	c'l (kN) (1)	W cos α (m)	W cos α tan ϕ' (kN) (2)	ψ tan ϕb (kN) (3)
1	26.78	1	5.9	-25.0	-0.423	-2.490	1.103	2	0.516	0.398	10.593	5.340	2.756	0.878
2	63.47	1	14.0	-15.0	-0.259	-3.614	1.035	2	0.516	0.398	9.939	13.488	6.961	0.824
3	105.95	1	23.3	-5.0	-0.087	-2.032	1.004	2	0.516	0.398	9.637	23.220	11.985	0.799
4	155.95	1	34.3	5.0	0.087	2.990	1.004	2	0.516	0.398	9.637	34.178	17.641	0.799
5	188.47	1	41.5	15.0	0.259	10.732	1.035	2	0.516	0.398	9.939	40.051	20.672	0.824
6	201.78	1	44.4	25.0	0.423	18.761	1.103	2	0.516	0.398	10.593	40.232	20.766	0.878
7	191.37	1	42.1	37.0	0.602	25.337	1.252	2	0.516	0.398	12.021	33.624	17.354	0.997
8	103.93	1.268	29.0	53.0	0.799	23.154	2.107	2	0.516	0.398	20.230	17.448	9.006	1.677
9			0.0		0.000	0.000	0.000		0.516	0.398	0.000	0.000	0.000	0.000
10			0.0		0.000	0.000	0.000		0.516	0.398	0.000	0.000	0.000	0.000
Total						72.839					92.588		107.140	7.676

FOS = 2.8474465

FOS for Unsaturated Soils, initial $\psi = -20cm$ with tree at bottom

Day 1

Slice No	z (cm)	b (m)	W (kN)	α (°)	sin α	Wsin α (kN) (4)	l (m)	ψ (kPa)	tan ϕ'	tan ϕ b	c'l (kN) (1)	Wcos α (m)	Wcos α tan ϕ' (kN) (2)	ψ tan ϕ b (kN) (3)
1	26.78	1	5.9	-25.0	-0.423	-2.490	1.103	2.02	0.516	0.398	10.593	5.340	2.756	0.887
2	63.47	1	14.0	-15.0	-0.259	-3.614	1.035	2.01	0.516	0.398	9.939	13.488	6.961	0.828
3	105.95	1	23.3	-5.0	-0.087	-2.032	1.004	2.01	0.516	0.398	9.637	23.220	11.985	0.803
4	155.95	1	34.3	5.0	0.087	2.990	1.004	2	0.516	0.398	9.637	34.178	17.641	0.799
5	188.47	1	41.5	15.0	0.259	10.732	1.035	2	0.516	0.398	9.939	40.051	20.672	0.824
6	201.78	1	44.4	25.0	0.423	18.761	1.103	2	0.516	0.398	10.593	40.232	20.766	0.878
7	191.37	1	42.1	37.0	0.602	25.337	1.252	2	0.516	0.398	12.021	33.624	17.354	0.997
8	103.93	1.268	29.0	53.0	0.799	23.154	2.107	2	0.516	0.398	20.230	17.448	9.006	1.677
9			0.0		0.000	0.000	0.000		0.516	0.398	0.000	0.000	0.000	0.000
10			0.0		0.000	0.000	0.000		0.516	0.398	0.000	0.000	0.000	0.000
Total						72.839					92.588		107.140	7.693

FOS = 2.8476785

Day 15

Slice No	z (cm)	b (m)	W (kN)	α (°)	sin α	Wsin α (kN) (4)	l (m)	ψ (kPa)	tan ϕ'	tan ϕ b	c'l (kN) (1)	Wcos α (m)	Wcos α tan ϕ' (kN) (2)	ψ tan ϕ b (kN) (3)
1	26.78	1	5.9	-25.0	-0.423	-2.490	1.103	2.33	0.516	0.398	10.593	5.340	2.756	1.023
2	63.47	1	14.0	-15.0	-0.259	-3.614	1.035	2.22	0.516	0.398	9.939	13.488	6.961	0.915
3	105.95	1	23.3	-5.0	-0.087	-2.032	1.004	2.16	0.516	0.398	9.637	23.220	11.985	0.863
4	155.95	1	34.3	5.0	0.087	2.990	1.004	2.1	0.516	0.398	9.637	34.178	17.641	0.839
5	188.47	1	41.5	15.0	0.259	10.732	1.035	2.1	0.516	0.398	9.939	40.051	20.672	0.865
6	201.78	1	44.4	25.0	0.423	18.761	1.103	2	0.516	0.398	10.593	40.232	20.766	0.878
7	191.37	1	42.1	37.0	0.602	25.337	1.252	2	0.516	0.398	12.021	33.624	17.354	0.997
8	103.93	1.268	29.0	53.0	0.799	23.154	2.107	2	0.516	0.398	20.230	17.448	9.006	1.677
9			0.0		0.000	0.000	0.000		0.516	0.398	0.000	0.000	0.000	0.000
10			0.0		0.000	0.000	0.000		0.516	0.398	0.000	0.000	0.000	0.000
Total						72.839					92.588		107.140	8.057

FOS = 2.8526718

Day 30

Slice No	z (cm)	b (m)	W (kN)	α (°)	sin α	Wsin α (kN) (4)	l (m)	ψ (kPa)	tan ϕ'	tan ϕ b	c'l (kN) (1)	Wcos α (m)	Wcos α tan ϕ' (kN) (2)	ψ tan ϕ b (kN) (3)
1	26.78	1	5.9	-25.0	-0.423	-2.490	1.103	2.67	0.516	0.398	10.593	5.340	2.756	1.172
2	63.47	1	14.0	-15.0	-0.259	-3.614	1.035	2.44	0.516	0.398	9.939	13.488	6.961	1.005
3	105.95	1	23.3	-5.0	-0.087	-2.032	1.004	2.32	0.516	0.398	9.637	23.220	11.985	0.927
4	155.95	1	34.3	5.0	0.087	2.990	1.004	2.2	0.516	0.398	9.637	34.178	17.641	0.879
5	188.47	1	41.5	15.0	0.259	10.732	1.035	2.11	0.516	0.398	9.939	40.051	20.672	0.869
6	201.78	1	44.4	25.0	0.423	18.761	1.103	2	0.516	0.398	10.593	40.232	20.766	0.878
7	191.37	1	42.1	37.0	0.602	25.337	1.252	2	0.516	0.398	12.021	33.624	17.354	0.997
8	103.93	1.268	29.0	53.0	0.799	23.154	2.107	2	0.516	0.398	20.230	17.448	9.006	1.677
9			0.0		0.000	0.000	0.000		0.516	0.398	0.000	0.000	0.000	0.000
10			0.0		0.000	0.000	0.000		0.516	0.398	0.000	0.000	0.000	0.000
Total						72.839					92.588		107.140	8.405

FOS = 2.8574483

Day 45

Slice No	z (cm)	b (m)	W (kN)	α (°)	sin α	Wsin α (kN) (4)	l (m)	ψ (kPa)	tan ϕ'	tan ϕ b	c'l (kN) (1)	Wcos α (m)	Wcos α tan ϕ' (kN) (2)	ψ tan ϕ b (kN) (3)
1	26.78	1	5.9	-25.0	-0.423	-2.490	1.103	3	0.516	0.398	10.593	5.340	2.756	1.317
2	63.47	1	14.0	-15.0	-0.259	-3.614	1.035	2.67	0.516	0.398	9.939	13.488	6.961	1.100
3	105.95	1	23.3	-5.0	-0.087	-2.032	1.004	2.5	0.516	0.398	9.637	23.220	11.985	0.999
4	155.95	1	34.3	5.0	0.087	2.990	1.004	2.31	0.516	0.398	9.637	34.178	17.641	0.923
5	188.47	1	41.5	15.0	0.259	10.732	1.035	2.17	0.516	0.398	9.939	40.051	20.672	0.894
6	201.78	1	44.4	25.0	0.423	18.761	1.103	2.02	0.516	0.398	10.593	40.232	20.766	0.887
7	191.37	1	42.1	37.0	0.602	25.337	1.252	2	0.516	0.398	12.021	33.624	17.354	0.997
8	103.93	1.268	29.0	53.0	0.799	23.154	2.107	2	0.516	0.398	20.230	17.448	9.006	1.677
9			0.0		0.000	0.000	0.000		0.516	0.398	0.000	0.000	0.000	0.000
10			0.0		0.000	0.000	0.000		0.516	0.398	0.000	0.000	0.000	0.000
Total						72.839					92.588		107.140	8.794

FOS = 2.862789

Day 60

Slice No	z (cm)	b (m)	W (kN)	α (°)	sin α	Wsin α (kN) (4)	l (m)	ψ (kPa)	tan ϕ'	tan ϕ b	c'l (kN) (1)	Wcos α (m)	Wcos α tan ϕ' (kN) (2)	ψ tan ϕ b (kN) (3)
1	26.78	1	5.9	-25.0	-0.423	-2.490	1.103	3.33	0.516	0.398	10.593	5.340	2.756	1.462
2	63.47	1	14.0	-15.0	-0.259	-3.614	1.035	2.88	0.516	0.398	9.939	13.488	6.961	1.187
3	105.95	1	23.3	-5.0	-0.087	-2.032	1.004	2.63	0.516	0.398	9.637	23.220	11.985	1.051
4	155.95	1	34.3	5.0	0.087	2.990	1.004	2.42	0.516	0.398	9.637	34.178	17.641	0.967
5	188.47	1	41.5	15.0	0.259	10.732	1.035	2.22	0.516	0.398	9.939	40.051	20.672	0.915
6	201.78	1	44.4	25.0	0.423	18.761	1.103	2.04	0.516	0.398	10.593	40.232	20.766	0.896
7	191.37	1	42.1	37.0	0.602	25.337	1.252	2	0.516	0.398	12.021	33.624	17.354	0.997
8	103.93	1.268	29.0	53.0	0.799	23.154	2.107	2	0.516	0.398	20.230	17.448	9.006	1.677
9			0.0		0.000	0.000	0.000		0.516	0.398	0.000	0.000	0.000	0.000
10			0.0		0.000	0.000	0.000		0.516	0.398	0.000	0.000	0.000	0.000
Total						72.839					92.588		107.140	9.150

FOS = 2.8676857

Day 75

Slice No	z (cm)	b (m)	W (kN)	α (°)	sin α	Wsin α (kN) (4)	l (m)	ψ (kPa)	tan ϕ'	tan ϕ b	c'l (kN) (1)	Wcos α (m)	Wcos α tan ϕ' (kN) (2)	ψ tan ϕ b (kN) (3)
1	26.78	1	5.9	-25.0	-0.423	-2.490	1.103	3.66	0.516	0.398	10.593	5.340	2.756	1.607
2	63.47	1	14.0	-15.0	-0.259	-3.614	1.035	3.1	0.516	0.398	9.939	13.488	6.961	1.277
3	105.95	1	23.3	-5.0	-0.087	-2.032	1.004	2.8	0.516	0.398	9.637	23.220	11.985	1.119
4	155.95	1	34.3	5.0	0.087	2.990	1.004	2.52	0.516	0.398	9.637	34.178	17.641	1.007
5	188.47	1	41.5	15.0	0.259	10.732	1.035	2.27	0.516	0.398	9.939	40.051	20.672	0.935
6	201.78	1	44.4	25.0	0.423	18.761	1.103	2.05	0.516	0.398	10.593	40.232	20.766	0.900
7	191.37	1	42.1	37.0	0.602	25.337	1.252	2	0.516	0.398	12.021	33.624	17.354	0.997
8	103.93	1.268	29.0	53.0	0.799	23.154	2.107	2	0.516	0.398	20.230	17.448	9.006	1.677
9			0.0		0.000	0.000	0.000		0.516	0.398	0.000	0.000	0.000	0.000
10			0.0		0.000	0.000	0.000		0.516	0.398	0.000	0.000	0.000	0.000
Total						72.839					92.588		107.140	9.519

FOS = 2.8727433

Day 90

Slice No	z (cm)	b (m)	W (kN)	α (°)	sin α	Wsin α (kN) (4)	l (m)	ψ (kPa)	tan ϕ'	tan ϕ b	c'l (kN) (1)	Wcos α (m)	Wcos α tan ϕ' (kN) (2)	ψ tan ϕ b (kN) (3)
1	26.78	1	5.9	-25.0	-0.423	-2.490	1.103	4	0.516	0.398	10.593	5.340	2.756	1.756
2	63.47	1	14.0	-15.0	-0.259	-3.614	1.035	3.32	0.516	0.398	9.939	13.488	6.961	1.368
3	105.95	1	23.3	-5.0	-0.087	-2.032	1.004	2.94	0.516	0.398	9.637	23.220	11.985	1.174
4	155.95	1	34.3	5.0	0.087	2.990	1.004	2.62	0.516	0.398	9.637	34.178	17.641	1.047
5	188.47	1	41.5	15.0	0.259	10.732	1.035	2.32	0.516	0.398	9.939	40.051	20.672	0.956
6	201.78	1	44.4	25.0	0.423	18.761	1.103	2.06	0.516	0.398	10.593	40.232	20.766	0.905
7	191.37	1	42.1	37.0	0.602	25.337	1.252	2	0.516	0.398	12.021	33.624	17.354	0.997
8	103.93	1.268	29.0	53.0	0.799	23.154	2.107	2	0.516	0.398	20.230	17.448	9.006	1.677
9			0.0		0.000	0.000	0.000		0.516	0.398	0.000	0.000	0.000	0.000
10			0.0		0.000	0.000	0.000		0.516	0.398	0.000	0.000	0.000	0.000
Total						72.839					92.588		107.140	9.879

FOS = 2.8776967

Day 105

Slice No	z (cm)	b (m)	W (kN)	α (°)	sin α	Wsin α (kN) (4)	l (m)	ψ (kPa)	tan ϕ'	tan ϕ b	c'l (kN) (1)	Wcos α (m)	Wcos α tan ϕ' (kN) (2)	ψ tan ϕ b (kN) (3)
1	26.78	1	5.9	-25.0	-0.423	-2.490	1.103	4.34	0.516	0.398	10.593	5.340	2.756	1.906
2	63.47	1	14.0	-15.0	-0.259	-3.614	1.035	3.54	0.516	0.398	9.939	13.488	6.961	1.458
3	105.95	1	23.3	-5.0	-0.087	-2.032	1.004	3.1	0.516	0.398	9.637	23.220	11.985	1.238
4	155.95	1	34.3	5.0	0.087	2.990	1.004	2.71	0.516	0.398	9.637	34.178	17.641	1.083
5	188.47	1	41.5	15.0	0.259	10.732	1.035	2.37	0.516	0.398	9.939	40.051	20.672	0.976
6	201.78	1	44.4	25.0	0.423	18.761	1.103	2.07	0.516	0.398	10.593	40.232	20.766	0.909
7	191.37	1	42.1	37.0	0.602	25.337	1.252	2	0.516	0.398	12.021	33.624	17.354	0.997
8	103.93	1.268	29.0	53.0	0.799	23.154	2.107	2	0.516	0.398	20.230	17.448	9.006	1.677
9			0.0		0.000	0.000	0.000		0.516	0.398	0.000	0.000	0.000	0.000
10			0.0		0.000	0.000	0.000		0.516	0.398	0.000	0.000	0.000	0.000
Total						72.839					92.588		107.140	10.244

FOS = 2.8827049

Day 120

Slice No	z (cm)	b (m)	W (kN)	α (°)	sin α	Wsin α (kN) (4)	l (m)	ψ (kPa)	tan ϕ'	tan ϕ b	c'l (kN) (1)	Wcos α (m)	Wcos α tan ϕ' (kN) (2)	ψ tan ϕ b (kN) (3)
1	26.78	1	5.9	-25.0	-0.423	-2.490	1.103	4.69	0.516	0.398	10.593	5.340	2.756	2.059
2	63.47	1	14.0	-15.0	-0.259	-3.614	1.035	3.76	0.516	0.398	9.939	13.488	6.961	1.549
3	105.95	1	23.3	-5.0	-0.087	-2.032	1.004	3.24	0.516	0.398	9.637	23.220	11.985	1.294
4	155.95	1	34.3	5.0	0.087	2.990	1.004	2.8	0.516	0.398	9.637	34.178	17.641	1.119
5	188.47	1	41.5	15.0	0.259	10.732	1.035	2.4	0.516	0.398	9.939	40.051	20.672	0.989
6	201.78	1	44.4	25.0	0.423	18.761	1.103	2.07	0.516	0.398	10.593	40.232	20.766	0.909
7	191.37	1	42.1	37.0	0.602	25.337	1.252	2	0.516	0.398	12.021	33.624	17.354	0.997
8	103.93	1.268	29.0	53.0	0.799	23.154	2.107	2	0.516	0.398	20.230	17.448	9.006	1.677
9			0.0		0.000	0.000	0.000		0.516	0.398	0.000	0.000	0.000	0.000
10			0.0		0.000	0.000	0.000		0.516	0.398	0.000	0.000	0.000	0.000
Total						72.839					92.588		107.140	10.593

FOS = 2.8874902

Day 135

Slice No	z (cm)	b (m)	W (kN)	α (°)	sin α	Wsin α (kN) (4)	l (m)	ψ (kPa)	tan ϕ'	tan ϕ b	c'l (kN) (1)	Wcos α (m)	Wcos α tan ϕ' (kN) (2)	ψ tan ϕ b (kN) (3)
1	26.78	1	5.9	-25.0	-0.423	-2.490	1.103	5.05	0.516	0.398	10.593	5.340	2.756	2.217
2	63.47	1	14.0	-15.0	-0.259	-3.614	1.035	4	0.516	0.398	9.939	13.488	6.961	1.648
3	105.95	1	23.3	-5.0	-0.087	-2.032	1.004	3.4	0.516	0.398	9.637	23.220	11.985	1.358
4	155.95	1	34.3	5.0	0.087	2.990	1.004	2.9	0.516	0.398	9.637	34.178	17.641	1.158
5	188.47	1	41.5	15.0	0.259	10.732	1.035	2.45	0.516	0.398	9.939	40.051	20.672	1.009
6	201.78	1	44.4	25.0	0.423	18.761	1.103	2.09	0.516	0.398	10.593	40.232	20.766	0.918
7	191.37	1	42.1	37.0	0.602	25.337	1.252	2	0.516	0.398	12.021	33.624	17.354	0.997
8	103.93	1.268	29.0	53.0	0.799	23.154	2.107	2	0.516	0.398	20.230	17.448	9.006	1.677
9			0.0		0.000	0.000	0.000		0.516	0.398	0.000	0.000	0.000	0.000
10			0.0		0.000	0.000	0.000		0.516	0.398	0.000	0.000	0.000	0.000
Total						72.839					92.588		107.140	10.983

FOS = 2.8928472

Day 150

Slice No	z (cm)	b (m)	W (kN)	α (°)	sin α	Wsin α (kN) (4)	l (m)	ψ (kPa)	tan ϕ'	tan ϕ b	c'l (kN) (1)	Wcos α (m)	Wcos α tan ϕ' (kN) (2)	ψ tan ϕ b (kN) (3)
1	26.78	1	5.9	-25.0	-0.423	-2.490	1.103	5.44	0.516	0.398	10.593	5.340	2.756	2.389
2	63.47	1	14.0	-15.0	-0.259	-3.614	1.035	4.2	0.516	0.398	9.939	13.488	6.961	1.730
3	105.95	1	23.3	-5.0	-0.087	-2.032	1.004	3.54	0.516	0.398	9.637	23.220	11.985	1.414
4	155.95	1	34.3	5.0	0.087	2.990	1.004	3	0.516	0.398	9.637	34.178	17.641	1.198
5	188.47	1	41.5	15.0	0.259	10.732	1.035	2.5	0.516	0.398	9.939	40.051	20.672	1.030
6	201.78	1	44.4	25.0	0.423	18.761	1.103	2.1	0.516	0.398	10.593	40.232	20.766	0.922
7	191.37	1	42.1	37.0	0.602	25.337	1.252	2	0.516	0.398	12.021	33.624	17.354	0.997
8	103.93	1.268	29.0	53.0	0.799	23.154	2.107	2	0.516	0.398	20.230	17.448	9.006	1.677
9			0.0		0.000	0.000	0.000		0.516	0.398	0.000	0.000	0.000	0.000
10			0.0		0.000	0.000	0.000		0.516	0.398	0.000	0.000	0.000	0.000
Total						72.839					92.588		107.140	11.357

FOS = 2.8979889

Day 165

Slice No	z (cm)	b (m)	W (kN)	α (°)	sin α	Wsin α (kN) (4)	l (m)	ψ (kPa)	tan ϕ'	tan ϕ b	c'l (kN) (1)	Wcos α (m)	Wcos α tan ϕ' (kN) (2)	ψ tan ϕ b (kN) (3)
1	26.78	1	5.9	-25.0	-0.423	-2.490	1.103	5.87	0.516	0.398	10.593	5.340	2.756	2.578
2	63.47	1	14.0	-15.0	-0.259	-3.614	1.035	4.42	0.516	0.398	9.939	13.488	6.961	1.821
3	105.95	1	23.3	-5.0	-0.087	-2.032	1.004	3.7	0.516	0.398	9.637	23.220	11.985	1.478
4	155.95	1	34.3	5.0	0.087	2.990	1.004	3.08	0.516	0.398	9.637	34.178	17.641	1.230
5	188.47	1	41.5	15.0	0.259	10.732	1.035	2.54	0.516	0.398	9.939	40.051	20.672	1.046
6	201.78	1	44.4	25.0	0.423	18.761	1.103	2.11	0.516	0.398	10.593	40.232	20.766	0.926
7	191.37	1	42.1	37.0	0.602	25.337	1.252	2	0.516	0.398	12.021	33.624	17.354	0.997
8	103.93	1.268	29.0	53.0	0.799	23.154	2.107	2	0.516	0.398	20.230	17.448	9.006	1.677
9			0.0		0.000	0.000	0.000		0.516	0.398	0.000	0.000	0.000	0.000
10			0.0		0.000	0.000	0.000		0.516	0.398	0.000	0.000	0.000	0.000
Total						72.839					92.588		107.140	11.754

FOS = 2.9034282

Day 180

Slice No	z (cm)	b (m)	W (kN)	α (°)	sin α	Wsin α (kN) (4)	l (m)	ψ (kPa)	tan ϕ'	tan ϕ b	c'l (kN) (1)	Wcos α (m)	Wcos α tan ϕ' (kN) (2)	ψ tan ϕ b (kN) (3)
1	26.78	1	5.9	-25.0	-0.423	-2.490	1.103	6.34	0.516	0.398	10.593	5.340	2.756	2.784
2	63.47	1	14.0	-15.0	-0.259	-3.614	1.035	4.63	0.516	0.398	9.939	13.488	6.961	1.908
3	105.95	1	23.3	-5.0	-0.087	-2.032	1.004	3.84	0.516	0.398	9.637	23.220	11.985	1.534
4	155.95	1	34.3	5.0	0.087	2.990	1.004	3.18	0.516	0.398	9.637	34.178	17.641	1.270
5	188.47	1	41.5	15.0	0.259	10.732	1.035	2.6	0.516	0.398	9.939	40.051	20.672	1.071
6	201.78	1	44.4	25.0	0.423	18.761	1.103	2.12	0.516	0.398	10.593	40.232	20.766	0.931
7	191.37	1	42.1	37.0	0.602	25.337	1.252	2	0.516	0.398	12.021	33.624	17.354	0.997
8	103.93	1.268	29.0	53.0	0.799	23.154	2.107	2	0.516	0.398	20.230	17.448	9.006	1.677
9			0.0		0.000	0.000	0.000		0.516	0.398	0.000	0.000	0.000	0.000
10			0.0		0.000	0.000	0.000		0.516	0.398	0.000	0.000	0.000	0.000
Total						72.839					92.588		107.140	12.172

FOS = 2.9091652

Day 195

Slice No	z (cm)	b (m)	W (kN)	α (°)	sin α	Wsin α (kN) (4)	l (m)	ψ (kPa)	tan ϕ'	tan ϕ b	c'l (kN) (1)	Wcos α (m)	Wcos α tan ϕ' (kN) (2)	ψ tan ϕ b (kN) (3)
1	26.78	1	5.9	-25.0	-0.423	-2.490	1.103	6.86	0.516	0.398	10.593	5.340	2.756	3.012
2	63.47	1	14.0	-15.0	-0.259	-3.614	1.035	4.84	0.516	0.398	9.939	13.488	6.961	1.994
3	105.95	1	23.3	-5.0	-0.087	-2.032	1.004	4	0.516	0.398	9.637	23.220	11.985	1.598
4	155.95	1	34.3	5.0	0.087	2.990	1.004	3.26	0.516	0.398	9.637	34.178	17.641	1.302
5	188.47	1	41.5	15.0	0.259	10.732	1.035	2.62	0.516	0.398	9.939	40.051	20.672	1.079
6	201.78	1	44.4	25.0	0.423	18.761	1.103	2.14	0.516	0.398	10.593	40.232	20.766	0.940
7	191.37	1	42.1	37.0	0.602	25.337	1.252	2	0.516	0.398	12.021	33.624	17.354	0.997
8	103.93	1.268	29.0	53.0	0.799	23.154	2.107	2	0.516	0.398	20.230	17.448	9.006	1.677
9			0.0		0.000	0.000	0.000		0.516	0.398	0.000	0.000	0.000	0.000
10			0.0		0.000	0.000	0.000		0.516	0.398	0.000	0.000	0.000	0.000
Total						72.839					92.588		107.140	12.599

FOS = 2.9150377

Day 210

Slice No	z (cm)	b (m)	W (kN)	α (°)	sin α	Wsin α (kN) (4)	l (m)	ψ (kPa)	tan ϕ'	tan ϕ b	c'l (kN) (1)	Wcos α (m)	Wcos α tan ϕ' (kN) (2)	ψ tan ϕ b (kN) (3)
1	26.78	1	5.9	-25.0	-0.423	-2.490	1.103	7.45	0.516	0.398	10.593	5.340	2.756	3.271
2	63.47	1	14.0	-15.0	-0.259	-3.614	1.035	5.1	0.516	0.398	9.939	13.488	6.961	2.101
3	105.95	1	23.3	-5.0	-0.087	-2.032	1.004	4.13	0.516	0.398	9.637	23.220	11.985	1.650
4	155.95	1	34.3	5.0	0.087	2.990	1.004	3.35	0.516	0.398	9.637	34.178	17.641	1.338
5	188.47	1	41.5	15.0	0.259	10.732	1.035	2.66	0.516	0.398	9.939	40.051	20.672	1.096
6	201.78	1	44.4	25.0	0.423	18.761	1.103	2.15	0.516	0.398	10.593	40.232	20.766	0.944
7	191.37	1	42.1	37.0	0.602	25.337	1.252	2	0.516	0.398	12.021	33.624	17.354	0.997
8	103.93	1.268	29.0	53.0	0.799	23.154	2.107	2	0.516	0.398	20.230	17.448	9.006	1.677
9			0.0		0.000	0.000	0.000		0.516	0.398	0.000	0.000	0.000	0.000
10			0.0		0.000	0.000	0.000		0.516	0.398	0.000	0.000	0.000	0.000
Total						72.839					92.588		107.140	13.074

FOS = 2.9215582

Day 225

Slice No	z (cm)	b (m)	W (kN)	α (°)	sin α	Wsin α (kN) (4)	l (m)	ψ (kPa)	tan ϕ'	tan ϕ b	c'l (kN) (1)	Wcos α (m)	Wcos α tan ϕ' (kN) (2)	ψ tan ϕ b (kN) (3)
1	26.78	1	5.9	-25.0	-0.423	-2.490	1.103	8.15	0.516	0.398	10.593	5.340	2.756	3.579
2	63.47	1	14.0	-15.0	-0.259	-3.614	1.035	5.32	0.516	0.398	9.939	13.488	6.961	2.192
3	105.95	1	23.3	-5.0	-0.087	-2.032	1.004	4.28	0.516	0.398	9.637	23.220	11.985	1.710
4	155.95	1	34.3	5.0	0.087	2.990	1.004	3.44	0.516	0.398	9.637	34.178	17.641	1.374
5	188.47	1	41.5	15.0	0.259	10.732	1.035	2.7	0.516	0.398	9.939	40.051	20.672	1.112
6	201.78	1	44.4	25.0	0.423	18.761	1.103	2.16	0.516	0.398	10.593	40.232	20.766	0.948
7	191.37	1	42.1	37.0	0.602	25.337	1.252	2	0.516	0.398	12.021	33.624	17.354	0.997
8	103.93	1.268	29.0	53.0	0.799	23.154	2.107	2	0.516	0.398	20.230	17.448	9.006	1.677
9			0.0		0.000	0.000	0.000		0.516	0.398	0.000	0.000	0.000	0.000
10			0.0		0.000	0.000	0.000		0.516	0.398	0.000	0.000	0.000	0.000
Total						72.839					92.588		107.140	13.599

FOS = 2.9286252

Day 240

Slice No	z (cm)	b (m)	W (kN)	α (°)	sin α	Wsin α (kN) (4)	l (m)	ψ (kPa)	tan ϕ'	tan ϕ b	c'l (kN) (1)	Wcos α (m)	Wcos α tan ϕ' (kN) (2)	ψ tan ϕ b (kN) (3)
1	26.78	1	5.9	-25.0	-0.423	-2.490	1.103	8.87	0.516	0.398	10.593	5.340	2.756	3.895
2	63.47	1	14.0	-15.0	-0.259	-3.614	1.035	5.59	0.516	0.398	9.939	13.488	6.961	2.303
3	105.95	1	23.3	-5.0	-0.087	-2.032	1.004	4.42	0.516	0.398	9.637	23.220	11.985	1.766
4	155.95	1	34.3	5.0	0.087	2.990	1.004	3.52	0.516	0.398	9.637	34.178	17.641	1.406
5	188.47	1	41.5	15.0	0.259	10.732	1.035	2.73	0.516	0.398	9.939	40.051	20.672	1.125
6	201.78	1	44.4	25.0	0.423	18.761	1.103	2.17	0.516	0.398	10.593	40.232	20.766	0.953
7	191.37	1	42.1	37.0	0.602	25.337	1.252	2.01	0.516	0.398	12.021	33.624	17.354	1.002
8	103.93	1.268	29.0	53.0	0.799	23.154	2.107	2	0.516	0.398	20.230	17.448	9.006	1.677
9			0.0		0.000	0.000	0.000		0.516	0.398	0.000	0.000	0.000	0.000
10			0.0		0.000	0.000	0.000		0.516	0.398	0.000	0.000	0.000	0.000
Total						72.839					92.588		107.140	14.126

FOS = 2.9359977

Day 255

Slice No	z (cm)	b (m)	W (kN)	α (°)	sin α	Wsin α (kN) (4)	l (m)	ψ (kPa)	tan ϕ'	tan ϕ b	c'l (kN) (1)	Wcos α (m)	Wcos α tan ϕ' (kN) (2)	ψ tan ϕ b (kN) (3)
1	26.78	1	5.9	-25.0	-0.423	-2.490	1.103	9.64	0.516	0.398	10.593	5.340	2.756	4.233
2	63.47	1	14.0	-15.0	-0.259	-3.614	1.035	5.86	0.516	0.398	9.939	13.488	6.961	2.414
3	105.95	1	23.3	-5.0	-0.087	-2.032	1.004	4.57	0.516	0.398	9.637	23.220	11.985	1.826
4	155.95	1	34.3	5.0	0.087	2.990	1.004	3.61	0.516	0.398	9.637	34.178	17.641	1.442
5	188.47	1	41.5	15.0	0.259	10.732	1.035	2.77	0.516	0.398	9.939	40.051	20.672	1.141
6	201.78	1	44.4	25.0	0.423	18.761	1.103	2.18	0.516	0.398	10.593	40.232	20.766	0.957
7	191.37	1	42.1	37.0	0.602	25.337	1.252	2.01	0.516	0.398	12.021	33.624	17.354	1.002
8	103.93	1.268	29.0	53.0	0.799	23.154	2.107	2	0.516	0.398	20.230	17.448	9.006	1.677
9			0.0		0.000	0.000	0.000		0.516	0.398	0.000	0.000	0.000	0.000
10			0.0		0.000	0.000	0.000		0.516	0.398	0.000	0.000	0.000	0.000
Total						72.839					92.588		107.140	14.692

FOS = 2.9437695

Day 270

Slice No	z (cm)	b (m)	W (kN)	α (°)	sin α	Wsin α (kN) (4)	l (m)	ψ (kPa)	tan ϕ'	tan ϕ b	c'l (kN) (1)	Wcos α (m)	Wcos α tan ϕ' (kN) (2)	ψ tan ϕ b (kN) (3)
1	26.78	1	5.9	-25.0	-0.423	-2.490	1.103	10.5	0.516	0.398	10.593	5.340	2.756	4.611
2	63.47	1	14.0	-15.0	-0.259	-3.614	1.035	6.2	0.516	0.398	9.939	13.488	6.961	2.554
3	105.95	1	23.3	-5.0	-0.087	-2.032	1.004	4.7	0.516	0.398	9.637	23.220	11.985	1.878
4	155.95	1	34.3	5.0	0.087	2.990	1.004	3.7	0.516	0.398	9.637	34.178	17.641	1.478
5	188.47	1	41.5	15.0	0.259	10.732	1.035	2.8	0.516	0.398	9.939	40.051	20.672	1.154
6	201.78	1	44.4	25.0	0.423	18.761	1.103	2.2	0.516	0.398	10.593	40.232	20.766	0.966
7	191.37	1	42.1	37.0	0.602	25.337	1.252	2.01	0.516	0.398	12.021	33.624	17.354	1.002
8	103.93	1.268	29.0	53.0	0.799	23.154	2.107	2	0.516	0.398	20.230	17.448	9.006	1.677
9			0.0		0.000	0.000	0.000		0.516	0.398	0.000	0.000	0.000	0.000
10			0.0		0.000	0.000	0.000		0.516	0.398	0.000	0.000	0.000	0.000
Total						72.839					92.588		107.140	15.319

FOS = 2.9523738

FOS for Unsaturated Soils, initial $\psi = -20cm$ with tree at centre of slope

c (kPa)	ϕ' (°)	ϕb (°)	γ (kN/m3)
9.6	27.3	21.7	22

Slice No	x (cm)	b (m)	W (kN)	α (°)	$\sin\alpha$	$W\sin\alpha$ (kN) (4)	l (m)	ψ (kPa)	$\tan\phi'$	$\tan\phi b$	c'l (kN) (1)	$W\cos\alpha$ (m)	$W\cos\alpha\tan\phi'$ (kN) (2)	$\psi l\tan\phi b$ (kN) (3)
1	26.78	1	5.9	-25.0	-0.423	-2.490	1.103	2.24	0.516	0.398	10.593	5.340	2.756	0.984
2	63.47	1	14.0	-15.0	-0.259	-3.614	1.035	2.3	0.516	0.398	9.939	13.488	6.961	0.948
3	105.95	1	23.3	-5.0	-0.087	-2.032	1.004	2.38	0.516	0.398	9.637	23.220	11.985	0.951
4	155.95	1	34.3	5.0	0.087	2.990	1.004	2.54	0.516	0.398	9.637	34.178	17.641	1.015
5	188.47	1	41.5	15.0	0.259	10.732	1.035	2.94	0.516	0.398	9.939	40.051	20.672	1.211
6	201.78	1	44.4	25.0	0.423	18.761	1.103	3.38	0.516	0.398	10.593	40.232	20.766	1.484
7	191.37	1	42.1	37.0	0.602	25.337	1.252	4.6	0.516	0.398	12.021	33.624	17.354	2.292
8	103.93	1.268	29.0	53.0	0.799	23.154	2.107	2.63	0.516	0.398	20.230	17.448	9.006	2.206
9			0.0		0.000	0.000	0.000		0.516	0.398	0.000	0.000	0.000	0.000
10			0.0		0.000	0.000	0.000		0.516	0.398	0.000	0.000	0.000	0.000
Total						72.839					92.588		107.140	11.090

FOS = 2.8943126

FOS for Unsaturated Soils, initial $\psi = -20cm$ with tree at top

c (kPa)	ϕ' (°)	ϕb (°)	γ (kN/m3)
9.6	27.3	21.7	22

Slice No	x (cm)	b (m)	W (kN)	α (°)	$\sin\alpha$	$W\sin\alpha$ (kN) (4)	l (m)	ψ (kPa)	$\tan\phi'$	$\tan\phi b$	c'l (kN) (1)	$W\cos\alpha$ (m)	$W\cos\alpha\tan\phi'$ (kN) (2)	$\psi l\tan\phi b$ (kN) (3)
1	26.78	1	5.9	-25.0	-0.423	-2.490	1.103	2	0.516	0.398	10.593	5.340	2.756	0.878
2	63.47	1	14.0	-15.0	-0.259	-3.614	1.035	2	0.516	0.398	9.939	13.488	6.961	0.824
3	105.95	1	23.3	-5.0	-0.087	-2.032	1.004	2	0.516	0.398	9.637	23.220	11.985	0.799
4	155.95	1	34.3	5.0	0.087	2.990	1.004	2	0.516	0.398	9.637	34.178	17.641	0.799
5	188.47	1	41.5	15.0	0.259	10.732	1.035	2.02	0.516	0.398	9.939	40.051	20.672	0.832
6	201.78	1	44.4	25.0	0.423	18.761	1.103	2.06	0.516	0.398	10.593	40.232	20.766	0.905
7	191.37	1	42.1	37.0	0.602	25.337	1.252	2.58	0.516	0.398	12.021	33.624	17.354	1.286
8	103.93	1.268	29.0	53.0	0.799	23.154	2.107	5.08	0.516	0.398	20.230	17.448	9.006	4.260
9			0.0		0.000	0.000	0.000		0.516	0.398	0.000	0.000	0.000	0.000
10			0.0		0.000	0.000	0.000		0.516	0.398	0.000	0.000	0.000	0.000
Total						72.839					92.588		107.140	10.583

FOS = 2.8873495